Université de Toulouse

THÈSE

En vue de l'obtention du

DOCTORAT DE L'UNIVERSITÉ DE TOULOUSE

Délivré par :

Université Toulouse 3 Paul Sabatier (UT3 Paul Sabatier)

Présentée et soutenue par :
Bruno Aliès
le lundi 17 décembre 2012

Titre :

Interactions des ions métalliques avec des formes tronquées du peptide amyloïde-ß liées à la maladie d'Alzheimer

---

École doctorale et discipline ou spécialité :
ED SDM : Chimie, Biologie, Santé - CO 042

Unité de recherche :
Laboratoire de Chimie de Coordination

Directeur(s) de Thèse :

Pr. Peter Faller
Dr. Christelle Hureau

Jury (noms, prénoms et qualité des membres) :

Dr. Jalila Simaan	Rapporteur	iSm2, Marseille
Dr. Claudio Gomes	Rapporteur	ITQB, Oeiras, Portugal
Pr. Wojciech Bal	Examinateur	IBB, Varsovie, Pologne
Pr. Jean-Pierre Mahy	Examinateur	ICMMO, Paris
Dr. Pierre Genevaux	Examinateur	LMGM, Toulouse
Pr. Peter Faller	Co-Directeur	LCC, Toulouse
Dr. Christelle Hureau	Directeur	LCC, Toulouse

Acknowledgement

I would like to thank the following people that I had the chance to know during my PhD. You may think that the contributions to my PhD of the announced people below are not equal. You may be right… but as the overall folding of a metallopeptide is due to the whole and intricate interactions, the "structure" of my PhD was highly dependent of cited people and determined by the wide contribution as each of these persons.

Thank you,

Metal ions

Christelle Hureau, for support (in French and in English) me during three years. I learnt a lot from you, in science, for sure but also on other aspects of life. You show me how a messy desk (not worse than mine) could be linked to a high scientific rigour, how determination can brave many obstacles. In spite of numerous phobias (not enough space to cite them, I tried to reduce the list), you remain more courageous than I on some points. I was a pleasure for me to have being guided by you across these three years (already…). Thank you for being my PhD supervisor.

Peter Faller, for recruiting me in the team against my initial choice. I was very pleased to enjoy your wide knowledge, your scientific frankness, your constant mood and availability. I'm still jealous about your great abstractions capacities (both scientific and the surrounding area) and your amazing effectiveness (amount / time). Late night beers and participations to my parties preserve your open-mindedness. Thank you for being my PhD co-supervisor.

Spectroscopic Techniques

Jalila Simaan, **Claudio Gomes**, **Wojciech Bal**, **Jean-Pierre Mahy**, **Pierre Genevaux**, for coming and for accepting to evaluated my PhD.

pI

Emmanuel Gras, for the pleasure I had to contradict you at lunchtime (and sometimes being right) and for the debates we had (sometimes productive).
Isabelle Sasaki, for late day discussions about lab, people, science, Japan… For showing me the cell's lab and for Christmas hand-made chocolates.
Vivane Peyrou-Maveyraud, for your constant smile and your friendly face
Emmanuelle Mothes, for introducing me to the SAFAS spectrofluorometer

Amino-acid Residues

Emmanuel Guillon, for coming at my PhD defence. For the nights and the days spent together on ESRF or Soleil beamlines. For your constant zest in science as in life (for when ironman?).
Stéphanie Sayen, for being the moderate persons on synchrotron's sessions. For taking care about experimental parameter and for writing them down when we were out-of-order.
Pier-Lorenzo Solari, **Isabelle Llorens**, **Emiliano Fonda**, **Stéphanie Belin**, **Olivier Proux**, **Jean-louis Hazemann**, for your key contribution in XAS measurements.
Vincent Picot and **Pierre Joseph,** for our collaboration into lab-on-chip.

Christian Bijani, for countless quantities of NMR tubes examined for my purposes.
Charles-Louis Serpentini, for taking care of CD spectrometer and give us old but useful deuterium lamps.
Lionel Rechignat, for numerous EPR tube examined for my purposes. For Grümo leadership, and for being our new TOC designer.

Peptide backbone and pH

Hélène (and Kévin), for sharing with me your solutions (ThT, Buffer…), for providing chocolates from Kévin and for your contribution to Aβ mutants paper.
Gilles, for interesting discussion about mathematical limits of series, for your organic synthesis expertise to my novice question.
Aurélien (Honraedt), for showing me (and took pictures) of the ever bigger synthetic crystals have ever seen.
Sabrina and **Sarah** (Cadet), for being "new" enthusiastic colleagues.
Carine, **George** and **Laurie**, for being kind co-workers from my university's promotion
Jeppe, **Markus**, **Fred**, **Sandra, Gana, Fanny** and **Ana** for parties, outdoor activities and dancing sessions
Samatha and **Madeleine**, for cooking bakery.
Helen, for time spent together running NMR spectra .
Fatima, for initiating Aβ full-length aggregation.
Maud, for being my trainee and performed investigations about ATCUN motif sequence, I hope we will soon succeed to promote this work.
Eva, **Pierre-Luc**, **Sambika** for your enthusiastic Spanish, South-west French and Indian style, respectively.
Fabien, **Pierre**, for being chatty colleagues.
Bertrand, for initiating me to QVPSP and HIMYM.
Emelyne, for your commitment outside your field of interest
Fred (Terrade), for the houseplant you donated to me
Anne, for joining me in a beer contest
Sara (from Spain) & **Sara** (Maria), for promising results in ROS
Thais, for exercising my English

Salt-bridges and H-bond

Pierre Dorlet, for accepting to loose with me at playing card and for letting me initiate you at scuba diving.
Emi Evangelio, for your wild character and for coming at my PhD defence. For hosting us in Barcelona, for sharing beers and cigarettes.
Remi Chauvin, for interesting discussions at lunchtimes and as a strong (and only) support against Manu's blah-blah.
Gwenanel Rapenne, for sending me in Florida as research trainee
Yves Génisson, for being my thesis sponsor
Laurent Sabater, for handling and taking care of my PhD supervisor
Stephanie, for taking care of my PhD co-supervisor
Clotide Policar, for her unwearied scientific enthusiasm and curiosity
Elodie Anxolabéhère-Mallart, for your post-doc advices
Claudio Gomes, **Joao Rodrigues**, **Bárbara Henriques** and the rest of the girls' team, for welcoming me in ITQB PBFS group.
Michel Caffarel, for your availability and for a brief course about quantum mechanics.

Erik Paul, for your availability and your advices about BMG spectrofluometer.
Frank Bussoti, for giving me opportunities to fully open the SAFAS spectrofluometer.

Temperature

Céline Deraeve, for welcoming me in your pratical lab class as novice teacher.
Vincent Pradines (and Diana), for introducing me to TEM, and being badminton idol
Aurélien Chollet, for beating my badminton idol
Marion and **Irene**, for your good mood
Anne Robert, for being my Master Degree supervisor and our knowledge exchange.
Jean-Luc Stigliani, for replacement when I was needed
Jean Bernadou, **Vania Bernardes-Genisson**, **Geneviève Pratviel**, for your technical (need of chemicals) or intellectual (scientific questions) help.

Ionic strength

Elsa & **Julie**, for hosting us during conference in Marseille.
Mathieu, for hosting me during conference in Paris.
Cha, **Mik**, **Paul**, for being my favourites physicist, and for answering to relativist questions (about synchrotron's electron) or mathematical questions (lim (n->+oo) [(n-1)/n]^n = 1/e) !
Ema, for back-flip dancing sessions.
Dré, for interesting discussion about linked between science and music.
Cédric, **Manu**, **Aurélie**, **Morgane**, **Alice** for sharing your couch / bed when I needed.
Karim, **Lisouille**, **Caro,** for your being my favourite Bachelor's class mate.
Florian (Pantillon), for jazz concerts
Kévin and **Jean**, for house duties (shopping, cooking, cleaning, parties organization) and entertainment
Valérie's family, for your kindness
Dad, for being the emergency CNRS supplier (creation of XAS sample holders, providing FLPC power supply, fuses for spectrofluometer…)
Mam, for the future organisation of the feast
Rémi, for being chess partner
Florian, for providing me your biological knowledge
Valérie, for sharing my life since… and for your love

Atmospheric pressure

And thank you to other people I may forget.

Issues

Amyloid plaques are one of the hallmarks in the brain of Alzheimer's disease (AD). These plaques are made of an aggregated peptide called amyloid-β (Aβ). Metal ions, more particularly Cu and Zn, are found in high amount in those plaques and have been proposed to play a major role in AD. Underlying processes of amyloid plaques formation and impacts of metal ions remain unclear. Nevertheless, evidence accumulate suggesting that Aβ peptide and metal ions interactions could be of paramount significance in AD. For instance, natively occurring Aβ sequence alterations of Aβ (truncation, mutation, etc) enhance AD and metal ions brain distribution correlate with amyloid plaques prone regions. This could be explained by the hypothesis that altered Aβ may be more toxic than native Aβ due to an aberrant coordination of Cu and that metal ions seem to modulate Aβ aggregation. In this context, the present manuscript follows these two researches axes. In the first one, named "coordination", we focused on the influence of Aβ sequence alterations to Cu coordination. In the second one, named "aggregation", we investigated the role of metal ions on the aggregation process with means of model peptides.

In the following chapters, we will try to reply to the following questions:

Coordination

- What is the coordination sphere of Cu(II) in Aβ and in its modified forms?
- How Cu(II) coordination depends on pH ?
- How mutations linked to early AD onset and truncations of Aβ disturb Cu(II) coordination?
- How the peptide sequence alterations affect Cu(II) affinity and coordination?

Aggregation

- Do Cu and Zn have the same effect on aggregation?
- How Cu and Zn modulate aggregation?
- Is Zn-induced aggregation pH dependent?
- Is transient Zn pool able to influence peptide aggregation?

Table of contents

I- AD

I. 1- Society

Alzheimer's disease (AD) is the major dementia (~70% of dementia are AD) which affected more than 35 million people worldwide. In the US, it is the sixth cause of death. As the disease is age-dependent (1 over 20 older than 65 year old, 1 over 5 older 85 year old), countries with high income and long life expectancy are more concerned. Nevertheless, extension of life expectancy is a phenomenon which occurs worldwide. In the coming decades, the number of Alzheimer's patients from the rich countries will be largely lower than the ones from other countries (see Figure 1). So, Alzheimer's disease generally considered as a rich people disease, is becoming an essential issue which need to be solved for the whole humanity. It is pointed out by the fact that dementia cost 1% of world's gross product. In spite of this crucial importance, AD remains, so far, an uncured disease.

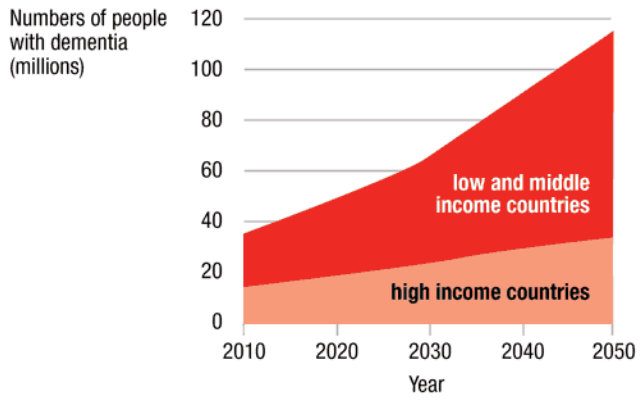

Figure 1: Expected number of people with dementia from low and middle (red) or high (orange) income countries on the next decades (from www.alz.co.uk/research/statistics).

I. 2- Symptoms

a- External

AD is characterized by a progressive lost of cognitive functions. The first noticeable symptom is the short-term memory loss. Then appear other disorders, difficulties to speak and to move. Recognition of people is also a faculty which is affected. In a later stage, the mood of AD patient becomes unstable. The patient may be aggressive, crying or laughing without reasons. At the terminal stage, patient do not show any emotions and the language is considerably reduced.

b- Internal

Brain's Volume

In AD, the size of the brain is notably reduced compared to a normal brain. A highly affected region is the hippocampus (brain's region related to information's acquisition). The decrease of the volume is concomitant with disease's progression. Methods used to investigate brain's anomalies are Position Emission Tomography (PET), Magnetic Resonance Imaging (MRI) and X-ray computed tomography. Nevertheless, differences in brain activity or in size at early stage of disease are too weak to be effectively used for diagnoses. Definitive diagnosis is made post mortem by showing the presence of the two hallmarks, amyloid plaques and neurofibrillary tangles.

Amyloid-plaques: aggregates of amyloid-β

Major hallmarks of AD are amyloid plaques and they were the first internal anomaly discovered by Alois Alzheimer more than a century ago. These plaques are found in the extracellular media of AD brain, and appear firstly in most affected brain's regions (*i.e* the hippocampus). They are constituted by aggregates of a peptide called Amyloid-β (Aβ). Aβ is mainly a 40 to 42 residue length peptide (see structure in annexe) issued from APP metabolism (see § I.4.a-Amyloid cascade). The function of Aβ is unclear. Due to its polar N-terminal and its apolar C-terminal parts, Aβ is amphiphilic (see sequence in § I.4.e-Metal ions Coordination to Aβ). Its tendency to aggregate is pretty high and Aβ forms *in vitro* similar type of aggregates like those formed *in vivo* (amyloid plaques). The aggregates could have a defined 3D structure, so called amyloids, which are often identified by the use of specific dyes such as Thioflavin T (see structure in annexe).

Neurofibrillary tangles: aggregates of Tau's proteins

Neurofibrillary tangles are the other major hallmark of AD but also appear in Pick's diseases. Neurofibrillary tangles consist of aggregated intraneuronal hyper-phosphorylated Tau proteins.[1] Tau proteins are highly expressed in neurons and their function is to stabilize long microtubules. Microtubules are essential to maintain the structure of the cell and to cellular transport. In neurones, long microtubules are required for neurotransmitter transport. In AD, Tau proteins are hyper-phosphorylated, which leads to incapacity to stabilize the microtubules. Consequently, microtubules are disrupted and the neuron becomes non-functional.

c- Predisposition and Risk Factors

Gender

Some studies suggest that women are more prone to develop AD than men (even when differences in life expectancy are taken into account). An explanation could be the decrease of steroids hormones in women due to menopause. Clinical trials by hormones supplement and genetic analysis of estrogens biosynthesis linked to AD seem to confirm this hypothesis and suggest estrogens play an important role in AD.[2]

Cholesterol

In spite of controversal studies, high level of cholesterol seems to enhance AD. It has been proposed that cholesterol increases Aβ concentration by promoting β-secretase at the expense of the α-secretase pathway (see scheme 1). Indeed, cholesterol is a membrane constituent and can modulate the enzymatic cleavage.[3]

Down's syndrome and Gene's mutations

Down's syndrome or trisomy 21 is characterized by a mental retardation, stunted growth and typical morphology. The APP gene is located on chromosome 21 and is consequently over-expressed resulting to early events of amyloid plaques formation and a type of AD development. Many mutations or polymorphisms on APP (precursor of Aβ), Presenilin (part of γ-secretase) and Apolipoprotein E (involved in clearance of Aβ)[4] genes have been pointed out to be at the origin of early AD onset.[5] These proteins are directly related to Aβ regulation and, as explained above, their metabolism is disrupted in AD. This in line with the amyloid cascade hypothesis stated below.

I. 3- Metal ions

a- Presence in the body

Fe, Zn and Cu are the most common transition metal ions in the body. Nevertheless, their quantities are rather low. Fe and Zn contribute for 4 g and 2 g to human weight, respectively. Cu is less present (70 mg). Other metals such as Mo or Co are found in low trace amount. They are involved in metabolism as essential cofactors.

b- Use of metals

Metals ions are involved in many tasks in the human body. Fe is well-known as dioxygen carrier in red blood cells. Fe has also other roles, for instance as oxidant catalyst in

cytochrome P450, for electron transfer in with the Iron-Sulfur cluster in complex III or hydrogen peroxide regulation in Catalase. In spite of its lower quantity, Cu is crucial. It is typically used for its redox chemistry. Cu can activate dioxygen for diverse enzymatic purposes.[6] Cu is involved in the respiratory chain as dioxygen reductant partner. Cu is also important in Fe metabolism (Ceruloplasmin) or in ROS management with Superoxide Dismutase (SOD). Zn is redox inactive (contrary to Cu or Fe) but can act as protein structures modulator or as Lewis-acid catalyst. It plays a major role in DNA transcription regulated by Zn finger proteins. Indeed, a secondary structure modification required for DNA interaction is induced by Zn coordination. Some proteases are Zn based. In those proteases, Zn destabilizes peptide-bond prior to the nucleophilic attack of water / hydroxide ion.

c- Metal Homeostasis

As explained above, metals, on one hand, are present at trace level in the body, and on the other hand, are essential in many pathways required for life. Those two parameters are absolutely vital because an overload is toxic and a lack is insufficient to maintain life's chemistry. Wilson's disease is a genetic disease which induced a mutation on an ATPase Cu efflux protein. The deficiency of this pump caused a Cu overload which lead to death without treatments. At the opposite, Menkes disease is characterized by the lack of Cu due to a mutation on an ATPase Cu influx. It causes severe development retardation and reduces life expectancy to five years. These two examples show how metals are necessary to life and how toxic they can be if in overload (see figure 2). So, metals homeostasis needs to be as tight as possible in a time and localization specific manner.

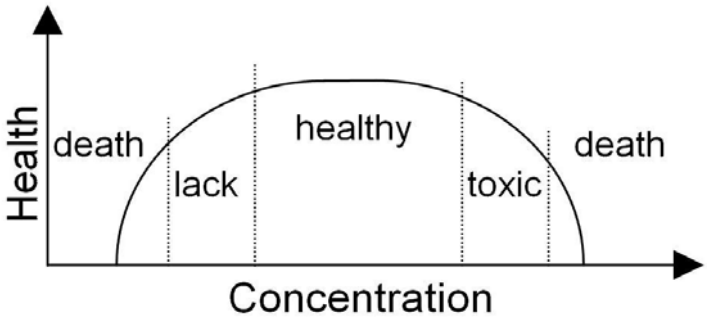

Figure 2: Tight regulation of metal ions is needed to maintain life

In human, brain represents 2% of the body weight, consumes 20% of dioxygen and contains 8% of total Cu (as pictured in figure 3). Considering those numbers and the fact that Cu is an efficient dioxyen activator,[6] it makes sense that the brain is highly sensible to Reactive Oxygen Species (ROS) and oxidative stress. In AD, metal homeostasis disruption has been proposed as an important parameter.[7]

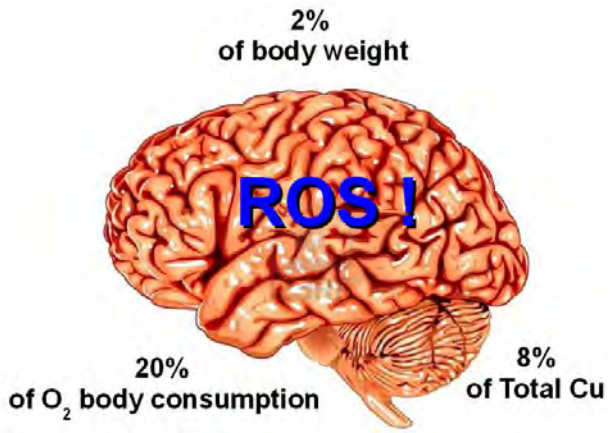

Figure 3: Brain's features which make it prone to oxidative stress.

I. 4- Amyloid-β peptide and Metals ions

a- Amyloid cascade

As explained above, Aβ peptide are found in AD brain as the main constituent in amyloid plaques and these amyloid plaques are a key evidence of the disease. Thus Aβ has been proposed to be crucial and may be involved in the aetiology of AD according to the amyloid cascade hypothesis (scheme 1).[8]

The Amyloid-β Precursor Protein (APP) is a transmembrane protein (major form has 695 amino acids) predominantly expressed in the brain with a large extracellular N-terminal domain. While its function remains unclear, its metabolism is well-known. APP could be cleaved by two pairs of proteases, either the α and γ or the β and γ secretases. By the first pair of enzymes, the resulting parts of the protein are not deleterious. If APP is cleaved by the β and γ secretases, one of the resulting part is the Aβ peptide.[9] Aβ is normally present in healthy brains but can accumulate and undergo "aggregation" in AD brains via a multistep process (see § I.4.b-Aggregation) resulting in amyloid plaques. The origins of accumulation and aggregation (via conformational change) in non-genetic AD are not clear. Various explanations have been proposed: metal ions interaction, overload of Aβ, reduction of Aβ degrading enzyme (such as Insulin-degrading enzyme)…[10]

Few years ago, amyloid plaques were believed to be the harmful species. Now, studies show no direct correlation between learning deficit and amyloid plaques, suggesting other forms of Aβ are much more toxic.[11] Aβ oligomeric species (Aβ forms between monomeric Aβ and amyloid plaques) are nowadays consider as the most deleterious compounds.[12]

Pathways by which Aβ oligomers are toxic to neurons and can trigger AD have been investigated. Several deleterious interactions with neurons have been proposed without consensus. Aβ oligomers may destabilize neuronal membranes and increase membrane permeability or interact with receptors.[13, 14]

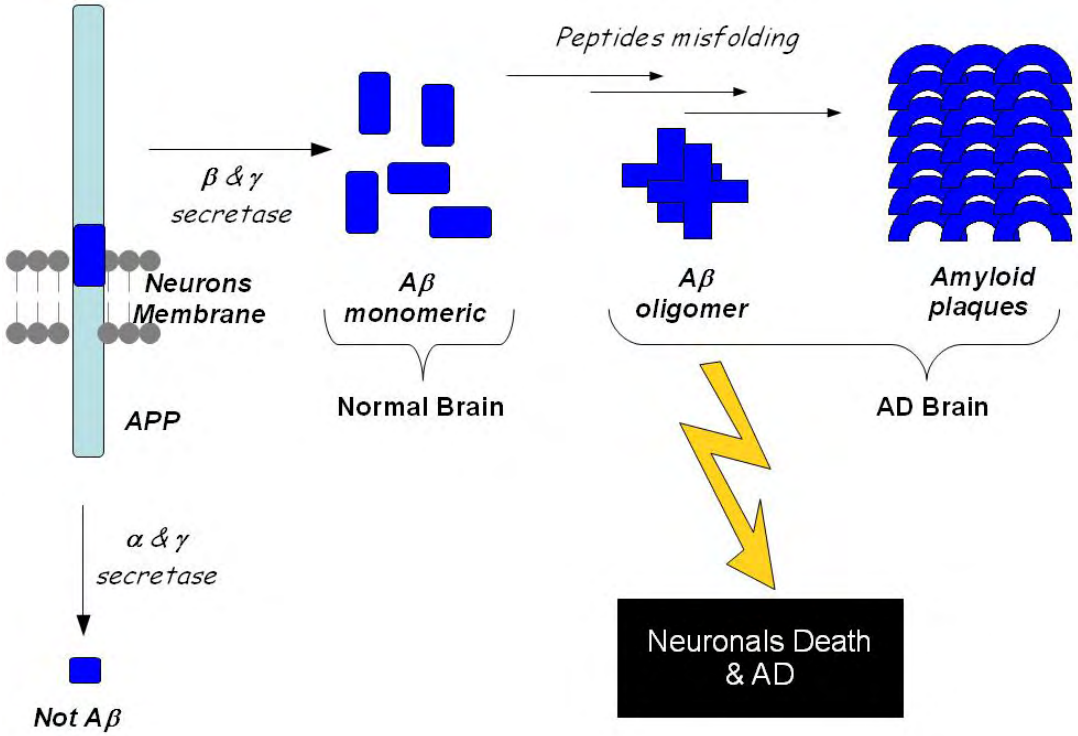

Scheme 1: Amyloid cascade pathway from APP to AD

b- Aggregation of Aβ

The major difference between peptides and proteins is the number of amino-acid. Due to this smaller number, peptides seem easier to look at compared to proteins. Here comes the tricky part, less amino-acids means less intermolecular interactions and thus less structured (or poorer 3D stability). Indeed, usually peptides are unfolded and so they have a wide range of possible 3D structures compared to proteins which are generally well-folded. This intrinsic structural instability gives to peptide tendency to seek for a lower free enthalpy (see figure 2 in ref [15]). Here begins the aggregation process.

There are two kinds of aggregates, amorphous and ordered (or amyloids). Specific dyes can be used to distinguish between amorphous and amyloids.[16] The major difference between those two types of aggregates is the well-defined 3D structures in case of amyloids.

In AD, amyloid plaques are made of fibrils amyloids. Amyloid fibrils are constituted of Aβ peptides with a high content of β-sheets (see figure 1 in ref [15]). Aβ and many of its derivatives could form amyloid fibrils under certain conditions. The rate, the amount and the

type of aggregates are highly dependent of various of parameters (pH, peptide sequence, concentration, metal ions…).

The mechanism of amyloid fibrils formation occurs in three basic steps: nucleation, elongation and termination (see figure 4).[17] The first step of the process, nucleation, is the rate limiting step. Indeed, this step needs several peptides in specific assembly modes. When the number and / or the shape of the nucleus are reached, elongation phase takes place. Elongation is similar to a non-covalent polymerisation. Monomeric peptides from the bulk are taken-up to extend the fibril. When the monomeric peptides concentration drops under a threshold, elongation stops. The quantity of fibrils remains stable, this is the plateau. The shape of amyloid formation kinetic is a sigmoid. Thus, fibrils aggregation can be fitted by mathematical model. Values found by the fitting equation give access to kinetic parameters (such as half-time) and allow comparing kinetic measurements.[18]

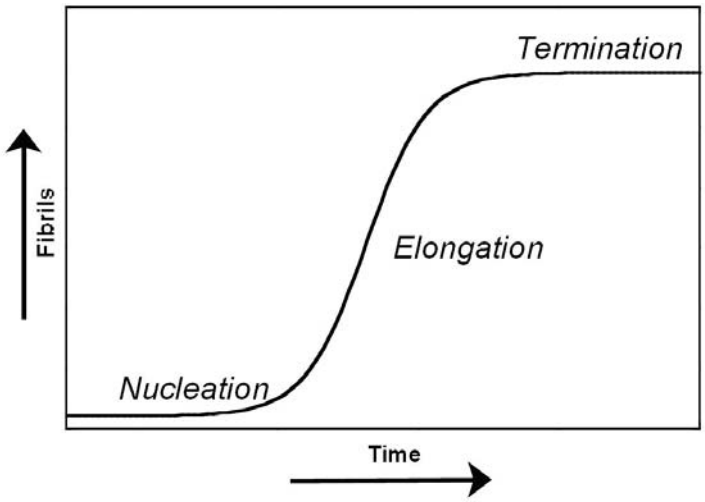

Figure 4: Formation of Amyloid fibrils: a three-step process.

c- Reactive Oxygen Species

Since O_2 is essential for many living organisms, these biological systems are exposed to Reactive Oxygen Species (ROS), a native byproduct of O_2 metabolism. In the presence of reducing agents, ROS can be produced via reduction of dioxygen. ROS include among others $O_2^{\bullet -}$, H_2O_2 and $^{\bullet}OH$. These molecules are reactive (or precursor of reactive molecules) that react with cell components such DNA, proteins or cell membranes. Modifications induced by ROS are harmful to life (damages, proteins inactivation or lipids peroxydation). In order to prevent such events, cell has mainly several protecting mechanisms, including the two enzymes, SOD and catalase. Increased ROS production leading to oxidative stress seems to

occur in AD. The reasons are ill defined, but for instance the modulation of the expression level of SOD and catalase may occurs in AD.[19]

d- Metals ions and Revised Amyloid Cascade

The hypothesis of implication of metal ions in AD is based on numerous facts. Firstly, Cu, Zn and Fe are highly accumulated in amyloid plaques.[20, 21] Secondly, AD brains show a dyshomeostasis of metal ions.[22,23] Also, brain's Zn distribution match with regions most prone to amyloid deposition (*i.e* hippocampus, amygdale and parietal lobe).[24] Thirdly, a large body of *in vitro* and *in vivo* experimental evidence supports metal ions implication in AD. Indeed, *in vitro* studies show that Cu and Zn can modulate Aβ aggregation.[25, 26] Chelators increase the resolubilisation of Aβ from isolated human amyloid plaques. *In vivo*, clioquinol chelator can dissolve amyloid deposit in transgenic mice's brains,[27] by metal chelation.[28] Zn transport knock-out transgenic mice show markedly reduced amyloid deposit.[29] Those examples demonstrate the importance of Cu and Zn in AD .

Metal ions, especially Cu, can be pretty efficient to catalyze ROS formation (see § I.3.b-Use of metal). This depends on its environment, i.e. the coordination chemistry. "Free" Cu or loosely bound Cu are efficient in ROS production. In contrast most Cu-proteins like cytochrome c oxidase are designed to minimize ROS production. Biological reductants react very poorly with dioxygen. In presence of Cu(II) and biological reductant (Glutathione, Ascorbate…), Cu(II) is reduced to Cu(I) and rapidly passes on its electron to dioxygen in solution to form superoxide (see scheme 2). This cycle goes on as long as the quantity of reductant is sufficient. The reaction produces also hydrogen peroxide and hydroxyl radical.

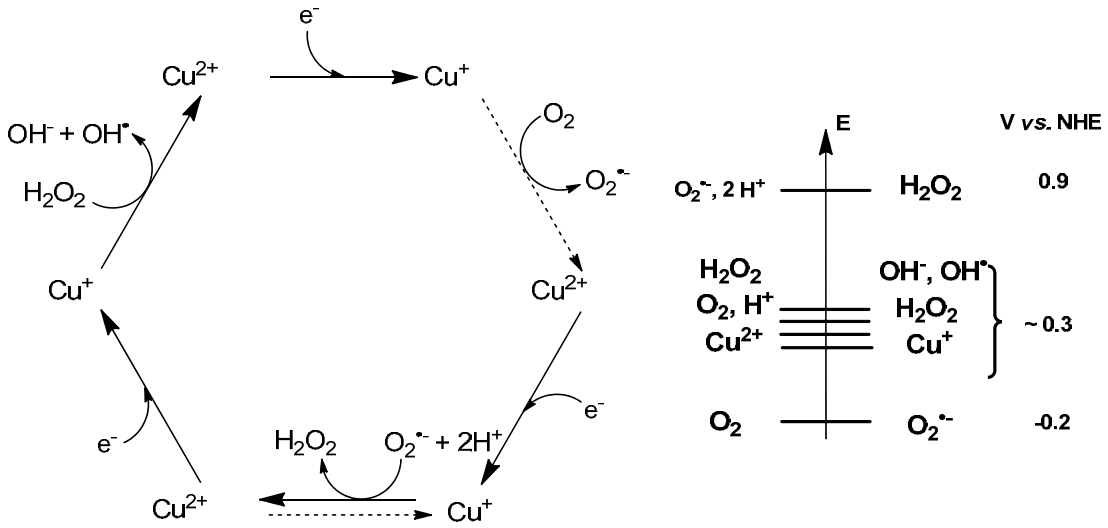

Scheme 2 : Cu catalysed ROS production adapted from ref 24

Oxidative stress present reported in AD could be explained by metal induced ROS production.[30] In this way, lossely bound Cu seems to correlate with AD's brain oxidative damages[7] and cell experiments have shown the toxicity of Aβ-Cu under reductive condition.[31] Moreover, transgenic mice with reduced level of MnSOD display more amyloid plaques and higher level of Aβ.[32] This indicates that oxidative damages can accentuate AD hallmarks, and thus ROS may be considered as a vicious circle in AD.

Overall, metal ions and Aβ are two actors of AD. Aβ can bind these metal ions and it has been proposed that Aβ-metal ions interactions could be a key event in AD. Amyloid cascade (see above scheme 1) shows the pathway from Aβ monomer to amyloid plaques. A trigger of this event may be metal ions coordination to Aβ. Another point is that Aβ-Cu complexes can produce ROS in presence of physiological reductant such as ascorbate. Aβ-metal mediated ROS production could explain oxidative damages found in AD brain and may be a central event of the disease. Thus, studies of Aβ-metal ions interactions are of paramount interest to explain both Aβ-aggregation and ROS production induced by metal ions.

e- Metal ions Coordination to Aβ

Aβ Sequence

As explained above, metal ions coordination to Aβ may help to understand molecular process linked to AD. Below, the figure 5 shows the sequence of Aβ1-42 (see also Aβ1-40 developed sequence in annexe), two parts can be clearly distinguished: in one side, the N-terminal part, polar and charged with several potential metals ligands; in the other side, the C-terminal part, largely hydrophobic. Because of this second part, the peptide is only soluble at very low concentrations (*i.e.* µM). This poor solubility is at the origin of aggregation but precludes the application of many spectroscopies, that require higher concentration in the soluble state. By looking at Figure 5, it is relatively clear that main binding sites of metal ions are located on the Aβ1-16 part rather than on the Aβ17-42 part. Therefore, in order to investigate metal coordination to Aβ at higher concentration, Aβ1-16 can be used due to its much higher solubility. However, Aβ1-16 does not form amyloid type aggregates, but it is clearly a valuable model for the soluble monomeric metal-Aβ1-40/42.[33]

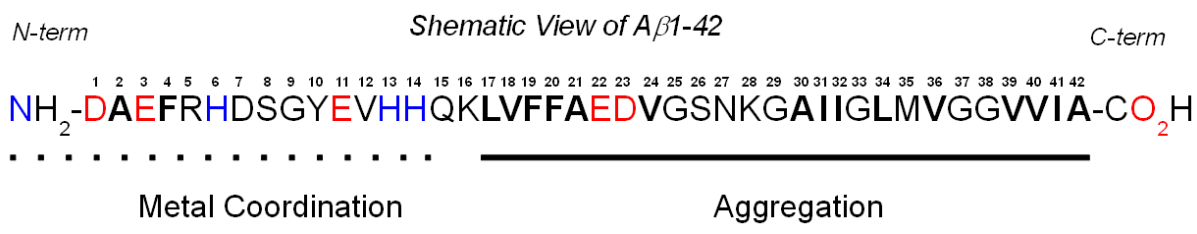

Figure 5a: Primary sequence of Aβ1-42 emphasizing the carboxylic acid functions (red), amine and imidazole (blue) and hydrophobic residues (bold).

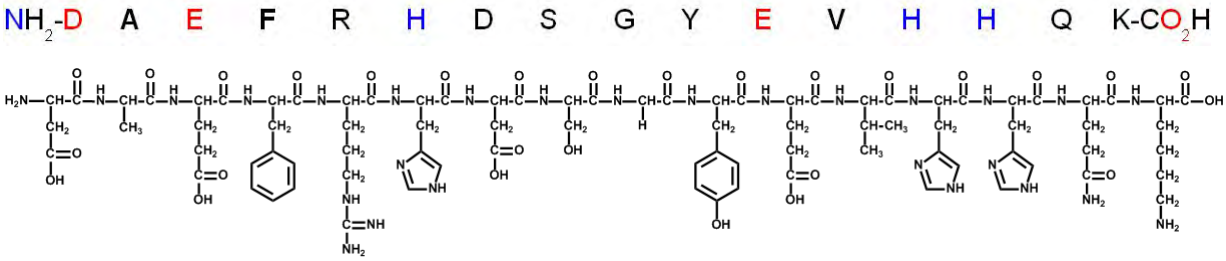

Figure 5b: Developed sequence of Aβ1-16 with the corresponding letter code amino-acid residues.

Fe(II)-Aβ

The most common oxidation states of Fe in body are Fe(III) and Fe(II). Nevertheless, the presence of the complex Aβ-Fe(III) is unlikely. The affinity of Aβ for Fe(III) is too low to compete with the formation of $Fe(OH)_3$ at physiological pH (pKs ~ 38).[34] An *in vitro* study conducts under strictly anaerobic conditions has shown that Fe(II) interact with Aβ1-16 and Aβ1-40.[34] It is worth noting that Met35 often suggested as a potential ligand was not involved in coordination. Based on NMR data, Bousejra-El-Garah et al. proposed the binding site depicted in Figure 6.

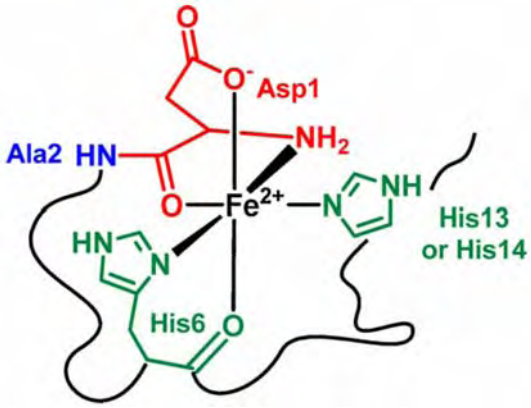

Figure 6: Proposed coordination of Fe(II) to Aβ1-16/40 from ref 27

Zn(II)-Aβ

Zn ion only exists as Zn(II). Its electronic structure (d^{10}) precludes many spectroscopic studies (EPR, CD or UV-vis). The Zn-Aβ coordination site has been studied by NMR (peptide chemical shift induced by Zn coordination) and by EXAFS.[35,36] Measurements of Zn(II) affinity on Aβ fragment by Isothermal Calorymetry (ITC) is also useful to recognize residues involved in Zn coordination.[37] In spite of a real consensus, several residues have been pointed out: Asp1 (N-terminal amine or side chain), Glu11 and His6-13-14.[38] Based on preliminary

results we obtained by NMR and XAS on Aβ and several mutants, we proposed the coordination shown below in Figure 7. Ligands proposed are His6; His13; Glu11 and Asp1 with COO^- and NH_2 depending on the pH.

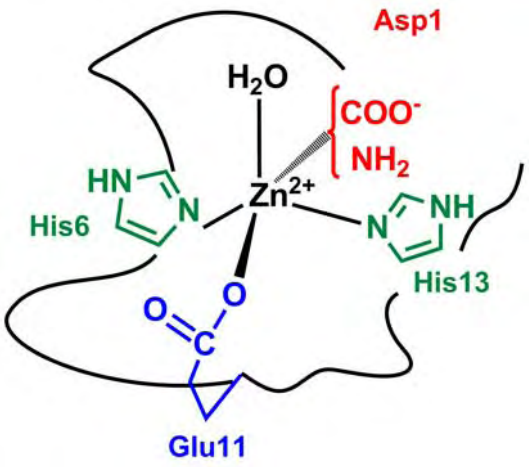

Figure 7: Proposed coordination of Zn(II) to Aβ

Cu(II)-Aβ

Cu(II) coordination to Aβ has been widely studied by many techniques.[39] Recently, a consensus has been found by advanced EPR and NMR spectroscopic methods.[40, 41] Aβ-Cu(II) coordination is pH dependent and display two kinds of coordination (species) around physiological pH (Figure 8). Interestingly, Aβ from murine show three mutations compared to human Aβ, R5G-Y10F-H13R, and do not develop AD. Interestingly, Cu coordination greatly differs between human and murin (see Figure 7). This may be one of the reasons why mice are preserved from AD.[42]

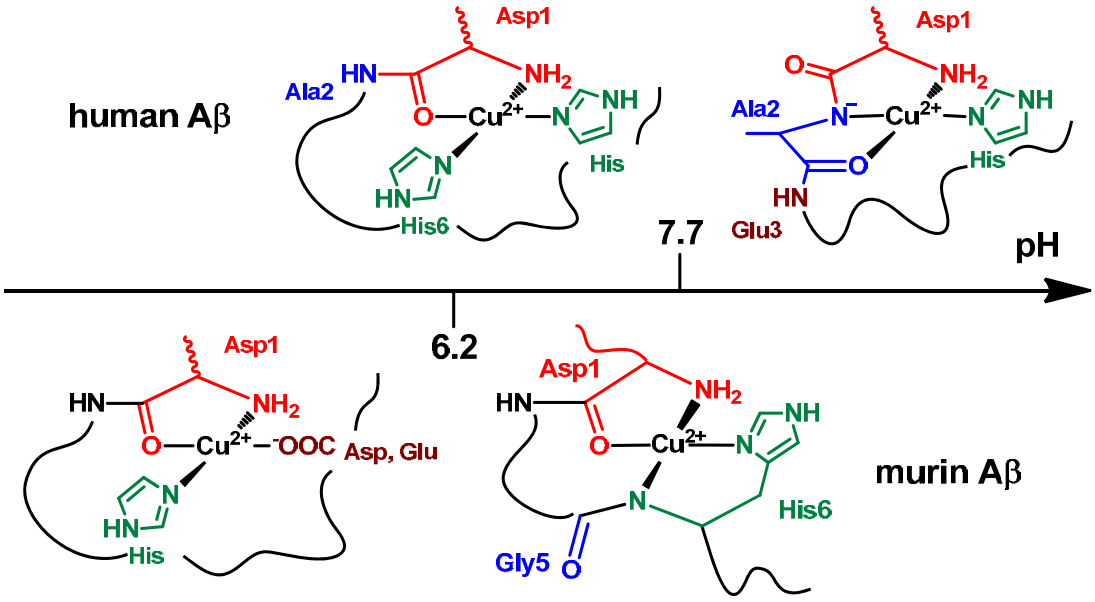

Figure 8: Cu(II) coordination to human and murin Aβ peptides and their pH dependence.

Cu(I)-Aβ

Like Zn(II), the electronic structure of Cu(I) is d^{10}. Its coordination to Aβ have been investigated by ^{1}H-NMR and by XANES.[43] Those spectroscopic data suggest that Cu(I) is coordinated to Aβ via two His in a diagonal geometry. The binding involves all 3 histidines, which are in equilibrium with the preferential His diad of His13 and His14 as depicted in Figure 8.

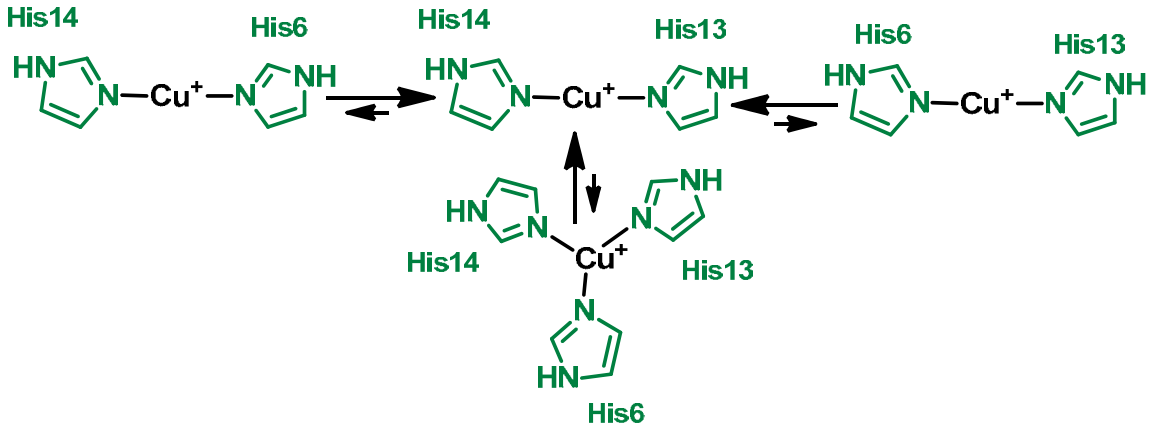

Figure 9 : Proposed Cu(I) coordination to Aβ adapted from ref [43].

References:

1. Hasegawa, M.; Morishima-Kawashima, M.; Takio, K.; Suzuki, M.; Titani, K.; Ihara, Y., Protein sequence and mass spectrometric analyses of tau in the Alzheimer's disease brain. *J. Biol. Chem.* **1992,** *267* (24), 17047-54.
2. Janicki, S.; Schupf, N., Hormonal Influences on Cognition and Risk for Alzheimer's Disease. *Curr. Neur. Neur. Rep.* **2010,** *10* (5), 359-366.
3. Fonseca, A. C. R. G.; Resende, R.; Oliveira, C. R.; Pereira, C. u. M. F., Cholesterol and statins in Alzheimer's disease: Current controversies. *Exp. Neur.* **2010,** *223* (2), 282-293.
4. Jiang, Q.; Lee, C. Y. D.; Mandrekar, S.; Wilkinson, B.; Cramer, P.; Zelcer, N.; Mann, K.; Lamb, B.; Willson, T. M.; Collins, J. L.; Richardson, J. C.; Smith, J. D.; Comery, T. A.; Riddell, D.; Holtzman, D. M.; Tontonoz, P.; Landreth, G. E., ApoE Promotes the Proteolytic Degradation of Aβ. *Neuron* **2008,** *58* (5), 681-693.
5. Bertram, L.; Lill, C. M.; Tanzi, R. E., The Genetics of Alzheimer Disease: Back to the Future. *Neuron* **2010,** *68* (2), 270-281.
6. Mirica, L. M.; Ottenwaelder, X.; Stack, T. D. P., Structure and Spectroscopy of Copper-Dioxygen Complexes. *Chem. Rev.* **2004,** *104* (2), 1013-1046.

7. James, S. A.; Volitakis, I.; Adlard, P. A.; Duce, J. A.; Masters, C. L.; Cherny, R. A.; Bush, A. I., Elevated labile Cu is associated with oxidative pathology in Alzheimer disease. *Free Radical Biol. Med.* **2012,** *52* (2), 298-302.
8. Hardy, J.; Selkoe, D. J., The Amyloid Hypothesis of Alzheimer's Disease: Progress and Problems on the Road to Therapeutics. *Science* **2002,** *297* (5580), 353-356.
9. Holtzman, D. M.; Morris, J. C.; Goate, A. M., Alzheimer's Disease: The Challenge of the Second Century. *Science Transl. Med.* **2011**, *3* (77), 77sr1.
10. Harrison, R. S.; Sharpe, P. C.; Singh, Y.; Fairlie, D. P.; Amara, S. G.; Bamberg, E.; Fleischmann, B.; Gudermann, T.; Hebert, S. C.; Jahn, R.; Lederer, W. J.; Lill, R.; Miyajima, A.; Offermanns, S.; Zechner, R., Amyloid peptides and proteins in review. Rev. Physiol. Biochem. Pharmacol. **2007**, *59*, pp 1-77.
11. Chen, G.; Chen, K. S.; Knox, J.; Inglis, J.; Bernard, A.; Martin, S. J.; Justice, A.; McConlogue, L.; Games, D.; Freedman, S. B.; Morris, R. G. M., A learning deficit related to age and β-amyloid plaques in a mouse model of Alzheimer's disease. *Nature* **2000,** *408* (6815), 975-979.
12. Klein, W. L.; Stine Jr, W. B.; Teplow, D. B., Small assemblies of unmodified amyloid β-protein are the proximate neurotoxin in Alzheimer's disease. *Neur. Aging* **2004,** *25* (5), 569-580.
13. Larson, M. E.; Lesné, S. E., Soluble Aβ oligomer production and toxicity. *J. Neurochem.* **2012** *120*, pp 125-139.
14. Williams, T. L.; Day, I. J.; Serpell, L. C., The Effect of Alzheimer's Aβ Aggregation State on the Permeation of Biomimetic Lipid Vesicles. *Langmuir* **2010,** *26* (22), 17260-17268.
15. Alies, B.; Hureau, C.; Faller, P., How Metal Ions affect Peptide aggregation: Models-peptide using as a probe. *Metallomics, In preparation*.
16. Hawe, A.; Sutter, M.; Jiskoot, W., Extrinsic Fluorescent Dyes as Tools for Protein Characterization. *Pharm. Res.* **2008,** *25* (7), 1487-1499.
17. Wetzel, R., Kinetics and Thermodynamics of Amyloid Fibril Assembly. *Acc. Chem. Res.* **2006,** *39* (9), 671-679.
18. Hellstrand, E.; Boland, B.; Walsh, D. M.; Linse, S., Amyloid β-Protein Aggregation Produces Highly Reproducible Kinetic Data and Occurs by a Two-Phase Process. *ACS Chem. Neurosc.* **2009,** *1* (1), 13-18.
19. Murakami, K.; Shimizu, T.; Irie, K., Formation of the 42-mer Amyloid β Radical and the Therapeutic Role of Superoxide Dismutase in Alzheimer's Disease. **2011,** *J. Amino Acids.*
20. Lovell, M. A.; Robertson, J. D.; Teesdale, W. J.; Campbell, J. L.; Markesbery, W. R., Copper, iron and zinc in Alzheimer's disease senile plaques. *Jour. Neur. Sci.* **1998,** *158* (1), 47-52.
21. Miller, L. M.; Wang, Q.; Telivala, T. P.; Smith, R. J.; Lanzirotti, A.; Miklossy, J., Synchrotron-based infrared and X-ray imaging shows focalized accumulation of Cu and Zn co-localized with β-amyloid deposits in Alzheimer's disease. *J. Struct. Biol.* **2006,** *155* (1), 30-37.
22. Bonda, D. J.; Lee, H.-g.; Blair, J. A.; Zhu, X.; Perry, G.; Smith, M. A., Role of metal dyshomeostasis in Alzheimer's disease. *Metallomics* **2011** *3* (3), 267-270.

23. Smith, M. A.; Harris, P. L.; Sayre, L. M.; Perry, G., Iron accumulation in Alzheimer disease is a source of redox-generated free radicals *Proc. Natl. Acad. Sci. USA* **1997,** *94,* 9866-9868.
24. Bush, A. I., Metal complexing agents as therapies for Alzheimer's disease. *Neur. Aging* **2002,** *23* (6), 1031-1038.
25. Pedersen, J. T.; Østergaard, J.; Rozlosnik, N.; Gammelgaard, B.; Heegaard, N. H. H., Cu(II) Mediates Kinetically Distinct, Non-amyloidogenic Aggregation of Amyloid-β Peptides. *J. Biol. Chem.* **2011** *286* (30), 26952-26963.
26. Noy, D.; Solomonov, I.; Sinkevich, O.; Arad, T.; Kjaer, K.; Sagi, I., Zinc-Amyloid β Interactions on a Millisecond Time-Scale Stabilize Non-fibrillar Alzheimer-Related Species. *J. Am. Chem. Soc.* **2008,** *130* (4), 1376-1383.
27. Bush, A. I., The metallobiology of Alzheimer's disease. *Trends Neurosci.* **2003,** *26* (4), 207-214.
28. Raman, B.; Ban, T.; Yamaguchi, K.-i.; Sakai, M.; Kawai, T.; Naiki, H.; Goto, Y., Metal Ion-dependent Effects of Clioquinol on the Fibril Growth of an Amyloid β Peptide. *J. Biol. Chem.* **2005,** *280* (16), 16157-16162.
29. Lee, J.-Y.; Cole, T. B.; Palmiter, R. D.; Suh, S. W.; Koh, J.-Y., Contribution by synaptic zinc to the gender-disparate plaque formation in human Swedish mutant APP transgenic mice. *Proc. Natl Acad. Sci.* **2002,** *99* (11), 7705-7710.
30. Hureau, C.; Faller, P., Aβ-mediated ROS production by Cu ions: Structural insights, mechanisms and relevance to Alzheimer's disease. *Biochimie* **2009,** *91* (10), 1212-1217.
31. Opazo, C.; Huang, X.; Cherny, R. A.; Moir, R. D.; Roher, A. E.; White, A. R.; Cappai, R.; Masters, C. L.; Tanzi, R. E.; Inestrosa, N. C.; Bush, A. I., Metalloenzyme-like Activity of Alzheimer's Disease β-Amyloid. *J. Biol. Chem.* **2002,** *277* (43), 40302-40308.
32. Li, F.; Calingasan, N. Y.; Yu, F.; Mauck, W. M.; Toidze, M.; Almeida, C. G.; Takahashi, R. H.; Carlson, G. A.; Flint Beal, M.; Lin, M. T.; Gouras, G. K., Increased plaque burden in brains of APP mutant MnSOD heterozygous knockout mice. *J. Neurochem.* **2004,** *89* (5), 1308-1312.
33. Faller, P.; Hureau, C., Bioinorganic chemistry of copper and zinc ions coordinated to amyloid-β peptide. *Dalton Trans.* **2009,** (7), 1080-1094.
34. Bousejra-ElGarah, F.; Bijani, C.; Coppel, Y.; Faller, P.; Hureau, C., Iron(II) Binding to Amyloid-β, the Alzheimer's Peptide. *Inorg. Chem.* **2011,** *50* (18), 9024-9030.
35. Gaggelli, E.; Janicka-Klos, A.; Jankowska, E.; Kozlowski, H.; Migliorini, C.; Molteni, E.; Valensin, D.; Valensin, G.; Wieczerzak, E., NMR Studies of the Zn^{2+} Interactions with Rat and Human β-Amyloid (1-28) Peptides in Water-Micelle Environment. *J. Phys. Chem. B* **2007,** *112* (1), 100-109.
36. Giannozzi, P.; Jansen, K.; Penna, G. L.; Minicozzi, V.; Morante, S.; Rossi, G.; Stellato, F., Zn induced structural aggregation patterns of β-amyloid peptides by first-principle simulations and XAS measurements. *Metallomics* **2012,** (2), 156-165.
37. Tsvetkov, P. O.; Kulikova, A. A.; Golovin, A. V.; Tkachev, Y. V.; Archakov, A. I.; Kozin, S. A.; Makarov, A. A., Minimal Zn^{2+} Binding Site of Amyloid-β. *Biophys. J.* **2010,** *99* (10), 84-86.

38. Migliorini, C.; Porciatti, E.; Luczkowski, M.; Valensin, D., Structural characterization of Cu^{2+}, Ni^{2+} and Zn^{2+} binding sites of model peptides associated with neurodegenerative diseases. *Coord. Chem. Rev.* **2012,** (256), 352-368.
39. Hureau, C.; Dorlet, P., Coordination of redox active metal ions to the amyloid precursor protein and to amyloid-β peptides involved in Alzheimer disease. Part 2: Dependence of Cu(II) binding sites with Aβ sequences. *Coord. Chem. Rev.* **2012,** (256), 2175-2187.
40. Dorlet, P.; Gambarelli, S.; Faller, P.; Hureau, C., Pulse EPR Spectroscopy Reveals the Coordination Sphere of Copper(II) Ions in the 1-16 Amyloid-β Peptide: A Key Role of the First Two N-Terminus Residues. *Angew. Chem. Int. Ed.* **2009,** *48* (49), 9273-9276.
41. Hureau, C.; Coppel, Y.; Dorlet, P.; Solari, P. L.; Sayen, S.; Guillon, E.; Sabater, L.; Faller, P., Deprotonation of the Asp1-Ala2 Peptide Bond Induces Modification of the Dynamic Copper(II) Environment in the Amyloid-β Peptide near Physiological pH. *Angew. Chem. Int. Ed.* **2009,** *48* (50), 9522-9525.
42. Eury, H.; Bijani, C.; Faller, P.; Hureau, C., Copper(II) Coordination to Amyloid β: Murine versus Human Peptide. *Angew. Chem. Int. Ed.* **2011**, *123* (4), 931-935.
43. Hureau, C.; Balland, V.; Coppel, Y.; Solari, P.; Fonda, E.; Faller, P., Importance of dynamical processes in the coordination chemistry and redox conversion of copper amyloid-β complexes. *J. Biol. Inorg. Chem.* **2009,** *14* (7), 995-1000.

Role of Metallic Ions in Amyloid Formation: General Principles from Model Peptides

Bruno Alies, Christelle Hureau, Peter Faller

Metallomics
Submitted

The following article reviewed general insight about role of metal ions on amyloid formation obtained by model peptides.

Role of Metallic Ions in Amyloid Formation: General Principles from Model Peptides

Bruno Alies,[a] Christelle Hureau[a] and Peter Faller[a]

CNRS ; LCC (Laboratoire de Chimie de Coordination) ; 205, route de Narbonne, F-31077 Toulouse, France. Université de Toulouse; UPS, INPT ; LCC ; F-31077 Toulouse, France

Abstract

The mechanistic understanding of peptides self-assembly mediated by metallic ions into amyloid or other structures has gained a lot of interest, mainly due to their importance in several neurodegenerative diseases. The use of short, easy-to-handle peptides has contributed to a better understanding of structure and mechanisms that are also relevant for the native and longer peptides involved in the neurodegenerative diseases. Here, we review the results obtained with such “model systems” with the aim to identify and discuss fundamental parameters determining the self-aggregation with a special focus on the role of metallic ions in this process.

Key words: amyloid, metallic ions, copper, zinc, self-assembly, aggregation, peptides

I) General principles of amyloid formation

I.1) Importance of the metal-peptide interaction in aggregation:

Peptide/protein aggregation occurs in many diseases, especially neurodegenerative diseases. For instance, amyloid-β peptides (Aβ), prion and α-synuclein proteins are involved in Alzheimer's disease (AD), Prion diseases and Parkinson's disease, respectively. Metallic ions are found in high concentration in the deposits of amyloidogenic peptides/proteins linked to these diseases and a large body of evidence suggests that metallic ions (mostly Cu, Zn and Fe) are involved in these diseases *via* various processes, including modification of the aggregation pathway.[1-4] This has led to numerous *in vitro* studies in order to delineate the effects of metallic ions on the aggregation of these peptides (for recent reviews see e.g. [4-7]).

More recently, aggregation of peptides into amyloid fibrils has also stimulated investigations in the field of material science, as a scaffold of fibrils with embedded metallic ions.[8, 9]

I.2) Interest in short "model" peptides:

It is clear that for material science the use of short, and thus cheaper and easy-to-handle peptides is an advantage. Short model peptides are also widely studied with the aim to learn about basic and general mechanisms on peptides aggregation. Also here, shorter peptides can be an advantage for a better reproducibility and accumulation of structural and mechanistic data (see for instance, [8-10]). This holds also for the interaction of a metallic ions with amyloidogenic peptides, which is the focus of the present review. Thus the review aims to reveal fundamental and general principles gained on short peptides regarding the impact of transition metallic ions (mostly Cu(II) and Zn(II)) on peptides aggregation into amyloids.

I.3) Amyloid versus non-amyloid aggregates:

Proteins or peptides can aggregate into different structures, going from completely unordered amorphous aggregates up to crystalline forms, which are highly ordered. Amyloids are ordered structures or at least have an ordered part, but are not crystalline. They form normally fibers/fibrils of about 10 nm diameter and can have a length up to several hundreds of μm. Therefore they are also often called amyloid fibrils. Amyloids consist of β-sheets that pile up to some extent.[11] This requires two principal interactions: i) one that makes the classical β-sheet, *i.e*. hydrogen bonds between the backbone amide groups. As this interaction is between the backbones only (average distance 4.8 Å), it can be adopted by all peptides/proteins; ii) to pile up the β-sheets, interactions between side chains are needed that

depend on the protein/peptide sequence. Interactions can be salt-bridges, H-bonds, and/or hydrophobic interactions. The average distance between the β-sheets is around 11 Å (Figure 1). The observation of these two distances by x-ray diffraction is one of the identification parameters of amyloids, together with the high content of β-sheet structure that can be determined by FTIR, RAMAN or CD, via the interaction with specific dyes (mostly Thioflavin T (ThT) and congo red) and by microscopy (TEM or AFM) for fibrillar forms. Another, important feature of amyloids is the seeding capacity: addition of a low amount of preformed amyloids triggers the aggregation of monomers rapidly, as they serve as templates for the aggregation (see also below).

In contrast to that, amorphous aggregates are supposed to be unordered and do not show the characteristic features mentioned above. "Unordered" means here a non-regular organisation of the peptide or protein. However, a protein can be structured (e.g. as α-helix or β-sheet) and aggregated by keeping at least part of its structure. On the other hand, amyloids can also have a part of the peptide/protein in a non-amyloid structure, which is *e.g.* the case of amyloid-β, where only 2/3 of the peptide (C-terminal part) is structured as amyloid, and the N-terminus part is unstructured.[11] Thus it is not always easy to recognize amyloid structures by electron microscopy only.

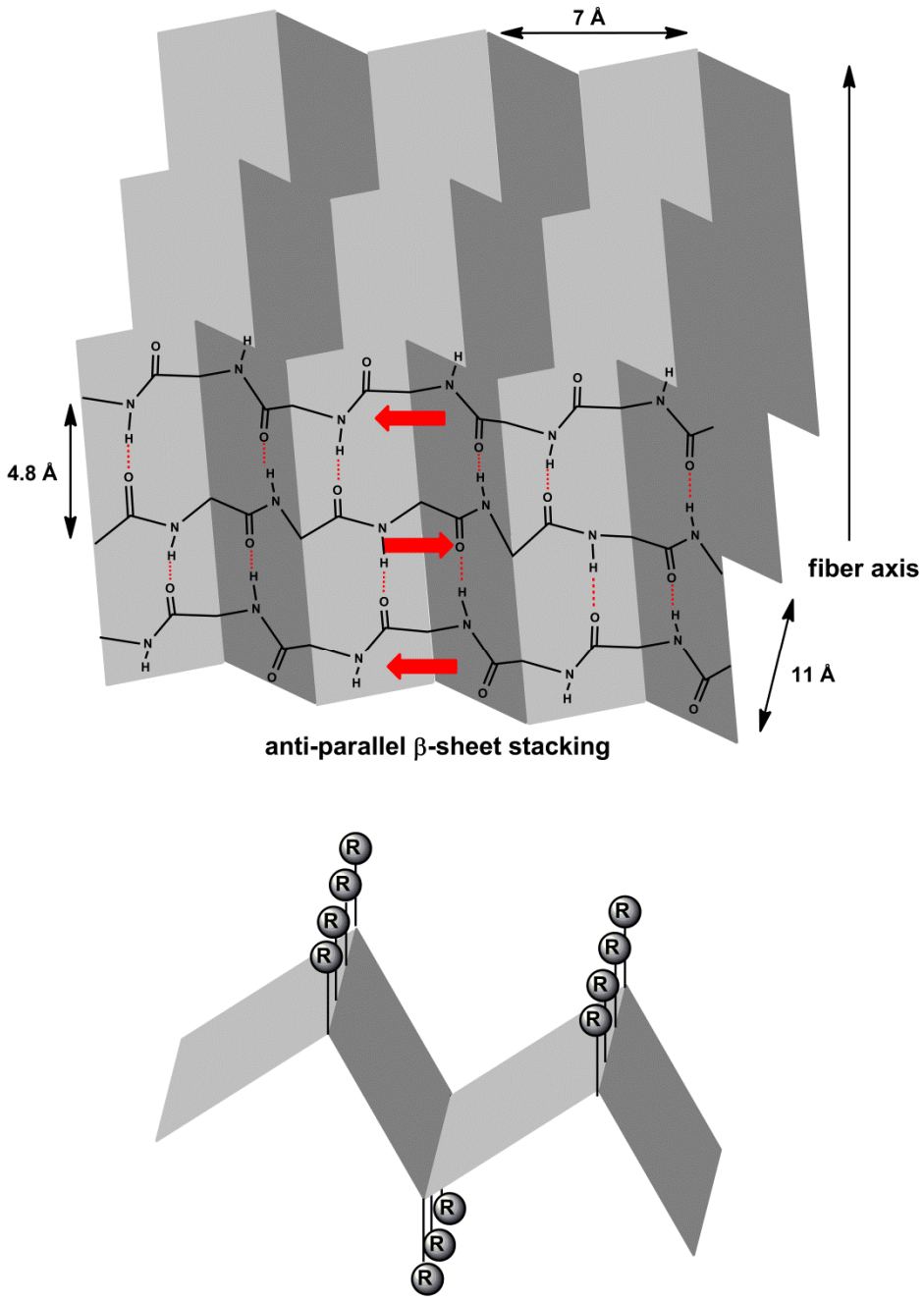

Figure 1. ***Top:*** Scheme of amyloid structure: amyloid structure can be parallel or, as shown here, anti-parallel β-sheet structure. Only the back-bone is shown in the first sheet. The red arrow indicates the direction of the backbone. The hydrogen bonds between the backbones are parallel to the fiber axis. The side chains are omitted for clarity but would point perpendicular to the paper sheet (to the front and to the back). ***Bottom:*** β-sheet turned by 90°. The side chains of the amino-acid residues are now shown and are above or below the plane made by the β-sheet structure. The same R is used here for clarity.

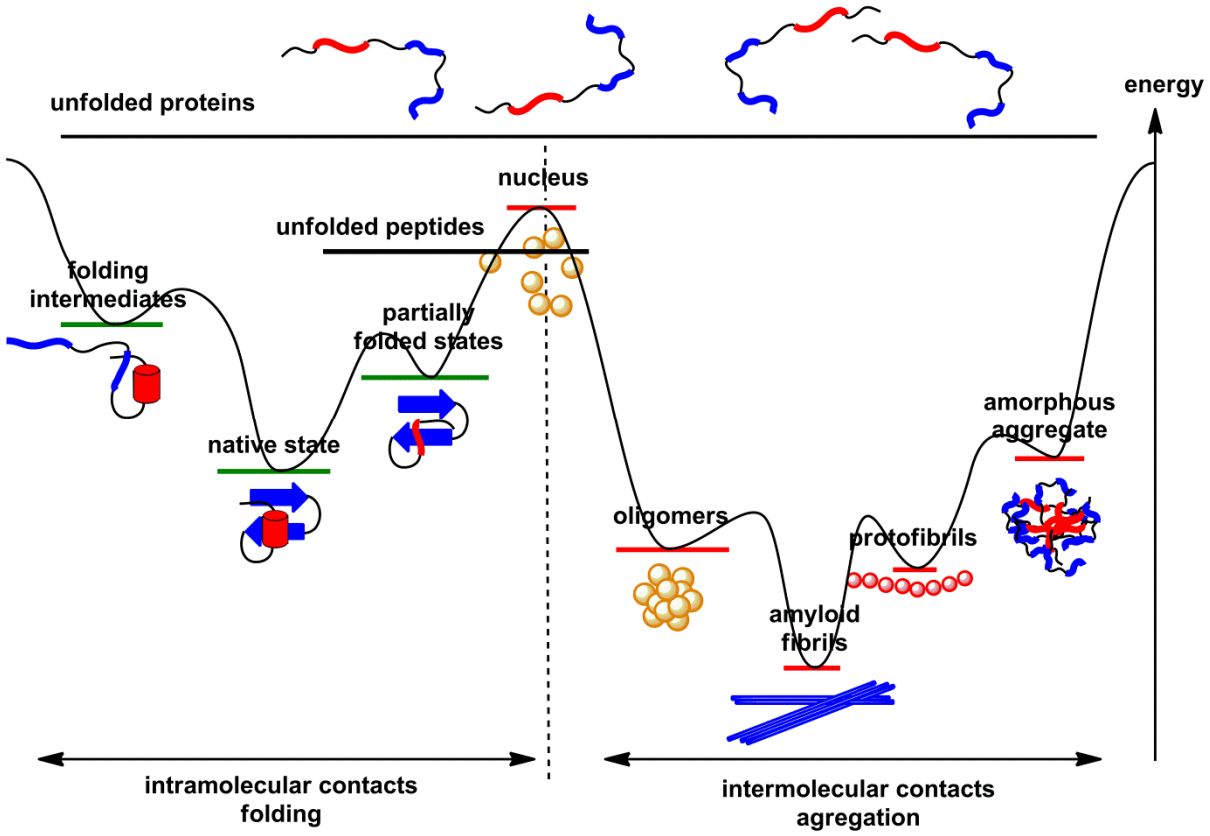

Figure 2. Diagram showing a scheme of the folding landscape with the respective energies of the various possible states of peptide/protein folding. Adapted from ref. [12].

I.4) Formation of amyloids:

To form amyloids, the monomeric peptides have to change their structure into β-sheet. In the case of a peptide in a random coil structure, *i.e.* of an unfolded peptide (Figure 2), it can transform directly into an amyloid[1]. In contrast, in a peptide/protein with a defined 3D structure (left part in Figure 2), it has first to unfold (at least partially) before it forms the β-sheets of the amyloid structure.

In general, it is admitted that the aggregation process consists of a nucleation and an elongation phases (Figure 3). In this mechanism, the nuclei are the highest energetic state (Figure 2, right) and hence the lowest populated one. Once this state is reached, the further aggregation is energetically favoured (elongation phase). As the assembly from the monomer to the nuclei is energetically unfavoured, it is very slow and rate-determining. This is the basic mechanism. Extensions of this mechanism have been suggested, including (i) fragmentation,

[1] Of course there could be other intermediates between the random coil structure and the β-sheets in the amyloid. E.g. Teplow and coll. showed that Aβ forms a partially alpha-helical intermediate from random coil to β-sheets.

i.e. break-down of amyloids, which increases the number of templates for elongation, and hence accelerates aggregation. This has been reported to improve the description for several systems ;[13] (ii) an additional conformational change, *i.e.* to formation of a nucleus involves a conformational change from its immediate precursor state. In this case the conformational change is the rate determining step, as elongation afterwards is fast.[14]

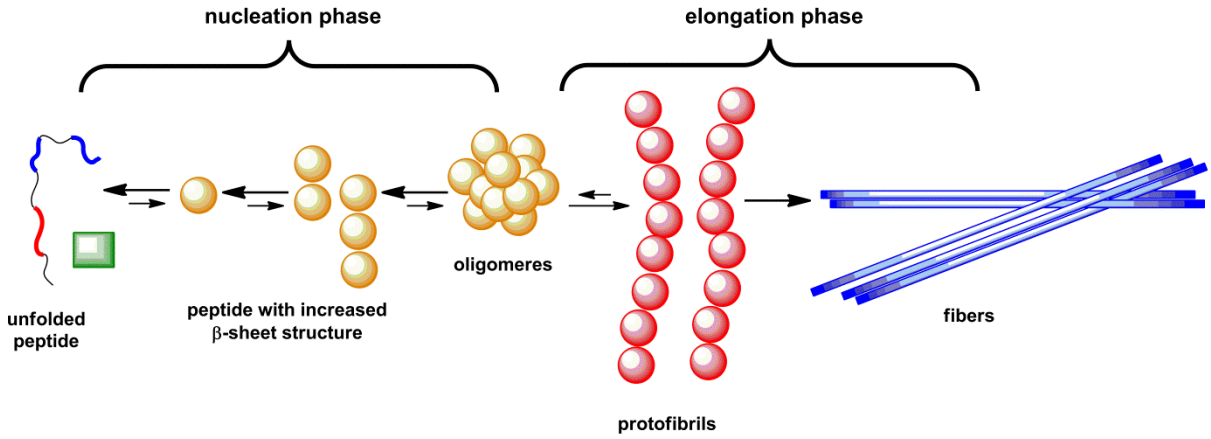

Figure 3. Basic view of the aggregation process of an unstructured peptide.

Amyloid formation is concentration dependent. Below a certain concentration (called critical concentration) no nuclei are formed and no amyloid formation occurs.[15] Above the critical concentration, aggregation occurs spontaneously but is often very slow due to formation of the nuclei (Figure 3). It can be accelerated by seeding with a preformed amyloid (Figure 4).

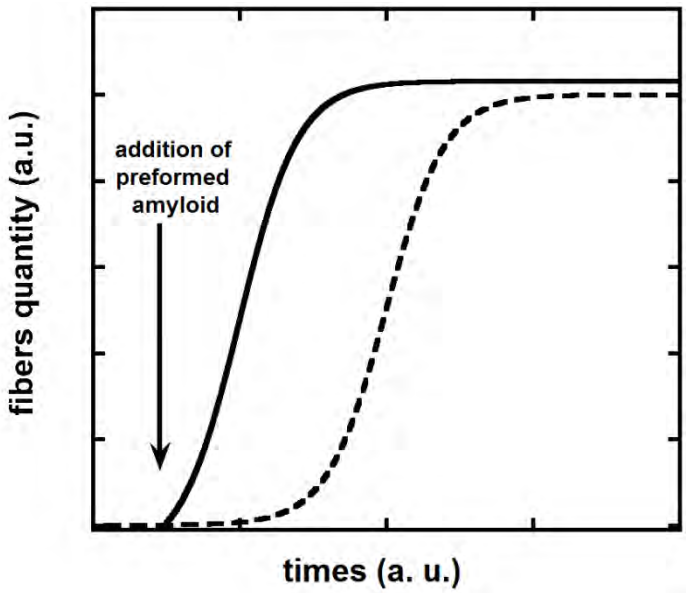

Figure 4. Theoretical curve of the aggregation process (dotted lines), which shows the typical sigmoid shape, due to nucleation, elongation and termination phases. Impact of adding a seed

(seeding experiment), *i.e.* adding a preformed amyloid that serves as a template for the addition of monomers and hence results in a immediate elongation (solid line).

II) Role of transition metallic ions in peptide aggregation

II.1) Introduction

Transition metal ions bind to peptides mostly through side chains of the amino-acid residues but backbone binding, via either carbonyl or deprotonated amide functions can also occur mainly in the case of Cu(II) ions. The main binding sites for Cu(II) and Zn(II) (but also Fe(II) and Cu(I)) are side chains of His and Cys and the N-terminal amine. The COO^- groups of Asp and Glu residues are also often encountered as well as the side-chain of Met. Metal binding to the side chains can directly interfere with the stacking between side chains (Figure 1, bottom). Interference with the β-sheet formation is also possible, either indirectly via side-chain binding or directly via binding to the backbone. The binding to the backbone often involves the N-terminus and adjacent metallacycle with backbone functional groups. Amides next to His are also involved, as His are a good anchor for metals.[16] Conceptually, the metal ions can induce aggregation by bridging two peptides, by inducing a more aggregation prone conformation or by reducing the overall charge. In contrast, they can impede aggregation into amyloids by inducing or stabilizing a less aggregation prone conformation or by increasing the overall net charge.

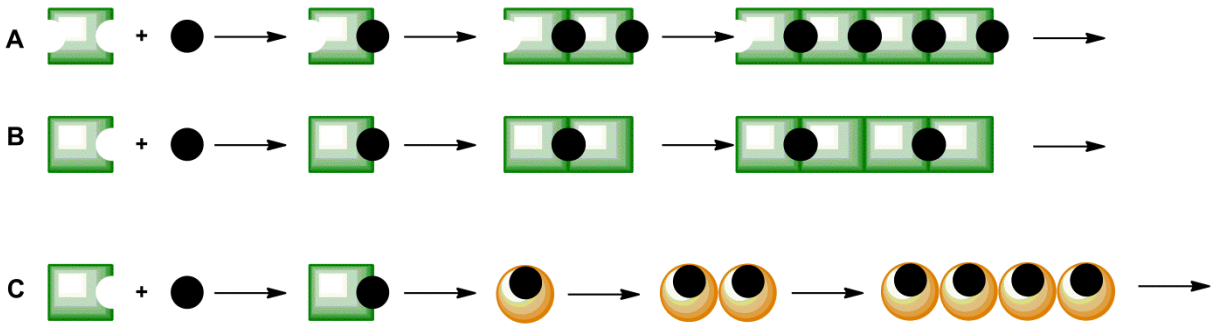

Figure 5. A, B: The metal ion bridges two peptides. In A, two metal ion binding sites are shared between two peptides leading to a 1:1 peptide:metal ion stoichiometry; in B the metal ion binding site is shared between two peptides leading to a 1:0.5 peptide:metal ion stoichiometry. C: Metal ion binding leads a peptide conformation more prone to aggregation.

In order to describe the effect of metal ions on the aggregation of amyloidogenic peptides, the following parameters are important:

(i) Where do the metal ions bind, *i.e.* what are their ligands? This depends of the type of amino acids and of their respective position in the sequence, and in case of structured peptides/proteins from their spatial organisation.

(ii) What metal ion is considered? Different metal ions have different coordination chemistry (preferences in geometry and type and number of ligands).

(iii) The affinity of the metal ion for the peptide. This determines occupancy and is linked to exchange rates.

(iv) Structural and overall charges changes induced by metal ion binding.

(v) Peptide to metal ratio.

These parameters are discussed in more detail in the following sections.

II.2) Primary Sequence as overall parameter

It is generally supposed that almost all peptides and proteins can adopt the amyloid structure. Above a certain concentration (often physiologically relevant) the amyloid structure becomes the most stable structure because it allows the maximal number of H-bonds between the backbone amides (Figure 1).[17] For unstructured (random coil) peptides, the formation is only dependent on the length of the peptide and on the type and position of the side chains. For peptides with 3D structure, the unfolding has to be considered as well. The importance in the side chains lies in their interactions with adjacent β-sheet that can be stabilized by electrostatic and hydrophobic interactions. The position of the amino acids in the sequence is thus important to match/interact with the amino acids from the other sheet. In a simple way, polyArg would not adopt a very stable amyloid structure (at neutral pH) since the charged side chains would induce strong electrostatic repulsion. In contrast poly-Gln can form amyloids (*e.g.* in Huntington disease)[18] because two neighbouring Gln side chains can form H-bonds. During the last years a lot of progress has been made on the identification of amyloidogenic peptides or stretches in protein by algorithms as well as in their design.[19]

In terms of metal-binding, the strongest interactions with transition metal ions (particularly Cu, Zn, Fe, Co, Ni,) are with side chains of His, Cys and the N-terminal amine functions, as stated above. There is not much freedom for “design” concerning N-terminal amine, either it is there (at the same position) or not (often acetylation is used). Mostly used

are His (see Table 1), because His are an intermediate base (in the HSAB theory) and thus it can bind strongly most of the transition metal ions. His are also the most important ligands in physiologically relevant peptides, like amyloid-β, prion protein, α-synuclein etc. Cys has often a stronger interaction with softer metal ions but it can be easily oxidized into disulfide bonds, and then the metal ion is released. In other words, experiments would have been done under anaerobic conditions. The other important ligands, but often of lower affinities are the carboxylates (Asp, Glu, C-terminus) and Met (for softer metal ions). Side chains of amino acids like Tyr, Ser, Lys, that are often found to bind metal ions in proteins due to a 3-D preorganization, but they are very rare in cases of unfolded peptide as their pKa are relatively high. They might only bind in absence of the stronger ligands.

II.3) Secondary Structure (In)Stability.

In the case of random coil peptides or proteins (often the case for short peptides, but also for some proteins) the main parameter to consider is where the ligands are positioned in the sequence, the induced structure around the metal site and the formation of amyloids (see above). In the case of peptides/proteins with a defined 3D-structure, formation of the amyloids includes a partial unfolding step. The metal ion binding can stabilize or destabilize the initial non-amyloid structure, and hence decrease or increase amyloid formation. For instance, Zn stabilizes the non-amyloid form of islet amyloid polypeptide linked to type II diabetes but promotes aggregation of amyloid-β.[20]

In general, the peptide/protein secondary structure could be a mixture of random coil, α-helix or β-sheet. The group of Koksch has established an interesting system to study this question. They used short model peptides that can adopt a coiled coil structure with a high α-helical content. Thus the conversion from α-helices to β-sheets (or not) can be monitored as well as the interaction with Cu(II) or Zn(II). For the peptide CCM (Table 1) an immediate formation of β-sheet was observed, in line with fast amyloid formation.{Pagel, 2005 #442} The β-sheet formation was slowed down by the addition of 40% TFE (Tri-Fluoro-Ethanol), a known inducer/stabilizator of α-helical structures that induced a conversion from a more α-helical structure to β-sheet. Addition of Zn(II) or Cu(II) in the presence of 40% TFE accelerated the conversion to β-sheet. This suggests that binding of Zn and Cu destabilized the α-helical structure and promoted the conversion to β-sheet and amyloid formation.[21]

II.4.) Metal Specificity

The metallic ions have specific coordination chemistry, *i.e.* preference for number and nature of ligands and geometry. In a very sensitive system like amyloid formation, each metal ion is thus expected to have a different impact (on kinetic, amount, structures of aggregates). Thus aggregation behaviour depends on nature, and hence, on the coordination specificity of the metal ion. The most studied ions, namely Cu(II) and Zn(II), are different. They differ by their electronic structure, Cu(II) is d^9 while Zn(II) is d^{10}. This one-electron difference is responsible for a main change in the coordination behaviour. Cu(II) prefers to be square planar (with one or two remote apical ligands) while Zn(II) is more usually tetrahedral or distorted pentacoordinated. Another main difference is that Cu(II) is a stronger Lewis acid than Zn(II). Cu(II) is strong enough to bind to backbone, as it can induce amide deprotonation from peptide bonds when stable metallacycle are formed with adjacent His side chain or N-terminal amine function.[16] Indeed, in all the studies published (Table 1) differences in the impact of these two metal ions have been reported. In general, Zn(II) is more potent in amyloid induction than Cu(II). The two exceptions are (i) : Zn(II) can inhibit the aggregation of the peptide iAPP, which is linked to type II diabetes;[22] (ii): on a coiled coil peptide called i+7 (Table 1). The aggregation kinetics of apo- i+7 and holo-i+7 with Cu(II) was similar, but Zn inhibited its conversion into β-sheet. The structural reasons are not known, but it was proposed that α-helical structure was stabilized by Zn binding to the two His (which are close in the α-helical structure). Cu would bind only one His, and hence does not stabilize the α-helical structure, but might in contrast stabilize the β-sheet.[21]

In the peptide Aβ11-28, the metal specificity has been studied in more detail, as the Cu(II) and Zn(II) binding sites have been determined. Cu(II) binds via the well-known NH_2-Xxx-Xxx-His motive (ATCUN), which included two deprotonated amide ligands between the N-terminal amine and the His side chain leading to a very stable arrangement of three metallacycles. Thus the peptide wraps around Cu(II) and that disturbs the alignment required to form β-sheet and amyloid (see Figure 6).[23] Zn(II) is not able to bind in the ATCUN motive, due to its lower Lewis acidity and lack of preference for the square planar geometry. Structural studies suggest that Zn(II) binds in between two peptides by the two carboxylates of Glu11 and the side chain of His14, and hence stabilizes interaction between peptides without disturbing too much the β-sheet alignment (see Figure 6).[24]

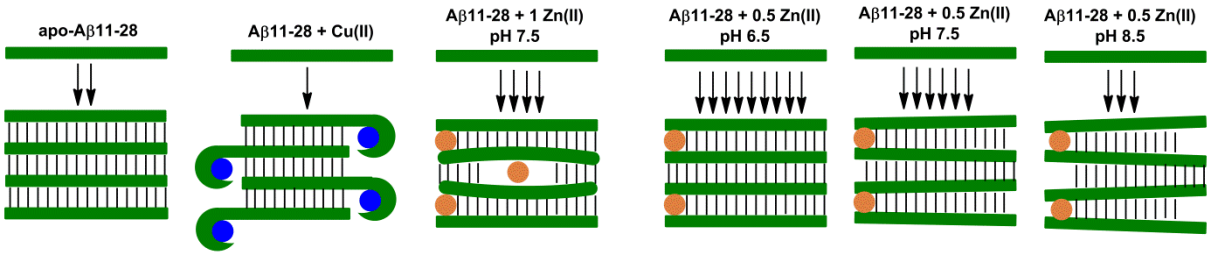

Figure 6: Modulation of Cu(II) (blue circles) and Zn(II) (orange circles) on the aggregation of the Aβ11-28 peptide. Cu(II) decreases fibril formation due to the lowering of H-bonds induced by formation of the Cu-ATCUN motif at the N-term part of the peptide. 0.5 equiv. of Zn(II) increases fibril formation via bridging two peptides. At low pH, coordination of the Zn(II) is more prone to formation of β-sheet than at pH 8.5. 1 equiv. of Zn(II) also increases fibril formation, but to a lesser extent due to unspecific binding and induced lowering of H-bonds.

The results obtained with the peptides Aβ13-20K16A and AcAβ13-20H14A can be explained in a similar manner.[25, 26] In the case of Aβ13-20K16A, Cu(II) inhibited aggregation, in contrast to AcAβ13-20H14A, where Cu(II) enhanced aggregation. For both peptides, it was proposed that Cu(II) bridges two peptides but with a different coordination site. Aβ13-20K16A binds Cu(II) by the two N-terminal His13/14 (N-terminal NH_2, the deprotonated amide between the two His and the Nδ of the imidazole ring of His14). This might diminish the H-bonds number (like in the case of Cu(II)-Aβ11-28). However, for Cu(II)-Aβ13-20K16A one equatorial position remains free (in contrast to Cu-Aβ11-28), and could be occupied by the His side-chain of another peptide to form a Cu-bridged dimer. Why such a Cu(II)-bridged dimer of Aβ13-20K16A does not promote amyloid formation is not clear, but could be due to structural reasons or to the relative low affinity of the monodentate ligand.[27] For Ac-Aβ13-20H14A, the only strong Cu(II) ligand available is the side chain His13. It was hypothesized that formation of Cu(II)-bridged dimers is increased and hence aggregation is favoured.[25]

II.5) Charge changes due to metal-binding

The overall charge is an important parameter for aggregation, as generally aggregation is faster when the overall charge approaches 0. Metal ion binding can induce changes in the overall charge. One has to consider two points: i) the metal ion carries a charge, like +2 for Cu(II) and upon binding to a peptide this charge has to be added, ii) metal ions can also induce the release of H^+ which has to be taken into account. For instance Cu(II) binding to the Aβ11-28 in the ATCUN motive releases about 3 protons at pH 7, and hence the overall change of the charge is -1. Thus the change in the overall charge due to the metal and the removed protons has to be taken into account for the differences between different metal ion like Zn and Cu.[7, 24, 28, 29] However, so far no study reported the isolated impact of the change in charge on peptide aggregation, as one would have to ascertain that two metal ions with different charge bind exactly with the same coordination.

For short peptides in the absence of metal ions, it has been proposed that amyloid formation is more efficient if the net charge is close to 0 but not exactly 0.[30] In line with that, on the system Zn-Aβ11-28, it was proposed that at net charge 0, aggregation is very fast and favours the formation of amorphous aggregates over fibrils. However, with time, a transition towards amyloids occurs. This indicates that too fast and massive aggregation will favour amorphous type aggregates, even when the amyloid structure is the thermodynamic more stable form.{Alies, 2012 #435}

II.6) pH dependence: changes in charge and metal coordination

pH dependence of peptides/proteins is a general feature, in the presence or absence of metal ions. For the peptide only (apo-peptide), this is due to the change in charge of the peptides/proteins induced by (de)protonation of side-chains and N/C-term parts. This changes the overall charge. As mentioned above, the more the overall charge approaches 0, or in other words the closer the pH is to the pI, the faster the aggregation is. In addition, in case of a structured peptide/protein such protonation changes can induce structural modification, and hence influence the aggregation (e.g. lowering the pH destabilizes often folded proteins which become then more prone to aggregation into amyloids).

In the case of holo-peptide, on top of the change of the protonation state described above, one has also to consider that the metal ion coordination to peptides (but also proteins, although to a lesser extend) are pH dependent. For instance, it has been proposed that a change of Zn coordination due to pH (coordination of N-terminal amine at higher pH) is

partially responsible for the slowdown of the amyloid formation at higher pH in case of the Aβ11-28 peptide (Figure 6).[28]

II.7) Affinity and Metal exchange

The apparent affinity (Ka at a given pH in a given buffer, *i.e.* the conditional Ka in presence of a competitor) of peptides/proteins has two-fold impact: i) it determines the occupation of the binding site, *i.e.* how much of the metal ion is bound to the peptide and ii) is related to the metal exchange, since Kd = k_{off}/k_{on}, where k_{off} is the dissociation rate of the metal-peptide complex and k_{on} the association rate, often considered as limited by diffusion process, for Cu and Zn peptide complex.[31]

Occupation: Dissociation constants of Cu(II) and Zn(II) for peptide cover several order of magnitude, with Kd_{cond} from fM (Cu(II)-ATCUN motive [27]) to µM (typical value for Zn-Aβ,[32]). Peptides without His, Cys and N-terminal amine might have a much weaker affinity.[33] Generally, the affinity follows the Irving Williams series, and hence Cu(II) has a higher affinity than Zn(II) for peptides. At typical µM concentration of peptide with apparent Kd in the µM range leads to a substantial fraction of unbound metal ion. This is the case for most of the peptides studied when bound to Zn(II), but to a much lesser extent when bound to Cu(II) (Table 1).

Affinity between monomeric and aggregated form: Does metal affinity to peptide differ between monomeric and aggregated forms ? In a recent study,[34] it has been shown for a specific peptide that affinity for Zn(II) was much higher with a peptide pool under β-sheet conformation. Indeed, in this peptide β-sheet formation allows to create a new Zn(II) binding site (due to vicinity of two His). Thus, metal ion affinity may be modified by the aggregation process. Also, Kozin et al. measure Zn(II) affinity to several Aβ portion by ITC and find that a shorter portion of a peptide could have better affinity than the peptide itself. It was rationalized by the fact salt bridge may involved important coordinating amino-residue side chain (such as glutamate or aspartate) which are not available to coordinate Zn in the full-length peptide but available in the shorter version of the peptide.[35] Nevertheless, for the full-length Aβ peptide, it seems not to be the case, since the affinity of Cu or Zn to peptide Aβ remains on the same order of magnitude in monomeric and aggregated forms.[36, 37]

Exchange: In general, binding of Cu(II) and Zn(II) to unstructured peptides is very fast and often diffusion controlled (~10^{-9} M^{-1} s^{-1}).[31] As a consequence, the k_{off} is also relatively fast, *e.g.* in the second to sub-second region for an apparent Kd in the nM to the µM region. In other words, for all the Zn-peptides studied and most of the Cu(II)-peptides (an exception

is the ATCUN motive) the metal bonds are labile and the exchange is quite fast, at least faster than the aggregation time scale and could hence affect the aggregation.

In line with this, in a very recent work,[24] we have shown that substoichiometric amounts of Zn(II) dramatically increase the rate of Aβ11-28 aggregation. It was proposed that Zn(II) is able to rapidly initiate the aggregation by forming a dimeric species inducing aggregation of the entire peptide pool due to fast exchange of Zn(II) between the aggregates formed and the remaining monomeric peptide. In other words, a transient binding of Zn was enough to induce aggregation of Aβ11-28. The fact that transient, substoichiometric Zn binding is enough to trigger aggregation of Aβ11-28 is of importance for the Zn-Aβ interaction in AD, because in glutamatergic neurones Zn(II) is transiently released into the synaptic cleft where Aβ can be localized. This could be enough to induce aggregation or secondary structure modification of the extracellular Aβ. Also, Zn(II) found in senile plaques of AD patients may act as a labile pool of Zn(II).

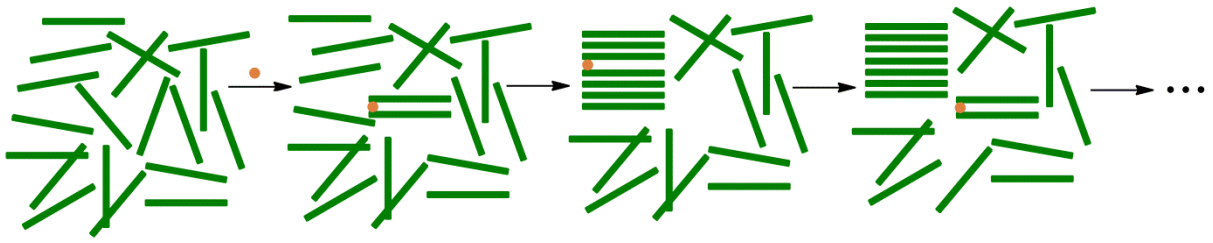

Figure 7. Substoichiometric Zn(II) triggering the Aβ11-28 aggregation. Zn(II) (red circle) binds to monomeric peptide and forms a transient Zn-bridged peptide dimer. This nucleates the aggregation. Zn(II) can leave this aggregated form and bind to other monomeric peptide to induce another nucleus for aggregation. The fast exchange of Zn(II) enables the formation of several nuclei, in contrast to the case when Zn(II) would be kinetically trapped in the aggregate. In the present case, Zn(II) can be considered as a catalyst of aggregation.

II.8) Stoichiometry

The stoichiometry or the metal/peptide ratio has also a significant impact. It was shown to affect fibrils formation of amyloid-involved disease's peptides.[22, 38] The stoichiometry has been also investigated on model peptides.[24, 26] Results show that Zn/peptide ratio modulate peptide aggregation in several ways, including kinetics, type of aggregates and shape of fibrils. In general, at metal/peptide ratios above 1 more amorphous type aggregates

are formed, in line with a more unspecific binding of the second metal ions favouring bridging of two peptides. This is the reason why an accurate determination of the peptide concentration is absolutely crucial, and parameters like counter ion or water content have to be taken into account when concentrations are determined by weight.[39]

Below the 1:1 ratio, the complexes formed can depend on the ratio, with formation of 1:1 or 1:2 metal:peptide complexes. Hence in the latter case, the aggregation will also depends on the metal:peptide ratio. This was observed for Zn-Aβ11-28 peptide. The amyloid formation was increased in kinetics and intensity (as determined by thioflavin T assay) for Zn / Abeta11-28 ratio from 0 to 0.5, but decreased from ratio 0.5 to 1. This was explained by the formation of a Zn_1-$(Aβ11\text{-}28)_2$ complex that aggregated rapidly into amyloids, and further Zn binding yielded a Zn_1-$(Aβ11\text{-}28)_1$ that formed more amorphous aggregates (Figure 6).[24]

Difference in stoichiometry contributes to a wide range of effects seen on metal-induced aggregation studies, but unfortunately, metal/peptide ratio is often not systematically varied and rigorously determined.

Conclusions

The use of small model peptides contributed much to the fundamental understanding of peptide self-assembly to form amyloid or other aggregates in the past years.

Several key parameters were determined:

1) Normally the binding site of flexible peptides are metal specific, *i.e.* Zn(II) binds differently than Cu(II). As a consequence, the structure is different, which has an impact on the self-assembly and amyloid formation.

2) Metal ion binding to peptides has an impact on the overall charge of the complex and this effect is pH-dependent.

3) Different metal to peptide stoichiometry can lead to different complexes. This can have a dramatic impact on the aggregation behaviour. An excess of metal ions may preferentially lead to unspecific amorphous aggregates.

4) Most metal bound to peptides are labile with a rapid metal exchange between peptides. This can have an important impact on aggregation, as the metal ions can be considered as a triggering/catalytic agent.

What can be learned from these model systems for more physiologically relevant peptides or proteins? The above mentioned studies revealed general principles and determined important parameters in the role of metal ions in amyloid formation. These insights will help significantly to the better understanding of the more complex native systems. This does not

mean that the more complex native systems behave exactly like the more simple shorter peptides discussed here. The native systems have to be studied separately as the impact of metal ion binding might be different for each peptide/proteins, but the principles and parameters discussed here will be very helpful tools for the more complicated systems.

Acknowledgements

We would like to thank all our present and former collaborators/students/colleagues for fruitful discussions.

Peptide Sequences / Name Used		Apo	Zn(II)	Cu(II)	Technique Used	Refs.
Aβ sequence based-design						
FEVHHQKLVFFA	Aβ10-21	+	++ xx	NS	SANS, EM	40
FEVQHQKLVFFA	Aβ10-21H13Q	+++ xxx	++ xxx			
HHQALVFFA-NH_2	Aβ13-21K16A	+++ x	++ xxx	-	CD, XAS, EM, AFM, EPR, IR, Tox	25, 26
Ac-HAQKLVFFA-NH_2	AcAβ13-21H14A	++ x	+++ xxx	+		
Ac-HHQKLVFFA-NH_2	AcAβ13-21	NS	NS	-		
EVHHQKLVFFAEDVGSNK	Aβ11-28	+ x	+++ xxx	-	ThT, Turbi, TEM, XANES, EPR	23, 24, 28, 29
EVHHQKLVFFAED	Aβ11-23	+ x	++ x	-		
HQKLVFFAED	Aβ14-23	+ x	++ xxx	++ xxx		
Coiled coil based-design						
Abz-LEVELKVLS KS LVKLEVELKVLSKSL	CC	-	-	-	CD	41
Abz-LEVELKVLHKHLHHLEVELKVLSKSL	CCM	-	+	+		
Abz-LKVELEKLKSELVVLHS HLEKLKSEL	i+2	++ x	+++ xxx	-	CD, ThT Fluo, TEM, EPR	34, 42
Abz-LKVELEKLKSELVVLHSELHKLKSEL	i+4	+++ xxx	-	-		
Abz-LKVELEVLKSELEKLHHELVKLKSEL	i+1	+++ xx	-	-	CD, IR	21
Abz-LKVELEVLHSELEKLHSELVKLKSEL	i+7	++ xxx	-	++ xx		
Ac-AEAEAKAKAEAEAKAKGGH-NH_2	EAK16(II)GGH	+++* +	NS	++	AFM, IR, NMR	43

Table 1: Schematic view of model peptides with induced-metal amyloid formation. Color and bold police in the sequences indicated : Histidine residue (red), N-term or C-term modification (blue), Change in the sequence (green or pink) ; (+) indicated a crude estimation of quantity of fibrils or β-sheet formed ; x indicated a crude estimation of rate of fibrils or β-sheet formation; (-) indicated no fribrils formation. (+ ; x ; -) signs are relative to the studies their come from.

Abbreviation used: Abz (o-animobenzoic acid) ; NS (Not Study) ; SANS (Small Angle Neutron Scattering) ; EM (Electronic Microscopy) ; CD (Circular Dischroim) ; XAS (X-ray Absorption Spectroscopy) ; AFM (Atomic Force Microscopy) ; EPR (Electronic Paramagnetic Resonance) ; IR (Infrared-Red) ; Tox (Toxicity on cells) ; ThT (Fluorescence of Thioflavin T) ; XANES (X-ray Absorption Near the Edge Structure) ; TEM (Transmision Electronic Microscopy)*: with $H2SO_4$ in order to compare $CuSO_4$

References.

1. Hureau, C., Coordination of redox active meatl ions to the APP and to the amyloid-β peptides involved in AD. Part 1: an overview. *Coord. Chem. Rev.* **2012,** *256* (19-20), 2164-2174.
2. Kozlowski, H.; Luczkowski, M.; Remelli, M.; Valensin, D., Copper, Zinc and iron in neurodegenerative diseases (Alzheimer's disease, Parkinson's disease and prion diseases). *Coord. Chem. Rev.* **2012,** *256* (19-20), 2129-2141.
3. Roberts, B. R.; Ryan, T. M.; Bush, A. I.; Masters, C. L.; Duce, J. A., The role of metallobiology and amyloid-β peptides in Alzheimer's disease. *J. Neurochem.* **2012,** *120* (Suppl 1), 149-166.
4. Tôugu, V.; Palumaa, P., Coordination of Zinc to the Aβ, APP, α-synuclein, PrP. *Coord. Chem. Rev.* **2012,** *256* (19-20), 2219-2224.
5. Hamley, I. W., The Amyloid Beta Peptide: A Chemist's Perspective. Role in Alzheimer's and Fibrillization. *Chem. Rev.* **2012,** *112* (10), 5147-5192.
6. Leal, S. S.; Botelho, H. M.; Gomes, C. M., Metals ions as modulators of protein conformation and misfolding in neurodegeneration. *Coord. Chem. Rev.* **2012,** *256* (19-20), 2253-2270.
7. Viles, J. H., Metal ions and amyloid formation in neurodegenerative diseases. *Coord. Chem. Rev.* **2012,** *256* (19-20), 2271-2284.
8. Cherny, I.; Gazit, E., Amyloids: not only pathological agents but also ordered nanomaterials. *Angew. Chem., Int. Ed. Engl.* **2008,** *47* (22), 4062-4069.
9. Hamley, I. W., Biological soft materials. *Angew. Chem., Int. Ed. Engl.* **2007,** *46* (24), 4442-4455.
10. Eisenberg, D.; Jucker, M., The amyloid state of proteins in human diseases. *Cell* **2012,** *148* (6), 1188-1203.
11. Tycko, R., Solid-state NMR studies of amyloid fibril structure. *Annu. Rev. Phys. Chem.* **2011,** *62*, 279-299.
12. Jahn, T. R.; Radford, S. E., The Yin and Yang of protein folding. *FEBS J.* **2005,** *272* (23), 5962-5970.
13. Knowles, T. P.; Waudby, C. A.; Devlin, G. L.; Cohen, S. I.; Aguzzi, A.; Vendruscolo, M.; Terentjev, E. M.; Welland, M. E.; Dobson, C. M., An analytical solution to the kinetics of breakable filament assembly. *Science* **2009,** *326*, 1533-1537.
14. Serio, T. R.; Cashikar, A. G.; Kowal, A. S.; Sawicki, G. J.; Moslehi, J. J.; Serpell, L.; Arnsdorf, M. F.; Lindquist, S. L., Nucleated conformational conversion and the replication of conformational information by a prion determinant. *Science* **2000,** *289* (5483), 1317-1321.
15. Wetzel, R., *Acc. Chem. Res.* **2006,** *39*, 671-679.
16. Hureau, C.; Dorlet, P., Coordination of redox active metal ions to the APP protein and to the amyloid-β peptides involved in Alzheimer disease.
Part 2: How Cu(II) binding sites depend on changes in the Aβ sequences. . *Coord. Chem. Rev.* **2012,** *256* (19-20), 2175-2187.
17. Baldwin, A. J.; Knowles, T. P.; Tartaglia, G. G.; Fitzpatrick, A. W.; Devlin, G. L.; Shammas, S. L.; Waudby, C. A.; Mossuto, M. F.; Meehan, S.; Gras, S. L.; Christodoulou, J.; Anthony-Cahill, S. J.; Barker, P. D.; Vendruscolo, M.; Dobson, C. M., Metastability of native

proteins and the phenomenon of amyloid formation. *J. Am. Chem. Soc.* **2011,** *133* (36), 14160-14163.
18. Temussi, P. A.; Masino, L.; Pastore, A., From Alzheimer to Huntington: why is a structural understanding so difficult? *EMBO J.* **2003,** *22* (3), 355-361.
19. Chiti, F.; Dobson, C. M., Protein misfolding, functional amyloid, and human disease. *Annu. Rev. Biochem.* **2006,** *75*, 333-366.
20. DeToma, A. S.; Salamekh, S.; Ramamoorthy, A.; Lim, M. H., Misfolded proteins in Alzheimer's disease and type II diabetes. *Chem. Soc. Rev.* **2012,** *41* (2), 608-621.
21. Hoernke, M.; Falenski, J. A.; Schwieger, C.; Koksch, B.; Brezesinski, G., Triggers for β-sheet formation at the hydrophobic-hydrophilic interface: high concentration, in-plane orientational order, and metal ion complexation. *Langmuir* **2011,** *27* (23), 14218-14231.
22. Brender, J. R.; Hartman, K.; Nanga, R. P.; Popovych, N.; de la Salud Bea, R.; Vivekanandan, S.; Marsh, E. N.; Ramamoorthy, A., Role of zinc in human islet amyloid polypeptide aggregation. *J. Am. Chem. Soc.* **2010,** *132* (26), 8973-8983.
23. Pradines, V.; Jurca Stroia, A.; Faller, P., Amyloid fibrils: modulation of formation and structure by copper(II). *New J. Chem.* **2008,** *32*, 1189-1194.
24. Alies, B.; Solari, P. L.; Hureau, C.; Faller, P., Dynamics of Zn-binding as a key feature in the formation of amyloid fibrils. *Inorg. Chem.* **2012,** *51* (1), 701-708.
25. Dong, J.; Canfield, J. M.; Mehta, A. K.; Shokes, J. E.; Tian, B.; Childers, W. S.; Simmons, J. A.; Mao, Z.; Scott, R. A.; Warncke, K.; Lynn, D. G., Engineering metal ion coordination to regulate amyloid fibril assembly and toxicity. *Proc. Natl. Acad. Sci. U. S. A.* **2007,** *104* (33), 13313-13318.
26. Dong, J.; Shokes, J. E.; Scott, R. A.; Lynn, D. G., Modulating amyloid self-assembly and fibril morphology with Zn(II). *J. Am. Chem. Soc.* **2006,** *128* (11), 3540-3542.
27. Trapaidze, A.; Hureau, C.; Bal, W.; Winterhalter, M.; Faller, P., Thermodynamic study of Cu2+ binding to the DAHK and GHK peptides by isothermal titration calorimetry (ITC) with the weaker competitor glycine. *J. Biol. Inorg. Chem.* **2012,** *17* (1), 37-47.
28. Alies, B.; La Penna, G.; Sayen, S.; Guillon, E.; Hureau, C.; Faller, P., Insights into the Mechanisms of Amyloid Formation of ZnII-Ab11-28: pH-Dependent Zinc Coordination and Overall Charge as Key Parameters for Kinetics and the Structure of ZnII-Ab11-28 Aggregates. *Inorg. Chem.* **2012,** *41* (14), 7897-7902.
29. Alies, B.; Pradines, V.; Alliot, I.; Sayen, S.; Guillon, E.; Hureau, C.; Faller, P., Metal-specific modulation of amyloid formation and structure in model peptides by zinc(II) *J. Biol. Inorg. Chem.* **2011,** *16* (2), 333-340.
30. Yoshimura, Y.; Lin, Y.; Yagi, H.; Lee, Y. H.; Kitayama, H.; Sakurai, K.; So, M.; Ogi, H.; Naiki, H.; Goto, Y., Distinguishing crystal-like amyloid fibrils and glass-like amorphous aggregates from their kinetics of formation. *Proc. Natl. Acad. Sci. U. S. A.* **2012,** *109* (36), 14446-14451.
31. Gaggelli, E.; Kozlowski, H.; Valensin, D.; Valensin, G., NMR studies on Cu(II)–peptide complexes: exchange kinetics and determination of structures in solution. *Mol. Biosyst.* **2005,** *1*, 79-84.
32. Zawisza, I.; Rozga, M.; Bal, W., Affinity of peptides (Aβ, APP, α-synuclein, PrP) for metal ions (Cu, Zn). *Coord. Chem. Rev.* **2012,** *256* (19-20), 2297-2307.

33. Nunes, A. M.; Zavitsanos, K.; Malandrinos, G.; Hadjiliadis, N., Coordination of Cu(2+)and Ni(2+) with the histone model peptide of H2B N-terminal tail (1-31 residues): A spectroscopic study. *Dalton Trans.* **2010,** *39* (18), 4369-4381.
34. Hoernke, M.; Koksch, B.; Brezesinski, G., Amyloidogenic peptides at hydrophobic-hydrophilic interfaces: coordination affinities and the chelate effect dictate the competitive binding of Cu2+ and Zn2+. *ChemPhysChem* **2011,** *12* (12), 2225-2229.
35. Tsvetkov, P. O.; Kulikova, A. A.; Golovin, A. V.; Tkachev, Y. V.; Archakov, A. I.; Kozin, S. A.; Makarov, A. A., Minimal Zn(2+) binding site of amyloid-β. *Biophys. J.* **2010,** *99* (10), L84-86.
36. Talmard, C.; Bouzan, A.; Faller, P., Zinc Binding to Amyloid-: Isothermal Titration Calorimetry and Zn Competition Experiments with Zn Sensors. *Biochemistry* **2007,** *46*, 13658-13666.
37. Sarell, C. J.; Syme, C. D.; Rigby, S. E.; Viles, J. H., Copper(II) binding to amyloid-beta fibrils of Alzheimer's disease reveals a picomolar affinity: stoichiometry and coordination geometry are independent of Abeta oligomeric form. *Biochemistry* **2009,** *48* (20), 4388-4402.
38. Pedersen, J. T.; Østergaard, J.; Rozlosnik, N.; Gammelgaard, B.; Heegaard, N. H., Cu(II) mediates kinetically distinct, non-amyloidogenic aggregation of amyloid-beta peptides. *J. Biol. Chem.* **2011,** *286* (30), 26952-26963.
39. Faller, P.; Hureau, C.; Dorlet, P.; Hellwig, P.; Coppel, Y.; Collin, F.; Alies, B., Methods and techniques to study the bioinorganic chemistry of metal-peptide complexes linked to neurodegenerative diseases. *Coord. Chem. Rev.* **2012,** *256* (19-20), 2381-2396.
40. Morgan, D. M.; Dong, J.; Jacob, J.; Lu, K.; Apkarian, R. P.; Thiyagarajan, P.; Lynn, D. G., Metal switch for amyloid formation: insight into the structure of the nucleus. *J. Am. Chem. Soc.* **2002,** *124* (43), 12644-12645.
41. Pagel, K.; Vagt, T.; Kohajda, T.; Koksch, B., From alpha-helix to beta-sheet--a reversible metal ion induced peptide secondary structure switch. *Organic and Biomolecular Chemistry* **2005,** *3* (14), 2500-2502.
42. Pagel, K.; Seri, T.; von Berlepsch, H.; Griebel, J.; Kirmse, R.; Böttcher, C.; Koksch, B., How Metal Ions Affect Amyloid Formation: Cu2+- and Zn2+-Sensitive Peptides. *ChemBioChem* **2008,** *9* (4), 531-536.
43. Yang, H.; Pritzker, M.; Fung, S. Y.; Sheng, Y.; Wang, W.; Chen, P., Anion effect on the nanostructure of a metal ion binding self-assembling peptide. *Langmuir* **2006,** *22* (20), 8553-8562.

La maladie d'Alzheimer (MA) est caractérisée entre autres par la présence de plaques amyloïdes retrouvées dans le cerveau des patients. Elles sont constituées d'agrégats de peptides Aβ dans lesquels est retrouvée une forte concentration d'ions Cu et Zn. Les ions métalliques peuvent être placés au cœur de la MA via la modulation de l'agrégation du peptide Aβ et/ou la production de d'espèces réactive de l'oxygène ROS ($O_2^{\bullet-}$; H_2O_2 ; $HO^{\bullet}$) délétères pour les neurones.[1,2,3] Il existe des formes génétiques de la MA, dans lesquelles la maladie se déclenche précocement. Certaines d'entre elles présentent des mutations sur le gène de l'APP (Amyloid Precusor Protein) conduisant à différents mutants du peptide Aβ tels que H6R-Aβ ou D7N-Aβ .[4]

Récemment, une autre modification du Aβ a été découverte. Il s'agit de formes tronquées sur la partie N-terminale et commençant, soit par le glutamate 3 (Aβ3), soit par la forme pyroglutamate correspondante (Aβp3). Ces peptides sont particulièrement intéressants. D'une part, ils sont retrouvés en forte proportion *in vivo* (représentant jusqu'à 25% du contenu en peptide Aβ des plaques).[5, 6] D'autre part, leur présence semble promouvoir la maladie.[7] On peut envisager l'hypothèse suivante pour expliquer la toxicité accrue de ces formes modifiées. Il est possible qu'une coordination différente des ions Cu à ces peptides entrainent la formation de plus de ROS ou/et conduisent à une agrégation des peptides plus néfaste pour les neurones.

La coordination du Cu(II) diffère-t-elle entre le peptide Aβ complet et ses formes modifiées considérées comme plus délétères ? Afin de répondre à cette question, nous nous sommes intéressés à la coordination du Cu(II) à ces différents peptides.

II- Coordination du Cu aux différentes formes du peptide Aβ

II. 1- Introduction

a- Coordination de [Cu(II)-Aβ]

Après de nombreuses études et controverses, la coordination ou plutôt les modes de coordination du Cu(II) sur Aβ semble aujourd'hui bien établie.[4] En effet, le peptide Aβ1-16, tronqué en position C-terminale (modèle du Aβ1-40/42 utilisé pour étudier la coordination du Cu, en raison de sa plus grande solubilité) présente deux types de coordination (notés composants I et II) autour du pH physiologique (*i.e.* pH 7.4). La géométrie du complexe est plan carré, néanmoins la possibilité d'un ligand apical COO^- (ou molécule d'eau) n'est pas

exclue. Dans le plan équatorial du composant I, le Cu(II) est lié par l'amine terminale de l'Asp1, la fonction carbonyle adjacente de la liaison peptidique Asp1-Ala2, le noyau imidazole de l'His6 et de l'His13 ou de l'His14 en équilibre. Dans le composant II, la déprotonation de la liaison peptidique Asp1-Ala2 entraine la coordination de la fonction amide correspondante, de la fonction carbonyle adjacent (Ala2-Glu3) et la décoordination d'un des deux noyaux imidazole d'une His (Schéma 1). Ces modes de coordinations ont été établis par différentes spectroscopies: DC, XAS, RMN,[8] et RPE pulsée couplée à l'utilisation de peptides marqués isotopiquement.[9]

Plus récemment, nous avons montré que le complexe Cu(II)-Aβ16 présente d'autres espèces (notées III, IV) à des pH plus élevés. Ces espèces (III, IV) correspondent à la déprotonation d'un NH amide (espèce III) puis de deux amides (espèce IV) supplémentaire. Ainsi, dans l'espèce III, le Cu(II) est lié par l'amine terminale, 2 fonctions amides déprotonées (des liaisons Asp1-Ala2 et Ala2-Glu3) et un noyau imidazole d'His. Dans l'espèce IV, le Cu(II) est lié par l'amine terminale, 3 fonctions amides déprotonées (des liaisons Asp1-Ala2, Ala2-Glu3 et Glu3-Phe4). Les pKa correspondant aux transitions I/II, II/III, III/IV sont de 7,8 ; 9,3 ; 10,1, respectivement (voir schéma 1 ci-dessous).

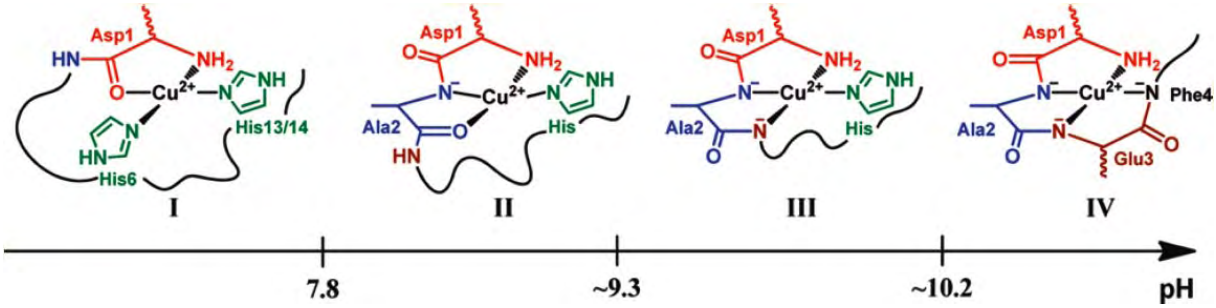

Schéma 1 : Modes de coordination du Cu(II) par le peptide Aβ1-16 en fonction du pH

b- Coordination de [Cu(II)-AcAβ]

Dans le cas du [Cu(II)-AcAβ1-16], où AcAβ1-16 correspond au peptide Aβ1-16 dans lequel l'amine terminale a été acétylée, nous avons montré que la coordination du Cu(II) diffère de celle du Aβ1-16. En effet, l'acétylation de l'amine empêche sa coordination. La coordination du Cu(II) dans le complexe Cu-AcAβ1-16 dépend aussi du pH et présente différentes espèces en fonction du pH, notées II', III', IV'. La coordination de Cu(II) dans ces espèces implique respectivement une, deux et trois fonctions amides déprotonées. Le plan de coordination équatorial des ions Cu(II) est complété par des noyaux imidazole d'His et/ou des fonctions CO de liaisons peptidiques.

Dès lors, on peut se demander : quel impact ont les modifications annoncées dans l'introduction sur la coordination du Cu(II) ?

c- Séquence des formes tronquées en N-terminal (Aβ3-16 & p3-16)

Ci-dessous, les séquences des peptides Aβ1-42, Aβ1-16, Aβ3-16, Aβp3-16 et AcAβ1-16 sont présentées. On remarque que les peptides Aβ1-16 et Aβ3-16 possèdent les mêmes ligands : l'amine terminale, 3 groupes imidazoles des residus His, 4 (resp. 3) fonctions carboxylate des residus Asp et Glu. Au contraire, l'amine terminale n'est plus disponible sur le peptide Aβp3-16 dû à la formation du cycle pyroglutamate qui bloque également la fonction COO^- du glutamate. Le peptide AcAβ1-16, lui non plus, ne dispose pas de l'amine terminale et sera donc utilisé comme contrôle de l'influence du NH_2 terminale.

Aβ1-42 NH_2-D**A**E**F**RHDSGYE**V**HHQK**LVFFA**EDVGSNKG**AII**G**L**M**V**GG**VVIA**-COOH

Aβ1-16 NH_2-D**A**E**F**RHDSGYE**V**HHQK-COOH

Aβ3-16 NH_2-E**F**RHDSGYE**V**HHQK-COOH

Aβp3-16 pE**F**RHDSGYE**V**HHQK-COOH

AcAβ1-16 AcNH-D**A**E**F**RHDSGYE**V**HHQK-COOH

Figure 1 : Séquences primaires des peptides Aβ1-42, Aβ1-16, Aβ3-16, Aβp3-16 et AcAβ1-16 (utilisant le code à une lettre), qui souligne leur origine commune, les ligands potentiels et les chaines latérales hydrophobes. Ligands azotés en bleu ; ligands oxygénés en rouge ; chaines latérales hydrophobes en gras.

II. 2- Méthodes et Techniques

a- Dichroïsme Circulaire (DC)

Le DC est une spectroscopie optique qui nécessite deux conditions pour être utilisée : de l'absorbance et de la chiralité. Cette technique présente l'avantage majeur de pouvoir sonder les modifications structurales au-delà de la première sphère de coordination (contrairement à la RPE). De plus, elle est généralement plus informative qu'un spectre UV-vis, car le signal peut être positif ou négatif (d'où une meilleure résolution des bandes d'absorbance).[10]

b- Résonance Paramagnétique Electronique (RPE)

La RPE est une technique de choix pour étudier la première sphère de coordination du Cu(II), de configuration électronqiue d^9. En effet, l'électron célibataire est sensible à la nature des ligands équatoriaux du Cu(II). Les paramètres RPE reflètent la nature des atomes coordinés et la géométrie du complexe. Dans notre cas, la RPE permet le suivi des espèces en fonction du pH de façon évidente.

c- Résonance Magnétique Nucléaire (RMN) ^{13}C et ^{1}H

La RMN permet de visualiser les atomes impliqués dans la coordination du Cu(II). Le Cu(II), paramagnétique, sera utilisé en quantité sub-stœchiométrique afin d'élargir spécifiquement le signal des atomes impliqués dans sa coordination. La RMN ^{13}C est particulièrement efficace pour les sonder la déprotonation d'un amide, notamment via la perte des signaux du Cα et CO adjacents. Le Cu(I) étant diamagnétique, les signaux sont déplacés par sa présence. Dans ce cas, la RMN ^{1}H est suffisante pour étudier la coordination du Cu(I) aux peptides. La difficulté majeure, d'un point de vue expérimental, est de garder le Cu sous sa forme réduite.

II. 3- Etude comparative et structurale

a- DC

La comparaison des spectres DC des complexes Cu(II)-Aβ1-16, Cu(II)-Aβ3-16, Cu(II)-Ac-Aβ1-16 et Cu(II)-Aβp3-16 en fonction du pH est intéressante. Dans la figure 2, on remarque de grandes similitudes entre les signatures spectroscopiques des complexes Cu(II)-Aβ3-16 et Cu(II)-Aβ1-16 ainsi qu'entre celles des complexes Cu(II)-Aβp3-16 et Cu(II)-AcAβ1-16. Dans le panneau A (Cu(II)-Aβ3-16 et Cu(II)-Aβ1-16), la forme des bandes d-d et de la bande négative à ~280nm correspondant à la transition LMCT $-NH_2$ est globalement la même. Néanmoins, on note quelques différences, une bande de faible intensité positive à ~650nm dans le cas du complexe Cu(II)-Aβ1-16 qui n'est pas présente chez le Cu(II)-Aβ3-16. De plus, sur le spectre du complexe Cu(II)-Aβ3-16, on observe un déplacement de la transition à 325nm (vers 315nm) correspondant à une bande de transfert de charge N^- vers Cu(II), et de la transition à 285nm (vers 275nm) correspondant à une bande de transfert de charge NH_2 vers Cu(II). Ce déplacement n'est pas présent sur le spectre du complexe Cu(II)-Aβ1-16. Dans le panneau B, on remarque que les signatures des complexes

Cu(II)-Aβp3-16 et Cu(II)-Ac-Aβ1-16 sont hautement identiques. Par ailleurs, comme attendu, la transition de transfert de charge NH_2 vers Cu(II) n'est pas détectée. Cette très grande ressemblance entre les signatures des complexes Cu(II)-Ac-Aβ1-16 et Cu(II)-Aβp3-16 et des complexes Cu(II)-Aβ1-16 et Cu(II)-Aβ3-16, confirme l'implication de l'amine N-terminale dans la coordination du Cu aux peptides Aβ1-16 et Aβ3-16.

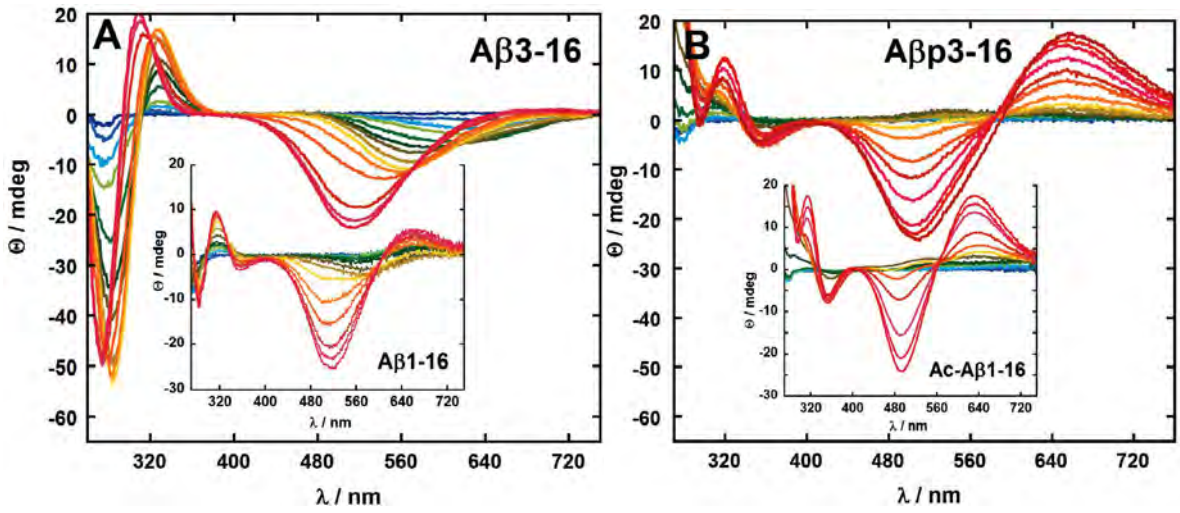

Figure 2 : Spectres de DC de Cu(II)-Aβ3-16 (panneau A) et Cu-Aβp3-16 (panneau B) en fonction du pH (d'acide bleu à basique rouge). En cartouche, les spectres DC de Cu(II)-Aβ1-16 (panneau A) et de Cu(II)-Ac-Aβ1-16 (panneau B). Conditions : [Cu-peptide] = 0.45mM ; ℓ=1cm ; T = 25°C.

Ainsi, on peut donc d'ores et déjà observer deux groupes de complexes. Le premier, dans lequel l'amine N-terminale est liée au Cu(II) (Cu(II)-Aβ1-16 et Cu(II)-Aβ3-16) et le second, dans lequel l'amine N-terminale étant bloquée, elle ne peut intervenir dans la complexation du Cu(II) (Cu(II)-Ac-Aβ1-16 et Cu(II)-Aβ3-16).

b- RPE

La figure 3 présente les complexes Cu(II)-peptide à différents pH organisés selon les groupes définis ci-dessus : l'un avec les peptides Aβ1-16 et Aβ3-16 (amine terminale libre) sur le panneau A, l'autre avec les peptides AcAβ1-16 et Aβp3-16 (amine terminale bloquée) sur le panneau B.

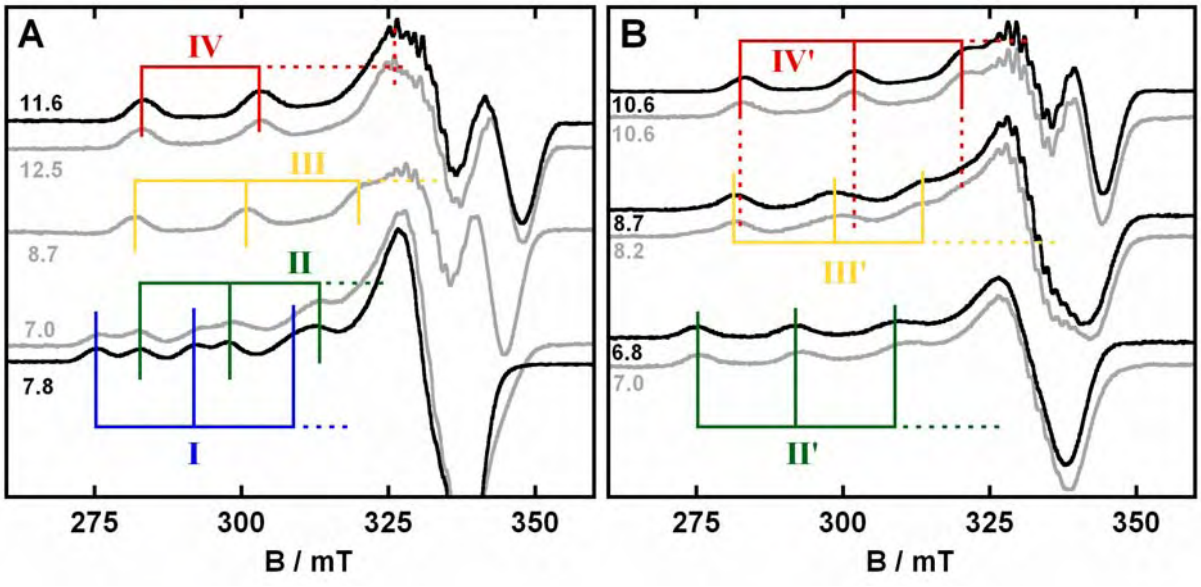

Figure 3 : Spectre RPE des complexes Cu(II)-peptides à une selection de pH. Panneau A, Cu(II)-Aβ1-16 (noir) et Cu(II)-Aβ3-16 (gris). Panneau B, Cu(II)- AcAβ1-16 (noir) et Cu(II)-Aβp3-16 (gris). [Cu(peptide] = 1 mM, T = 110 K, v = 9.5 GHz.

Sur le panneau A, on constate que les complexes Cu(II)-Aβ3-16 et Cu(II)-Aβ1-16 présentent les mêmes signatures spectroscopiques, mais à des pH différents. En particulier, l'espèce III est nettement plus visible sur le spectre du complexe Cu(II)-Aβ3-16 que sur celui de Cu(II)-Aβ1-16 (données non montrées). Cela est dû à sa présence sur une grande plage de pH (voir tableau 1). Le pKa de I / II est vue à ~ pH 7,0 dans le cas du peptide Aβ3-16 et à ~ pH 7,8 ans le cas du peptide Aβ1-16 (voir le panneau A de la Figure 3).

Dans le panneau B, à l'instar du DC, les spectres RPE des complexes Cu(II)-AcAβ1-16 et Cu(II)-Aβp3-16 sont hautement semblables. En effet, les différents modes de coordination du Cu(II) sont observés pour des pH très proches (voir tableau 1). Le DC et la RPE suggère donc que les modes de coordination du Cu(II) par les peptides Aβp3-16 et AcAβ1-16 sont similaires, tout comme leur dépendance en fonction du pH.

Il faut noter ici que l'utilisation de la RPE, comme unique technique, et sur une plage de pH réduite peut conduire à des erreurs d'interprétation. En effet, les espèces II' et III' possèdent des paramètres RPE très proches des espèces I et II, respectivement. Cette erreur fut commise dans les travaux de Drew et al., où il fut conclu que la coordination du Cu(II) aux peptides Aβ3-16 et Aβp3-16 était semblable (puisque les complexes Cu(II)-AcAβ1-16 et Cu(II)-Aβp3-16 présentent les mêmes signatures RPE) et par conséquent que la fonction NH_2 terminale n'était pas impliquée dans la coordination du Cu(II) par les deux peptides.[11]

Peptide	pKa I / II	pKa II / III	pKa III / IV
Aβ1-16	7.8	9.3	10.1
Aβ3-16	7.0	7.5	10.0
	pKa I' / II'	pKa II' / III'	pKa III' / IV'
Aβp3-16	5.3	7.6	8.8
AcAβ1-16	5.2	7.5	8.7

Tableau 1 : Valeurs des pKa des complexes Cu(II)-Aβ1-16, Cu(II)-Aβ3-16, Cu(II)-Aβp3-16 et Cu(II)-AcAβ1-16 basées sur la spéciation des signatures RPE des différentes espèces en fonction du pH

c- RMN ^{13}C

Afin d'aller plus loin dans l'exploration de la sphère de coordination du Cu(II), et en particulier pour identifier les résidus impliqués dans la coordination du Cu(II), nous avons utilisé la RMN du ^{13}C en absence et en présence de Cu(II).

Cu(II)-Aβ3-16

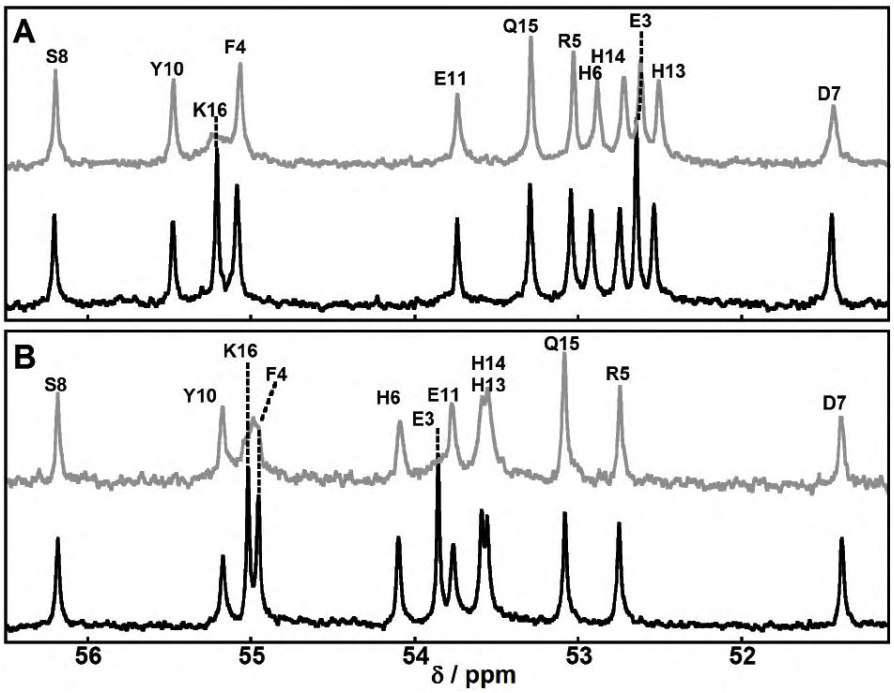

Figure 4 : RMN ^{13}C centré sur les Cα du peptide Aβ3-16 à pH 6,0 (panneau A) et à pH 8,6 (panneau B) en absence (noir) et en présence (gris) de Cu(II). Les lignes en pointillés indiquent les résidus affectés par l'ajout de Cu(II). Condition : [Aβ3-16] = 10 mM, T = 25 °C, [Cu(II)]=200µM à pH 6,0 ; [Cu(II)]=3mM à pH 8,6, ν = 125,.8 MHz.

Dans la figure 4, on observe le spectre RMN ^{13}C du peptide Aβ3-16 dans la zone des Cα à pH 6,0 (panneau A) et pH 8,6 (panneau B) avec (gris) et sans (noir) Cu(II). Le but est de comparer la coordination du Cu(II) dans l'espèce I et dans l'espèce II de Cu(II)-Aβ3-16. Il faut noter que lorsque le Cu(II) est lié par deux fonctions amides déprotonées ou plus, il n'y a plus d'échange du Cu(II) entre peptide et, en conséquence, le signal du peptide est totalement effacé. Le signal restant est donc celui du peptide libre ou du peptide lié au Cu(II) dans l'espèce II. Ainsi, en se plaçant à pH 6,0 et pH 8,6, la coordination reflétée par la RMN sera celle de l'espèce I et de l'espèce II, respectivement. On constate qu'aux deux pH, le signal Cα du Glu3 est largement affecté par l'ajout de Cu(II), ce qui est attribué à la coordination du NH_2 terminal (celui-ci étant adjacent au Cα du Glu3). On remarque aussi que le signal du Cα de la Lys16 (adjacent au COO^- terminal) est affecté. Les groupements carboxylates sont généralement très affectés par l'addition du Cu(II). En effet, ils sont flexibles et peuvent intervenir dans la coordination du Cu(II) comme ligand apical ou lors de l'échange rapide du Cu(II) entre les peptides. Cet élargissement n'est donc pas spécifique. Par ailleurs, le groupe COO^- de la Lys16 n'est pas pertinent d'un point de vue biologique puisqu'il n'existe pas dans le peptide complet. A pH 8,6, on constate que le signal du Cα de la Phe4 est particulièrement affecté en présence de Cu(II). Cela indique la déprotonation de la fonction amide de la liaison Glu3-Phe4 dans l'espèce II du Cu(II)-Aβ3-16. Les signaux du Cα ainsi que du CO (non montré) de His6 sont aussi élargis par l'addition de Cu(II).

Cu(II)-Aβp3-16

Ci-dessous, la figure 5 présente le spectre RMN ^{13}C du peptide Aβp3-16 en présence (gris) et en l'absence de Cu(II) (noir) dans deux zones d'intérêt: Cα (panneau A) et CO (panneau B). Les signaux Cα des groupements COO^- sont affectés pour les raisons évoquées précédemment. Comme attendu, le signal Cα du pyroGlu3 n'est pas affecté puisqu'il n'intervient pas dans la coordination du Cu(II). Les différents signaux des résidus His 6, 13, 14 sont, quant à eux, largement affectés. Cependant, on notera que les signaux Cα et CO des His13 et 14 sont plus touchés que ceux de l'His6 par l'ajout du Cu(II).

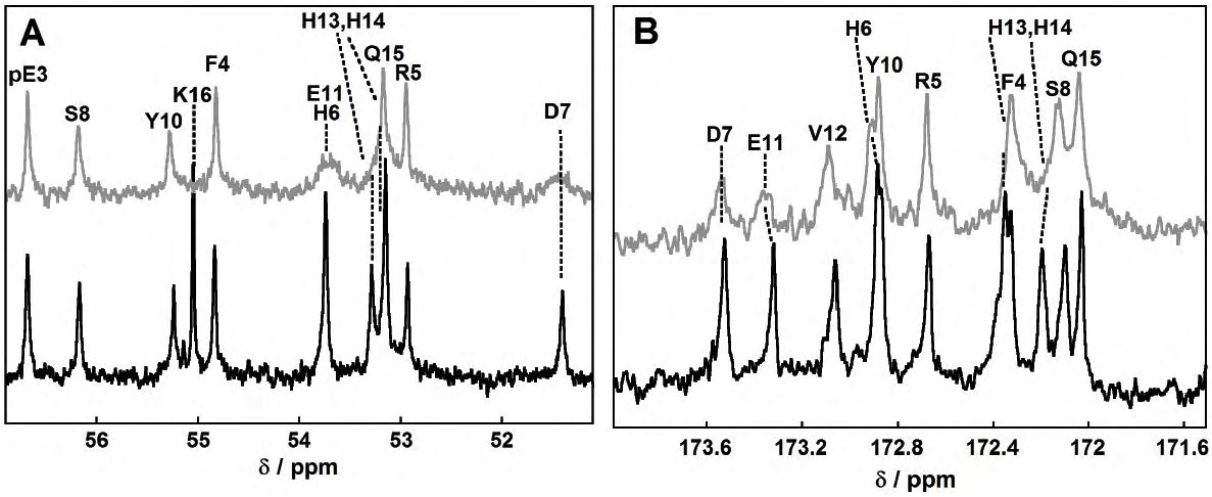

Figure 5 : RMN ^{13}C centré sur les Cα (panneau A) et les CO (panneau B) du du peptide Aβp3-16 à pH 7,0 en absence (noir) et en présence (gris) de Cu(II). Condition : [Aβp3-16] = 5 mM, [Cu(II)]=250µM, T = 25 °C, ν = 125,8 MHz.

d- Cu(I) & RMN ^{1}H

Dans l'hypothèse de la toxicité du complexe Cu-Aβ *via* la formation de ROS, le Cu(I) est essentiel. En effet, la production de ROS nécessite le cycle redox Cu(II)/Cu(I). Dans ce contexte, nous nous sommes intéressés à la coordination du Cu(I) aux peptides Aβ.

Afin d'étudier si la coordination du Cu(I) diffère entre les différents peptides Aβ1-16, Aβ3-16 et Aβp3-16, nous nous sommes basés sur la méthode et les conditions décrites dans une précédente publication de l'équipe.[12] Grâce aux spectres RMN ^{1}H des peptides avec et sans Cu(I), nous avons pu identifier les résidus impliqués dans la coordination du Cu(I) (non montré). Les signaux des résidus His subissent une modification en présence de Cu(I). La manière dont ces signaux sont déplacés et élargis par l'ajout de Cu(I) sur les peptides Aβ3-16 et Aβp3-16 est hautement semblable aux modifications observées pour le peptide Aβ1-16. Ces informations suggèrent que la coordination du Cu(I) est inchangée entre les peptides Aβ1-16, Aβ3-16 et Aβp3-16. Il a été proposé que le Cu(I) est lié par le peptide Aβ1-16 via un couple préférentiel d'His (His13/14) en équilibre avec d'autres modes de coordination : couples d'His6/14 ou His6/13 ou via transitoirement les trois histidines.[12] Le comportement par RMN ^{1}H des peptides Aβ3-16 et Aβp3-16 en présence de Cu(I) étant identique à celui du peptide Aβ1-16, nous proposons donc la même coordination du Cu(I) pour les peptides Aβ1-16, Aβ3-16 et Aβp3-16 (voir § I.4.e-Metal ions Coordination to Aβ Cu(I) figure 8).

III. 4- Affinité

La connaissance de l'affinité d'un ion métallique pour un peptide est une donnée importante. En effet, ci-celle détermine si l'interaction ions métalliques – peptides est possible dans le vivant, indique le sens des équilibres entre peptides en compétition et permet de quantifier la fraction liée et la fraction libre. De plus, l'affinité est hautement dépendante de la coordination. Aussi, d'importantes modifications dans l'affinité suggère une coordination différente (et réciproquement).

Peptide	**Cu(II) Affinité (10^{10} M^{-1})**	**Cu(I) Affinité (10^{6} M^{-1})**
Aβ1-16	1.1 ± 0.1	7.5 ± 1.0
Aβ3-16	0.33 ± 0.02	9.2 ± 0.9
Aβp3-16	0.008 ± 0.001	6.5 ± 0.5
AcAβ1-16	0.01 ± 0.001	12 ± 1.3

Tableau 2 : Valeurs d'affinité conditionnelle (i.e. affinité absolue à un pH, donné ici pH 7.4) des ions Cu(II) et Cu(I) pour les peptides étudiés.

a- Cu(I)

Les valeurs d'affinité du Cu(I) pour les peptides Aβ1-16, Aβ3-16, Aβp3-16 et AcAβ1-16 ont été obtenues par compétition avec la ferrozine suivant la procédure décrite dans la ref [13]. Les valeurs d'affinité obtenues sont similaires pour les quatre peptides et comprise entre ~7-12 $x10^{6}M^{-1}$ (voir tableau 2). Ces valeurs proches sont en accord avec une coordination du Cu(I) identique pour les quatre peptide Aβ1-16, Aβ3-16, Aβp3-16 et AcAβ1-16.

b- Cu(II)

Les affinités conditionnelles ont été obtenues par compétition des complexes peptidiques avec de la glycine (chélateur du Cu(II) de faible affinité) suivie par dichroïsme circulaire. Dans la figure 6, on observe la décroissance de la concentration en complexes avec l'augmentation de la concentration en glycine. Les courbes simulées selon la ref [14] permettent obtenir les valeurs de l'affinité conditionnelle indiquées dans le tableau 2. On constate que l'ordre d'affinité est le suivant : Aβ1-16 > Aβ3-16 >> Aβp3-16 ~ AcAβ1-16. Les affinités relatives du Cu(II) pour les peptides Aβ1-16, Aβ3-16, Aβp3-16 ont été calculées par différentes méthodes (données non montrées) et ont donné des résultats en accord avec les affinités conditionnelles mesurées. Il apparait clairement que la protection de l'amine

terminale que ce soit par acétylation ou par formation d'un cycle pyroglutamate diminue significativement l'affinité des peptides pour le Cu(II) en accord avec les modes de coordination précédemment déduits des études spectroscopiques.

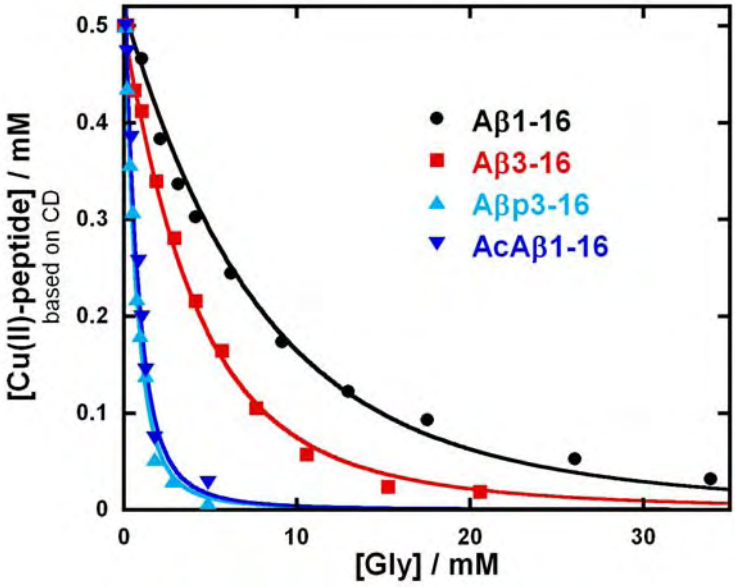

Figure 6 : Concentration en complexe déterminé par DC en fonction de la concentration en glycine. Les points proviennent de l'expérience, les courbes sont simulées à partir des valeurs d'affinité reportées dans le tableau 2. Condition : [peptide-Cu] = 500µM ; [HEPES] = 100mM pH 7,4 ; ℓ=1cm ; les longueurs d'ondes en DC utilisées pour mesurer la concentration en complexe sont 315nm pour Cu(II)-Aβ1-16, 282nm pour Cu(II)-Aβ3-16, 280nm pour Cu(II)-Aβp3-16 et Cu(II)-AcAβ1-16.

II. 5- Coordination du Cu(II) sur Aβ3-16 et Aβp3-16

a- Cu(II)-Aβp3-16

Les différentes expériences décrites ci-dessus suggèrent que la coordination du Cu(II) aux peptides Aβp3-16 et AcAβ1-16 sont similaires (DC, RPE, affinité). De plus, l'effet du Cu(II) sur les spectres RMN ^{13}C du peptide Aβp3-16 montre l'implication de préférentielle des His13 et His14. Les paramètres RPE de l'espèce II' sont en adéquation avec une coordination de type (N^-, 2His, N/O). Moins d'informations sont disponibles pour l'espèce III' du Aβp3-16. Néanmoins, la formation d'un metallacycle étant plus favorable en direction du N-terminal,[4] la déprotonation de la fonction amide de l'His13 est probable. Basé sur ces arguments, les coordinations du Cu(II) lié par le peptide Aβp3-16 sont proposées dans le schéma 2.

b- Cu(II)-Aβ3-16

L'étude par RPE en fonction du pH du complexe Cu(II)-Aβ3-16 (figure 3) présente des similitudes avec celle de Cu(II)-Aβ1-16, néanmoins les différences importantes des valeurs de pKa entre les différentes espèces suggèrent une coordination non semblable à un pH donné (voir tableau 1). De plus, l'apparition de la bande DC à 330 nm sur une plage de pH ~7.5 - 10 laissant place à une bande DC à 310 nm entre pH 10 – 12 suggère que la coordination du Cu(II)-Aβ3-16 diffère de celle de Cu(II)-Aβ1-16 pour les espèces II et III (figure 2). En effet, le Cu(II)-Aβ1-16 présente la bande DC à 310nm sur une plage de pH 7.5-12. La valeur du pKa déterminée en DC (330nm vers 310nm) pour le passage de l'espèce absorbant à 330 nm à celle absorbant à 310 nm est de 9,8, ce qui est très proche de la valeur du pKa(III / IV) déterminée par RPE. Ces données indiquent donc un « retour » du Cu(II)-Aβ3-16 vers une coordination semblable à celle de Cu(II)-Aβ1-16 pour l'espèce IV. A pH 7,4, l'affinité du Cu(II) pour le peptide Aβ3-16 est environ trois fois plus faible que celle du peptide Aβ1-16. Ceci est un argument supplémentaire qui soutient une coordination du Cu(II) différente (tableau 2) entre les deux peptides. Grâce à la RMN ^{13}C qui montre que les siganux du Cα et du CO de l'His6 sont préférentiellement affectées dans l'espèce II et aux autres arguments énoncés ci-dessus, les modes de coordinations du Cu(II)-Aβ3-16 sont proposées dans le schéma 2. Pour l'espèce I, tout comme dans le cas du peptide Aβ1-16, le site du Cu(II) fait intervenir, l'amine terminale, la fonction carbonyle adjacente et deux noyaux imidazole de deux His. Pour les espèces II et III, la formation d'un second métallacycle, non-adjacent au metallacycle en position N-terminale est proposée, métallacycle qui fait intervenir le noyau imidazole de l'His6 et le groupement CO ou la fonction amide deprotonée de la liaison His6-Asp7 dans les espèces II et III, respectivement. Dans l'espèce IV, on retrouve une coordination de type Aβ1-16 avec la formation de trois métallacyle consécutifs centrés sur la partie N-terminale.

Cette forte modification de coordination pour les espèces II et III du complexe Cu(II)-Aβ3-16 comparativement au complexe Cu(II)-Aβ3-16 est probablement dû à l'Arg5. En effet, il a été montré que la mutation de l'Arg5 du peptide Aβ1-16 en Gly favorise la déprotonation de la fonction peptidique Gly5-His6 au lien de la déprotonation de la liaison peptidique Asp1-Ala2 dans le peptide non muté.[15] Aussi, l'arginine, résidu encombrant et chargé pourrait gêner l'approche du Cu(II), empêchant une coordination proche de l'Arg5 dans les espèces II et III du complex Cu(II)-Aβ3-16. A plus haut pH dans l'espèce IV, la formation de trois

metallacycles deviennent suffisamment favorable pour un retour vers une coordination semblable à celle du Cu(II)-Aβ1-16.

Outre la différence de sites pour les espèces II et III. La valeur du pKa(I / II) est également significativement différente. Ceci est du à une stabilisation moins grande de la fonction amide dans la liaison Glu3-Phe4 (peptide Aβ3-16) par rapport à Asp1-Ala2 (peptide Aβ1-16) due à une interaction de type hydrogène moins forte entre le groupement COO^- du Glu3 et de la fonction amide adjacente (formation d'un cycle à 7) par rapport à celle formée entre le groupement COO^- de l'Asp1 et de la fonction amide adjacente (formation d'un cycle à 6).

Ainsi, bien que les ligands disponibles soient les mêmes entre les peptides Aβ1-16 et Aβ3-16, la coordination à pH physiologique est radicalement différente. L'étude de la coordination du Cu(II) au peptide Aβ3-16 illustre donc parfaitement le fait que des résidus n'intervenant pas directement dans la coordination du Cu(II) peuvent néanmoins avoir un effet majeur sur celle-ci.

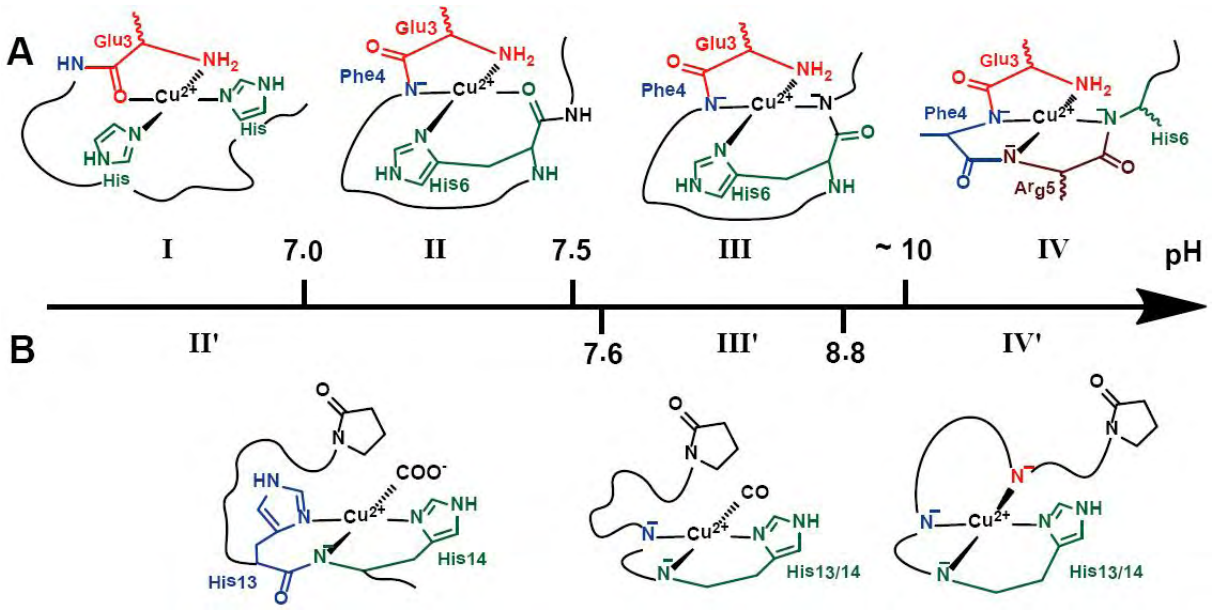

Schéma 2 : Coordination du Cu(II) pour les complexes Cu(II)-Aβ3-16 (A) et Cu(II)-Aβp3-16 (B) en fonction du pH.

II. 6- H6R-Aβ, D7N-Aβ et autres mutants

a- pKa

Basé sur le même type d'approche, nous nous sommes intéressés à la coordination du Cu(II) sur une série de mutants dont les mutants familiaux H6R-Aβ et D7N-Aβ responsables d'un déclenchement précoce de la maladie d'Alzheimer.

Peptide	pKa I / II	pKa II / III	pKa III / IV
Aβ1-16	7.8	9.3	10.2
D1N-Aβ	6.0	9.0	10.3
D7N-Aβ	7.7	9.1	10.6
E3Q-Aβ	7.6	8.5	9.7
E11Q-Aβ	7.5	9.3	10.1
H6A-Aβ	7.3	9.6	
H6R-Aβ	7.2	9.7	
H13A-Aβ	7.5	9.5	10.2
H14A-Aβ	7.5	9.6	10.4

Tableau 3 : Valeurs des pKa des différentes espèces Cu-peptides pour Aβ1-16 et ses mutants, basées sur la spéciation des signatures RPE des différentes espèces détectées en fonction du pH.

Parmi les différents mutants étudiés, certains ont une influence sur les répartitions des espèces, *i.e.* la valeur des pKa entre les différentes espèces (voir tableau 3). Les mutants H13A et H14A ont pour effet de favoriser la formation de l'espèce II. En effet, l'espèce II requiert une histidine de moins que l'espèce I (voir schéma 1). Les complexes Cu(II)-D1N-Aβ et le Cu(II)-E3Q-Aβ présentent notamment des valeurs de pKa(I / II) (mutant D1N) et pKa(II / III) (mutant E3Q) fortement différentes de celles du complexe Cu(II)-Aβ1-16. Ces grands écarts de pKa peuvent être expliqués par la présence (Aβ1-16) ou l'absence (E3Q-Aβ et D1N-Aβ) des liaisons hydrogènes stabilisantes entre les fonctions carboxylates et les NH d'amides à déprotoner selon le schéma ci-dessous :

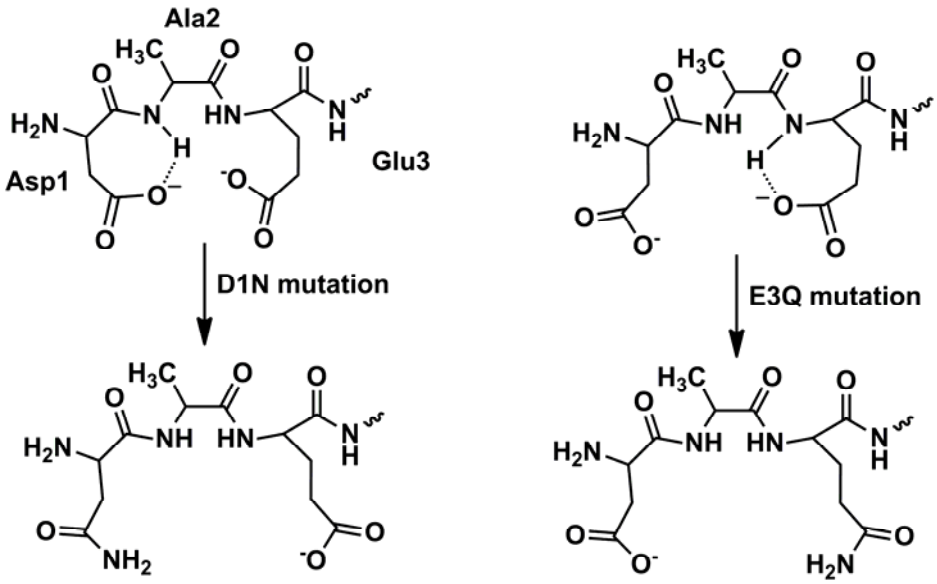

Schéma 3: Influence des liaisons H sur les valeurs de pKa(I/II) et pKa(II/III).

b- H6R et D7N

D7N : Les valeurs des pKa des espèces du complexe Cu(II)-D7N-Aβ et les donnés DC diffèrent peu par rapport à celles du complexe Cu(II)-Aβ1-16. Il est donc raisonnable de penser que la coordination du Cu(II) par le D7N-Aβ ne sera significativement différente de celle par le peptide Aβ1-16.

H6R : Les complexes Cu(II)-H6R-Aβ et Cu(II)-H6A-Aβ, quant à eux, montrent de grandes différences de pKa(I / II) comparativement au complexe Cu(II)-Aβ1-16 (voir Tableau 1) et un passage direct entre espèces II et IV. Les différences des spectres DC en fonction du pH entre les complexes Cu(II)-Aβ1-16 et Cu(II)-H6R-Aβ, suggèrent l'implication simultanée des His13 et His14 dans le dernier cas. De plus, les spectres RMN ^{13}C du peptide H6R-Aβ en présence ou en absence de Cu(II), suggèrent la coordination de l'amine terminale, des His13 et His14 et l'implication du CO de l'His13 dans l'espèce I. La formation de l'espèce I du complexe Cu(II)-H6R-Aβ nécessite deux histidines, or l'His6 est maintenant remplacée par une Arg, laissant seulement His13 et His14 disponibles. Au delà de pH 7,3, la RPE et le DC indique la déprotonation d'une fonction amide et l'implication d'une seule histidine. Si le pH augmente encore (*i.e.* pH > 9.7), on retrouve par DC et RPE, les signatures d'une coordination semblable à l'espèce IV du Cu(II)-Aβ (voir schéma 1). Le passage direct de l'espèce II à l'espèce IV est du à la décoordination simultanée du noyau His et de la fonction carbonyle adjacente formant un metallacycle. La coordination proposée pour le complexe Cu(II)-H6R-Aβ autour du pH physiologique vous est présentée dans le schéma 4 ci-dessous. Cette coordination largement différente de celle obtenue avec le peptide Aβ1-16 semble avoir les répercussions sur les propriétés d'agrégation et redox du complexe.[16]

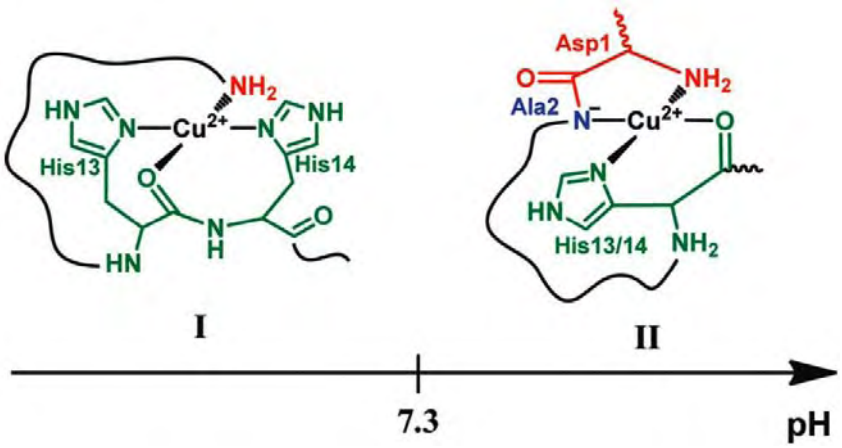

Schéma 4: Espèces I et II proposées pour le complexe Cu(II)-H6R-Aβ autour du pH physiologique

II. 7- Conclusion

Par ces résultats nous avons montré que :

- la coordination du Cu(II)-Aβ présente différentes espèces en fonction du pH

- la fonction N-terminale a un rôle majeur dans la coordination du Cu(II) et son blocage change considérément la coordination et diminue fortement l'affinité pour le Cu(II)

- la seconde sphère de coordination joue un rôle majeur sur la première sphère de coordination du Cu(II) (influence de l'Arg5, mutation D1N)

- la coordination du Cu(II) est très sensible à de faibles modifications de la séquence du peptide amyloïde β

Références :

1. Ashley, I. B.; Rudolph, E. T., Therapeutics for Alzheimer's Disease Based on the Metal Hypothesis. *Neurother.* **2008,** *5* (3), 421-432.

2. Hureau, C.; Faller, P., AB-mediated ROS production by Cu ions: Structural insights, mechanisms and relevance to Alzheimer's disease. *Biochimie* **2009,** *91* (10), 1212-1217.

3. Holtzman, D. M.; Morris, J. C.; Goate, A. M., Alzheimer's Disease: The Challenge of the Second Century. *Science Transl. Med.* **2011** 3 (77), 77sr1.

4. Hureau, C.; Dorlet, P., Coordination of redox active metal ions to the amyloid precursor protein and to amyloid-β peptides involved in Alzheimer disease. Part 2: Dependence of Cu(II) binding sites with Aβ sequences. *Coord. Chem. Rev.* **2012** (256), 2175-2187.

5. Güntert, A.; Döbeli, H.; Bohrmann, B., High sensitivity analysis of amyloid-beta peptide composition in amyloid deposits from human and PS2APP mouse brain. *Neurosci.* **2006,** *143* (2), 461-475.

6. Harigaya, Y.; Saido, T. C.; Eckman, C. B.; Prada, C.-M.; Shoji, M.; Younkin, S. G., Amyloid β Protein Starting Pyroglutamate at Position 3 Is a Major Component of the Amyloid Deposits in the Alzheimer's Disease Brain. *Biochem. Biophys. Res. Commun.* **2000,** *276* (2), 422-427.
7. Schilling, S.; Zeitschel, U.; Hoffmann, T.; Heiser, U.; Francke, M.; Kehlen, A.; Holzer, M.; Hutter-Paier, B.; Prokesch, M.; Windisch, M.; Jagla, W.; Schlenzig, D.; Lindner, C.; Rudolph, T.; Reuter, G.; Cynis, H.; Montag, D.; Demuth, H.-U.; Rossner, S., Glutaminyl cyclase inhibition attenuates pyroglutamate Aβ and Alzheimer's disease-like pathology. *Nat. Med.* **2008,** *14* (10), 1106-1111.
8. Hureau, C.; Coppel, Y.; Dorlet, P.; Solari, P. L.; Sayen, S.; Guillon, E.; Sabater, L.; Faller, P., Deprotonation of the Asp1-Ala2 Peptide Bond Induces Modification of the Dynamic Copper(II) Environment in the Amyloid-beta Peptide near Physiological pH. *Angew. Chem. Int. Ed.* **2009,** *48* (50), 9522-9525.
9. Dorlet, P.; Gambarelli, S.; Faller, P.; Hureau, C., Pulse EPR Spectroscopy Reveals the Coordination Sphere of Copper(II) Ions in the 1-16 Amyloid-beta Peptide: A Key Role of the First Two N-Terminus Residues. *Angew. Chem. Int. Ed.* **2009,** *48* (49), 9273-9276.
10. Faller, P.; Hureau, C.; Dorlet, P.; Hellwig, P.; Coppel, Y.; Collin, F.; Alies, B., Methods and techniques to study the bioinorganic chemistry of metal-peptide complexes linked to neurodegenerative diseases. *Coord. Chem. Rev.* **2012** (256), 2381-2396.
11. Drew, S. C.; Masters, C. L.; Barnham, K. J., Alzheimer's Aβ Peptides with Disease-Associated N-Terminal Modifications: Influence of Isomerisation, Truncation and Mutation on Cu^{2+} Coordination. *PLoS ONE* **2010** *5* (12), e15875.
12. Hureau, C.; Balland, V.; Coppel, Y.; Solari, P.; Fonda, E.; Faller, P., Importance of dynamical processes in the coordination chemistry and redox conversion of copper amyloid-β complexes. *J. Biol. Inorg. Chem.* **2009,** *14* (7), 995-1000.
13. Alies, B.; Badei, B.; Faller, P.; Hureau, C., Reevaluation of Copper(I) Affinity for Amyloid-β Peptides by Competition with Ferrozine - An Unusual Copper(I) Indicator. *Chem. Eur. J.* **2012** *18* (4), 1161-1167
14. Trapaidze, A.; Hureau, C.; Bal, W.; Winterhalter, M.; Faller, P., Thermodynamic study of Cu^{2+} binding to the DAHK and GHK peptides by isothermal titration calorimetry (ITC) with the weaker competitor glycine. *J. Biol. Inorg. Chem.* **2011** *17* (1), 37-47.
15. Eury, H.; Bijani, C.; Faller, P.; Hureau, C., Copper(II) Coordination to Amyloid β: Murine versus Human Peptide. *Angew. Chem. Int. Ed.* **2011** *123* (4), 931-935.
16. Shin, B.-k.; Saxena, S., Substantial Contribution of the Two Imidazole Rings of the His13-His14 Dyad to Cu(II) Binding in Amyloid-β (1-16) at Physiological pH and Its Significance. *J. Phys. Chem. A* **2011** *115* (34), 9590-9602.

pH-Dependent Cu(II) Coordination to Amyloid-β Peptide: Impact of Sequence Alterations, Including the H6R and D7N Familial Mutations

Bruno Alies, Hélène Eury, Christian Bijani, Lionel Rechignat, Peter Faller, and Christelle Hureau

Inorganic Chemistry
2011, *50* (21), 11192-11201

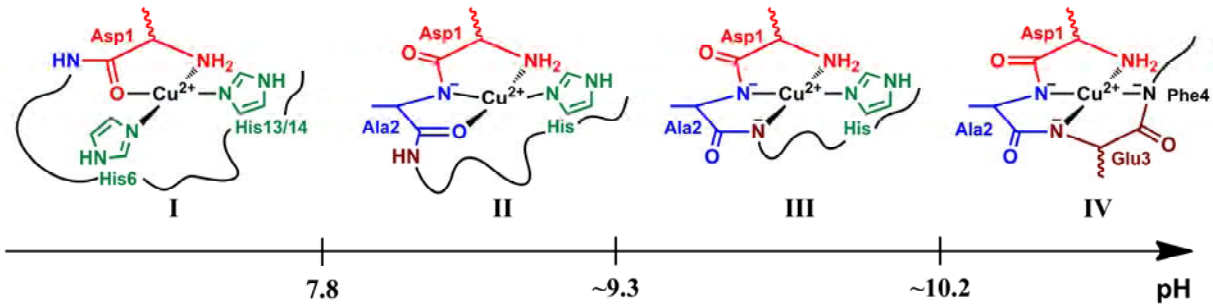

The following article is described in the previous chapter. It is a study about Cu coordination to Aβ and to a series of pertinent mutant. Their pH-dependent Cu coordination has been closely investigated.

Inorganic Chemistry

ARTICLE

pubs.acs.org/IC

pH-Dependent Cu(II) Coordination to Amyloid-β Peptide: Impact of Sequence Alterations, Including the H6R and D7N Familial Mutations.

Bruno Alies,[†] Hélène Eury,[†] Christian Bijani, Lionel Rechignat, Peter Faller, and Christelle Hureau*

CNRS, LCC (Laboratoire de Chimie de Coordination), 205, route de Narbonne, F-31077 Toulouse, France, and Université de Toulouse, UPS, INPT, LCC, F-31077 Toulouse, France

Supporting Information

ABSTRACT: Copper ions have been proposed to intervene in deleterious processes linked to the development of Alzheimer's disease (AD). As a direct consequence, delineating how Cu(II) can be bound to amyloid-β (Aβ) peptide, the amyloidogenic peptide encountered in AD, is of paramount importance. Two different forms of [Cu^{II}(Aβ)] complexes are present near physiological pH, usually noted components **I** and **II**, the nature of which is still widely debated in the literature, especially for **II**. In the present report, the phenomenological pH-dependent study of Cu(II) coordination to Aβ and to ten mutants by EPR, CD, and NMR techniques is described. Although only indirect insights can be obtained from the study of Cu(II) binding to mutated peptides, they reveal very useful for better defining Cu(II) coordination sites in the native Aβ peptide. Four components were identified between pH 6 and 12, namely, components **I**, **II**, **III** and **IV**, in which the predominant Cu(II) equatorial sites are {$-NH_2$, CO (Asp1−Ala2), N_{im} (His6), N_{im} (His13 or His14)}, {$-NH_2$, N^- (Asp1−Ala2), CO (Ala2−Glu3), N_{im}}, {$-NH_2$, N^- (Asp1−Ala2), N^- (Ala2−Glu3), N_{im}} and {$-NH_2$, N^- (Asp1−Ala2), N^- (Ala2−Glu3), N^- (Glu3−Phe4)}, respectively, in line with classical pH-induced deprotonation of the peptide backbone encountered in Cu(II) peptidic complexes formation. The structure proposed for component **II** is discussed with respect to another coordination model reported in the literature, that is, {CO (Ala2−Glu3), 3 N_{im}}. Cu(II) binding to the H6R-Aβ and D7N-Aβ peptides, where the familial H6R and D7N mutations have been linked to early onset of AD, has also been investigated. In case of the H6R mutation, some different structural features (compared to those encountered in the native [Cu^{II}(Aβ)] species) have been evidenced and are anticipated to be important for the aggregating properties of the H6R-Aβ peptide in presence of Cu(II).

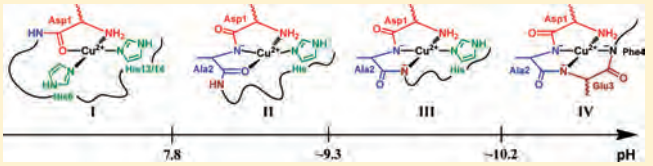

INTRODUCTION

Alzheimer's disease (AD) is the most common cause of dementia in the elderly population with an estimated prevalence of 30 million people worldwide, a number that is expected to quadruple in 40 years.[1] AD is a complex multifactorial neurodegenerative disease in which many genetic and environmental factors are involved. The underlying mechanisms of AD are not clear, but there is evidence and a relatively wide agreement that the so-called amyloid cascade is a key and early event in the development of AD. This hypothesis proposes an increased extracellular accumulation of a peptide, called amyloid-β (Aβ), which leads to its aggregation, first into oligomers, then into protofibrils and last into amyloid plaques, a hallmark of AD. This hypothesis suggests that the mismetabolisms of Aβ and of its precursor protein are initiating events in AD pathogenesis. Formation of Aβ aggregates would further instigate pathological events, including formation of intracellular neurofibrillary tangles (another hallmark of AD), disruption of synaptic connections, ultimately leading to neuronal cells death and dementia.[1−6] Aβ is typically a 39−43 residue polypeptide and consists of a hydrophilic N-terminal domain (1−28) and a C-terminal hydrophobic domain (29−39/43). In vivo, the most prevalent forms of Aβ consist of 40 (Aβ40) and 42 amino acids (Aβ42). The longer form Aβ42 is more prone to aggregation and more toxic to neurons than Aβ40, in agreement with the amyloid cascade hypothesis. Metal ions (Cu, Fe, Zn) have been proposed to play a key role in the development of AD. In vivo, in cello, and in vitro experiments strongly suggest that metal ions and in particular Cu ions are involved in AD. Cu ions can bind to Aβ and modulate its aggregation. Furthermore [Cu(Aβ)] oligomeric forms can catalyze the production of ROS (reactive oxygen species) in presence of physiological reducing agents (e.g., ascorbate), which finally leads to neuronal cells death (for reviews, see refs 7−14).

Copper coordination to the Aβ peptides has been proposed as an important event in the amyloid cascade and deciphering the Cu environment when bound to Aβ peptides is still a burning and controversial topic. At physiological pH, two equatorial binding modes coexist. The one predominant at lower pH is constituted of two equivalent sets of ligands (noted **Ia** and **Ib**), where the terminal $-NH_2$ (from Asp1), the CO from the Asp1−Ala2 peptide bond, a N from imidazole ring of His6 and from His13 (component **Ia**) or from His14 (component **Ib**) are involved.[15−19] The two components have been proposed to be in equilibrium in 1:1 ratio,[15,17] and thus in the following the mixture of **Ia** and **Ib** will be noted component **I**. However, a recent study reported

Received: August 10, 2011
Published: October 06, 2011

ACS Publications © 2011 American Chemical Society

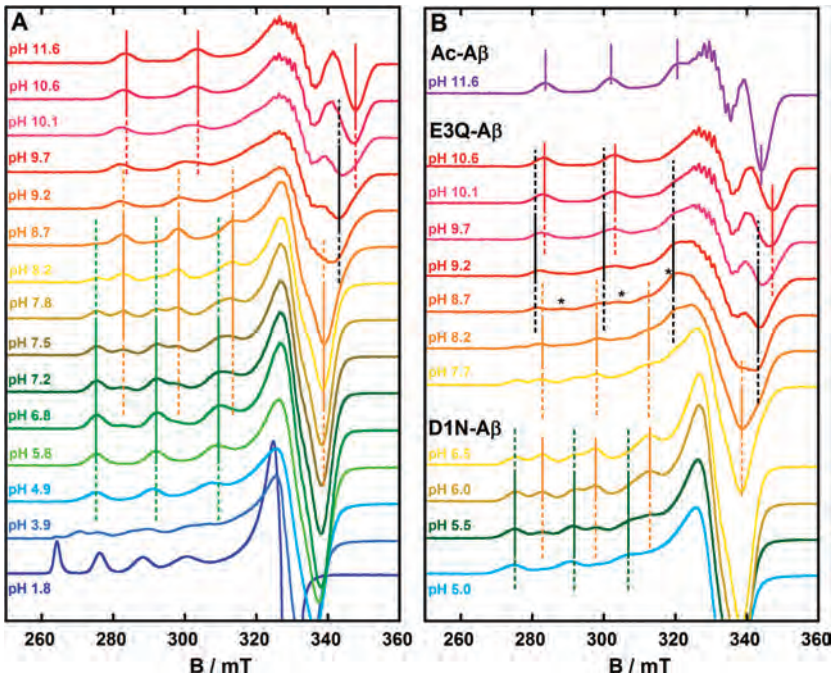

Figure 1. EPR spectra of [Cu^{II}(peptide)] complexes as a function of pH. Panel A: Peptide = Aβ16. Panel B: Peptide = D1N-Aβ, E3Q-Aβ, or Ac-Aβ. Component **I** is designated by green lines, component **II** by orange lines, component **III** by black lines and components **IV** and **IV′** by red and purple lines, respectively. Plain lines indicate pH values where a component is predominant in solution and dotted lines pH range where a component is present in solution but not predominant. [Cu^{II}(peptide)] = 1 mM in D_2O. ν = 9.5 GHz, amplitude modulation = 0.5 mT, microwave power = 20 mW. T = 110 K. * indicates the presence of a minor species, which is not detected in the EPR spectra of other [Cu^{II}(peptide)] species, with $g_{\|}$ = 2.17(8) and $A_{\|}$ = 160 × 10^{-4} cm^{-1} EPR parameters (see Supporting Information for identification of this species).

that a third component, where the two His involved in Cu(II) coordination are the His13 and His14, is also present, this third component (noted **Ic**) being more prone to formation of unstructured aggregates than **Ia** and **Ib**.[20] Regarding the second component (**II**), predominant at higher pH, there are two divergent hypotheses.[19] Mainly on the basis of S-band EPR and HYSCORE data on ^{13}C and ^{15}N isotopically labeled peptides, it was proposed that component **II** is made of the CO group from the Ala2−Glu3 peptide bond and the imidazole rings of the three His.[18] In the second proposition, also deduced from HYSCORE data on ^{13}C and ^{15}N isotopically labeled peptides[15] but from NMR data as well,[16] the $-NH_2$ terminal, the amidyl function N^- from the Asp1−Ala2 peptide bond, the CO from the Ala2−Glu3 peptide bond, and one among the three imidazole rings of His are the functions predominantly involved in equatorial Cu(II) binding. Regarding the apical positions, the debate is still open but involvement of carboxylate groups has been proposed in the literature.[15,16,18]

Here, we report a EPR, CD, and NMR study of Cu(II) binding to the Aβ peptide and to ten mutants that allow discrimination between the two proposed Cu(II) binding models in **II** (see above). Moreover, we describe the pH dependent Cu(II) binding to this series of peptides from pH 4 to 12. While such a pH range is not biologically pertinent, study performed outside the physiological range do help disentangling Cu(II) coordination features around physiological pH. Indeed, the Cu(II) peptidic species are generally obtained from each other by successive deprotonation (protonation) of the peptide when the pH is increased (decreased).[21,22] Moreover, such a wide study is of interest from a chemical point of view since it provides general rules for Cu(II) coordination to peptides. We thus characterized two new components (noted **III** and **IV**) at pH higher than 8.

In this study, the impact on Cu(II) binding properties of the two English (H6R) and Tottori−Japanese (D7N) mutations linked to early onset familial AD were also investigated. In vitro studies of Aβ40 and Aβ42 peptides incorporating either the H6R or the D7N mutations have evidenced that the two mutations alter Aβ assembly at its earliest stages, as well as monomer folding and oligomerization process. Moreover, it was shown that the oligomers of the mutated peptides are more toxic to cultured neuronal cells than the wild type oligomers.[23,24] Trace Cu(II) have not been taken into account in these studies but might influence the aggregation process. Moreover, His6 intervenes in Cu(II) binding and Asp7 is a putative Cu ligand in the wild-type peptide. These are the reasons why it is worth determining how the H6R and the D7N mutations can modify Cu(II) coordination in these rare familial forms of AD. Although beyond the scope of the present phenomenological study, it would be very important to relate the impact of these mutations on the biological properties of the peptides with the difference in the Cu(II) coordination described here.

RESULTS

1. EPR pH-Dependent Study of Cu(II) Binding to Aβ16 Peptides and Mutants. The shorter Aβ16 peptide is used in the present study. Number of previous works have unambiguously shown that it represents the minimum Aβ sequence involved in Cu(II) binding.[25−27] The pH-dependent EPR signature of Cu(II) binding to the Aβ16 peptide is shown in Figure 1 together with spectra of Cu(II) species obtained with the D1N-Aβ and E3Q-Aβ mutants and the N-terminally acetylated (Ac-Aβ) peptide at selected pH values. The EPR signatures of the [Cu^{II}(Aβ)]

dx.doi.org/10.1021/ic201739n |*Inorg. Chem.* 2011, 50, 11192–11201

Table 1. EPR Parameters of Components I−IV and I′−IV′ and of Other [$^{63}Cu^{II}$(peptide)] Complexes for Comparison

	I		II		III		IV				
peptide	$g_{\|}$ [a]	$A_{\|}$ [a]	$g_{\|}$ [a]	$A_{\|}$ [a]	$g_{\|}$ [a]	$A_{\|}$ [a]	$g_{\|}$ [a]	$A_{\|}$ [a]	pK_a(I/II) [b]	pK_a(II/III) [b]	pK_a(III/IV) [b]
human	2.26(2)	184	2.22(6)	161	2.19(1)	194	2.17(3)	203	7.8	9.3	10.2
D1N-Aβ	2.26(3)	180	2.23(0)	160	2.19(1)	194	2.17(4)	201	6.0	9.0	10.3
D7N-Aβ	2.26(2)	184	2.22(7)	160	2.18(8)	194	2.17(4)	197	7.7	9.1	10.6
E3Q-Aβ	2.26(3)	183	2.22(4)	161	2.19(0)	194	2.17(3)	201	7.6	8.5	9.7
E11Q-Aβ	2.26(5)	184	2.22(5)	161	2.18(7)	194	2.17(0)	202	7.5	9.3	10.1
H6A-Aβ	2.26(8)	185	2.22(8)	164			2.17(2)	202	7.3	9.6	
H6R-Aβ	2.26(6)	180	2.22(7)	162			2.17(1)	205	7.2	9.7	
H13A-Aβ	2.26(3)	180	2.23(0)	162			2.17(5)	202	7.5	9.5	10.2
H14A-Aβ	2.26(9)	182	2.22(7)	163			2.17(5)	202	7.5	9.6	10.4
DAHK[28]					2.19	199					
GGGGH[29]			2.23(0)	156	2.19(9)	200	2.17(1)	206			
GGGGG[29]							2.17(1)	206			
	I′		II′		III′		IV′				
Ac-Aβ	2.32(0)	168	2.27(3)	187	2.23(0)	171	2.19(1)	190	5.2	7.5	8.7
GGGTH[30]							2.20	200			

[a] Parallel spin Hamiltonian parameters were obtained directly from the experimental spectra and were calculated from the second and the third hyperfine lines in order to remove second-order effects. $A_{\|}$ parameters are given in 10^{-4} cm^{-1}. [b] pK_a values are roughly estimated from EPR spectra, and with the exception of pK_a(**I**/**II**) that can be estimated accurately, the two others pK_a values are given with an uncertainty of ±0.3 pH unit.

complexes are complicated and generally correspond to the superimposition of several components simultaneously present in solution at a given pH. This is particularly obvious at low pH (near pH 4), at physiological pH where two species coexist (the well-described components **I** and **II**, indicated by green and orange colors in Figure 1, respectively) and at pH near 10. In this latter case, two among the three coexisting components can be well identified: the first one is predominant at pH 8.7 (component **II**) and the other one is predominant above pH 10.6 (that will be noted component **IV**, in red in Figure 1). The third component (noted **III**, in black in Figure 1) is present only as a minor component and is thus difficult to identify. The EPR parameters determined for these four components (**I**−**IV**) are given in Table 1. Regarding the other [Cu^{II}(peptide)] complexes (peptide = Ac-Aβ, D1N-Aβ, E3Q-Aβ, D7N-Aβ, H6A-Aβ, H6R-Aβ, E11Q-Aβ, H13A-Aβ, and H14A-Aβ) studied here (see Figures S1−S3 in the Supporting Information), none of them with the exception of the [Cu^{II}(Ac-Aβ)] has significantly different EPR parameters compared to those of [Cu^{II}(Aβ16)] species (Table 1 and see below for details). Hence, components relative to [Cu^{II}(Ac-Aβ)] will be noted **I**′−**IV**′. Nevertheless, pK_a values corresponding to transition between the various components depend on the nature of the peptide involved in Cu(II) binding (Table 1). Note that the pK_a values are defined as the pH values where the EPR signatures of two components contribute equally to the EPR intensity and thus have been estimated by considering that only two components are simultaneously present in solution.

*a. Components **I** and **II**.* Regarding component **I**, there is now a consensus that the Cu(II) ion lies in an equatorial binding site made of the terminal amine $-NH_2$ group, the imidazole ring of His6, the one of His13 or His14 (in equilibrium) and a carbonyl function,[15−19] the apical position being likely occupied by a carboxylate group.[15,16,18] Species **II**, in which the Cu(II) coordination remains to be elucidated is characterized by EPR parameters that differ from those of component **I** by a concomitant decrease in the $g_{//}$ and $A_{//}$ and are classical for 3N1O or 4N binding site[31] (Table 1). The pK_a of the **I**/**II** transition is approximately 7.8, in line with previous studies.[32,33] In Figure 1, panel B, the EPR pH dependent signatures of Cu(II) bound to the D1N-Aβ mutant is reminded. While the EPR parameters of components **I** from [Cu^{II}(Aβ16)] and [Cu^{II}(D1N-Aβ)] complexes are very similar, the pK_a(**I**/**II**) value is approximately 6.0 in case of the [Cu^{II}-(D1N-Aβ)] complexes, thus significantly lower than that of the [Cu^{II}(Aβ16)] complexes. The D1N mutant was previously studied by the group of Szalai[33] and the decrease in the pK_a(**I**/**II**) was attributed to the breakage of a H-bond network (due to the replacement of the Asp1 anionic carboxylate by a neutral group), which would facilitate the deprotonation of a peptide function during the process leading to component **II**. However, in this pioneer work the peptide function undergoing the deprotonation was not identified.

Regarding the other Cu(II) complexes studied here, none of them with the exception of the [Cu^{II}(Ac-Aβ)] has significantly different EPR parameters compared to [Cu^{II}(Aβ16)]. This strongly suggests that none of the mutated residues is essential for creating the Cu(II) equatorial binding sites and that it can be replaced by an identical residue but located at another position in the peptide sequence. Differences between pK_a(**I**/**II**) values are observed and the most important ones are detected for the [Cu^{II}(H6A-Aβ)] and [Cu^{II}(H6R-Aβ)] complexes, pK_a(**I**/**II**) values being approximately 0.5 pH unit below that of [Cu^{II}(Aβ16)]. This suggests that even if His6 has been proposed to be always equatorially bound to the Cu(II) center in species **I**,[15,17] it can be replaced by either the His13 or His14 thus leading to the equatorial coordination of the His13-His14 diad. In such a coordination environment, geometric constraints accounting for formation of component **II** at a lower pH than in the native [Cu^{II}(Aβ16)] species may be anticipated. On the contrary, the H13A or H14A mutations have only a slight impact on the pK_a(**I**/**II**) values (Table 1), in line with the equilibrium between

dx.doi.org/10.1021/ic201739n |*Inorg. Chem.* 2011, 50, 11192–11201

these two His residues for one equatorial binding position previously proposed.[15,17]

*b. Component **III**.* Component **III** is hardly distinguishable in the pH dependent EPR traces of [Cu^{II}(Aβ16)], being only discernible by the fourth hyperfine feature (black line at B = 343 mT in Figure 1, panel A). Indeed, the three other hyperfine lines are mixed with those of components **II** and **IV** and cannot be well isolated. The reason for such a mixture between components **II**, **III**, and **IV** is likely close pK_a(**II**,**III**) and pK_a(**III**,**IV**) values. To better characterize component **III**, the E3Q mutant is helpful. Indeed, in the [Cu^{II}(E3Q-Aβ)] mutant, component **III** is more easily detected, pK_a(**II**/**III**) and pK_a(**III**/**IV**) values being sufficiently different (estimated to 8.5 and 9.7, respectively). Similar to what was proposed for the D1N-Aβ mutant, we can hypothesize that the Glu3 carboxylate function stabilizes a deprotonable function in its protonated form by H-bond interactions, and that in the [Cu^{II}(E3Q-Aβ)] complex, the H-bond network is broken leading to deprotonation of the function at a lower pK_a(**II**/**III**) value. It is worth noting that mutation of the two other carboxylate functions (leading to D7N and E11Q mutants) do not affect neither the EPR signatures of the corresponding Cu(II) complexes nor their pH dependence compared to [Cu^{II}(Aβ16)]. Parameters of component **III** are close to those observed when the Cu(II) is bound to the ATCUN motif (encountered in peptide with N-terminal XXH- sequence). In such species, the Cu(II) is bound via the $-NH_2$ terminal, the His and the two amidyl functions in between these two residues. For instance, such equatorial Cu(II) coordination is encountered in the N-terminal binding site of the serum albumin having the DAHK sequence.[28] Nevertheless, some minor differences are observed that can be attributed to the formation of three adjacent metallacycles in the ATCUN case, a structural feature that cannot be observed in the present case due to the position of the His compared to the $-NH_2$ group, the closest His residue being far from the terminal amine by 5 amino-acids. Such ATCUN type coordination in component **III** will be further confirmed by NMR studies (see below).

It is also worth noticing that component **III** cannot be detected in the EPR pH-dependent spectra of the [Cu^{II}(H6A-Aβ)] and [Cu^{II}(H6R-Aβ)] complexes. This suggests that His6 is more involved than His13 or His14 in Cu(II) binding in component **III**.

*c. Component **IV**.* The $g_{\|}$ and $A_{\|}$ parameters of component **IV** of [Cu^{II}(peptide)] complexes, with the exception of the [Cu^{II}-(Ac-Aβ)] are characteristic of a 4N equatorial binding mode,[31] where the Cu(II) ion is bound via the terminal $-NH_2$ and three amidyl functions. Indeed, very similar EPR parameters have been reported for the [Cu^{II}(GGGGG)] complex, where the $-NH_2$ is the sole Cu(II) anchoring function and thus where the Cu(II) equatorial site is completed by amidyl groups from adjacent peptide bonds.[29] Such Cu(II) coordination is often encountered in peptidic fragments where other potential ligands are replaced by amidyl functions adjacent to the $-NH_2$ anchoring point when the pH is increased. At high pH, the other possibility is to have a nitrogen atom from the imidazole ring of an His residues as the anchoring point and adjacent amidyl functions that entered is the Cu(II) coordination sphere.[22] This is encountered when the terminal $-NH_2$ is not available for Cu(II) binding, for instance when it is acetylated.[30] In this case, the EPR parameters are different from those observed here in the component **IV** but similar to those observed in component **IV**′ corresponding to complex [Cu^{II}(Ac-Aβ)] at high pH (Figure 1, panel B and Table 1). This agrees with the involvement of the N-terminal amine in equatorial Cu(II) coordination in [Cu^{II}(Aβ16)] at high pH. Note that involvement of the terminal $-NH_2$ function has already been identified by EPR and ENDOR experiments performed on labeled [Cu^{II}(^{15}N-(Asp1)-Aβ16] species.[15] A second consequence is that, Cu(II) center in component **IV** is likely bound by the terminal -NH_2 and the three adjacent amidyl functions while in component **IV**′ by one of the three His and three adjacent amidyl functions, the His residue(s) involved remaining to be identified.

d. [Cu^{II}(Ac-Aβ)] Species. Acetylation of the terminal amine lead to a series of new type of components that can be obtained from component **IV**′ by successive protonation of the amidyl functions, leading to a {$-N_{im}$, $2N^-$, X} equatorial binding site in **III**′ and {$-N_{im}$, N^-, X, Y} in **II**′ and {$-N_{im}$, X, Y, Z} in **I**′, where X, Y, and Z can be either His or CO ligands. Further identification of the exact nature of components **I**′−**IV**′ is beyond the scope of the present paper and is not physiologically relevant for the understanding of Cu(II) coordination to Aβ. Nevertheless, an important point to note is that EPR parameters of components **II**′ and **III**′ are very close to those of components **I** and **II**, respectively and that pK_a(**II**′/**III**′) is also very close to pK_a(**I**/**II**) (Table 1). As a consequence, the pH dependent EPR spectra of [Cu^{II}(Aβ16)] and [Cu^{II}(Ac-Aβ)] complexes will be by chance very similar near physiological pH. This may have led to misinterpretation of comparative EPR data of [Cu^{II}(Aβ16)] and [Cu^{II}(Ac-Aβ)] when recorded only near physiological pH and to the erroneous conclusion that $-NH_2$ is involved in Cu(II) apical position in component **I**.[34]

2. CD pH-Dependent Study of Cu(II) Binding to Aβ16 Peptides and Mutants. EPR is a powerful technique to determine the Cu(II) binding site but reveals information concerning only the equatorial plane. As a consequence, CD can be used to monitor structural modifications that occur outside from the first coordination shell and in apical position. pH-dependent CD spectra of four chosen examples of [Cu^{II}(peptide)] complexes that are representative of the four types of CD signatures obtained in the present study, are shown in Figure 2 ([Cu^{II}(Aβ16)], [Cu^{II}(Ac-Aβ)], [Cu^{II}(H6A-Aβ)], [Cu^{II}(E3Q-Aβ)]).

a. [Cu^{II}(Aβ16)] Type Family. pH dependent CD signatures of this family is shown in Figure 2, panel A. Weak d−d transitions are observed at λ = 670 and 590 nm, which increase in intensity upon increasing pH, reaching a maximum at a pH ∼7.5. A new d−d band at λ = 510 nm is observed when the pH is raised above 7.5. In the UV domain, the intensity of the λ = 315 and 285 nm bands increase from pH approximately 7 and 3, respectively. The former band has been attributed to amide to Cu(II) charge transfer transition (LMCT) while the latter to amine to Cu(II) LMCT. The band detected at λ = 265 nm, which has tentatively been attributed to imidazole to Cu(II) LMCT,[21] increases in intensity from pH approximately 8.5. pH dependent behavior of these features indicates that (i) $-NH_2$ is bound to Cu(II) from pH 3 and remains bound to Cu(II) at any higher pH, (ii) amidyl groups start to bind Cu(II) at pH approximately 7, and (iii) binding of amidyl functions to Cu(II) enhances the molar extinction coefficient of the His to Cu(II) LMCT and of the d−d transitions detected at 265 and 590 nm, respectively. The [Cu^{II}(H13A-Aβ)], [Cu^{II}(H14A-Aβ)] and [Cu^{II}(E11Q-Aβ)] complexes belong to this family (Supporting Information Figures S5 and S6) and thus behave very similarly to the [Cu^{II}(Aβ16)], suggesting that (i) both His13 and His14 are not simultaneously involved in Cu(II) binding in the whole pH range and that

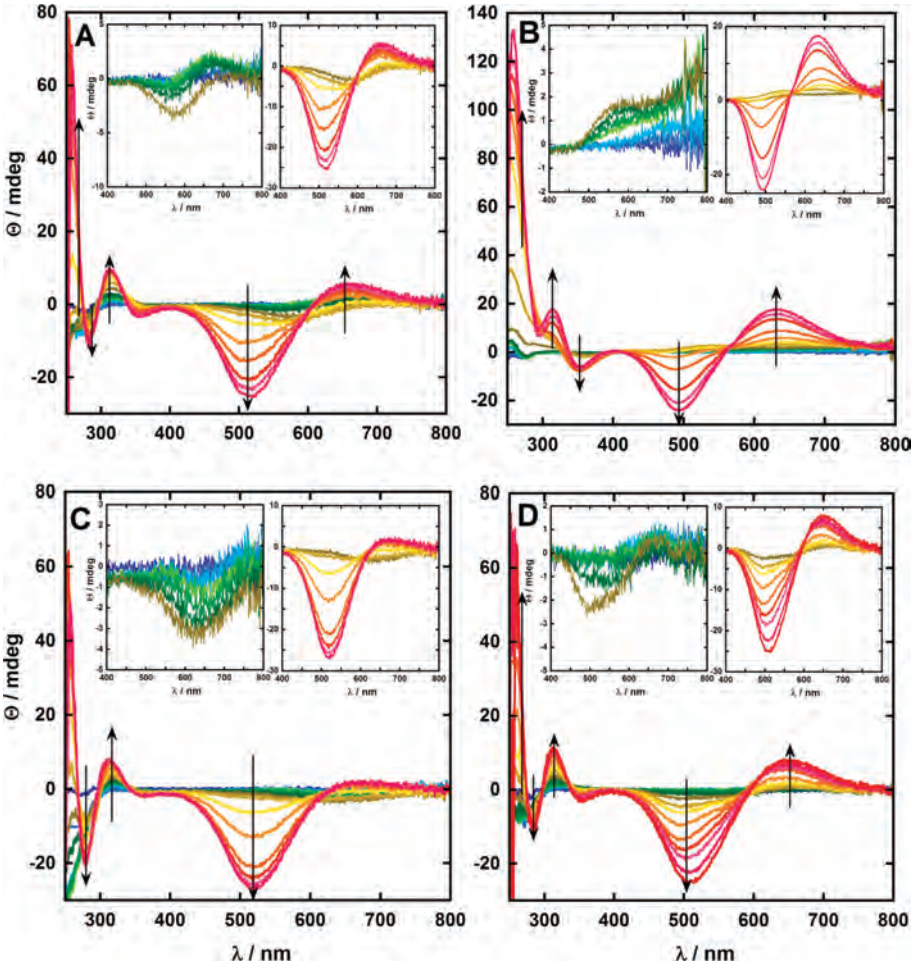

Figure 2. Effect of pH on the CD spectra of [Cu^{II}(peptide)] complexes, from pH approximately 3 (blue line) to pH approximately 12 (red line). Panel A: [Cu^{II}(Aβ16)]. Panel B: [Cu^{II}(Ac-Aβ)]. Panel C: [Cu^{II}(H6A-Aβ)]. Panel D: [Cu^{II}(E3Q-Aβ16)]. Left insets: pH from approximately 3 to approximately 7.5. Right insets: pH from approximately 7.5 to approximately 12. [Cu^{II}(peptide)] = 0.5 mM, ℓ =1 cm, T = 20 °C. Arrows indicate the formation of relevant bands with pH increase. For exact pH values see Supporting Information, Figures S4−S6.

(ii) carboxylate group from Glu11 is not an essential element of Cu(II) binding sites.

b. [Cu^{II}(Ac-Aβ)]. pH-dependent CD signature of [Cu^{II}(Ac-Aβ)] is unique compared to all the other [Cu^{II}(peptide)] complexes studied here (Figure 2, panel B). The continuous increase of bands at λ = 630, 490, 360, 315, and 265 nm is observed when the pH is increased. Two main differences with the [Cu^{II}(Aβ16)] data are the absence of the λ = 285 nm band characteristic of $-NH_2$ to Cu(II) LMCT, in line with acetylation of N-terminal amine and a significantly higher intensity of the λ = 265 nm band, especially at high pH, compared to all the others [Cu^{II}(peptide)] complexes, in agreement with the formation of binding sites centered on His anchoring residue, as previously proposed on the basis of the EPR data analysis.

c. [Cu^{II}(H6A-Aβ)]/[Cu^{II}(H6R-Aβ)] Type Family. These mutations lead to three mains differences in the pH-dependent CD signatures of the [Cu^{II}(peptide)] complexes (Figure 2, panel C and Supporting Information Figure S5), which are (i) a negative d−d band at λ = 630 nm from pH 3 to approximately 7.5; (ii) a more pronounced λ = 285 nm band, and (iii) a λ = 265 nm band, the growth of which begins in the negative part of the CD spectra from pH 3 to approximately 7.5 and the intensity of which remains weaker than in the [Cu^{II}(Aβ16)] type family complexes at higher pH. These modifications may be attributed to the simultaneous involvement of His13 and His14 in Cu(II) binding, a feature that is not detected in the [Cu^{II}(Aβ16)] type family (see above), thus leading to an important reshuffling of the peptide conformation. Sign change in the λ = 265 nm band at pH ~7.5 may also be interpreted as transition between the His13−His14 diad involved in Cu(II) coordination to only one His bound to Cu(II). These CD data are consistent with the EPR data, since it confirms that both His13 and His14 can be simultaneously bound to Cu(II). However, if the EPR traces of both [Cu^{II}(H6A-Aβ)] and [Cu^{II}(H6R-Aβ)] complexes are very close to that of the [Cu^{II}-(Aβ16)], their CD signatures differ significantly, in line with modifications occurring outer from the first coordination shell.

d. [Cu^{II}(E3Q-Aβ)] Type Family. The pH dependent CD spectra of Cu(II) complexes obtained with the triple E3QD7NE11Q mutants and the D1N, E3Q, and D7N mutants (Figure 2, panel D and Supporting Information Figures S4 and S6) are slightly different from that of the [Cu^{II}(Aβ16)] type family by having weaker d−d band intensities up to pH 7.5 (especially in the E3Q and E3QD7NE11Q cases) and then a stronger intensity at λ = 650 nm at higher pH, except for the [Cu^{II}(D1N)] complex that exhibits a weaker intensity. This may reflect involvement of the Glu3 and Asp7 residues in apical Cu(II) binding or an outer first

dx.doi.org/10.1021/ic201739n |*Inorg. Chem.* 2011, 50, 11192–11201

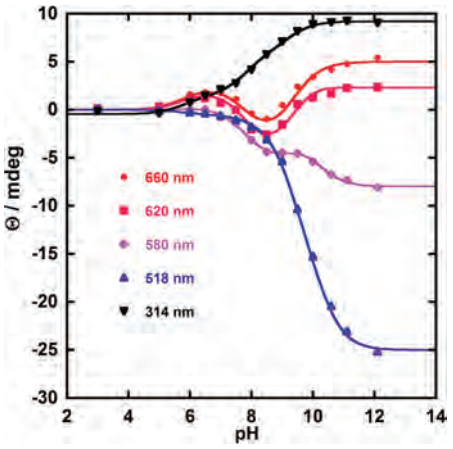

Figure 3. pH-dependent CD absorbance of $[Cu^{II}(A\beta16)]$ complex at λ = 660 (red plain circles), 620 (pink plain squares), 580 nm (purple plain diamonds), 518 nm (blue plain triangles), and 314 nm (black plain triangles). Solid lines are the fits of the curves with pK_a = 5.8, 7.9, 9.3, and 10.3. $[Cu^{II}(A\beta16)]$ = 0.5 mM, ℓ =1 cm, T = 20 °C.

sphere contribution of the Glu3 and Asp7 residues, for instance by creating salt bridge with the Arg5 residue. Furthermore, the CD data obtained here are in line with contribution of the Asp1 residue in Cu(II) apical position even if the different pH-dependent CD signature of the $[Cu^{II}(D1N\text{-}A\beta)]$ complex is mainly due to the low pK_a(**I**/**II**) value.

e. pK_a Determination. Using EPR data it was possible to evaluate the pK_a between various components. As exemplified in Figure 3 in the case of the $[Cu^{II}(A\beta16)]$ complex, this could also be achieved by simulation of the CD data. Simulations of the pH-dependent absorbance curves at several selected wavelengths with a unique set of pK_a values were performed and pK_a(**I**/**II**) = 7.9, pK_a(**II**/**III**) = 9.3, and pK_a(**III**/**IV**) = 10.3 values were found. These results were fully consistent with EPR data suggesting that no significant pH drift occurs upon freezing the EPR samples. In the course of simulation, it appears that more than 3 pK_a values were necessary to correctly fit the curves. More precisely, below pH 6, the intensities of the λ = 620 and 660 nm undergo significant increase. The pK_a value corresponding to transition between component **I** and this newly detected component (noted **0**) is estimated to be 5.8. Regarding the EPR data, it appears that the EPR signature of component **0** is indiscernible to that of component **I**. Hence, a possible explanation is that this pK_a corresponds to the deprotonation of the third Cu(II) unbound His leading to modification of peptide arrangement but not to direct change in the equatorial Cu(II) coordination.

3. NMR Studies of Cu(II) Binding to Aβ in Component III and to H6R-Aβ Mutant in Components I and II. In an attempt to better characterize the new components **III** and **IV**, we used NMR spectroscopy that was previously revealed to be a powerful technique to better disentangle Cu(II) binding to Aβ peptides[16,32] and to others peptides or proteins.[35,36] Indeed the paramagnetism of the Cu(II) ion induces broadening of NMR features that depends on the proximity of the Cu(II) ion. Hence, it is possible to map which residues are affected by the presence of Cu(II) and thus involved in its coordination. ^{13}C NMR spectra of the apo-Aβ and holo-Aβ (0.3 equiv of Cu(II)) recorded at pH 9.8 (where component **III** is predominant) are compared to those of the apo-Aβ and holo-Aβ (0.1 equiv of Cu(II)) at pH 8.7 (Figure 4). Cu(II)-induced broadening of the ^{13}C peaks are weaker at pH 9.8

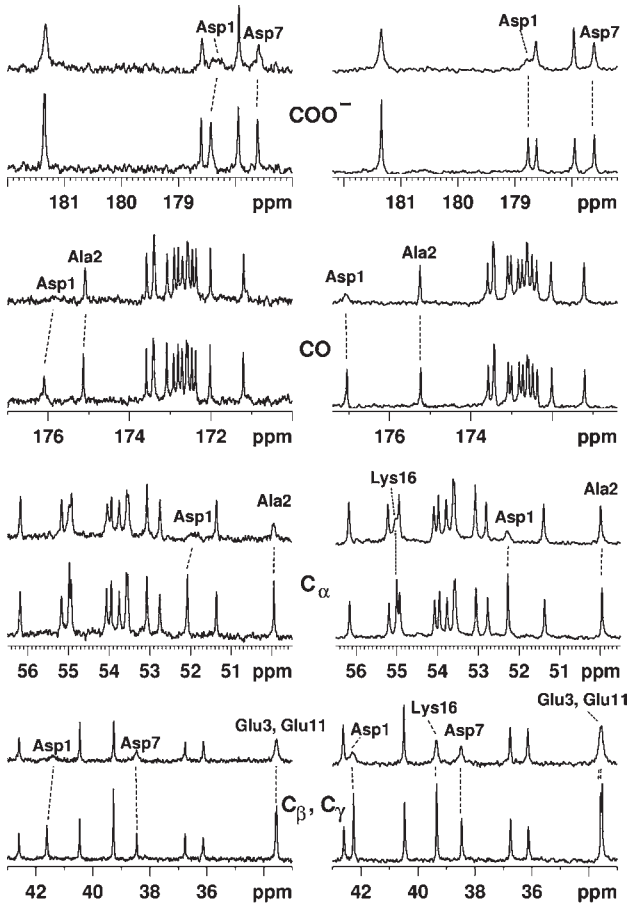

Figure 4. $^{13}C\{^1H\}$ NMR spectra of 10 mM Aβ peptide in D_2O (bottom spectra) and in presence of 0.1 equiv of Cu(II) (top spectra) at pH 8.7 (left) and of 0.3 equiv of Cu(II) (top spectra) at pH 9.8 (right). T = 25 °C, ν = 125.8 MHz. Shift of some peaks is due to slight modification in the pH value induced by Cu(II) addition.

although the Cu(II) stoichiometry is 3-fold higher. Moreover, no new ^{13}C signals, with the exception of the C_α and C_β of Lys16, are affected by the Cu(II) addition at pH 9.8 compared to pH 8.7. This behavior is attributed to the formation of a "ATCUN" type Cu(II) binding motif $\{-NH_2, 2N^-, N_{im}\}$ in component **III**. Indeed, it was previously evidenced that in such a coordination site, Cu(II) exchange between peptides is too slow to affect all the peptides present in solution. On the contrary, Cu(II) stays bound to a portion of peptide and then lead to the total disappearance of its NMR signals.[28] Thus in the present case, Cu(II) effect on Aβ NMR peaks corresponding to component **III** is not observable. The broadening effect observed is due to the presence of a small portion of component **II** (in pH-dependent equilibrium with component **III**). As a direct consequence, NMR revealed inappropriate for the study of components **III** and **IV**.

The H6R mutation is a familial mutation that was associated with early onset of AD. Moreover, significant modifications of the pH-dependent CD signature of $[Cu^{II}(H6R\text{-}A\beta)]$ complexes were observed compared to that of $[Cu^{II}(A\beta16)]$. These are the reason why components **I** and **II** of the $[Cu^{II}(H6R\text{-}A\beta)]$ complexes were also studied by ^{13}C NMR. In general, Cu(II) effect on the ^{13}C NMR spectra of the H6R mutant and on the Aβ16 peptide[16] are similar (Supporting Information Figure S7). More precisely, binding of both His13 and His14 in component **I** (see

dx.doi.org/10.1021/ic201739n |*Inorg. Chem.* 2011, 50, 11192–11201

CD part) may induce the binding of the CO function in between the two His residues, as proposed by calculations.[37] However, such a binding do not change the impact of Cu(II) to the ^{13}C NMR spectra of H6R-Aβ compared to Aβ16. Indeed, coordination of CO function from His residues was previously detected in the Aβ16 case and attributed to equilibrium in solution between $\{-NH_2, CO (Asp1), 2N_{Im}\}$ and $\{-NH_2, CO (His), 2N_{Im}\}$.[16] The main differences observed on the CO and C_α regions at pH 8.6, where component **II** is predominant, are shown in Figure 5. Both the CO functions and C_α atoms from His13 and His 14 residues are more broadened in the case of the H6R mutant. However, broadening of the CO and C_α ^{13}C atoms from the Ala2 residue, previously attributed to coordination of the amidyl function from the Asp1−Ala2 peptide bond, is still observed. Thus, this suggests that the deprotonation of the Asp1−Ala2 peptide bond also occurs in the H6R mutant but in this latter case, it does not induce the binding of the adjacent CO function (from Ala2 to Glu3). Indeed, CO functions from His residues may principally be involved in Cu(II) binding.

DISCUSSION

1. Coordination Sites of Cu(II) in Components I−IV. The proposed equatorial Cu(II) binding sites in components **I**−**IV** are shown in Scheme 1. Component **I** has been proposed by several groups.[15−19] In this species, the Cu(II) center is bound via the terminal amine, two His residues and a CO function mainly originating from the Asp1−Ala2 peptide bond.

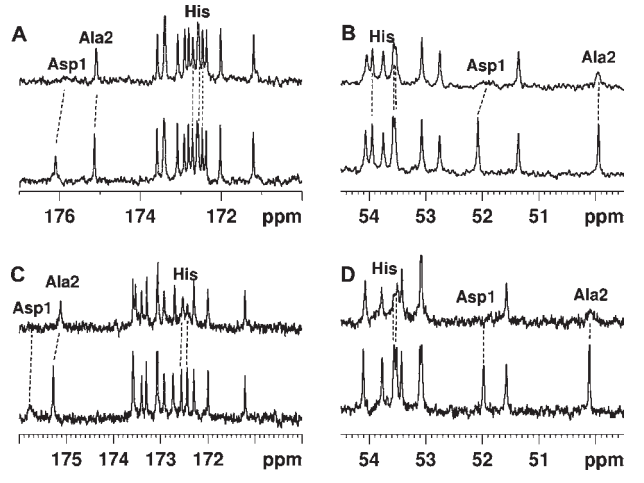

Figure 5. $^{13}C\{^1H\}$ NMR spectral regions of 10 mM Aβ16 peptide in D_2O (bottom spectra) and in presence of 0.1 equiv of Cu(II) (top spectra) at pH 8.7 (panels A and B) and of 5 mM H6R-Aβ peptide in D_2O (bottom spectra) and in presence of 0.05 equiv. of Cu(II) (top spectra) at pH 8.6 (panels C and D) T = 25 °C, ν = 125.8 MHz. Shift of some peaks is due to slight modification in the pH value induced by Cu(II) addition.

While consensus has been recently reached on Cu(II) coordination sphere in component **I**, this is not the case for component **II**. Indeed two models have principally appeared in the last years. In the first one, Cu(II) is bound via the carbonyl function from Ala2−Glu3 and the imidazole rings of the three His (model noted 1)[17,18] and in the second one, Cu(II) is bound via the terminal amine, the adjacent amide function from Asp1−Ala2, one out of the three His and the CO function from Ala2−Glu3 (model noted 2).[15,16] In the present study, new key insights have been obtained regarding the Cu(II) binding sphere in component **II**. First, an interesting feature is that Cu(II) complexes of the three H6A, H13A, and H14A mutants have EPR parameters identical to those of $[Cu^{II}(A\beta16)]$, indicating that the simultaneous equatorial coordination of the three His to the Cu(II) center is unlikely. Otherwise, this would imply that in complexes obtained with the His mutants, the His residues is replaced by a ligand that would influence the Cu(II) electronic properties in a very similar way, a possibility that we cannot however fully ruled out. Second, component **III** is identified as $\{-NH_2, 2N^-, N_{im}\}$ (see below) and thus it is difficult to rationalize why the terminal $-NH_2$ amine bound to Cu(II) in components **I** and **III**, will be unbound in the intermediate component **II**. Third, transition from components **I**−**II** (and to **III** and **IV**) is pH driven and thus should be concomitant to deprotonation of peptide function. In case of model 1, all the residues that can undergo deprotonation (i.e., the three His residues) are already deprotonated at pH below the pK_a(**I**/**II**) value and hence this model fails to explain the effect of pH in transition from **I** to **II**. Fourthly, contrarily to model 2, model 1 does not explain the variation in the pK_a(**I**/**II**) and pK_a(**II**/**III**) observed in $[Cu^{II}(D1N\text{-}A\beta)]$ and $[Cu^{II}(E3Q\text{-}A\beta)]$ complexes, respectively (see below). Fifthly, intervention of CO from Ala2−Glu3 preferentially to that of another peptide bond remains unexplained in model 1 whereas the deprotonation of the adjacent Asp1−Ala2 amide bond in model 2 justifies the intervention of the Ala2−Glu3 CO function in Cu(II) binding. Lastly, the EPR parameters of the very simple $[Cu^{II}(GGGGH)]$ complex (see Table 1), containing only one His residues in its sequence, are virtually identical to those found here for components **II**−**IV**, indicating that only one His can be bound to Cu(II) in components **II** and **III**.[29]

Regarding component **III**, EPR parameters, as well as NMR data support an "ATCUN" type Cu(II) site $\{-NH_2, 2N^-, Nim\}$. A $\{-NH_2, 3N^-\}$ Cu(II) equatorial site is proposed for component **IV** based on the EPR parameters and the difference with EPR signature of $[Cu^{II}(Ac\text{-}A\beta)]$. These propositions are in line with those previously reported by Kowalik et al. in their pioneer work,[21] except for component **IV** that was identified as $\{-N_{im}, 3N^-\}$. Moreover, in the present study attribution of each equatorial binding atoms has been proposed, that is, **I** = $\{-NH_2$, CO

Scheme 1. Proposed Equatorial Cu(II) Binding Sites of $[Cu^{II}(A\beta)]$ as a Function of pH

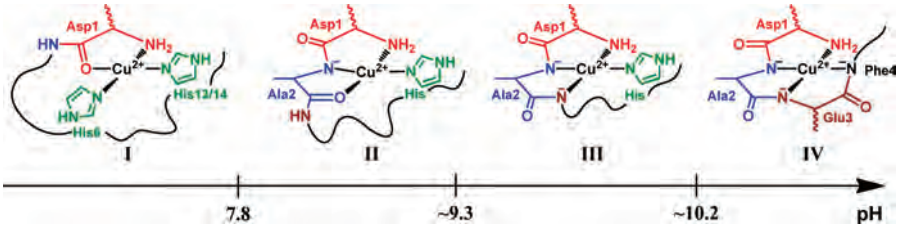

dx.doi.org/10.1021/ic201739n |Inorg. Chem. 2011, 50, 11192–11201

Scheme 2. D1N Mutation Decreases the pKa(I/II) Value by Precluding the $COO^- \cdots H-N$ (Asp1−Ala2) Interaction (7-Membered Metallacycle) while the E3Q Mutation Decreases the pKa(II/III) Value by Precluding the $COO^- \cdots H-N$ (Ala2−Glu3) Interaction (7-Membered Metallacycle)

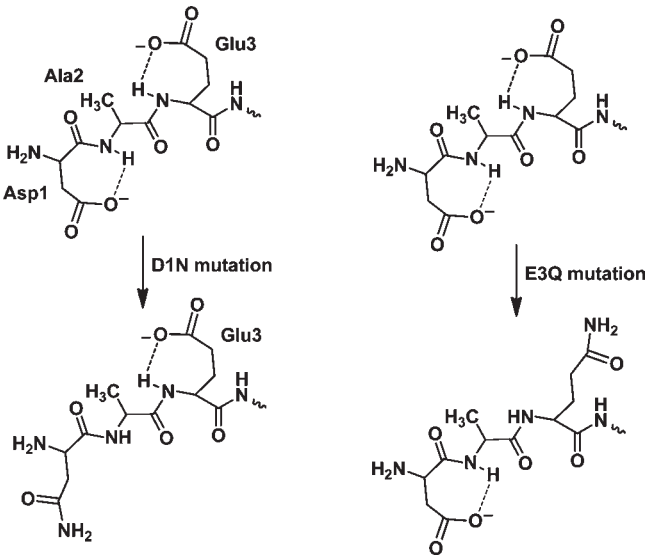

(Asp1−Ala2), N_{im} (His6), N_{im} (His13 or His14)}, **II** = {$-NH_2$, N^- (Asp1−Ala2), CO (Ala2−Glu3), N_{im}}, **III** = {$-NH_2$, N^- (Asp1−Ala2), N^- (Ala2−Glu3), N_{im}}, and **IV** = {$-NH_2$, N^- (Asp1−Ala2), N^- (Ala2−Glu3), N^- (Glu3−Phe4)}

Regarding involvement of carboxylate groups in Cu(II) apical position, the CD data obtained are in line with previous propositions that suggest a preferential role of the Asp1 residue.[15,16,18] Implication of the Glu3, Asp7, and Glu11 carboxylate groups in equilibrium with the one of Asp1 was also suggested for component **I**.[16] The CD data obtained here agree with this possibility except for the Glu11 residue, for the involvement of which no evidence was found.

D1N and E3Q mutations induced change in pK_a values between **I**/**II** and **II**/**III**, respectively (Table 1). More precisely, D1N mutation decrease the pK_a(**I**/**II**) value by more than one pH unit and the E3Q mutation decrease the pK_a (**II**/**III**) by more than 0.5 pH unit (Table 1). As previously pointed out,[33] this may be related to the breakage of H-bond network when carboxylate functions are modified to amide and subsequent easier deprotonation of peptide functions, here identified as the Asp1−Ala2 and Ala2−Glu3 peptide bonds, respectively. This is illustrated in Scheme 2, where the interventions of Asp1 and Glu3 are exemplified on the basis of model 2 for component **II**.

2. Coordination of Cu(II) to the H6R and D7N Familial Mutants. Among the various mutants studied here, Cu(II) coordination to the two H6R and D7N familial mutants linked to early onset of AD were investigated. While, regarding to Cu(II) coordination, the D7N mutation have no significant impact, the [Cu^{II}(H6R-Aβ)] complexes show differences with [Cu^{II}(Aβ16)]. More precisely, the pK_a(**I**/**II**) is significantly lower (about 0.5 pH unit) in the former case than in the latter, implying that at physiological pH the two components **I** and **II** will be differently distributed. More importantly, Cu(II) is differently bound in both components **I** and **II** of [Cu^{II}(H6R-Aβ)] and [Cu^{II}(Aβ)]. Proposed Cu(II) equatorial binding sites of [Cu^{II}(H6R-Aβ)] complexes are shown in Scheme 3. The most striking difference

Scheme 3. Proposed Equatorial Cu(II) Binding Sites of [Cu^{II}(H6R-Aβ)] as a Function of pH

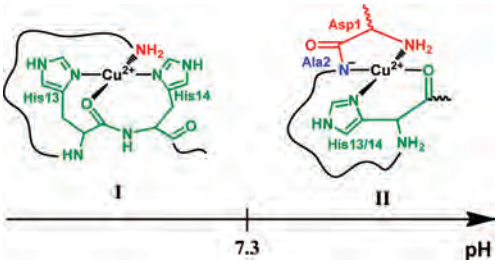

with [Cu^{II}(Aβ16)] is due to the concomitant involvement of His13 and His14 in Cu(II) binding in **I**, leading to outer first coordination shell effects observed by CD. Such equatorial binding of the His13-His14 diad (as minor form) in [Cu^{II}(Aβ16)] species compared to coordination of the His6 plus His13 or His14 (as major form) has been recently proposed to be linked to formation of amorphous aggregates.[20] In the [Cu^{II}(H6R-Aβ)] species, only the His13-His14 diad does intervene in Cu(II) equatorial binding in component **I**, and thus, the H6R mutation may be anticipated to be responsible of formation of only amorphous aggregates. In component **II**, intervention of CO from His13-His14 and His14-Gln15 peptide bonds in Cu(II) equatorial binding may also explained why component **III** is not detected in [Cu^{II}(H6R-Aβ)] complexes. Indeed, decoordination of the CO and the adjacent imidazole ring from His13 or His14 (forming a 6-membered metallacycle) residues may be concomitant, thus leading directly to a component **IV** (identical to the one obtained in case of the [Cu^{II}(Aβ)] species) from component **II**. Lastly, the [Cu^{II}(H6R-Aβ)] and [Cu^{II}(H6A-Aβ)] complexes have the same spectroscopical signatures implying that nature of the replacing residue in the H6 mutant is not a key factor.

CONCLUDING REMARKS

In the present paper, we reported the pH-dependent study of Cu(II) coordination to the Aβ peptide and to a series of mutants. While results obtained here are in perfect agreement with the Cu(II) equatorial binding site previously proposed in the literature for component **I** {$-NH_2$, CO (Asp1−Ala2), 2 N_{im}}, they also strongly supports a {$-NH_2$, N^-, CO (Ala2−Glu3), N_{im}} site in component **II**. Cu(II) complexes outside the physiological pH range have also been studied for expanding the number of spectroscopic references of Cu(II) peptidic species. Among the various mutants studied, the two familial H6R and D7N mutants were investigated and while the D7N mutation does not impact significantly Cu(II) coordination to Aβ, the H6R one leads to modification in Cu(II) binding that may also influence the peptide aggregating properties. During the course of these studies, the EPR and CD revealed to be complementary spectroscopies. Indeed, while EPR is a powerful technique to determine the Cu(II) equatorial environment, CD was very useful in disentangling effects outside the first coordination shell and for instance lead to the detection of a new species near pH 5.5.

EXPERIMENTAL SECTION

1. Sample Preparation. Studies were performed in H_2O or in D_2O. However, for clarity and consistency, we decided to use the notation pH even when the measurements were made in D_2O. pD was

dx.doi.org/10.1021/ic201739n |Inorg. Chem. 2011, 50, 11192–11201

measured using a classical glass electrode according to pD = $pH_{reading}$ + 0.4, and the pD value was adjusted according to ref 38 to be in ionization conditions equivalent to those in H_2O.

Aβ16 peptide (sequence DAEFRHDSGYEVHHQK and referred to as Aβ in the following), Ac-Aβ peptide corresponding to the N-terminally acetylated Aβ peptide, the D1N-Aβ (sequence NAEFRHDSGYEVHHQK), E3Q-Aβ (sequence DAQFRHDSGYEVHHQK), H6R-Aβ (sequence DAEFRRDSGYEVHHQK), H6A-Aβ (sequence DAEFRADSGYEVHHQK), D7N-Aβ (sequence DAEFRHNSGYEVHHQK), E11Q-Aβ (sequence DAEFRHDSGYQVHHQK), H13A-Aβ (sequence DAEFRHDSGYEVAHQK), H14A-Aβ (sequence DAEFRHDSGYEVHAQK), and the triple E3QD7NE11Q-Aβ C-terminally protected Aβ peptide (sequence DAQFRHNSGYQVHHQK-NH_2) were bought from GeneCust (Dudelange, Luxembourg) with purity grade >98%.

Stock solutions of peptide were prepared by dissolving the powder in Milli-Q water or in D_2O (resulting pH ~2). Peptide concentration was then determined by UV−visible absorption of Tyr10 considered as free tyrosine ($(\varepsilon_{276}$- $\varepsilon_{296}) = 1410\ M^{-1}cm^{-1}$) and the solution was diluted down to the appropriate concentration in peptide.

pH was adjusted using NaOH/HCl (H_2O) or NaOD/DCl (D_2O). All pH values are given with a ± 0.2 pH unit error.

a. Circular Dicroism (CD) Samples. Stock solution of peptide was diluted down to 0.5 mM in pure Milli-Q water; 0.9 equiv of Cu^{II} was added from 0.1 M $Cu(SO_4)$ stock solution.

b. Electron Paramagnetic Resonance (EPR) Samples. Stock solution of peptide was diluted down to 1.0 mM in D_2O; 0.9 equivalent of $^{63}Cu^{II}$ was added from 0.1 M $^{63}Cu(NO_3)_2$ stock solution. Samples were frozen in quartz tube, with addition of 10% glycerol as a cryoprotectant.

c. Nuclear Magnetic Resonance (NMR) Samples. Stock solution of H6R-Aβ peptide was diluted to about 5 mM in D_2O. Substoichiometric quantity (~0.05 equiv) of Cu^{II} from $Cu(SO_4)$ in D_2O was added. Cu^{II} to H6R-Aβ ratio was reduced to a minimum in the free peptide solution by working at 10 mM peptide concentration without buffer that is the primary source of paramagnetic contamination. Indeed a too high Cu^{II} to Aβ ratio would induce an uncontrolled broadening of NMR signals, a problem that may contributes to the loss of signals in the apo-peptide solution in previous studies.[39,40] Substoichiometric Cu^{II} ratio (0.05 equiv of Cu^{II} per Aβ peptide) was used. Indeed, this ratio is large enough to induce selective broadening of specific residues of all the peptides present in solution (because of fast exchange of Cu^{II} between peptides).

2. Spectroscopic Measurements. *a. Circular Dichroism (CD).* CD spectra were recorded on a JASCO circular dichroism spectrometer at 20 °C. Data were collected with a 1 nm sampling interval and 2 scans were averaged and a baseline spectrum was subtracted for each spectrum.

b. Electron Paramagnetic Resonance (EPR). EPR data were recorded using an Elexsys E 500 Bruker spectrometer, operating at a microwave frequency of approximately 9.5 GHz. All spectra were recorded using a microwave power of 20 mW across a sweep width of 150 mT (centered at 310 mT) with a modulation amplitude of 0.5 mT. Experiments were carried out at 110 K using a liquid nitrogen cryostat.

c. Nuclear Magnetic Resonance (RNMR). 1D ^1H and ^{13}C experiments and 2D experiments were recorded on a Bruker Avance 500 spectrometer equipped with a 5 mm triple resonance inverse Z-gradient probe (TBI ^1H, ^{31}P, BB) and a Bruker Avance 600 spectrometer equipped with a 5 mm triple resonance inverse (TCI ^1H, ^{13}C, ^{15}N) Z-gradient cryoprobe, respectively. All chemical shifts are relative to tetramethylsilane. 1D-NMR and 2D-NMR spectra were collected at 298 and 288 K in pure D_2O, respectively. Accumulation lasts c.a. Sixteen hours for the $^{13}C\{1H\}$ NMR experiments and 24 h for the 2D $^1H-^1H$ TOCSY, $^1H-^{13}C$ HSQC, and $^1H-^{13}C$ HMBC experiments.

All the ^1H and ^{13}C signals were assigned on the basis of chemical shifts, spin−spin coupling constants, splitting patterns and signal intensities, and by using $^1H-^1H$ TOCSY, $^1H-^{13}C$ HSQC, and $^1H-^{13}C$ HMBC experiments.

■ ASSOCIATED CONTENT

Ⓢ Supporting Information. pH-dependent EPR and CD spectra of [Cu^{II}(peptide] complexes, ^{13}C NMR spectra of H6R-Aβ, and assignments of the ^1H and ^{13}C signals of the H6R-Aβ peptide. This material is available free of charge via the Internet at http://pubs.acs.org.

■ AUTHOR INFORMATION

Corresponding Author

*E-mail: christelle.hureau@lcc-toulouse.fr. Phone: (+33) 5 61 33 31 62. Fax: (+33) 5 61 55 30 03.

Author Contributions

†These authors contributed equally to this work.

■ ACKNOWLEDGMENT

Authors thank the ANR (Agence Nationale de la Recherche), ANR Grant Neurometals NT09-488591. We thank Dr. L. Frémond for earlier results obtained on Cu(II) binding to H13A-Aβ and H14A-Aβ, Drs. L. Sabater, G. La Penna and P. Dorlet for fruitful discussions. Charles-Louis Serpentini is acknowledged for its participation in recording the CD data.

■ REFERENCES

(1) Holtzman, D. M.; Morris, J. C.; Goate, A. M. *Sci. Transl. Med.* **2011**, *3*, 77sr1.
(2) Castellani, R. J.; Smith, M. A. *J. Pathol.* **2011**, *224*, 147–152.
(3) Hardy, J.; Selkoe, D. J. *Science* **2002**, *298*, 789–791.
(4) Maccioni, R. B.; Muñoz, J. P.; Barbeito, L. *Arch. Med. Res.* **2001**, *32*, 367–381.
(5) Simón, A. M.; Frechilla, D.; del Rio, J. *Rev. Neurol.* **2010**, *50*, 667–675.
(6) Cappai, R.; Barnham, K. J. *Neurochem. Res.* **2008**, *33*, 526–532.
(7) Adlard, P. A.; Bush, A. I. *J. Alzheimer Dis.* **2006**, *10*, 145–163.
(8) Bush, A. I. *Trends Neurosci.* **2003**, *26*, 207–214.
(9) Cuajungco, M. P.; Faget, K. Y. *Brain Res. Rev.* **2003**, *41*, 44–56.
(10) Faller, P.; Hureau, C. *Dalton Trans.* **2009**, 1080–1094.
(11) Hureau, C.; Faller, P. *Biochimie* **2009**, *91*, 1212–1217.
(12) Kozlowski, H.; Janicka-Klos, A.; Brasun, J.; Gaggelli, E.; Valensin, D.; Valensin, G. *Coord. Chem. Rev.* **2009**, *253*, 2665–2685.
(13) Molina-Holgado, F.; Hider, R. C.; Gaeta, A.; Williams, R.; Francis, P. *Biometals* **2007**, *20*, 639–654.
(14) Smith, D. G.; Cappai, R.; Barnham, K. J. *Biochim. Biophys. Acta* **2007**, *1768*, 1976–1990.
(15) Dorlet, P.; Gambarelli, S.; Faller, P.; Hureau, C. *Angew. Chem., Int. Ed.* **2009**, *48*, 9273–9276.
(16) Hureau, C.; Coppel, Y.; Dorlet, P.; Solari, P. L.; Sayen, S.; Guillon, E.; Sabater, L.; Faller, P. *Angew. Chem., Int. Ed.* **2009**, *48*, 9522–9525.
(17) Drew, S. C.; Noble, C. J.; Masters, C. L.; Hanson, G. R.; Barnham, K. J. *J. Am. Chem. Soc.* **2009**, *131*, 1195–1207.
(18) Drew, S. C.; Masters, C. L.; Barnham, K. J. *J. Am. Chem. Soc.* **2009**, *131*, 8760–8761.
(19) Drew, S. C.; Barnham, K. J. *Acc. Chem. Res.* **2011**, DOI: 10.1021/ar200014u.
(20) Shin, B.-k.; Saxena, S. *J. Phys. Chem. A* **2011**, *115*, 9590–9602.
(21) Kowalik-Jankowska, T.; Ruta, M.; Wisniewska, K.; Lankiewicz, L. *J. Inorg. Biochem.* **2003**, *95*, 270–282.
(22) Kozlowski, H.; Bal, W.; Dyba, M.; Kowalik-Jankowska, T. *Coord. Chem. Rev.* **1999**, *184*, 319–346.
(23) Ono, K.; Condron, M. M.; Teplow, D. B. *J. Biol. Chem.* **2010**, *285*, 23186–23197.

(24) Hori, Y.; Hashimoto, T.; Wakutani, Y.; Urakami, K.; Nakashima, K.; Condron, M. M.; Tsubuki, S.; Saido, T. C.; Teplow, D. B.; Iwatsubo, T. *J. Biol. Chem.* **2007**, *282*, 4916–4923.
(25) Karr, J. W.; Kaupp, L. J.; Szalai, V. A. *J. Am. Chem. Soc.* **2004**, *126*, 13534–13538.
(26) Minicozzi, V.; Stellato, F.; Comai, M.; Dalla Serra, M.; Potrich, C.; Meyer-Klaucke, W.; Morante, S. *J. Biol. Chem.* **2008**, *283*, 10784–10792.
(27) Syme, C. D.; Nadal, R. C.; Rigby, S. E.; Viles, J. H. *J. Biol. Chem.* **2004**, *279*, 18169–18177.
(28) Hureau, C.; Eury, H.; Guillot, R.; Bijani, C.; Sayen, S.; Solari, P. L.; Guillon, E.; Faller, P.; Dorlet, P. *Chem.—Eur. J.* **2011**, *17*, 10151–10160.
(29) Várnagy, K.; Szabó, J.; Sóvágó, I.; Malandrinos, G.; Nick, H.; Sanna, D.; Micera, G. *J. Chem. Soc., Dalton Trans.* **2000**, 467–472.
(30) Hureau, C.; Charlet, L.; Dorlet, P.; Gonnet, F.; Spadini, L.; Anxolabéhère-Mallart, E.; Girerd, J.-J. *J. Biol. Inorg. Chem.* **2006**, *11*, 735–744.
(31) Peisach, J.; Blumberg, W. E. *Arch. Biochem. Biophys.* **1974**, *165*, 691–708.
(32) Eury, H.; Bijani, C.; Faller, P.; Hureau, C. *Angew. Chem., Int. Ed.* **2011**, *50*, 901–905.
(33) Karr, J. W.; Szalai, V. A. *J. Am. Chem. Soc.* **2007**, *129*, 3796–3797.
(34) Sarell, C. J.; Syme, C. D.; Rigby, S. E.; Viles, J. H. *Biochemistry* **2009**, *48*, 4388–4402.
(35) Rasia, R. M.; Bertoncini, C. W.; Marsh, D.; Hoyer, W.; Cherny, D.; Zweckstetter, M.; Griesinger, C.; Jovin, T. M.; Fernández, C. O. *Proc. Natl. Acad. Sci. U.S.A.* **2005**, *102*, 4294–4299.
(36) Gaggelli, E.; Bernardi, F.; Molteni, E.; Pogni, R.; Valensin, D.; Valensin, G.; Remelli, M.; Luczkowski, M.; Kozlowski, H. *J. Am. Chem. Soc.* **2005**, *127*, 996–1006.
(37) Raffa, D. F.; Gómez-Balderas, R.; Brunelle, F.; Rickard, G. A.; Rauk, A. *J. Biol. Inorg. Chem.* **2005**, *10*, 887–903.
(38) Delgado, R.; Da Silva, J. J. R. F.; Amorim, M. T. S.; Cabral, M. F.; Chaves, S.; Costa, J. *Anal. Chim. Acta* **1991**, *245*, 271–282.
(39) Danielsson, J.; Pierattelli, R.; Banci, L.; Graslund, A. *FEBS J.* **2007**, *274*, 46–59.
(40) Hou, L.; Zagorski, M. G. *J. Am. Chem. Soc.* **2006**, *128*, 9260–9261.

Copper coordination to native N-terminally modified versus full-length amyloid-β: second sphere effects determine the species present at physiological pH

Bruno Alies, Christian Bijani, Stephanie Sayen,
Emmanuel Guillon, Peter Faller, Christelle Hureau

Inorganic Chemistry
Accepted

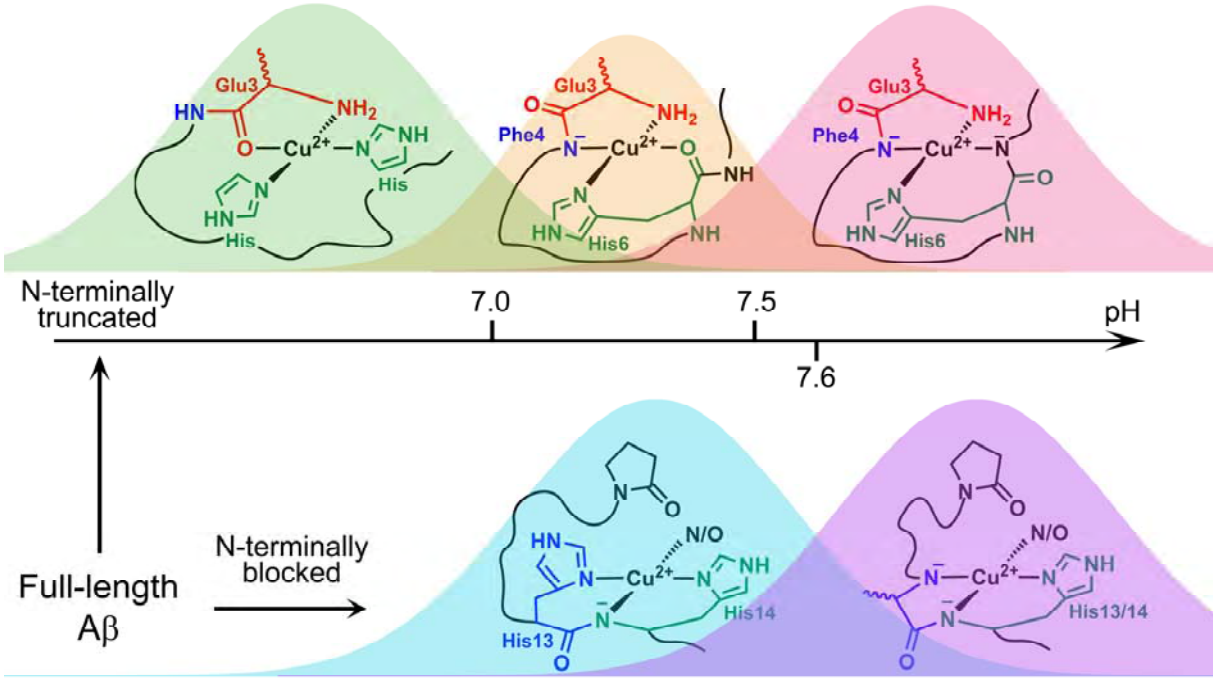

The following article is summarized in the previous chapter. It is a comprehensive study about Cu coordination to the deleterious N-terminal truncated Aβ peptides.

Inorganic Chemistry

Article

pubs.acs.org/IC

Copper Coordination to Native N-Terminally Modified versus Full-Length Amyloid-β: Second-Sphere Effects Determine the Species Present at Physiological pH

Bruno Alies,*[,†,‡] Christian Bijani,[†,‡] Stéphanie Sayen,[§] Emmanuel Guillon,[§] Peter Faller,[†,‡] and Christelle Hureau*[,†,‡]

[†]Laboratoire de Chimie de Coordination (LCC), CNRS, 205 route de Narbonne, F-31077 Toulouse, France

[‡]UPS, INPT, LCC, Université de Toulouse, F-31077 Toulouse, France

[§]Groupe de Chimie de Coordination, Institut de Chimie Moléculaire de Reims (ICMR, CNRS UMR 7312), Université de Reims Champagne-Ardenne, BP 1039, 51687 Reims Cedex 2, France

Supporting Information

ABSTRACT: Alzheimer's disease is characterized by senile plaques in which metallic ions (copper, zinc, and iron) are colocalized with amyloid peptides of different sequences in aggregated forms. In addition to the full-length peptides (Aβ1-40/42), N-terminally truncated Aβ3-40/42 forms and their pyroglutamate counterparts, Aβp3-40/42, have been proposed to play key features in the aggregation process, leading to the senile plaques. Furthermore, they have been shown to be more toxic than the full-length Aβ, which made them central targets for therapeutic approaches. In order to better disentangle the possible role of metallic ions in the aggregation process, copper(II) coordination to the full-length amyloid peptides has been extensively studied in the last years. However, regarding the N-terminally modified forms at position 3, very little is known. Therefore, copper(I) and copper(II) coordination to those peptides have been investigated in the present report using a variety of complementary techniques and as a function of the pH. Copper(I) coordination is not affected by the N-terminal modifications. In contrast, copper(II) coordination is different from that previously reported for the full-length peptide. In the case of the pyroglutamate form, this is due to preclusion of N-terminal amine binding. In the case of the N-terminally truncated form, alteration in copper(II) coordination is caused by second-sphere effects that impact the first binding shell and the pH-dependent repartition of the various [Cu(peptide)] complexes. Such second-sphere effects are anticipated to apply to a variety of metal ions and peptides, and their importance on changing the first binding shell has not been fully recognized yet.

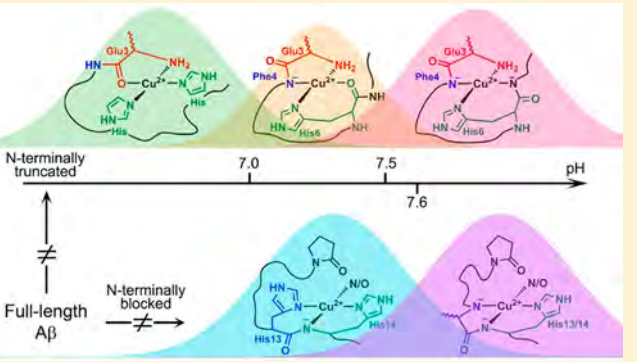

INTRODUCTION

Amyloid-β (Aβ) is mainly a 40/42 amino acid residue peptide that is normally present under physiological conditions, especially in the brain. Despite a wide number of studies, its biological function is still under debate.[1] Aβ is well-known to be the main component of senile plaque, a typical feature that occurs in the brain of Alzheimer's disease (AD) patients.[2] According to the amyloid cascade hypothesis, aggregation of the monomeric Aβ into the fibrils detected in the senile plaque plays a causal role in AD.[3] The amyloid cascade contains several aggregation stages (oligomers, protofibrils, and fibrils), and aggregation intermediates (often called oligomers) have been proposed to instigate further pathological events, including the formation of intracellular neurofibrillary tangles, another hallmark of AD, and disruption of synaptic connections, which would lead ultimately to neuronal cell death and dementia.[3−5] They are now considered to be more toxic than the senile plaques or higher molecular weight aggregates,[5−7] via various events including the production of reactive oxygen species (ROS), which have also been implicated in the pathological process. Metal ions such as copper, iron, and zinc are found at hundreds of micromolars in senile plaques.[8,9] Their effects on Aβ aggregation and their involvement in the generation of ROS, two key features in the amyloid cascade, underline an important role of metallic ions in AD.[10−12]

In order to gain insight into the role of metallic ions in AD, coordination of copper to Aβ1-40/42 has been widely studied. It was shown that copper(II)[13−15] and copper(I)[16] bind to the first 16 amino acid residues and, hence, the C-terminally truncated Aβ1-16 peptide is widely accepted as a valuable model of copper binding to monomeric Aβ1-40/42. Copper(II) binds Aβ with an apparent K_d in the low nanomolar range (at pH 7.4),[17−19] and copper coordination is pH-dependent.

Received: September 27, 2012

 © XXXX American Chemical Society dx.doi.org/10.1021/ic302097d | Inorg. Chem. XXXX, XXX, XXX−XXX

Near physiological pH, [Cu^{II}(Aβ)] species are found under two kinds of coordination modes (called "components" I and II),[20,21] in which the copper(II) geometry is square-planar. Components I and II have been characterized using electron paramagnetic resonance (EPR), including studies on copper(II) binding to specifically labelled Aβ peptides,[22−24] circular dichroism (CD),[25] and nuclear magnetic resonance (NMR).[15,26] The four copper(II) equatorial ligands in component I are NH_2 from the N-terminal Asp1, CO from the Asp1−Ala2 peptide bond, and two nitrogen atoms from the His rings of His6 and His13 or His14, with the latter two being in dynamical exchange for the fourth copper(II) equatorial position. In component II, the four ligands are the NH_2 terminal amine that remains coordinated, the deprotoned N^- amide group from the Asp1−Ala2 bond that replaces the corresponding CO group, the adjacent CO group from the Ala2−Glu3 peptide bond, and a side chain from one His (His6, His13, or His14 in dynamical exchange).

Recently, the species obtained at higher pH, i.e., components III and IV, have been characterized as well.[27] Component III equatorial ligands consist of $-NH_2$ (Asp1), two adjacent deprotonated amides N^- (from Asp1−Ala2 and Ala2−Glu3 peptide bonds), and one His. Component IV involves the N-terminal NH_2 (Asp1) and three adjacent deprotonated amides N^- (from Asp1−Ala2, Ala2−Glu3, and Glu3−Phe4 peptide bonds). Hence, the Roman numbers refer to the number of deprotonated amide function(s) involved in copper(II) binding (from I to IV for components involving from 0 to 3 deprotonated amide functions).

Regarding copper(I) coordination to the monomeric Aβ peptide, a consensual proposition has recently emerged in the literature: the copper(I) center is linearly bound by two side chains of His residues,[16,28] with equilibrium between the three possible pairs of His, His6−His13, His6−His14, and His13−His14, with the latter one being proposed as the predominant species.[29,30]

Aβ1-40/42 and familial mutants are not the only forms of interest. N-Terminally modified peptides such as the Aβ3-40/42 truncated forms, the sequence of which begins by glutamate 3, and the pyroglumate Aβp3-40/42 counterpart have been found in AD brains in high amount (up to 25% of Aβ in plaques are pyroglutamate forms[31,32]) and have been extensively studied in the last years for several reasons. First, they have been shown to be more toxic than the full-length Aβ1-40/42,[33−37] possibly via modification of the amyloid plaque morphology.[38] Second, the N-term cyclization in Aβp3-40/42 slows down peptide degradation.[39] Third, the aggregation process of Aβ1-40/42 could change because of seeding effects of the pyroglutamate forms.[40−42]

Considering the role of copper ions in Aβ aggregation and ROS production processes linked to AD, it seems interesting to investigate the coordination chemistry of copper(I) and copper(II) to those N-terminally modified forms Aβ3-40/42 and Aβp3-40/42. So far, only one EPR study on the coordination chemistry copper(II) binding to models of Aβ3-40/42 and Aβp3-40/42, i.e., Aβ3-16 and Aβp3-16, was published.[43] On the basis of similar EPR parameters determined for the two [Cu^{II}(Aβ3-16)] and [Cu^{II}(Aβp3-16)] species, the authors suggested that copper(II) coordination to the Aβ3-16 and Aβp3-16 peptides are similar but with different pH dependence regarding the repartition of components I and II. As in [Cu^{II}(Aβp3-16)], copper(II) coordination via the terminal amine is precluded by the pyroglutamate ring; they thus proposed that the N-terminal amine is not directly involved in copper(II) binding in the [Cu^{II}(Aβ3-16)] complexes either. This result seems highly questionable because it has been shown in many studies and on several different Aβ peptide sequences that when the N-terminal amine is available, it takes part of the coordination sphere of copper(II) regardless of the pH values.[25,27]

In order to get a better description of copper(II) coordination to Aβ3-16 and Aβp3-16 peptides and possibly to disentangle the role of the $-NH_2$ terminus in copper(II) binding in such Aβ-modified forms, we have used EPR but also extended the analysis with complementary methods, i.e., ^{13}C NMR, CD, and X-ray absorption near-edge structure (XANES). In addition to these new pieces of data on copper(II), we have determined copper(I) coordination by ^1H NMR, and to complete the study, we have evaluated the copper(II) and copper(I) affinity for both N-terminally modified peptides. This complete set of analyses provided the first results on copper(I) and new insights into the coordination of copper(II) to such N-terminally modified peptides.

EXPERIMENTAL SECTION

Copper Solutions. Copper(II) used was from $CuSO_4·5H_2O$ and purchased from Sigma. A stock solution of copper(II) (∼1 M) was prepared in D_2O. [Cu^I(MeCN)$_4$](BF_4) (MeCN = methyl cyanide) was bought from Sigma-Aldrich and kept under an inert atmosphere until use. A copper(I) stock solution (0.16 M) was prepared in MeCN.

Ferrozine [5,6-diphenyl-3-(2-pyridyl)-1,2,4-triazine-4,4″-disulfonic acid monosodium salt hydrate] was bought from Alfa-Aesar. A 0.1 M stock solution was prepared in water.

HEPES buffer (sodium salt of 2-[4-(2-hydroxyethyl)piperazin-1-yl]ethanesulfonic acid) was bought from Fluka (bioluminescence grade).

A phosphate buffer was prepared from K_2HPO_4 and KH_2PO_4 bought from Sigma-Aldrich.

Peptides. Aβ1-16 peptide (sequence DAEFRHDSGYEVHHQK), Ac-Aβ peptide corresponding to the N-terminally acetylated Aβ1-16 peptide, Aβ3-16 (sequence EFRHDSGYEVHHQK), and Aβp3-16 corresponding to the N-terminally pyroglumate form of the Aβ3-16 peptide (sequence (pEFRHDSGYEVHHQK) were bought from GeneCust (Dudelange, Luxembourg) with purity grade >98%

Cu(peptide) Sample Preparation. Studies were performed in H_2O or D_2O. However, for clarity and consistency, we decided to use the notation pH even when the measurements were made in D_2O. The pD was measured using a classical glass electrode according to pD = pH* + 0.4, and the apparent pH value was adjusted according to ref 44, pH = (pD − 0.32)/1.044, or equivalently to ref 45, pH = 0.929pH* + 0.41, to be in ionization conditions equivalent to those in H_2O.

Stock solutions of peptide were prepared by dissolving the powder in Milli-Q water or D_2O (resulting pH ∼ 2). The peptide concentration was then determined by UV−vis absorption of Tyr10 considered as free tyrosine ($\varepsilon_{276} - \varepsilon_{296}$ = 1410 M^{-1} cm^{-1}), and the solution was diluted to the appropriate concentration in peptide. The pH was adjusted using NaOH/HCl (H_2O) or NaOD/DCl (D_2O). All pH values are given with a ±0.2 pH unit error.

Circular Dichroism (CD) Samples. A stock solution of peptide was diluted to 0.5 mM in pure Milli-Q water. A total of 0.9 equiv of Cu^{II} was added from a 0.1 M $Cu(SO_4)$ stock solution.

Electron Paramagnetic Resonance (EPR) Samples. A stock solution of peptide was diluted to 1.0 mM in D_2O. A total of 0.9 equiv of $^{63}Cu^{II}$ was added from a 0.1 M $^{63}Cu(NO_3)_2$ stock solution. Samples were frozen in quartz tubes after the addition of 10% glycerol as a cryoprotectant.

Nuclear Magnetic Resonance (NMR) Samples. For NMR copper(II) experiments, a stock solution of Aβ3-16 or Aβp3-16 peptide was diluted to about 10 mM in D_2O. A substoichiometric

dx.doi.org/10.1021/ic302097d | Inorg. Chem. XXXX, XXX, XXX−XXX

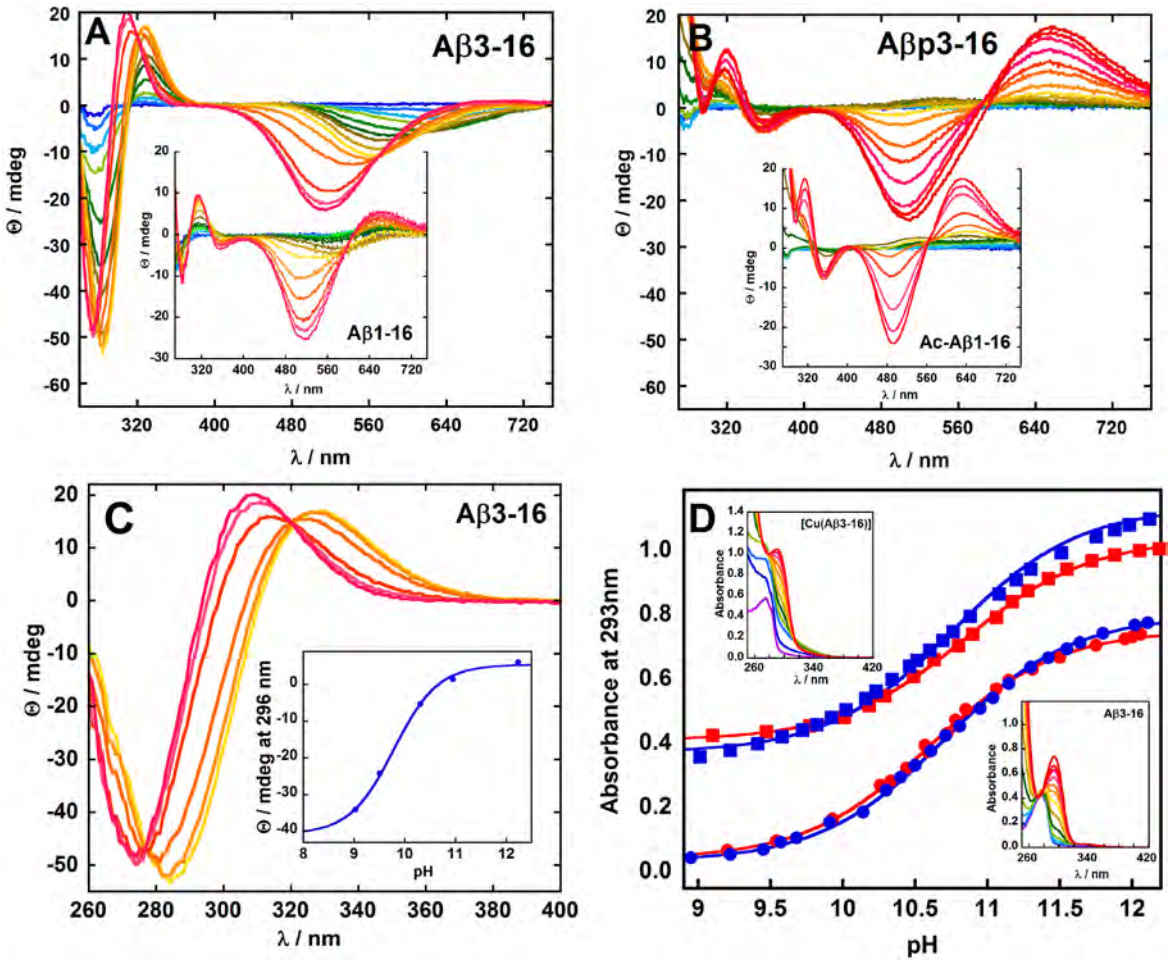

Figure 1. pH dependence of copper(II) coordination to Aβ3-16 (panel A) and Aβ1-16 (inset in panel A) and to Aβp3-16 (panel B) and Ac-Aβ1-16 (insert panel B) from acidic (blue) to basic (red) pH values. Panel C: Zoom on the UV band of [Cu(Aβ3-16)] between pH 9 and 12 and pH dependence of the UV band at 296 nm detected by CD (inset in panel C). Panel D: pH dependence of the UV band at 293 nm detected by UV−vis for Aβ1-16 (blue) and Aβ3-16 (red) peptides and of the corresponding copper(II) complexes. Insets in panel D are the UV−vis spectrum of Aβ3-16 and [Cu(Aβ3-16)]. [Cu^{II}(peptide)] = 0.45 mM (panels A−C), [Cu^{II}(peptide)] = 0.3 mM (panel D), and l = 1 cm.

quantity (ca. 0.02 equiv at pH 6 or 0.3 equiv at pH 8.6 for the Aβ3-16 peptide and 0.05 equiv at pH 7 for the for the Aβp3-16 peptide) of copper(II) from $Cu(SO_4)$ in D_2O was added. Indeed, a too high copper(II)-to-Aβ ratio would induce an uncontrolled broadening of NMR signals because of paramagnetism of the copper(II). Nevertheless, this ratio needs to be enough to induce selective broadening of specific residues of all of the peptides present in solution [via exchange of copper(II) between peptides].

For NMR copper(I) experiments, copper(I) was produced in situ, by the direct addition (1.5 equiv) of a fresh-made $Na_2S_2O_3$ stock solution (0.1 M) into an NMR tube previously degassed with water-saturated argon containing the peptides and copper(II), both at 1 mM concentration. The NMR tube was sealed under argon, measured as soon as possible to prevent possible oxidation. In such conditions, no significant pH drift due to the addition of $Na_2S_2O_3$ was measured.

UV−Vis Samples. For ferrozine titration experiments, copper(I) stock solutions (5 mM) were prepared in an argon-degassed HEPES buffer [0.1 M, pH 7.4, containing 5% (v/v) MeCN] and degassed with water-saturated argon just before use. UV−vis monitoring of the stock solution under argon was performed to ensure that under these conditions no dismutation occurred. Less than 2% of copper(II) was detected, a content that can be neglected in analysis of the titration curve.

CD. CD spectra were recorded at 20 °C on a Jasco J-815 CD spectrometer, with a Peltier PTC423 temperature controller. Data were collected with a 1 nm sampling interval, and two scans were averaged and a baseline spectrum was subtracted for each spectrum.

EPR. EPR data were recorded using an Elexsys E 500 Bruker spectrometer, operating at a microwave frequency of approximately 9.5 GHz. All spectra were recorded using a microwave power of 20 mW across a sweep width of 150 mT (centered at 310 mT) with a modulation amplitude of 0.5 mT. Experiments were carried out at 110 K using a liquid-nitrogen cryostat.

NMR. 1D ^1H and ^{13}C NMR experiments and 2D experiments were recorded on a Bruker Avance 500 spectrometer equipped with a 5-mm triple-resonance inverse Z-gradient probe (TBI ^1H, ^{31}P, BB). All chemical shifts are relative to tetramethylsilane. 1D and 2D NMR spectra were collected at 298 K in pure D_2O, respectively. Accumulation lasted ca. 16 h for the $^{13}C\{^1H\}$ NMR experiments and 24 h for the 2D $^1H-^1H$ TOCSY, $^1H-^{13}C$ HSQC, and $^1H-^{13}C$ HMBC experiments.

All of the ^1H and ^{13}C NMR signals were assigned on the basis of chemical shifts, spin−spin coupling constants, splitting patterns, and signal intensities and by using $^1H-^1H$ TOCSY, $^1H-^{13}C$ HSQC, and $^1H-^{13}C$ HMBC experiments.

XANES. Measurements were carried out at the SOLEIL Synchrotron Facility (St. Aubin, France), which was operating with a ring current of 400 mA. Cu K-edge XANES spectra were collected on the SAMBA beamline using a Si(220) double crystal monochromator and two large silicon mirrors for high-energy harmonics rejection. The liquid samples were injected in special sample holders

dx.doi.org/10.1021/ic302097d | *Inorg. Chem.* XXXX, XXX, XXX−XXX

and cooled down to 20−30 K using a helium-flow cryostat. The spectra were collected in fluorescence mode by measuring the Cu Kα fluorescence with a seven-element germanium detector (Canberra). Three scans of 25 min each were averaged. Data from each detector channel were inspected for glitches or dropouts before inclusion in the final average. Energy calibration was achieved by recording a copper foil for the Cu edge and assigning the first inflection point of the absorption spectrum to 8980.3 eV. XANES spectra were background-corrected by linear regression through the preedge region and a polynomial through the postedge region and normalized to the edge jump. No significant photoreduction of the samples occurs during the measurements.

RESULTS

Structural Data on [Cu(Aβ3-16)] and [Cu(Aβp3-16)]. *pH Dependence on the CD Study of [Cu^{II}(Aβ3-16)] and [Cu^{II}(Aβp3-16)].* CD is a powerful tool to sense structural changes due to metal-ion coordination to peptide. In the case of copper(II) complexes, the d−d and charge-transfer transitions can be studied between 450 to 750 nm and between 250 and 400 nm, respectively.[46] CD is thus sensitive to structural changes in the first copper(II) coordination sphere but also to modifications beyond the first shell.[47] pH-dependent CD spectra were recorded for the four [Cu^{II}(Aβ1-16)], [Cu^{II}(Aβ3-16)], [Cu^{II}(Ac-Aβ1-16)], and [Cu^{II}(Aβp3-16)] complexes (Figure 1A,B). All four studied complexes show different signatures, underlining different first and second coordination shells. Nevertheless, general trends can be observed. In all of the complexes, the intensity of the deprotonated amide-to-copper(II) ligand-to-metal charge-transfer (LMCT) transitions increases from pH ∼ 6, indicating participation of the deprotonated amide in copper(II) binding above this pH value. Furthermore, the d−d transition bands evolve from approximately 650 nm at low pH to 500 nm at high pH. This hypsochromic shift indicates a copper(II) environment that gets enriched in nitrogen atoms (compared to oxygen atoms) at higher pH, in line with successive amide backbone deprotonation and subsequent copper(II) binding with a pH increase. Another important feature is the strong similarity between [Cu^{II}(Aβ1-16)] and [Cu^{II}(Aβ3-16)] on the one side and [Cu^{II}(Ac-Aβ1-16)] and [Cu^{II}(Aβp3-16)] on the other side (compare parts A and B of Figure 1 and parameters listed in Table 1). Thus, two families can be made: [Cu^{II}(Aβ1-16)]-like families obtained when the peptide possesses a free $-NH_2$ terminus (Figure 1A) and [Cu^{II}(Ac-Aβ1-16)]-like families when the peptide has the $-NH_2$ terminus blocked (Figure 1B). Two clear spectral differences between the two families can be observed: (i) A negative band at ∼280 nm attributed to NH_2-to-copper(II) LMCT appears only in the former family. This indicates the involvement of the $-NH_2$ terminal amine in copper(II) binding regardless of the pH. Such a CD feature is not observed in the latter family in line with a $-NH_2$ terminal amine, which is blocked either via acetylation (Ac-Aβ1-16) or via pyroglutamate formation (Aβp3-16). (ii) On the [Cu^{II}(Ac-Aβ1-16)] and [Cu^{II}(Aβp3-16)] spectra, an intense positive CD band is observed at ∼645 nm, while on [Cu^{II}(Aβ1-16)] and [Cu^{II}(Aβ3-16)] spectra, such a band is not detected. These two main differences strongly suggest two highly different copper(II) sites between [Cu^{II}(Aβ1-16)] and [Cu^{II}(Aβ3-16)], on the one hand, and [Cu^{II}(Ac-Aβ1-16)] and [Cu^{II}(Aβp3-16)], on the other hand, regardless of the pH range. Such strong dissimilarities are reminiscent of first-coordination-shell effects. In a more thorough analysis, minor differences, indicative of second-

Table 1. EPR Parameters and CD Data of the Four Different [Cu(Aβ1-16)], [Cu(Aβ3-16)], [Cu(AcAβ1-16)], and [Cu(Aβp3-16)] Species as a Function of the pH and Corresponding pK_a Values[a]

	I			II			III			IV			pK_a			
peptide	$g_{\parallel}$[b]	$A_{\parallel}$ ($\times 10^{-4}$ cm^{-1})	λ_{max} (nm)	$g_{\parallel}$	$A_{\parallel}$ ($\times 10^{-4}$ cm^{-1})	λ_{max} (nm)	$g_{\parallel}$	$A_{\parallel}$ ($\times 10^{-4}$ cm^{-1})	λ_{max} (nm)	$g_{\parallel}$	$A_{\parallel}$ ($\times 10^{-4}$ cm^{-1})	λ_{max} (nm)	I/II	II/III	III/IV	ref
Aβ1-16	2.26(2)	184	660+	2.22(6)	161	580−	2.19(1)	194		2.17(3)	203	516−, 660+	7.8	9.3	10.1	27
Aβ3-16	2.25(4)	182	640−	2.22(3)	160	602−	2.19(0)	201	574−	2.16(7)	212	515−	7.0	7.5	10.0	this work
Aβ3-16	2.26(1)	183					2.19(4)	193								43

	I′			II′			III′			IV′			pK$_a$			
peptide	$g_{\parallel}$[b]	$A_{\parallel}$ ($\times 10^{-4}$ cm^{-1})	λ_{max} (nm)	$g_{\parallel}$	$A_{\parallel}$ ($\times 10^{-4}$ cm^{-1})	λ_{max} (nm)	$g_{\parallel}$	$A_{\parallel}$ ($\times 10^{-4}$ cm^{-1})	λ_{max} (nm)	$g_{\parallel}$	$A_{\parallel}$ ($\times 10^{-4}$ cm^{-1})	λ_{max} (nm)	I′/II′	II′/III′	III′/IV′	ref
AcAβ1-16	2.32(0)	168		2.27(3)	187	580+	2.23(0)	171	645+, 485−	2.19(1)	190	635+, 495−	5.2	7.5	8.7	27
Aβp3-16	2.31(0)	169		2.26(4)	180	560+	2.23(0)	161	656+, 500−	2.19(0)	187	657+, 510−	5.3	7.6	8.8	this work
Aβp3-16				2.26(1)	183					2.19(4)	193					43

[a]In the CD data, the ± sign indicates the positive/negative nature of the band. [b]Numbers into parentheses are the third digit of the $g_{\parallel}$ value, which is given with an error of ±0.005.

dx.doi.org/10.1021/ic302097d | Inorg. Chem. XXXX, XXX, XXX−XXX

sphere effects, are observed between the CD spectra of [Cu^{II}(Aβ1-16)] and [Cu^{II}(Aβ3-16)] complexes. For instance, d−d transitions are slightly different, with positive CD bands detected in the [Cu^{II}(Aβ1-16)] spectrum and only negative CD bands in the case of the [Cu^{II}(Aβ3-16)] complex. Also the two $-NH_2$-to-copper(II) and deprotonated amide-to-copper(II) LMCT bands are detected near 315 and 285 nm, respectively, in the case of the [Cu^{II}(Aβ1-16)] complex, while the same bands shift from 330 to 310 nm and from 285 to 275 nm with an increase of the pH (pK_a = 9.8; Figure 1C) in the case of the [Cu^{II}(Aβ3-16)] complex. This pK_a value is close to that expected for deprotonation of the Tyr10 residue, and thus to examine whether Tyr10 deprotonation is at the origin of such a band shift in the case of the Aβ3-16 peptide, UV−vis pH titration was performed for both peptides (Aβ1-16 and Aβ3-16) and corresponding copper(II) complexes (Figure 1D). Deprotonation of the Tyr residue is close between the apo- and holopeptide and between the two peptides (pK_a = 10.7 ± 0.1). Hence, the shift in the N^--to-copper(II) LMCT band observed near pH 9.8 only detected for the [Cu^{II}(Aβ3-16)] species is not linked to deprotonation of the Tyr residue, indicating a difference in the second-sphere environment between [Cu^{II}(Aβ3-16)] and [Cu^{II}(Aβ1-16)] that does not persist above pH 9.8. Indeed above this pH value, both complexes exhibit the same N^--to-copper(II) LMCT at 315 nm (Figure 1A,C). In addition, it appears that no Tyr10 coordination to copper(II) is observed either in the case of the [Cu^{II}(Aβ1-16)] complex, as previously reported,[15,24,25,48,49] or in the case of the [Cu^{II}(Aβ3-16)] complex, in line with the absence of tyrosinate-to-copper(II) LMCT transition detected near 400 nm.[50]

pH Dependence on the EPR Study of [Cu^{II}(Aβ3-16)] and [Cu^{II}(Aβp3-16)]. EPR has been widely used to gain insight into copper(II) coordination because different copper(II) environments and geometries lead to different EPR parameters.[46] In particular, EPR parameters are correlated to the number, chemical nature, and charge of the equatorial ligands.[51] The pH dependence of the EPR fingerprints of the four [Cu(Aβ1-16)], [Cu(Aβ3-16)], [Cu(Ac-Aβ3-16)], and [Cu(Aβp3-16)] complexes have been studied over a wide pH range (3−12; Figure S1 in the Supporting Information). This allowed determination of the speciation, i.e., the different types of coordination environments and their relative abundance as a function of the pH. With respect to the previous work,[27] the different components encountered in [Cu(Aβ1-16)] and [Cu(Aβ3-16)] (respectively [Cu(Ac-Aβ)] and [Cu(Aβp3-16)]) were denoted as I−IV (respectively I′−IV′). According to the two families observed by CD, we have regrouped in Figure 2A the EPR spectra of [Cu(Aβ1-16)] (black) and [Cu(Aβ3-16)] (gray) and in Figure 2B the EPR spectra of [Cu(Ac-Aβ1-16)] (black) and [Cu(Aβp3-16)] (gray), where the spectra are compared at some selected pH values. In Figure 2A, the two lower traces display the EPR signatures of the two components I (blue) and II (green) in a 1:1 ratio of [Cu(Aβ1-16)] (black, pH 7.8) and [Cu(Aβ3-16)] (gray, pH 7.0). The EPR signatures are very similar, in line with the same type of first-sphere copper(II) coordination in the two peptides for both components I and II. The EPR parameters (Table 1) of components I and II are consistent with a 3N1O coordination mode, as previously discussed in the case of the Aβ1-16 peptide.[13,17,21,25] The middle trace [Cu(Aβ3-16)] (yellow, pH 8.7) is attributed to component III, a component that is hardly detected in the case of [Cu(Aβ1-16)][27] because of the

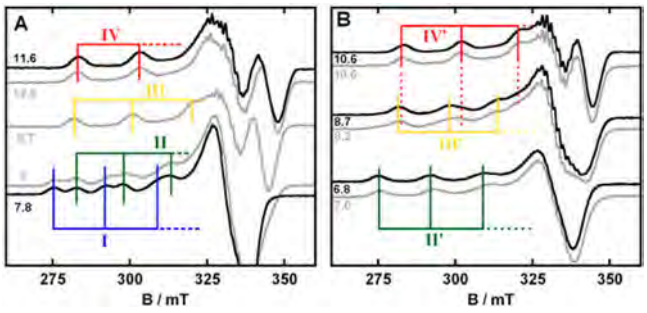

Figure 2. EPR spectra of copper(II) peptide complexes at selected pH values. Panel A: [Cu(Aβ1-16)] (black); [Cu(Aβ3-16)] (gray). Right panel B: [Cu(AcAβ1-16)] (black); [Cu(Aβp3-16)] (gray). [Cu-(peptide)] = 1 mM in D_2O, ν = 9.5 GHz, amplitude modulation = 0.5 mT, microwave power = 20 mW, and T = 110 K.

simultaneous presence of components II and IV. The two upper traces [Cu(Aβ1-16)] (black, pH 11.6) and [Cu(Aβ3-16)] (gray, pH 12.5) show the signature of component IV (red) of both complexes. EPR parameters of components III and IV are consistent with a 4N coordination sphere. In Figure 2B, EPR spectra of [Cu(Ac-Aβ3-16)] (black) and [Cu(Aβp3-16)] (gray) are compared at different pH values. The two complexes display the same EPR signatures at similar pH values. Three different components are observed. The high similarities between the EPR fingerprints of [Cu(Ac-Aβ3-16)] and [Cu(Aβp3-16)] suggest that the coordination of copper-(II) will be similar in both peptides whatever the pH. Hence, the four components observed from pH 5 are denoted as I′−IV′, corresponding to complexes with 0 to 3 deprotonated amides bound to copper(II), with respect to previous work.[27] Together with the EPR parameters, the pK_a values between two successive components are reported in Table 1. From these pK_a values, it is possible to evaluate the relative proportion of the different components at a given pH. For the physiological pH 7.4, in the case of [Cu(Aβ1-16)] having a pK_a(I/II) = 7.7,[27] the major component is I with a weak contribution of component II. In contrast, for [Cu(Aβ3-16)] with a pK_a(I/II) = 7.0 [evaluated from the 50:50 proportion of components I and II at pH 7.0 (Figure 2A)] and a pK_a(II/III) = 7.5 [evaluated from the 50:50 proportion of components II and III (Figure S2 in the Supporting Information)], the main component is II with a significant contribution of component III. Consequently, the type of copper(II) coordination at physiological pH is significantly different between the two peptides. For [Cu-(Aβp3-16)] species with pK_a(II′/III′) = 7.6 [evaluated from the 50:50 proportion of components II′ and III′ (Figure S2 in the Supporting Information)], II′ is the major component at pH 7.4 with a large contribution of component III′, as is also the case for the [Cu(Aβp3-16)] complex. This underlines the fact that, for those two latter species, the EPR parameters *and* pH dependence are highly similar, indicating, as expected, that the influence of modification on the N-term is weak regarding copper(II) coordination.

In ref 27 and in this work, parallel spin Hamiltonian parameters were obtained directly from the experimental spectra and were calculated from the second and third hyperfine lines in order to remove second-order effects. Errors on the hyperfine couplings are $\pm 5 \times 10^{-4}$ cm^{-1} and on the pK_a values ±0.2.

^{13}C NMR Study of [Cu^{II}(Aβ3-16)] and [Cu^{II}(Aβp3-16)]. In order to identify ligands involved in copper(II) coordination in

dx.doi.org/10.1021/ic302097d | *Inorg. Chem.* XXXX, XXX, XXX−XXX

the different species of [Cu^{II}(Aβ3-16)] and [Cu^{II}(Aβp3-16)], the NMR data (^{1}H, ^{13}C, and 2D NMR experiments) of the corresponding peptide in the absence and presence of substoichiometric copper(II) amounts at several pH values were recorded (Figures 3 and 4 and S3−S12 in the Supporting Information). Because copper(II) is paramagnetic and its binding to Aβ peptides is dynamic, a small stoichiometry of copper(II) will induce specific broadening of the NMR signals of residues involved in copper(II) coordination.[47] Nevertheless, because of the dynamics in solution, ^{13}C NMR can hardly distinguish the transient ligands from more stable ligands (i.e., ^{13}C NMR signals of COO^- and aromatic rings of His are both highly affected by the presence of copper(II) because they are likely involved in copper(II) exchange between peptides; see, for instance, Figures S3, S4, and S10 in the Supporting Information, panels B and F, respectively).[26] Such transient ligands may also be involved in the formation of Cu(Aβ)$_2$ species, as recently suggested by Pedersen and co-workers,[52] although in a our previous NMR study of copper binding to Aβ1-16, we found no direct evidence for the formation of such species in a significant amount.[26]

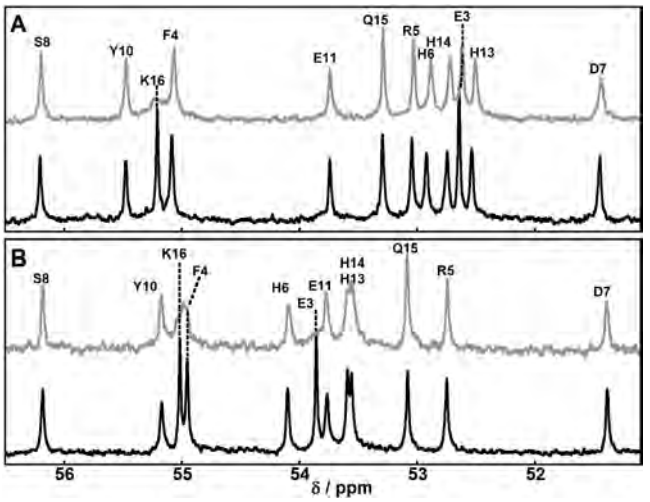

Figure 3. Cα region of the ^{13}C NMR spectrum of Aβ3-16 peptide in the absence (black) or presence (gray) of 0.02 equiv of Cu^{II} at pH 6.0 (panel A) and of 0.3 equiv of Cu^{II} at pH 8.6 (panel B). The signals affected by copper(II) addition are indicated by dotted lines. [Aβ3-16] = 10 mM, T = 25 °C, and ν = 125.8 MHz.

In addition to that, NMR analysis of copper(II) binding to the peptides is limited to components with less than two deprotonated amide ligands (i.e., components I, II, and II′). Indeed, copper(II) coordination involving two or more deprotonated amide groups results in a too slow copper(II) exchange and the copper(II) paramagnetic effect broadens the signal of bound peptide beyond detection. Then only the signal of a copper(II)-unbound peptide or copper(II) bound to peptide in another detectable component remains.[27,53]

Figure 3A shows the ^{13}C NMR spectrum of the Cα area of Aβ3-16 peptide in the absence and presence of 0.02% copper(II) at pH 6.0. The two signals most strongly affected belong to Lys16 and Glu3. The signal of Cα from Glu3 undergoes a large broadening, which is in line with the $-NH_2$ terminus bound to copper(II). The broadening of the Cα signal from Lys16 is attributed to binding of the free COO^- C terminus, as observed earlier for Aβ1-16.[26] However, this may not be relevant for the full-length peptide because the Aβ1-16 C terminus was not protected. Hence, the involvement of the $-NH_2$ terminal amine in copper(II) binding by the Aβ3-16 peptide is confirmed by the NMR experiments, as were previously reported for the Aβ1-16 and murine counterparts.[26,54]

In order to figure out copper(II) coordination in component II, ^{13}C NMR was performed at higher pH. There is no pH where component II is exclusively present. Thus, pH 8.6 was chosen because only components II and III are present, but component III cannot be detected by ^{13}C NMR, in line with the presence of two deprotonated amide groups in the copper(II) binding site (see above). Hence, only changes due to component II are observed. Cα from Glu3 remains largely affected, indicating that the N-terminal NH_2 stays coordinated to the copper(II) in component II. The main change between pH 6.0 and 8.6 is the broadening of Cα from Phe4, which is attributed to deprotonation of the NH group from the Glu3−Phe4 peptide bond and its coordination to copper(II). At pH 8.6, the Cα and CO from His (Figure S4 in the Supporting Information, panels A and C) are broadened by copper(II) addition, and on the Cα/Hα correlation peak (Figure S5 in the Supporting Information), His6 is preferentially affected compared to the other two His residues, in line with the CO group of His6 involved in copper(II) binding.

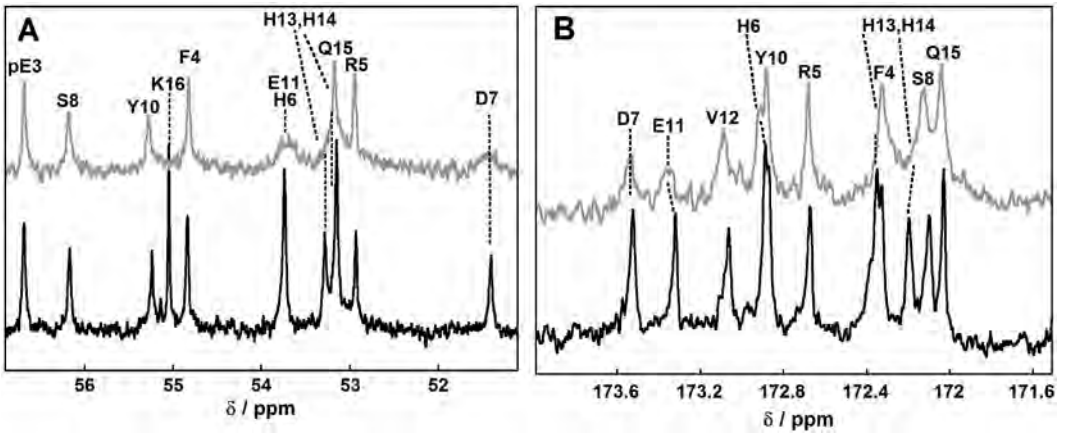

Figure 4. Cα (panel A) and CO (panel B) regions of ^{13}C NMR spectra of the Aβp3-16 peptide in the absence (black) or presence of 0.05 equiv of Cu^{II} (gray) at pH 7.0. The signals affected by copper(II) addition are indicated by dotted lines. [Aβp3-16] = 10 mM, T = 25 °C, and ν = 125.8 MHz.

dx.doi.org/10.1021/ic302097d | Inorg. Chem. XXXX, XXX, XXX−XXX

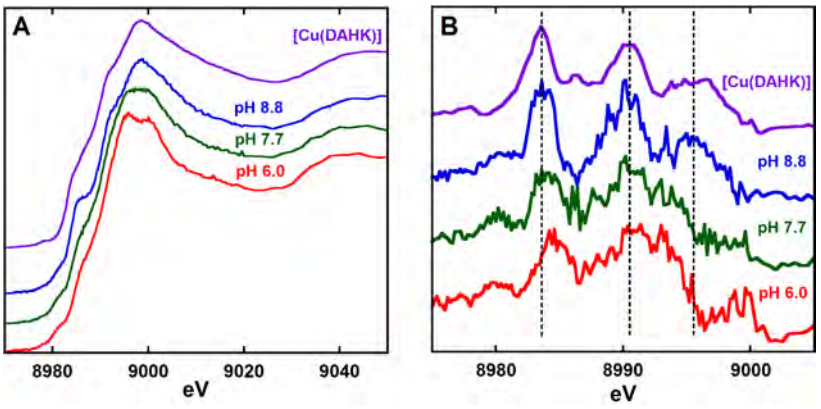

Figure 5. XANES spectra (A) and derivatives of the XANES spectra (B) of [Cu(Aβ3-16)] (red, pH 6.0; green, pH 7.7; blue, pH 8.8) and [Cu(DAHK)] (purple) complexes. Conditions: [Cu(peptide)] = 2 mM in H_2O and T = 20 K, except for [Cu(DAHK)] (see ref 21 for conditions).

At both pH values, the Cδ/Hδ and Cε/Hε of the His rings are also affected (Figures S3 and S4, panel F, and S8 and S9 in the Supporting Information), indicating His involvement in copper(II) binding in both components. Thus, taking into account the EPR and CD results, the experimental data are best explained by the following equatorial coordination site of copper(II) when linked to the Aβ3-16 peptide: component I {NH_2; CO; 2Im (His)} and component II {NH_2; N^- (Glu3−Phe4); Im (His6); CO (His6)}. On the basis of what was proposed on the [Cu(Aβ1-16)] species,[21] the CO function in component I of [Cu(Aβ3-16)] might come from the Glu3 amino acid residue. Indeed, this will induce the formation of a stable five-coordinated metallacycle with the $-NH_2$ terminal amine. In contrast, while in component II of the [Cu(Aβ1-16)] complex, the Glu3 CO group adjacent to the Asp1−Ala2 deprotonated amide was proposed to be involved in copper(II) binding,[22,26] in the case of [Cu(Aβ3-16)], the CO group is proposed to be that of His6 based on its selective broadening detected by NMR. It has to be noted that, based only on the size of the metallacycle formed, the {Im (His6), CO (His6)} binding is less favorable than that of {N^- (Glu3), CO (Arg5)}. Thus, the binding of CO (His6) instead of CO (Arg5) may be linked to the peculiar nature of the Arg5 side chain (bulky and charged).

In Figure 4, the two panels display the ^{13}C NMR spectra of Aβp3-16 at pH 7.0 with (gray) and without (black) copper(II) with focus on the CONH (left) and Cα (right) areas. Attempts to record the NMR data at higher pH were unfruitful because broadening was not specific enough, in line with copper(II) bound by two or more deprotonated amide groups in components III′ and IV′. In contrast to component II of [Cu(Aβ3-16)] (Figure 3B, bottom), Phe4 is not affected in the case of the Aβp3-16 peptide, in line with copper(II) coordination to the N-term part (including the deprotonated amide of the Glu3−Phe4 bond) that is precluded by the presence of the pyroglutamate cycle. As a general trend, peaks from the His residues are strongly affected by added copper(II) (Figures S10−S12 in the Supporting Information), as exemplified by Cα and CO (Figure 4). In general, His13 and His14 are more affected than His6. As in component II′, there is one deprotonated amide group bound to the copper(II) center (see above); this might be explained by the preferential involvement of the deprotonated amide from the His13−His14 peptide bond rather than the His6−Asp7 bond, with the involvement of the deprotonated amide group from Arg5−His6 being discarded on the basis of previous results on copper(II) binding to Aβ1-16.[26,54] Such a His13−N^-−His14 tripodal copper(II) binding has also been proposed using theoretical calculations[55,56] and is in line with potentiometric studies of copper(II) binding to Ac-Y10A-Aβ8-16 peptides.[57] Cα and CO from Asp7 and Glu11 are also affected by copper(II). Nevertheless, it seems that such a broadening is due to COO^- coordination to copper(II) because the side chain is more strongly affected than the backbone carbon and hydrogen atoms. This indicates a possible implication of Asp7 and Glu11 in copper(II) binding via COO^-. As was previously observed, Cα from Lys16 is affected because of COO^- binding. According to results obtained by other techniques, the most likely ligands of copper(II) in component II′ of [Cu(Aβp3-16)] are {N^- (His13−His14); Im (His13); Im (His14); Im (His6); COO^- (Asp7, Glu11)}.

XANES Study of [Cu^{II}(Aβ3-16)] and [Cu^{II}(Aβp3-16)]. XANES spectra were recorded for [Cu(Aβ3-16)] and [Cu(Aβp3-16)] species at selected pH values (Figures 5 and S13 in the Supporting Information). In line with previous measurements by CD, EPR, and NMR, pH-dependent spectral modifications were observed because of copper(II) coordination changes with the pH for both complexes. More particularly, in the case of [Cu(Aβ3-16)], component III can be predominantly detected at pH 8.8, a situation that was not encountered for the [Cu(Aβ1-16)] species studied in the past.[27] The XANES signature of component III was compared to that of the well-described [Cu(DAHK)] peptide, where DAHK represents the N-terminal sequence of the human serum albumin.[53] In this latter species, the copper(II) site is made of the N-terminal amine, the side chain of the His residues, and the two deprotonated amides in between,[53,58] and such copper(II) coordination is predominant over a wide pH range.[59] It is worth noting that the XANES spectrum of [Cu(Aβ3-16)] at pH 8.8 (component III) and its derivative (parts A and B in Figure 5, respectively) are very similar to those reported for [Cu(DAHK)] at pH 7.4.[53] This supports a similar type of first coordination sphere for copper(II) in [Cu(Aβ3-16)], i.e., the $-NH_2$, one N^-, and one imidazole ring of His, in line with the studies described above.

^{1}H NMR Study of [Cu^I(Aβ3-16)] and [Cu^I(Aβp3-16)]. To complete the structural data on copper binding to the N-terminally truncated Aβ peptides, we have performed ^{1}H NMR studies of [Cu^I(Aβ3-16)] and [Cu^I(Aβp3-16)] species. In Figure 6, ^{1}H NMR spectra of the Aβ3-16 and Aβp3-16 peptides

dx.doi.org/10.1021/ic302097d | Inorg. Chem. XXXX, XXX, XXX−XXX

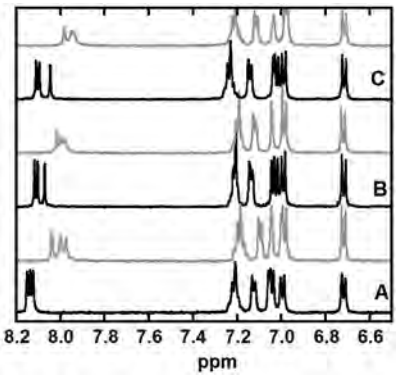

Figure 6. ^{1}H NMR spectra of Aβ1-16 (A), Aβ3-16 (B), and Aβp3-16 (C) peptides (black) and in the presence of 0.9 equiv of Cu^I (gray) in a phosphate buffer of 0.2 M and pH 6.7. [peptide] = 1 mM.

in the presence of 0.9 equiv of Cu^I are compared to that obtained in the case of the reference Aβ1-16 peptide.[29] Similar effects of copper(I) addition on the apopeptide signature are observed for the three peptides, i.e., a shift of the two aromatic protons from the three His. In the case of Hε (see the Supporting Information for nomenclature details), a downshift is observed that is more important for two of the three His signals (Figure 6). Concomitantly, those latter signals are more broadened. In the case of Hδ, the changes observed are more subtle and more difficult to analyze.[29] In addition to modifications on the aromatic domain, some changes are also observed in the aliphatic region for the three peptides (Figure S14 in the Supporting Information) mainly involving Gly9 to Val12 residues, modifications that can be attributed in the case of the Aβ1-16 peptide to the folding imposed by copper(I) coordination to the His13−His14 dyad.[30] Copper(I) coordination to Aβ1-16 was proposed to be dynamic including the different species in equilibrium.[29] The major form was copper(I) binding to His13 and His14 (His13−Cu^I−His14) in a linear fashion.[16,28] This form was in equilibrium with two minor forms, i.e., His6−Cu^I−His13 and His6−Cu^I−His14. The shifts and broadening of the NMR signals due to copper(I) addition to either Aβ3-16 or Aβp3-16 peptide are highly similar to what was observed for Aβ1-16, strongly indicating that the copper(I) coordination site is the same in the three peptides. Thus, truncation or pyroglutamate formation at the N-terminus does not affect copper(I) binding. This confirms that the N-terminal amine is not involved in copper(I) binding.

Affinity Measurements on [Cu^{II}(Aβ3-16)] and [Cu^{II}(Aβp3-16)]. In addition to structural insight, affinity for copper(II) and copper(I) is an important parameter to evaluate because it determines whether Aβ peptide is able to bind copper ions in a biological environment, in the presence of competitive ligands.

In order to evaluate the affinities of copper(II) for the Aβ3-16 and Aβp3-16 and the Aβ1-16 and Ac-Aβ counterparts, competition experiments with a well-known copper(II) chelator, i.e., glycine amino acid, have been performed and followed by CD (Figure 7). The CD data were reproduced by considering the formation of a 1:1 Cu−peptide complex, leading to determination of the apparent affinity constant as a function of the Gly concentration. Then, the conditional affinity is deduced from the following equation, where the conditional affinity value is the affinity at a given (pH, T) couple.

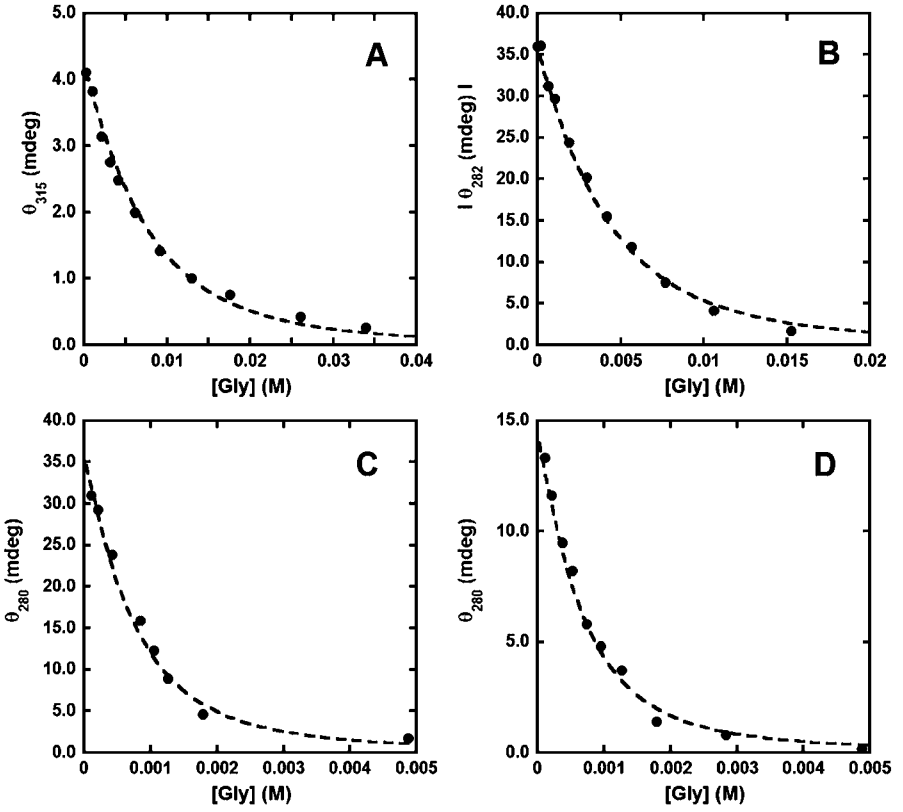

Figure 7. Gly-induced decrease of a [Cu(peptide)] LMCT band in CD spectra, together with the corresponding simulated curve: (A) [Cu(Aβ1-16)], λ = 315 nm; (B) [Cu(Aβ3-16)], λ = 282 nm; (C) [Cu(Ac-Aβ)], λ = 280 nm; (D) [Cu(Aβ1-16)], λ = 280 nm. [Cu(peptide)] = 0.5 mM, [HEPES] = 100 mM, and pH 7.4.

dx.doi.org/10.1021/ic302097d | *Inorg. Chem.* XXXX, XXX, XXX−XXX

$$ {}^{\mathrm{cond}}K^{\mathrm{A}\beta} = {}^{\mathrm{app}}K^{\mathrm{A}\beta}\left(1 + \frac{[\mathrm{Gly}]_0}{K_{\mathrm{d}_1}^{\mathrm{Gly}}}\frac{1}{1 + 10^{-\mathrm{pH}+\mathrm{p}K_{\mathrm{a}}^{\mathrm{Gly}}}} + \frac{[\mathrm{Gly}]_0^{\,2}}{K_{\mathrm{d}_1}^{\mathrm{Gly}}K_{\mathrm{d}_2}^{\mathrm{Gly}}}\frac{1}{(1 + 10^{-\mathrm{pH}+\mathrm{p}K_{\mathrm{a}}^{\mathrm{Gly}}})^2} + \frac{[\mathrm{HEPES}]_0}{K_{\mathrm{d}}^{\mathrm{HEPES}}(1 + 10^{-\mathrm{pH}+\mathrm{p}K_{\mathrm{a}}^{\mathrm{HEPES}}})}\right) $$

$$ \mathrm{p}K_{\mathrm{a}}^{\mathrm{HEPES}} = 7.41, \quad K_{\mathrm{d}}^{\mathrm{HEPES}} = 10^{-3.22}; \quad \mathrm{p}K_{\mathrm{a}}^{\mathrm{Gly}} = 9.53, \quad K_{\mathrm{d}_1}^{\mathrm{Gly}} = 10^{-8.2}, \quad K_{\mathrm{d}_2}^{\mathrm{Gly}} = 10^{-6.9} $$

Competition with the HEPES buffer has also been included but is negligible compared to competition with Gly, except for very low Gly concentration. HEPES data are from ref 60; Gly data are from the NIST database and ref 61.

Values thus obtained are reported in Table 2 and, for the Aβ1-16 peptide, are in line with most recent values reported in the literature.[18,48] Aβp3-16 and Ac-Aβ peptides have very similar affinities for the copper(II) ion, indicating that the way that the free N-terminal is blocked has only a minor impact on copper(II) coordination. In contrast, the affinity of the Aβ3-16 peptide is about 3 times weaker than that of the Aβ1-16 peptide. These relative affinity values have also been obtained by competition between Aβ1-16 and Aβ3-16 or Aβp3-16, followed by CD and fluorescence (see the Supporting Information). Acetylation or pyroglutamate formation on the N-terminal amine leads to a decrease in the affinity by 2 orders of magnitude, in line with the previous data obtained by calorimetric titration.[48,62]

Table 2. Conditional Affinity Constants of [Cu^{II}(peptide)] and [Cu^{I}(peptide)] Species (0.1 M HEPES, pH 7.4) and Corresponding Standard Deviation Constants

peptide	copper(II) affinity ($\times 10^{10}$ M^{-1})	copper(I) affinity ($\times 10^{6}$ M^{-1})	ref
Aβ1-16	1.1 ± 0.1	7.5 ± 1.0	63
Aβ3-16	0.33 ± 0.02	9.2 ± 0.9	
Aβp3-16	0.008 ± 0.001	6.5 ± 0.5	
Ac-Aβ1-16	0.01 ± 0.001	12 ± 1.3	63

Affinity Measurements on [Cu^{I}(Aβ3-16)] and [Cu^{I}(Aβp3-16)]. In a recent study of copper(I) binding to Aβ1-16, we have established that ferrozine is a copper(I) chromophore of moderate affinity and is thus suitable for competition experiments with Aβ peptides.[63] The copper(I) affinities of Aβ3-16 and Aβp3-16 peptides determined using this method are given in Table 2 and compared to those of Aβ1-16 and Ac-Aβ1-16 peptides. These four values are very close, indicating that the copper(I) site is maintained in the different peptides in line with the data obtained by NMR and the involvement of His residues only.

DISCUSSION

Copper(I) Coordination to N-Terminally Modified Aβ Peptides. Regarding copper(I) coordination to the Aβ1-16, Ac-Aβ1-16, Aβ3-16, and Aβp3-16 peptides, no significant structural and thermodynamic change is observed between the peptides in line with the involvement of only His side chains in copper(I) binding that are conserved in the four peptides.

Copper(II) Coordination to N-Terminally Truncated Aβ Peptides. The proposed copper(II) binding to the Aβ3-16 peptide as a function of the pH is described in Scheme 1. It is worth noting that, as previously described in the case of [Cu(Aβ1-16)], several species are in equilibrium at a given pH value[26] and consequently only the main form is drawn in Scheme 1. The involvement of the $-NH_2$ terminal of Aβ3-16 is supported by the ^{13}C NMR data in both components I and II, where a strong paramagnetic relaxation enhancement effect is observed for the signals of the Aβ3-16 N-terminal region. On the basis of previous data on [Cu(Aβ1-16)] and on the data obtained here, equatorial copper(II) coordination is completed by the CO group from the Glu3−Phe4 bond and the side chain of two His residues in component I. In component II, a strong broadening effect on Phe4 Cα was detected in line with binding of the amidyl from the Glu3−Phe4 peptide bond. Also, coordination of the CO from the His6−Asp7 bond occurs

Scheme 1. Proposed [Cu(Aβ3-16)] (A) and [Cu(Aβp3-16)] (B) Complexes as a Function of the pH

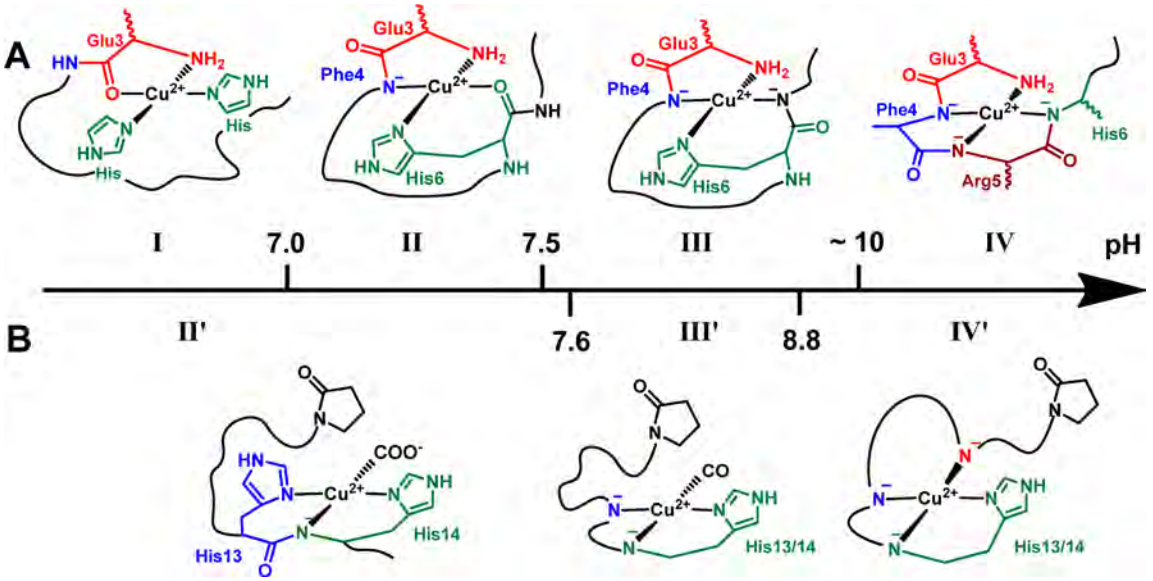

dx.doi.org/10.1021/ic302097d | Inorg. Chem. XXXX, XXX, XXX−XXX

concomitant with decoordination of the second His side chain. This was mainly proposed on the basis of different spectral CD signatures compared to the parent [Cu(Aβ1-16)] complex ruling out the formation of two adjacent metallacycles, as in the [Cu(Aβ1-16)] case. Such CO (His 6) binding is likely unfavored on a thermodynamic point of view and may explain why component II evolves toward component III with a very low pK_a value compared to other Aβ mutants and is thus very minor in solution. In component III, the {$-NH_2$, $2N^-$, and His} binding set is deduced from the NMR, EPR, and XANES measurements, and thus deprotonation of the peptide bond His6−Asp7 is proposed. The presence of two distant metallacycles is proposed from the positions of the CD, $-NH_2$-to-copper(II) and N^--to-copper(II) LMCT bands that are different compared to those of the [Cu(Aβ1-16)] complex, where two adjacent metallacycles were observed. Hence, components II and III are slightly different between [Cu(Aβ1-16)] and [Cu(Aβ3-16)]. Indeed, in the former case, two adjacent metallacycles were proposed between $-NH_2$(Asp1)−Cu^{II}−N^-(Asp1−Ala2) and N^-(Asp1−Ala2)−Cu^{II}−CO(Ala2−Glu3) (component II) or N^-(Asp1−Ala2)−Cu^{II}−CO(Ala2−Glu3) (component III), while in the latter case, two remote metallacycles are proposed between $-NH_2$(Glu3)−Cu^{II}−N^-(Glu3−Phe4) and Im(His6)−Cu^{II}−CO(His6−Asp7) (component II) or Im(His6)−Cu^{II}−N^-(His6−Asp7) (component III). Such a trend is quite unusual because, in general, the formation of metallacycles centered on two different (N-term and His) sites is disfavored compared to the formation of several metallacycles centered on either the N-term or the side chain of His residues,[57] with the best anchoring site being strongly dependent on the peptide sequence and distance between the N-term and His.[64−66] Such a difference might originate from the presence of Arg5 that precludes the formation of the second adjacent metallacycle in the present case (see below). In component IV, the copper(II) site is strongly reshuffled, leading to a copper(II) bound to the N-terminal amine and the three adjacent deprotonated amide groups, as observed in the case of the [Cu(Aβ1-16)] complex, in line with a shift of the position of the LMCT bands in CD toward the position observed in [Cu(Aβ1-16)] for three adjacent metallacycles. Decoordination of the anchoring His at high pH may be the driving force of such a reorganization. Such His decoordination in favor of a third amide coordination at high pH is reminiscent of what was previously reported for other His-containing peptides, when the His residues lies in the fourth position or beyond from the N-terminal anchoring site (reviewed in ref 67). This is particularly true for the simplest GGGH peptide[68] and the Aβ one.[27]

Copper(II) Coordination to Pyroglutamate Forms of Aβ Peptides. For copper(II) binding to the Aβp3-16 peptides, as expected from preclusion of the NH_2 terminal binding, His act(s) as anchoring residues for copper(II). In component II′, all of the available data converge toward a copper(II) binding site made by two imidazole rings from His, a deprotonated amidyl function, and either a carboxylate function or an imidazole ring from the third His residue, where the former proposition is favored based on the drastic broadening observed by NMR on the Asp7 and Glu11 side chains. In component III′, detected at higher pH, EPR data are in line with deprotonation of a second amidyl function, leading to a copper(II) binding site made by one (anchoring) imidazole ring from His, two deprotonated amidyl functions, and a carbonyle or a carboxylate function or an imidazole ring from the second His residue. On the basis of the similarity of the EPR data reporting copper(II) binding to the Ac-GGGTH-NH_2 peptide in component III′,[69] in which the copper(II) site was one imidazole ring from His, two deprotonated amidyl functions, and a carbonyle function, the former possibility is favored. In component IV′, a third amidyl function replaces the carbonyl one, leading to a {His, $3N^-$} copper(II) binding site.

Copper(II) Coordination to N-Terminally Modified Aβ Peptides: First-Coordination-Sphere Effects. The results obtained here by multiple complementary techniques (NMR, CD, XANES, and EPR) on copper(I) and copper(II) binding to Aβ3-16 and Aβp3-16 agree in terms of the nature of the different components observed as a function of the pH. According to these results, pH-dependent copper(II) coordination models are proposed in Scheme 1. For copper(II), the N-terminal amine plays a crucial role in line with its participation in copper(II) anchoring. Indeed, the absence of the free N-terminal amine reduces the copper(II) affinity, and the copper(II) site is located around the His residues only. This is the reason why the spectroscopic features of [Cu(Aβ3-16)] compare well with [Cu(Aβ1-16)], on the one hand, and [Cu(Aβp3-16)] with [Cu(Ac-Aβ1-16)], on the other hand. The two major CD differences between the two peptide groups is the shape of d−d and $-NH_2$ LMCT bands. The same distinction can be made regarding the EPR data obtained as a function of the pH. However, the EPR results alone can be misleading, especially in the absence of the attribution of all components as a function of the pH. This was the case for Drew et al.,[43] who concluded that copper(II) binds to Aβ3-16 and Aβp3-16 peptides in a similar way because of similar EPR parameters. They only detected the EPR signatures of two components for both Aβ3-16 and Aβp3-16 peptides, a "low-pH" component predominant at pH 6.3 (Aβ3-16) and pH 6.9 (Aβp3-16), and a "high-pH" component predominant at pH 8.5 (Aβ3-16) and above pH 9 (Aβp3-16).[43] Including their EPR data in Table 1 clearly shows that for the [Cu(Aβ3-16)] complex their "low-pH" component corresponds to component I and their "high-pH" form to component III. This is in line with a component II that never predominates in solution and is thus difficult to detect properly. Similarly, for the [Cu(Aβp3-16)] species, their "low-pH" form corresponds to component II′ and their "high-pH" form to component IV′. As can be seen in Table 1, components I and II′, on the one hand, and III and IV′, on the other hand, have comparable EPR parameters, hence the ill-interpretation of the EPR data in ref43. Thus, the full component assignments over a large pH range and the use of complementary methods such as CD and NMR are crucial to correctly assigning the components because the same EPR parameters do not imply the same copper(II) coordination sphere.

Copper(II) affinities for the different peptide studies here are in line with the coordination site proposed based on spectroscopic data. Indeed, copper(II) binding to the N-terminal amine of Aβ3-16 (and Aβ1-16) is also in agreement with the significant drop of the copper(II) affinity due to free N-terminal amine blocked in the case of Ac-Aβ1-16 and Aβp3-16 peptides. It is also worth noting that the copper(II) affinity for Aβ3-16 is slightly weaker than that for the Aβ1-16 peptide, while copper(II) coordination to the two peptides at pH 7.4 is different. Indeed, at pH 7.4, the main component in [Cu(Aβ1-16)] is I, including one metallacycle, whereas the main component in [Cu(Aβ3-16)] is II, including two metallacycles. Thus, the affinity measurements indicate that the formation of a

dx.doi.org/10.1021/ic302097d | Inorg. Chem. XXXX, XXX, XXX−XXX

Scheme 2. Proposed Interaction To Rationalize the Different Species pK_a(I/II) Values Determined between the [Cu(peptide)] Complexes[a]

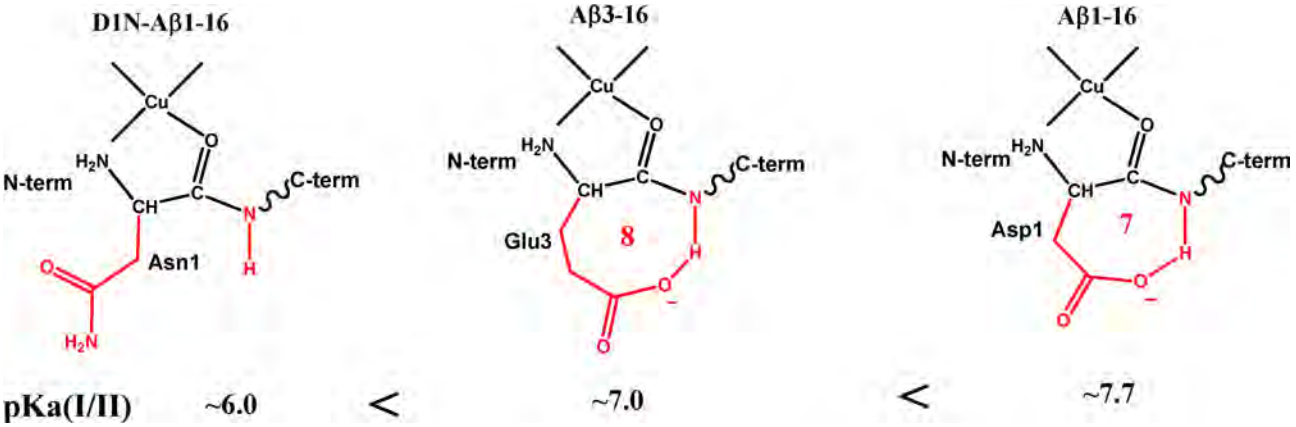

[a]In red, the N−H that undergoes deprotonation in component II (upper scheme) and the residue proposed to be involved with it.

second metallacyle is not favorable in terms of the copper(II) affinity. Such a similar trend has been recently observed for Cu(peptide) model systems encompassing two or three metallacycles.[70]

Copper(II) Coordination to N-Terminally Modified Aβ Peptides: Effects beyond the First Coordination Sphere. The four complexes [Cu(Aβ1-16)], [Cu(Aβ3-16)], [Cu(Ac-Aβ1-16)], and [Cu(Aβp3-16)] successively switch from component I/I′ to IV/IV′ via an additional amidyl binding for each further species. However, the pK_a values between two successive components are significantly different in the case of the [Cu(Aβ1-16)] and [Cu(Aβ3-16)] complexes (Table 1), while they are close in the case of [Cu(Ac-Aβ1-16)] and [Cu(Aβp3-16)]. In the latter case, this could be explained by the fact that a free N-terminal is not available for copper(II) coordination, leading to the same set of ligands for both Aβp3-16 and AcAβ. In contrast, the high variation in the pK_a(I/II) values between the [Cu(Aβ1-16)] and [Cu(Aβ3-16)] complexes can be rationalized by second-sphere effects (Scheme 2) in line with the pK_a(I/II) value previously determined for the mutants D1N and E3Q, respectively.[27,71] The key step between component I/II is deprotonation of the NH amide backbone. If the −NH function is stabilized by its involvement in intramolecular interaction such as hydrogen bonding, then the pK_a value between two successive components will be higher. This is typically the case for pK_a(I/II) values within the series of [Cu(D1N-Aβ1-16)], [Cu(Aβ3-16)], and [Cu(Aβ1-16)] species in which pK_a(I/II) is ~6.2,[27,71] ~7.0, and ~7.7, respectively. The highest stabilization of component I is observed for the [Cu(Aβ1-16)] complex, where the NH is stabilized by the hydrogen bond from COO^- of Asp1 forming a seven-membered ring. In [Cu(Aβ3-16)], a more moderate stabilization occurs because of the formation of an an eight-membered metallacycle (compared to seven-membered). No stabilization is detected in [Cu(D1N-Aβ1-16)] because the lone pair NH_2 of Asn1 is mainly delocalized on the adjacent carbonyl and can thus not be involved in hydrogen-bond interaction.

The Arg5 residue, while not directly involved in copper(II) coordination, seems to play a crucial role in copper(II) binding to [Cu(Aβ1-16)] by precluding the formation of a second metallacycle adjacent to the first $-NH_2-Cu^{II}-N^-$ cycle, in contrast to what was previously observed in the case of [Cu(Aβ1-16)]. Similar Arg5 effects were observed in the comparative study of copper(II) binding to the human and to its R5G mutant because replacement of Arg5 by Gly induces deprotonation of the Gly5−His6 peptide bond instead of the Asp1−Ala2 bond in the human case.[54] Also, Arg indirect effects, i.e., effects not related to binding of the side chain of Arg to Cu, were encountered in other studies. For instance, the copper(II) binding site of angiotensin II (sequence DRVYIH), initially observed around His6, moves to the N-term part with deprotonation of the D1−R2 and R2−V3 bonds at high pH.[72] This is reminiscent of what was observed here between components III and IV, where the metal center site has been reshuffled at high pH with deprotonation of the F4−R5 and R5−H6 bonds. Also, in sequence with specific nickel(II) peptide bond hydrolysis, Arg was shown to increase particularly the hydrolytic activity compared to other amino acids.[65] In the present case, the exact origin of such an Arg5 effect needs further investigation to be correctly depicted.

CONCLUDING REMARKS

The present study has revealed the copper(I) and copper(II) binding spheres to the two biologically relevant truncated forms of the Alzheimer peptide Aβ, i.e., Aβ3-16 and Aβp3-16. The application of a multispectroscopic approach (NMR, EPR, CD, and XANES) including affinity studies was crucial to deciphering the different components of the [Cu(peptide)] complexes and to identifying the most likely ligands in the component present at pH close to the physiological value. It turned out that, when available, the free N-terminal amine is the main anchor for copper(II) binding, as observed in the [Cu(Aβ1-16)] with [Cu(Aβ3-16)] complexes. When the N-terminal amine is blocked, as observed in the [Cu(Ac-Aβ1-16)] and [Cu(Aβp3-16)] complexes, His will take over the anchoring role. In addition to that feature, the present data also reveal an important role of the second-sphere environment because pH-dependent copper(II) coordination to Aβ1-16 and Aβ3-16 is significantly different. Hence, at physiological pH, the main coordination sites are altered in Aβ3-16 compared to Aβ1-16, with component I or II being predominant in the latter or former case, respectively. This also implies that Aβ modification of residues not directly involved in copper(II) binding does change the copper(II) binding site and can thus impact the aggregation and ROS production properties of the [Cu-

dx.doi.org/10.1021/ic302097d | Inorg. Chem. XXXX, XXX, XXX−XXX

(peptide)] complexes. Such a scenario might be of particular interest in the case of familial AD in which Aβ mutation has been reported. A well-known copper(II) coordination chemistry to these important N-terminally modified Aβ forms is a prerequisite for further studies on aggregation and toxicity. Such studies are currently in progress in our group.

■ ASSOCIATED CONTENT

Ⓢ Supporting Information

pH-dependent EPR, NMR, and XANES spectra of [Cu^{II}(peptide] complexes, assignments of the ^{1}H and ^{13}C NMR signals of the Aβ3-16 and Aβp3-16 peptides, NMR spectra of [Cu^{I}(peptide] complexes, and CD and Tyr10 fluorescence competition experiments. This material is available free of charge via the Internet at http://pubs.acs.org.

■ AUTHOR INFORMATION

Corresponding Author

*E-mail: bruno.alies@lcc-toulouse.fr (B.A.), christelle.hureau@lcc-toulouse.fr (C.H.). Tel.: (+33) 5 61 33 31 62. Fax: (+33) 5 61 55 30 03.

Notes

The authors declare no competing financial interest.

■ ACKNOWLEDGMENTS

Financial support from ANR NEUROMETALS (Agence Nationale de la Recherche; Grant Neurometals NT09-488591) as well as SOLEIL for the provision of synchrotron radiation on the SAMBA beamline (Proposal 20110116) is acknowledged. E. Renaglia is ackowledged for recording of the Tyr10 fluorescence data.

■ REFERENCES

(1) Puzzo, D.; Arancio, O. *J. Alzheimer's Dis.* **2012**, DOI: 10.3233/JAD-2012-129033.
(2) Holtzman, D. M.; Morris, J. C.; Goate, A. M. *Sci. Transl. Med.* **2011**, *3*, 77sr1.
(3) Hardy, J.; Selkoe, D. J. *Science* **2002**, *297*, 353−356.
(4) Klein, W. L.; Stine, W. B., Jr.; Teplow, D. B. *Neurobiol. Aging* **2004**, *25*, 569−580.
(5) Haass, C.; Selkoe, D. J. *Nat. Rev. Cell. Mol. Biol.* **2007**, *8*, 101−112.
(6) Gadad, B. S.; Britton, G. B.; Rao, K. S. *J. Alzheimer's Dis.* **2011**, *24*, 223−232.
(7) Ono, K.; Yamada, M. *J. Neurochem.* **2011**, *117*, 19−28.
(8) Lovell, M. A.; Robertson, J. D.; Teesdale, W. J.; Campbell, J. L.; Markesbery, W. R. *J. Neurol. Sci.* **1998**, *158*, 47−52.
(9) Miller, L. M.; Wang, Q.; Telivala, T. P.; Smith, R. J.; Lanzirotti, A.; Miklossy, J. *J. Struct. Biol.* **2006**, *155*, 30−37.
(10) Roychaudhuri, R.; Yang, M.; Hoshi, M. M.; Teplow, D. B. *J. Biol. Chem.* **2009**, *284*, 4749−4753.
(11) Donnelly, P. S.; Xiao, Z.; Wedd, A. G. *Curr. Opin. Chem. Biol.* **2007**, *11*, 128−133.
(12) Adlard, P. A.; Bush, A. I. *J. Alzheimer's Dis.* **2006**, *10*, 145−163.
(13) Karr, J. W.; Kaupp, L. J.; Szalai, V. A. *J. Am. Chem. Soc.* **2004**, *126*, 13534−13538.
(14) Minicozzi, V.; Stellato, F.; Comai, M.; Dalla Serra, M.; Potrich, C.; Meyer-Klaucke, W.; Morante, S. *J. Biol. Chem.* **2008**, *283*, 10784−10792.
(15) Syme, C. D.; Nadal, R. C.; Rigby, S. E.; Viles, J. H. *J. Biol. Chem.* **2004**, *279*, 18169−18177.
(16) Shearer, J.; Szalai, V. A. *J. Am. Chem. Soc.* **2008**, *130*, 17826−17835.
(17) Faller, P.; Hureau, C. *Dalton Trans.* **2009**, 1080−1094.
(18) Sarell, C. J.; Syme, C. D.; Rigby, S. E.; Viles, J. H. *Biochemistry* **2009**, *48*, 4388−4402.
(19) Zawisza, I.; Rózga, M.; Bal, W. *Coord. Chem. Rev.* **2012**, *256*, 2297−2307.
(20) Hureau, C. *Coord. Chem. Rev.* **2012**, *256*, 2164−2174.
(21) Hureau, C.; Dorlet, P. *Coord. Chem. Rev.* **2012**, *256*, 2175−2187.
(22) Dorlet, P.; Gambarelli, S.; Faller, P.; Hureau, C. *Angew. Chem., Int. Ed.* **2009**, *48*, 9273−9276.
(23) Drew, S. C.; Masters, C. L.; Barnham, K. J. *J. Am. Chem. Soc.* **2009**, *131*, 8760−8761.
(24) Drew, S. C.; Noble, C. J.; Masters, C. L.; Hanson, G. R.; Barnham, K. J. *J. Am. Chem. Soc.* **2009**, *131*, 1195−1207.
(25) Kowalik-Jankowska, T.; Ruta, M.; Wisniewska, K.; Lankiewicz, L. *J. Inorg. Biochem.* **2003**, *95*, 270−282.
(26) Hureau, C.; Coppel, Y.; Dorlet, P.; Solari, P. L.; Sayen, S.; Guillon, E.; Sabater, L.; Faller, P. *Angew. Chem., Int. Ed.* **2009**, *48*, 9522−9525.
(27) Alies, B.; Eury, H.; Bijani, C.; Rechignat, L.; Faller, P.; Hureau, C. *Inorg. Chem.* **2011**, *50*, 11192−11201.
(28) Himes, R. A.; Park, G. Y.; Siluvai, G. S.; Blackburn, N. J.; Karlin, K. D. *Angew. Chem., Int. Ed.* **2008**, *47*, 9084−9087.
(29) Hureau, C.; Balland, V.; Coppel, Y.; Solari, P. L.; Fonda, E.; Faller, P. *J. Biol. Inorg. Chem.* **2009**, 995−1000.
(30) Furlan, S.; Hureau, C.; Faller, P.; La Penna, G. *J. Phys. Chem. B* **2010**, *114*, 15119−15133.
(31) Harigaya, Y.; Saido, T. C.; Eckman, C. B.; Prada, C. M.; Shoji, M.; Younkin, S. G. *Biochem. Biophys. Res. Commun.* **2000**, *276*, 422−427.
(32) Jawhar, S.; Wirths, O.; Bayer, T. A. *J. Biol. Chem.* **2011**, *286*, 38825−38832.
(33) Wirths, O.; Breyhan, H.; Cynis, H.; Schilling, S.; Demuth, H. U.; Bayer, T. A. *Acta Neuropathol. (Berlin)* **2009**, *118*, 487−496.
(34) Schlenzig, D.; Rönicke, R.; Cynis, H.; Ludwig, H. H.; Scheel, E.; Reymann, K.; Saido, T.; Hause, G.; Schilling, S.; Demuth, H. U. *J. Neurochem.* **2012**, *121*, 774−784.
(35) Schilling, S.; Zeitschel, U.; Hoffmann, T.; Heiser, U.; Francke, M.; Kehlen, A.; Holzer, M.; Hutter-Paier, B.; Prokesch, M.; Windisch, M.; Jagla, W.; Schlenzig, D.; Lindner, C.; Rudolph, T.; Reuter, G.; Cynis, H.; Montag, D.; Demuth, H. U.; Rossner, S. *Nat. Med.* **2008**, *14*, 1106−1111.
(36) Frost, J. L.; Liu, B.; Kleinschmidt, M.; Schilling, S.; Demuth, H. U.; Lemere, C. A. *Neurodegener. Dis.* **2012**, *10*, 265−270.
(37) Wittnam, J. L.; Portelius, E.; Zetterberg, H.; Gustavsson, M. K.; Schilling, S.; Koch, B.; Demuth, H. U.; Blennow, K.; Wirths, O.; Bayer, T. A. *J. Biol. Chem.* **2012**, *287*, 8154−8162.
(38) Güntert, A.; Döbeli, H.; Bohrmann, B. *Neuroscience* **2006**, *143*, 461−475.
(39) Wirths, O.; Bethge, T.; Marcello, A.; Harmeier, A.; Jawhar, S.; Lucassen, P. J.; Multhaup, G.; Brody, D. L.; Esparza, T.; Ingelsson, M.; Kalimo, H.; Lannfelt, L.; Bayer, T. A. *J. Neural Transm.* **2010**, *117*, 85−96.
(40) Schlenzig, D.; Manhart, S.; Cinar, Y.; Kleinschmidt, M.; Hause, G.; Willbold, D.; Funke, S. A.; Schilling, S.; Demuth, H. U. *Biochemistry* **2009**, *48*, 7072−7078.
(41) Schilling, S.; Lauber, T.; Schaupp, M.; Manhart, S.; Scheel, E.; Böhm, G.; Demuth, H. U. *Biochemistry* **2006**, *45*, 12393−12399.
(42) Nussbaum, J. M.; Schilling, S.; Cynis, H.; Silva, A.; Swanson, E.; Wangsanut, T.; Tayler, K.; Wiltgen, B.; Hatami, A.; Rönicke, R.; Reymann, K.; Hutter-Paier, B.; Alexandru, A.; Jagla, W.; Graubner, S.; Glabe, C. G.; Demuth, H. U.; Bloom, G. S. *Nature* **2012**, *485*, 651−655.
(43) Drew, S. C.; Masters, C. L.; Barnham, K. J. *PloS One* **2011**, *5*, e15875.
(44) Delgado, R.; Da Silva, J. J. R. F.; Amorim, M. T. S.; Cabral, M. F.; Chaves, S.; Costa, J. *Anal. Chim. Acta* **1991**, *245*, 271−282.
(45) Krezel, A.; Bal, W. *J. Inorg. Biochem.* **2004**, *98*, 161−166.
(46) Solomon, E. I. *Inorg. Chem.* **2006**, *45*, 8012−8025.
(47) Faller, P.; Hureau, C.; Dorlet, P.; Hellwig, P.; Coppel, Y.; Collin, F.; Alies, B. *Coord. Chem. Rev.* **2012**, *256*, 2381−2396.

(48) Hong, L.; Carducci, T. M.; Bush, W. D.; Dudzik, C. G.; Millhauser, G. L.; Simon, J. D. *J. Phys. Chem. B* **2010**, *114*, 11261−11271.
(49) Karr, J. W.; Akintoye, H.; Kaupp, L. J.; Szalai, V. A. *Biochemistry* **2005**, *44*, 5478−5487.
(50) Livera, C.; Pettit, L. D.; Bataille, M.; Krembel, J.; Bal, W.; Kozlowski, H. *J. Chem. Soc., Dalton Trans.* **1988**, 1357−1360.
(51) Peisach, J.; Blumberg, W. E. *Arch. Biochem. Biophys.* **1974**, *165*, 691−708.
(52) Pedersen, J. T.; Teilum, K.; Heegaard, N. H. H.; Østergaard, J.; Adolph, H.-W.; Hemmingsen, L. *Angew. Chem., Int. Ed.* **2011**, *50*, 2532−2535.
(53) Hureau, C.; Eury, H.; Guillot, R.; Bijani, C.; Sayen, S.; Solari, P. L.; Guillon, E.; Faller, P.; Dorlet, P. *Chem.—Eur. J.* **2011**, *17*, 10151−10160.
(54) Eury, H.; Bijani, C.; Faller, P.; Hureau, C. *Angew. Chem., Int. Ed.* **2011**, *50*, 901−905.
(55) Raffa, D. F.; Rickard, G. A.; Rauk, A. *J. Biol. Inorg. Chem.* **2007**, *12*, 147−164.
(56) Raffa, D. F.; Gómez-Balderas, R.; Brunelle, P.; Rickard, G. A.; Rauk, A. *J. Biol. Inorg. Chem.* **2005**, *10*, 887−902.
(57) Damante, C. A.; Osz, K.; Nagy, Z.; Pappalardo, G.; Grasso, G.; Impellizzeri, G.; Rizzarelli, E.; Sóvágó, I. *Inorg. Chem.* **2008**, *47*, 9669−9683.
(58) Harford, C.; Sarkar, B. *Acc. Chem. Res.* **1997**, *30*, 123−130.
(59) Sokolowska, M.; Krezel, A.; Dyba, M.; Szewczuk, Z.; Bal, W. *Eur. J. Biochem.* **2002**, *269*, 1323−1331.
(60) Sokołowska, M.; Bal, W. *J. Inorg. Biochem.* **2005**, *99*, 1653−1660.
(61) Kiss, T.; Sovago, I.; Gergely, A. *Pure Appl. Chem.* **1991**, *63*, 597−638.
(62) Sacco, C.; Skowronsky, R. A.; Gade, S.; Kenney, J. M.; Spuches, A. M. *J. Biol. Inorg. Chem.* **2012**, *17*, 531−541.
(63) Alies, B.; Badei, B.; Faller, P.; Hureau, C. *Chem.—Eur. J.* **2012**, *18*, 1161−1167.
(64) Bal, W.; Jezowska-Bojczuk, M.; Kozlowski, H.; Chruscinski, L.; Kupryszewski, G.; Witczuk, B. *J. Inorg. Biochem.* **1995**, *57*, 235−247.
(65) Jancsó, A.; Selmeczi, K.; Gizzi, P.; Nagy, N. V.; Gajda, T.; Henry, B. *J. Inorg. Biochem.* **2011**, *105*, 92−101.
(66) Pettit, L. D.; Pyburn, S.; Bal, W.; Kozlowski, H.; Bataille, M. *J. Chem. Soc., Dalton Trans.* **1990**, 3565−3570.
(67) Kozłowski, H.; Kowalik-Jankowska, T.; Jezowska-Bojczuk, M. *Coord. Chem. Rev.* **2005**, *249*, 2323−2334.
(68) Várnagy, K.; Szabó, J.; Sóvágó, I.; Malandrinos, G.; Nick, H.; Sanna, D.; Micera, G. *J. Chem. Soc., Dalton Trans.* **2000**, 467−472.
(69) Hureau, C.; Charlet, L.; Dorlet, P.; Gonnet, F.; Spadini, L.; Anxolabéhère-Mallart, E.; Girerd, J.-J. *J. Biol. Inorg. Chem.* **2006**, *11*, 735−744.
(70) Trapaidze, A.; Hureau, C.; Bal, W.; Winterhalter, M.; Faller, P. *J. Biol. Inorg. Chem.* **2012**, *17*, 37−47.
(71) Karr, J. W.; Szalai, V. A. *J. Am. Chem. Soc.* **2007**, *129*, 3796−3797.
(72) Decock-Le Reverend, B.; Liman, F.; Livera, C.; Pettit, L. D.; Pyburn, S.; Kozlowski, H. *J. Chem. Soc., Dalton Trans.* **1988**, 887−894.

Le processus d'agrégation, dans lequel des peptides passent d'une forme monomérique à un assemblage complexe, apparait dans de nombreuses maladies comme celle d'Alzheimer. Divers éléments suggèrent que les ions métalliques tels que le Zn(II) et Cu(II) sont impliqués dans ce phénomène. Afin de mieux comprendre l'implication des ions métalliques sur l'agrégation de peptides, nous nous sommes intéressés à des peptides modèles. Ces modèles nous ont permis de mettre au jour, l'importance du mode de coordination des ions métalliques et ses différents impacts sur l'agrégation. Ce chapitre résume les trois articles qui suivent.

III- Agrégation

III. 1- Problématiques

Comment les ions métalliques Cu(II) et Zn(II) influencent-t-ils le processus d'agrégation ? Autrement dit, quels sont les caractéristiques déterminantes de l'interaction peptide-metal et quelles sont les conséquences engendrées sur la structuration du peptide ? Comment ces ions métalliques peuvent modifier l'agrégation ?

Afin de répondre à ces différentes questions, nous nous sommes intéressés à différents peptides modèles nommés Aβ11-28 et Aβ14-23 avec un intérêt plus prononcé pour le premier d'entre eux. La séquence de ces peptides est issue du peptide Amyloïde-β (Aβ1-42), élément clé de la maladie d'Alzheimer. Bien que certains de ces peptides tronqués soit retrouvés *in vivo,*[1] le but de ces recherches n'est pas de mimer un type particulier d'interaction métal-peptide, mais plutôt de comprendre les processus clés et généralisables du lien entre métaux, peptide et agrégation. En effet, cette problématique dépasse largement le cadre de la maladie d'Alzheimer. Les mêmes acteurs interviennent dans d'autres maladies,[2] telles que Parkinson, Creutzfeld-Jakob, SLA (Sclérose Latérale Amyotrophique) ou encore dans le diabète de type II[3] (voir tableau 1). L'agrégation ou plutôt l'auto-assemblage de peptides via l'utilisation d'ions métalliques comme modulateur est aussi un des sujets d'intérêt pour les bio/nano technologies. Une meilleure connaissance fondamentale de ce sujet d'étude (Lien entre Peptide – Métaux – Agrégation) couvre donc un large domaine de connaissances et d'applications.

Proteine / Peptide	Maladie Associée
Amyloïde-β	Alzheimer
α-syncleine	Parkinson
Superoxide Dismutase	SLA
Amylin	Diabète de type 2
Prion	Creutzfeldt-Jakob

Tableau 1 : Exemple de peptide ou de protéine dont l'agrégation est impliquée dans une maladie.

Revenons maintenant au choix des peptides, il est basé sur les deux points essentiels :

- Possibilité de lier des ions métalliques
- Tendance à l'agrégation

Cela est rendu possible grâce la conservation de la partie de séquence du peptide Aβ qui contient :

- Des ligands potentiels (comme Histidine et aussi, N-term, C-term, squelette peptiques, Aspartate, Glutamate)

- Un fort regroupement de résidus **hydrophobes** (Phenylalanine, Leucine, Alanine…)

Les séquences des peptides Aβ1-42, Aβ11-28, Aβ11-23, Aβ14-23 possédant les caractéristiques précédemment énoncées, vous sont présentées ci-dessous.

Aβ1-42 NH_2-D**A**E**F**RHDSGYE**V**HHQK**LVFFA**EDVGSNKG**AII**G**L**M**V**GG**VVIA**-COOH

Aβ11-28 NH_2-E**V**HHQK**LVFFA**ED**V**GSNK-COOH

Aβ14-23 NH_2-HQK**LVFFA**ED-COOH

Figure 1 : Séquences de peptides (utilisant le code à une lettre) qui souligne leur origine commune, les ligands potentiels et les chaines latérales hydrophobes. Ligands azotés en bleu ; ligands oxygénés en rouge ; chaines latérales hydrophobes en gras.

Dans le choix des peptides modèles, on note clairement deux parties, la partie N-term avec des ligands des métaux et la partie C-term avec le « noyau » hydrophobe du peptide Aβ (LVFFA). Maintenant que nous avons nos modèles, comment étudier l'effet du Cu(II) et du Zn(II) sur l'agrégation de ses peptides ?

III. 2- Méthodes et Principes :

Différentes techniques permettent d'observer l'agrégation et donc l'influence des ions métalliques sur celle-ci. Chacune d'entre-elles possède ses spécificités, ses avantages et ses limites.

a- Mécanisme de l'agrégation

Le mécanisme de l'agrégation est généralement décrit par trois phases successives : la nucléation, l'élongation et le plateau. La nucléation est décrite comme l'étape cinétiquement déterminante et correspond à la formation de noyaux (= oligomères). Lorsque le seuil critique de taille d'agrégat (noyaux) est atteint, l'élongation commence, elle est caractérisée par l'empilement en feuillet-β de peptides. Ces empilements forment ainsi les fibres. Enfin, quand le nombre de peptides vient à manquer pour continuer l'empilement, on arrive au plateau. La formation de fibre s'arrête.[4] La forme de cette cinétique (avec x = le temps et y = quantité de fibres) est une sigmoïde. La cinétique est généralement suivie par fluorescence de la Thioflavine T (voir ci-dessous). Un paramètre caractéristique de cette sigmoïde est le $t_{1/2}$, il correspond au temps nécessaire pour atteindre la moitié de la valeur maximale.[5]

b- Agrégation : fibrillaire ou amorphe ?

Le terme d'agrégation sera utilisé de manière indifférenciée pour désigner tout type d'agrégats, qu'il s'agisse agrégats amyloïde ou amorphes. Une amyloïde est constituée d'un empilement de peptides organisés en feuillets-β. Au contraire, un agrégat amorphe n'aura pas de structure tridimensionnelle bien définie. De plus, celui-ci est généralement plus enclin à devenir insoluble (précipitation) qu'un agrégat amyloïde.

c- Fluorescence et ThT

La fluorescence est une technique intrinsèquement sensible, encore faut-il avoir un fluorophore adéquat. La Thioflavine T (ThT) est une molécule qui a la propriété de changer sa fluorescence (λ_{exc} et λ_{emi} differents) et d'exacerber sa fluorescence en présence de fibres (voir figure 2 et structure en annexe). Aussi, suivre la fluorescence de la ThT, c'est suivre l'agrégation amyloïde du peptide. Ses avantages : elle permet la quantification, le suivi cinétique et présente une forte spécificité pour les fibres amyloïde (elle interagit peu avec les agrégats amorphes). Comme la ThT peut être utilisée à faible concentration, son influence sur la formation de fibres est minimisée. Ses inconvénients : la fluorescence de la ThT peut être quenchée par Cu(II) et l'interaction de la ThT avec les fibres reste mal décrite.

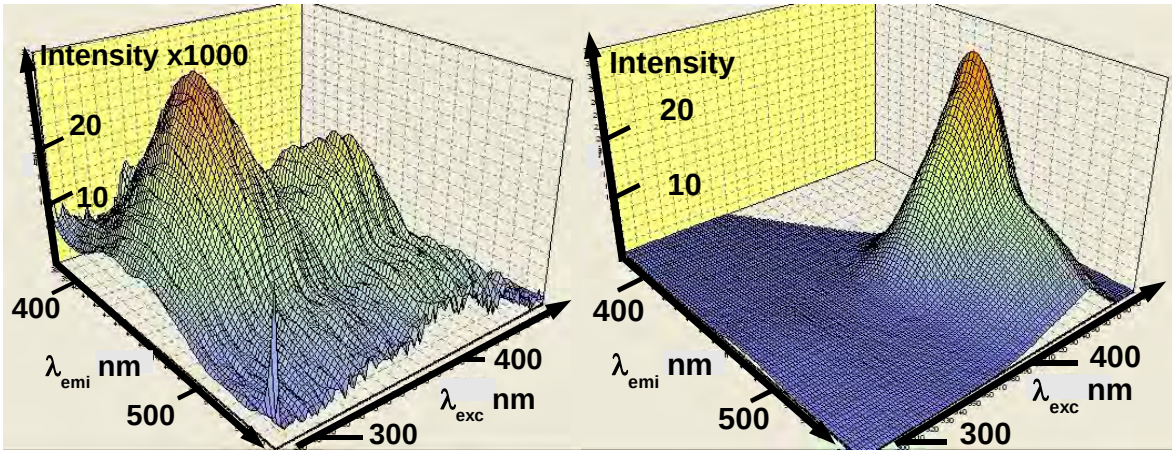

Figure 2 : Spectre de 3D de la Fluorescence de la ThT (x: λ_{emi} ; y: λ_{exc} ; z: intensité) en l'absence (intensité env. x1000) à gauche, et en présence de fibres à droite. Conditions : [ThT] =100µM; [HEPES] = 100mM; T = 20°C.

d- Absorbance et turbidité

La turbidité mesure le trouble d'une solution. Le suivi de l'absorbance à une longueur d'onde fixée où l'échantillon ne présente pas absorption électronique. Aussi, « l'absorbance » mesuré est dû à la diffusion de lumière, est donc comparable à une mesure de turbidité. Sa mesure permet de suivre l'agrégation. Cette mesure est plutôt représentative de l'état global d'agrégation que spécifique de l'agrégation amorphe ou fibrillaire.

e- MET et fibres

La Microscopie Electronique à Transmission (MET), à la différence de la microscopie optique, permet de visualiser des objets de l'ordre du nanomètre. Dans notre utilisation, la coloration négative à l'acétate d'uranyle révèle les assemblages de peptides. Cette technique sert à distinguer les différents types d'agrégats rencontrés (amorphe / fibrillaire).

f- XANES et ions metalliques

La spectroscopie de structure près du front d'absorption de rayons X (ou XANES en anglais pour X-ray Absorption Near Edge Structure) est principalement réalisée sur synchrotron. Le spectre obtenu correspond à l'absorption dans le domaine des rayons X de l'élément considéré sur une courte plage d'énergie (contrairement à l'EXAFS). Celle-ci peut être utilisée comme une signature contenant des informations sur la nature de l'élément, son degré d'oxydation ainsi que sa coordination. Dans notre cas, les éléments étudiés seront des complexes peptidiques de Cu ou de Zn.

Il est nécessaire d'utiliser différentes techniques et de coupler les résultats provenant de celles-ci afin d'obtenir une image globale.

III. 3- Expérience

a- Importance de la monomérisation

Ci-dessous, la figure 3 représente tout l'intérêt de partir du même état initial pour étudier le processus d'agrégation. En effet, le suivi par fluorescence de la ThT montre que deux différents lots (carré et cercle noir) d'un même peptide en l'absence d'ions métalliques (apo) dans les mêmes conditions ne présentent pas la même agrégation. L'hypothèse est la suivante, la différence entre ces deux lots provient de deux états de pré-agrégation différents. Le lot « carré noir » contient plus de pré-agrégats que le lot « cercle noir ». Aussi, dans les conditions de l'expérience un lot agrège spontanément alors que l'autre est stable. Pour pallier ce problème, ces deux lots sont soumis à une pré-incubation à pH 12 afin de monomériser les pré-agrégats présents. Le point isoélectrique de ces peptide étant autour de pH ~6, l'augmentation de pH augmente la charge négative sur le peptide ce qui permet la dissociation des pré-agrégats. La même expérience est alors reconduite dans les mêmes conditions que précédemment et les deux lots (carré et rond blanc) se comportent alors de manière identique.

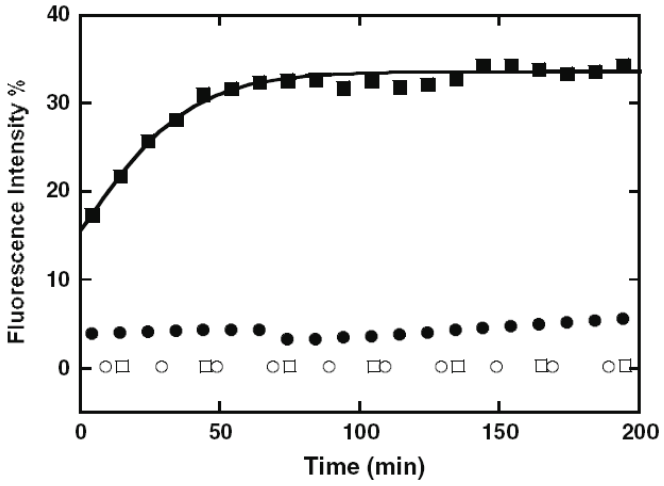

Figure 3 : Fluorescence de la ThT au cours du temps de apo-Aβ11-28 provenant de différents lots (carré et rond) avec (blanc vide) et sans (noir plein) préincubation à pH 12.
Conditions : [Aβ11-28] = 300µM, [Hepes] = 100mM pH 7,4, [ThT] = 10µM.

Cette expérience démontre l'importance de l'état initial dans le cas de l'agrégation. Afin d'éviter de considérer ce paramètre majeur, toutes les expériences suivantes seront

réalisées à partir de solutions de peptides pré-incubées à pH 12, dosées par UV-vis, diluées à 1.2 mM, aliquotées, congelées à l'azote liquide et enfin placées à -20°C.

b- Effet du Cu(II) et Zn(II) sur Aβ11-28 et Aβ14-23

Etudions maintenant les différents peptides en présence des ions Cu(II) et Zn(II) à l'aide des techniques annoncées ci-dessus. La figure 4 nous présente une étude comparative du comportement de Aβ11-28 et Aβ14-23 en présence des deux ions métalliques d'intérêt par fluorescence de la ThT, turbidité et MET. Dans la figure 4, on constate des comportements similaires entre Aβ11-28 et Aβ14-23 :

- L'apo-peptide n'agrège pas sur la durée de l'expérience
- Le Zn(II) déclenche l'agrégation

Malgré ces comportements similaires, on notera des différences sur la vitesse et sur l'intensité d'agrégation induite par le Zn ($t_{1/2}$ (Aβ11-28) >> $t_{1/2}$ (Aβ14-23)).

Il est aussi très intéressant de remarquer les comportements diamétralement opposés de Aβ11-28 et de Aβ14-23 vis-à-vis du Cu(II). Alors que le Cu(II) inhibe l'agrégation du peptide Aβ11-28, il la déclenche sur Aβ14-23. On notera sur le Aβ14-23 que la fluorescence de la ThT est quenchée par le Cu(II) car les autres techniques montrent la présence de l'agrégation induite par le Cu(II). Deux idées se détachent de cette figure:
L'agrégation induite par les ions métalliques dépend, d'une part, de la séquence du peptide (Aβ11-28 ≠ Aβ14-23) et d'autre part, de l'ion métallique (Cu(II) ≠ Zn(II)). La coordination permet-t-elle de faire le lien ? Afin d'en savoir plus, nous nous sommes intéressés de plus près aux types de coordinations.

c- Coordination du Cu(II), Aβ11-28 vs Aβ14-23

La séquence du Aβ11-28 contient un motif ATCUN (Amino Terminal Cu and Ni binding). Le motif ATCUN est défini par la séquence suivante : NH_2-XXH-R (avec X≠P). On le retrouve dans différents types d'Albumines et dans d'autres peptides.[6] Ce motif est caractérisé par sa propriété à lier un ion Cu(II) ou un ion Ni(II) avec une forte affinité. La coordination au métal se fait via quatre atomes d'azote provenant de l'amine terminale (NH_2), les deux amides déprotonés suivant (N^-) et du Nδ de l'Histidine en troisième position. Lorsque le Cu est lié, la partie du N-terminale est alors enroulée autour du Cu. Le Cu-ATCUN a des caractéristiques précises dans des nombreuses spectroscopies (UV-vis ; RPE…). Il a été montré que la coordination du Cu(II) par le Aβ11-28 se fait via le motif ATCUN.[7]

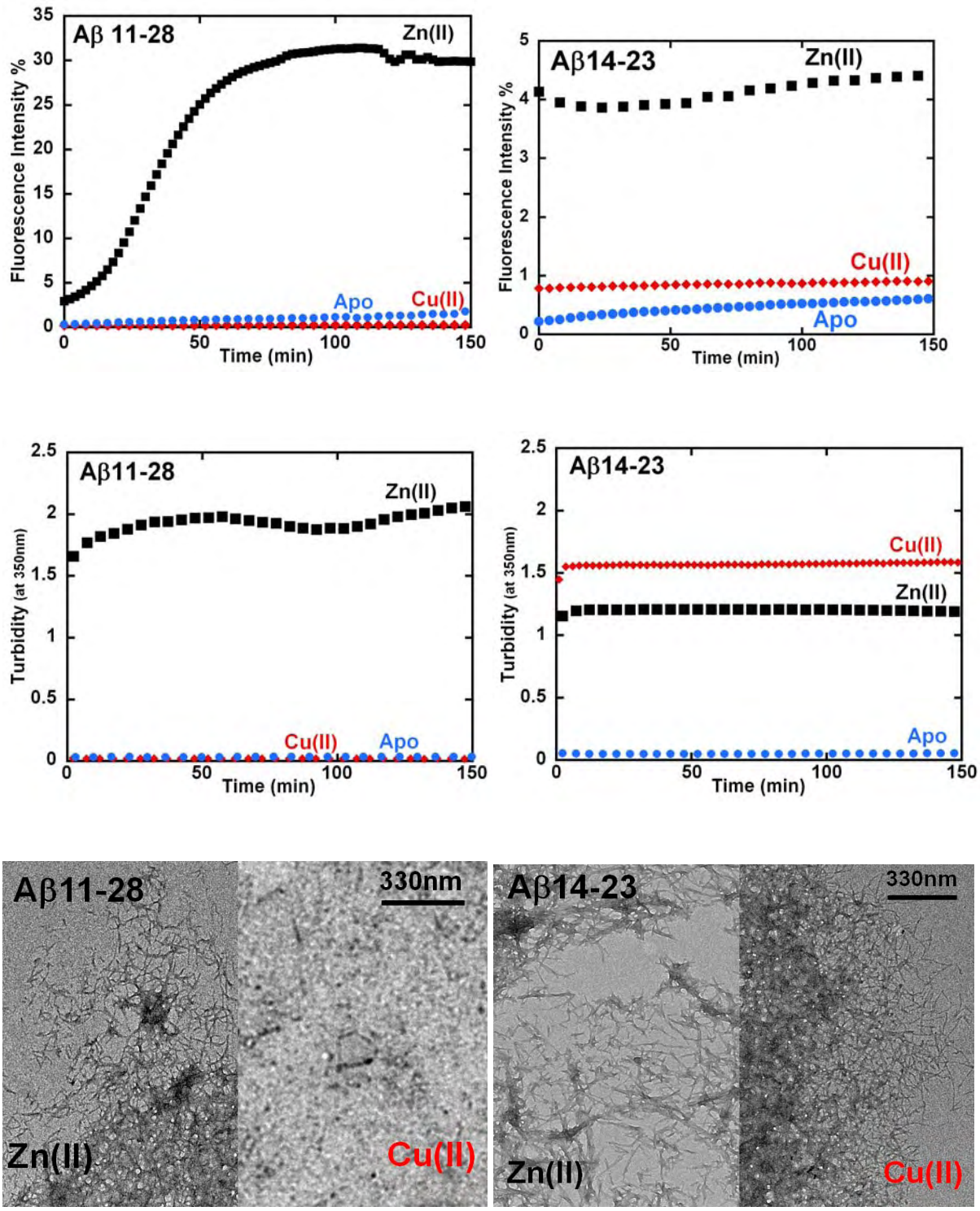

Figure 4 : Fluorescence de la ThT (dessus), turbidité (milieu) au cours du temps et MET (dessous) après incubation, des peptides Aβ11-28 (gauche) et Aβ14-23 (droite) en absence (cercle bleu) ou en présence de 0.9 équivalent de Zn(II) (noir, carré) ou de Cu(II) (rouge, losange). Condition : [peptide] = 300µM; [Hepes] = 100mM pH 7,4 ; [ThT] = 10µM seulement pour la fluorescence.

Dans le cas du Aβ14-23, le motif ATCUN n'est pas présent. La coordination sera donc nécessairement différente. Bien que la géométrie précise des ligands reste floue, les données structurales suggèrent l'implication de l'histidine en N-term, bidentate avec l'amine NH_2 terminale et l'imidazole. Il est donc très probable que le Cu soit lié *via* deux peptides Aβ14-23.

La nature de la coordination semble bel et bien être à la source des différents comportements d'agrégation vis-à-vis de la présence de Cu(II). En effet, la coordination du Cu sur le Aβ11-28 via le motif ATCUN entraine l'enroulement du N-terminal, réduisant le nombre de liaisons hydrogène possibles et donc l'agrégation. Au contraire, dans le cas du peptide Aβ14-23, l'implication de deux peptides « recrutés » pour lier le Cu, augmentera fortement la possibilité de créer des liaisons hydrogènes entre eux. Cet effet aura donc tendance à l'accentuer l'agrégation (voir schéma ci-contre).

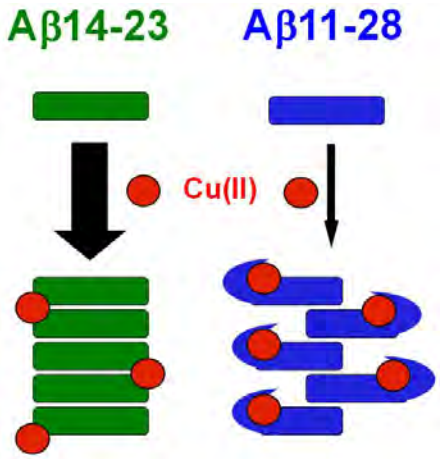

Schéma 1 : Effet de la coordination du Cu(II) sur l'agrégation de Aβ11-28 et Aβ14-23. A la différence du Aβ14-23, la coordination du Cu(II) par le Aβ11-28 provoque un enroulement du peptide autour du Cu, réduisant le nombre de liaisons hydrogène possibles et donc l'agrégation

d- Coordination du Zn(II) au Aβ11-28

Quel soit le peptide, le Zn(II) semble promouvoir l'agrégation (voir figure 4). Quel rôle joue la coordination dans ce phénomène ? Afin de répondre à cette question, l'interaction Zn(II) – Aβ11-28 a été étudiée en détail.

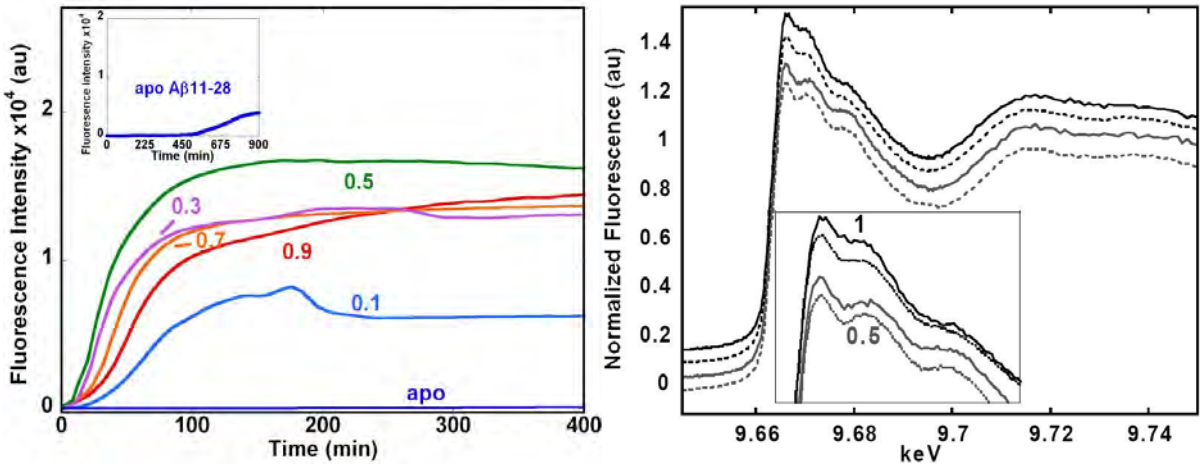

Figure 5 : A gauche, fluorescence de la ThT au cours du temps de Aβ11-28 en présence de Zn(II) à différentes stœchiométries (0éq bleu foncé ; 0.1éq bleu clair ; 0.3éq rose ; 0.5éq vert ; 0.7éq orange ; 0.9éq rouge). A droite, le XANES au seuil du Zn de Aβ11-28 en présence de 1 (noir) ou 0.5 (gris) équivalent de Zn(II) avant (ligne en pointillés) ou après l'agrégation (ligne continue). En cartouche, l'agrandissement de la zone autour de 9.67 keV. Conditions : Fluorescence de la ThT : [Aβ11-28] = 300 µM; [Zn(II)] = 0-270 µM ; [HEPES] = 100 mM, pH 7,4 ; [ThT] = 10 µM ; XANES : [Aβ11-28] = 2.4 mM ; [Zn(II)] = 1.2 or 2.2 mM; [HEPES] = 50 mM, pH 7,0.

La figure 5, panneau de gauche, nous présente la fluorescence de la ThT du Aβ11-28 à différentes stœchiométries. On y remarque que la vitesse ainsi que l'intensité de l'agrégation ne sont pas proportionnelles à la stœchiométrie en Zn(II). Ces deux paramètres sont maximisés pour un ratio Zn(II)/Aβ11-28 = 0.5. Le panneau de droite nous montre la signature en spectroscopie XANES du peptide Aβ11-28 en présence de 0.5 ou 1 équivalent de Zn(II) avant et après l'agrégation. On constate tout d'abord que la coordination du Zn(II) ne semble pas changer au cours de l'agrégation (la ligne en pointillés et la ligne continue sont identiques). Par contre, la stœchiométrie du Zn(II) semble avoir un rôle sur coordination du Zn(II). En effet, l'agrandissement au seuil du Zn montre une différence entre le ratio 0.5 (en gris) et 1 (en noir). De plus, les spectres XANES enregistrés pour des stœchiométries inférieures à 0.5 équivalent sont comparables à celui à 0.5 équivalent, tandis que les spectres de stœchiométries supérieures à 0.5 sont comparables à celui à 1 équivalent.

Ces deux éléments distincts convergent vers la même idée : la formation d'un dimère Zn-(Aβ11-28)$_2$. La formation de ce dimère serait donc à l'origine de l'effet accélérateur du Zn(II) sur l'agrégation des différents peptides. Qu'en est-il des ligands impliqués dans la formation de ce possible dimère ?

Rien de tel que la RMN pour nous apporter des informations structurales manquantes. Ci-dessous, la figure 6 de gauche, présente le spectre RMN ^{1}H centré sur les protons aromatiques, de Aβ11-28 et de tetra-peptide modèles de séquence NH_2-EVXX-NH_2 (Aβ11-14) avec et sans Zn(II). Lorsque le Zn(II) est ajouté à Aβ11-28, il provoque le déplacement préférentiel de deux protons d'une histidine. Le but est d'identifier l'histidine mise en jeu dans la coordination du Zn(II). Ce déplacement est aussi visible sur le spectre des peptides EVHH (C) et EVRH (B) mais pas sur celui de EVHG (A). Cela suggère fortement l'implication de l'histidine 14 dans la coordination du Zn(II). De plus, les protons Hβ du Glu11 de Aβ11-28 et du Glu de EVHH sont affectés par la présence de Zn(II) (non montré).

Basé sur ces indices, nous avons proposé un modèle de la coordination du Zn(II) par deux peptides Aβ11-28, avec comme ligands le COO^- du Glu11 et l'imidazole de l'His14. La possibilité d'autres ligands par exemple une molécule d'eau n'est pas exclue (l'analyse des données d'EXAFS privilégie un Zn pentacoordiné plutôt que tetracoordiné). Ce modèle est présenté dans la figure 6 de droite, où l'on suppose l'induction de feuillets-β parallèles par la coordination du Zn(II) au COO^- du Glu11 et au noyau imidazole de l'His14, expliquant ainsi la tendance à l'agrégation du Aβ11-28 en présence de Zn(II).

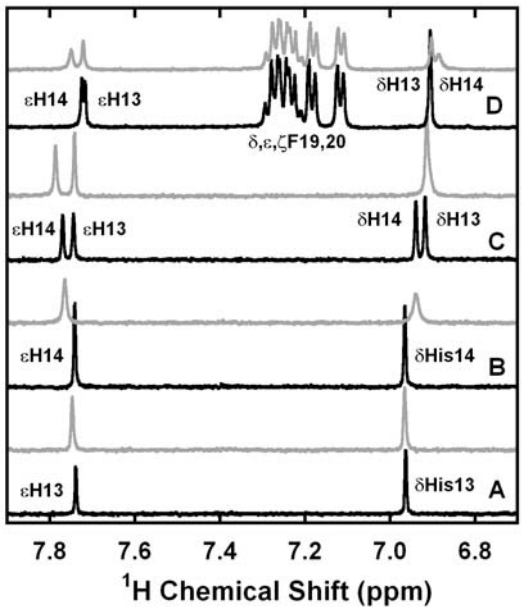

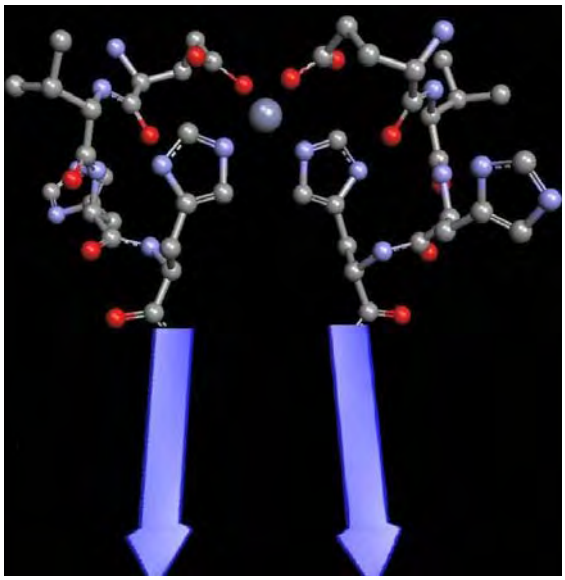

Figure 6 : (A gauche) ^{1}H RMN, avec (gris) et sans Zn(II) (noir) de peptides EVHG (A), EVRH (B), EVHH (C), and Aβ11-28 (D). Conditions: [peptide] = 300 μM; [Zn(II)] = 270 μM; [Tris-D_{11}] = 100 mM, pH 7,5. (A droite) Modèle proposé pour le complexe Zn(Aβ11-28).

Résumons les points précédents, la coordination du Zn(II) contrairement à celle du Cu(II) induit la formation d'un dimère, via les résidus Glu11 et His14, à l'origine de l'agrégation rapide induite par le Zn(II) à pH 7,4. Qu'en est-il à d'autres pH ? Comment évoluent l'agrégation et la coordination ?

e- Effet du pH

Ci-dessous, la figure 7 décrit la dépendance de l'agrégation de Aβ11-28 en fonction du pH en présence de 0.5 équivalent de Zn(II). Les paramètres de l'étude sont les vitesses ($t_{1/2}$) et les intensités des plateaux déterminés par la fluorescence de la ThT et par turbidité. La figure 7 du dessus nous présente une expérience typique au cours du temps à un pH donné. On peut y extraire les $t_{1/2}$ et les intensités des plateaux (flèches et ligne horizontale) provenant de la mesure en simultané à la fois de la turbidité et la fluorescence de la ThT. Cette expérience a été répétée sur une plage de pH autour du pH physiologique (*i.e* 7,4). Les paramètres d'intensité (plateau d'intensité) et de vitesse ($t_{1/2}$) en fonction du pH sont regroupés dans la figure 7 du milieu et dans la figure 7 du dessous, respectivement.

Dans la figure du milieu et du dessous, on note tout d'abord que les comportements vis-à-vis du pH détectés par les deux méthodes sont clairement différents. En effet, dans la figure du milieu, alors que l'intensité du plateau en turbidité est très dépendante du pH, l'intensité du plateau en fluorescence est relativement constante quel que soit le pH. On trouve la tendance inverse si on s'intéresse aux $t_{1/2}$ (figure 7 du dessous). Le $t_{1/2}$ en fluorescence de la ThT augmente avec le pH, alors que le $t_{1/2}$ en turbidité est rapide et constant.

Ainsi, nous sommes donc en présence de deux phénomènes distincts. D'une part, la précipitation mesurée par la turbidité apparait toujours rapidement quelque soit le pH, néanmoins la quantité de précipité (ou l'intensité du plateau en turbidité) est très dépendante de celui-ci (maximum pour ~ pH 7,3). D'autre part, la vitesse de formation des fibres amyloïde mesurée par la fluorescence de la ThT ralentit avec l'augmentation du pH alors que l'intensité maximum atteinte varie peu en fonction du pH.

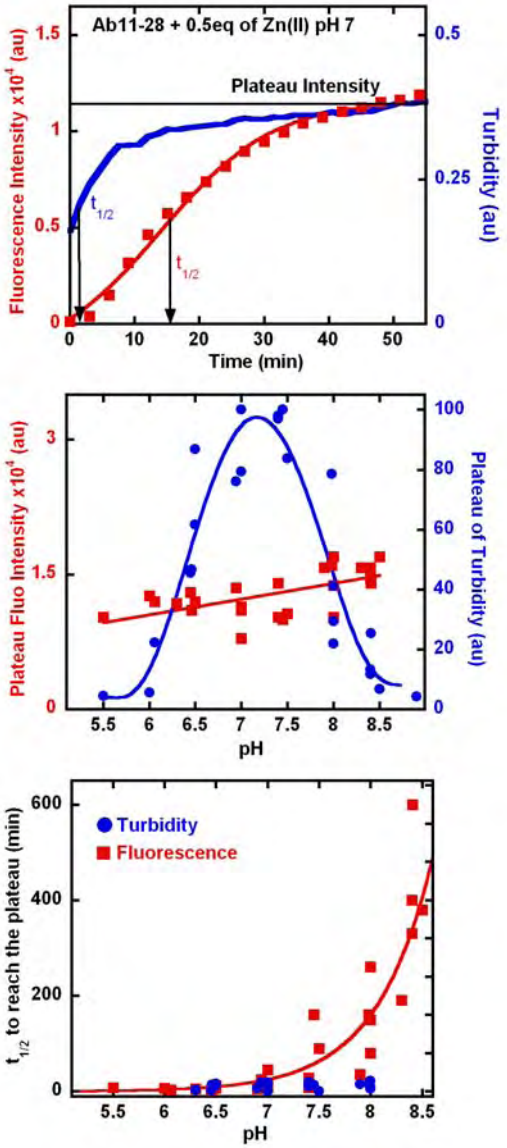

La précipitation d'un composé dans l'eau se produit généralement lorsque celui-ci devient globalement neutre. Le point isoélectrique (pI) est le pH auquel un composé devient globalement neutre. Dans le cas du Aβ11-28, sa charge globale évolue de 0 à pH 6,3, -1 à pH 7,3, à -2 à pH 8.4. Si l'on considère la formation du dimère $Zn(Aβ11\text{-}28)_2$ avec la coordination proposée ci-dessus, la charge globale attendue sera de +2 à pH 6,3, 0 à pH 7,3, à -2 à pH 8,4. La charge globale du $Zn.(Aβ11\text{-}28)_2$ est donc bien en accord avec l'allure du plateau de turbidité en fonction du pH et permet d'expliquer celui-ci.

Figure 7 ci-contre : (Dessus) Fluorescence de la ThT (échelle de gauche rouge, carré rouge) et turbidité (échelle de droite bleu, ligne bleu) au cours du temps de Aβ11-28 en présence de 0.5éq de Zn(II) à pH 7,0. La ligne noire indique l'intensité du plateau, les flèches noires correspondent au temps nécessaire pour atteindre la moitié de l'intensité maximale. (Milieu) Intensité des plateaux de la fluorescence de la ThT (échelle de gauche rouge, carré rouge) et de turbidité (échelle de droite bleu, cercle bleu) en fonction du pH de Aβ11-28 avec 0.5 éq Zn(II). (Dessous) $t_{1/2}$ de la fluorescence de la ThT (carré rouge) et de la turbidité (cercle bleu) de Aβ11-28 avec 0.5 éq de Zn(II) en fonction du pH. Conditions : [Aβ11-28] = 300 µM ; [Zn(II)] =150µM ; [Tampon] = 100 mM ; MES pour pH 5,5-6, PIPES pour pH 6-7, HEPES pour pH 7-8, POPSO pour pH 8-8,5.

La vitesse de formation des fibres dépend du pH (Figure 8 du dessous). Afin de mieux comprendre ce phénomène, nous avons suivi la coordination du Zn(II) au peptide Aβ11-28 à différents pH par XANES et RMN (figure 8). Dans les spectres XANES (Figure 8 de gauche) présentés ci-dessous, on constate que l'allure de seuils de $Zn_{0.5}$-Aβ11-28 à pH 6,5 et à pH 7,5 sont identiques mais diffèrents de celui à pH 8,5. Cela suggère fortement un changement de la coordination du Zn(II) au Aβ11-28 entre pH 7,5 et pH 8,5. Le pKa de l'amine terminal étant précisément dans cette gamme, sa coordination au Zn(II) est possible. Afin de vérifier cette

hypothèse, nous avons étudié par spectroscopie ^{1}H RMN le déplacement du signal du proton Hα-Cα-NH_2 lors de l'ajout de Zn(II) (Fig. 8 de droite). L'expérience montre qu'à partir de pH 7,7, un déplacement spécifique de cette résonnance apparait (le signal de His14 est aussi déplacé sur toute la gamme de pH étudié, données non montrées). Ce déplacement s'accentue avec l'augmentation du pH. En accord avec le XANES, ce déplacement indique la coordination de l'amine terminale à un pH supérieur à 7,7. De plus, on voit par RMN que l'His14 et le Glu11 ne semblent pas se décoordiner du Zn(II) (non montré) à plus haut pH, le NH_2 semble donc plutôt s'ajouter aux autres ligands que de s'y substituer.

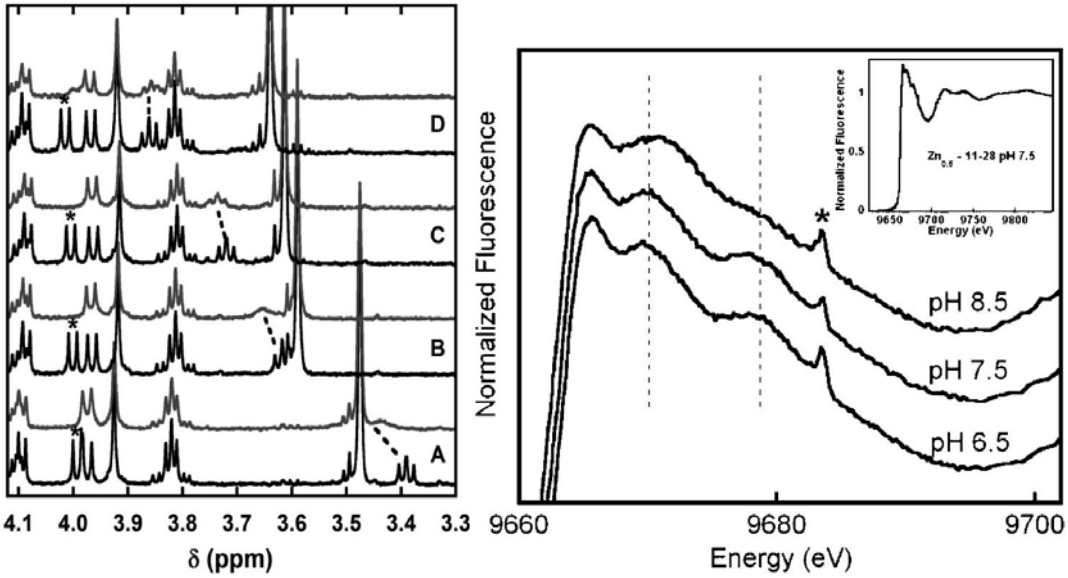

Figure 8 : (A gauche) Agrandissement au seuil du Zn des spectres XANES de Aβ11-28 en présence de 0.5 équivalent de Zn(II) à différents pH. En cartouche, le spectre XANES complet de Aβ11-28 en présence de 0.5 équivalent de Zn(II) à pH 7,5. L'astérisque pointe un artéfact dû au détecteur. Condition : [Aβ11-28] = 2mM ; [Zn(II)] = 1mM ; [Tampon] = 50mM (A droite) ^{1}H RMN de Aβ11-28 en l'absence (noir, tracé du bas) et en présence de Zn(II) (gris, tracé du haut) à pH 9,1 (A), pH 8,0 (B), pH 7,7 (C), pH 7,3 (D). L'astérisque pointe le H-Cα de Val12, fortement affecté par l'ajout de Zn(II) dû à sa proximité avec le Glu11. Les traits en pointillés indiquent le déplacement du proton du H-Cα-NH_2 dû à l'addition de Zn(II). Condition : [Aβ11-28] = 300µM ; [Zn(II)] = 270µM ; [Tris D_{11}] = 100mM.

Afin étudier l'impact de la coordination du NH_2 terminal sur l'agrégation, l'équipe de G. LaPenna a réalisé des calculs de dynamique moléculaire sur deux modèles. Le premier modèle $Zn(Ab11\text{-}28)_2$, noté I, dans lequel le Zn est coordiné par 2 COO^- des Glu11 et 2 noyau imidazole des His14 coorespond au peptide Aβ11-28 en présence de Zn(II) à bas pH. Le second modèle $Zn(Ab11\text{-}28)_2$, noté II, dans lequel le Zn est coordiné par 1 COO^- (Glu11) 2 NH_2 et 2 noyaux imidazole (His14) (la modélisation montre que le départ d'un carboxylate est nécessaire à l'arrivé des deux NH_2). Les deux modèles choisis présentent une conformation

initiale en feuillets-β comme retrouvée dans les agrégats d'Aβ. La modélisation montre que la conformation en feuillets-β est plus stable dans le modèle I que dans le modèle II, et que par conséquent, l'arrivé du NH_2 déstabilise la conformation initiale en feuillet-β. Ces résultats sont en accord avec l'observation de la réduction de la vitesse d'agrégation avec l'augmentation de pH (Schéma 2, ci-dessous).

Plusieurs des aspects énoncés ci-dessus peuvent être résumés dans le schéma 2 ci-dessous. Il représente les différences de coordination induit par le métal (Cu ≠ Zn sur Aβ11-28) ou par les peptides (Zn.Aβ11-28 pH 7,4 ≠ Zn.Aβ11-28 pH 8,5 et Cu.Aβ11-28 ≠ Cu.Aβ14-23) ainsi que l'influence de cette coordination sur la tendance à l'agrégation.

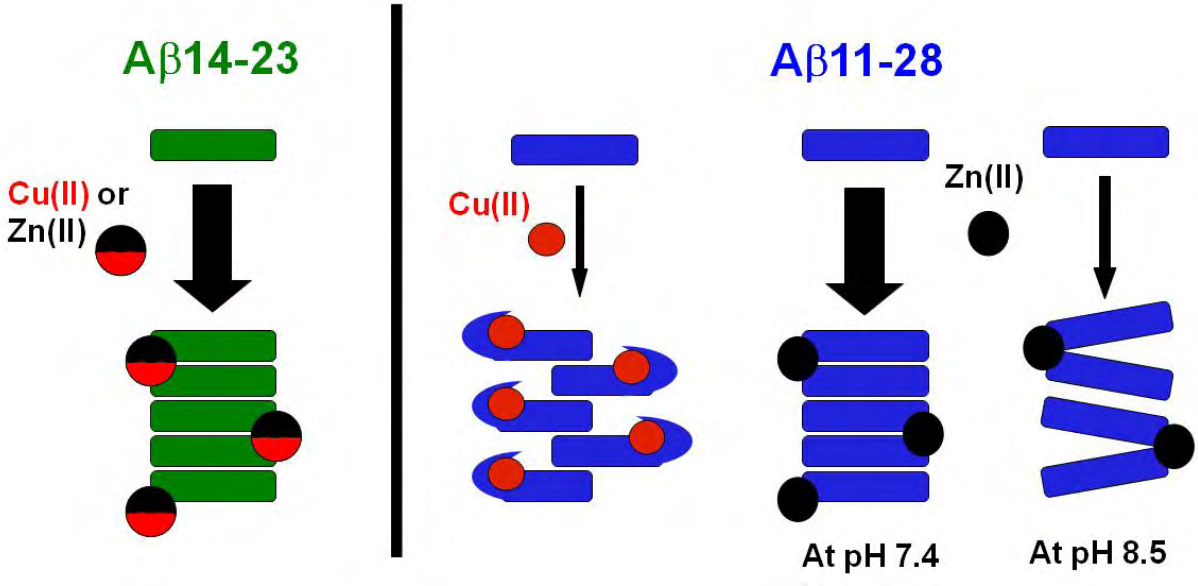

Schéma 2 : Coordination schématique du Cu(II) et du Zn(II) sur Aβ14-23 et Aβ11-28 ainsi que l'effet de celle-ci sur l'agrégation. A la différence du Aβ14-23, la coordination du Cu(II) par le Aβ11-28 provoque l'inhibition de l'agrégation (voir schéma 1). Le Zn(II) accélère l'agrégation chez le Aβ11-28 comme le Aβ14-23. A haut pH, la coordination du Zn(II) au Aβ11-28 change, ce qui contribue au ralentissement de l'agrégation.

f- Dynamique

On sait que le Aβ présente une affinité modérée pour le Zn(II) avec un Kd de l'ordre du µM.[8] Une affinité similaire est attendue pour Aβ11-28 (même type de ligands disponible). On peut alors se poser plusieurs questions : Le Zn(II) est-il en échange entre les peptides ? Est-il labile après l'agrégation ? Que se passe-t-il si on le retire ? Afin de répondre à ces questions, nous avons mené les expériences suivantes.

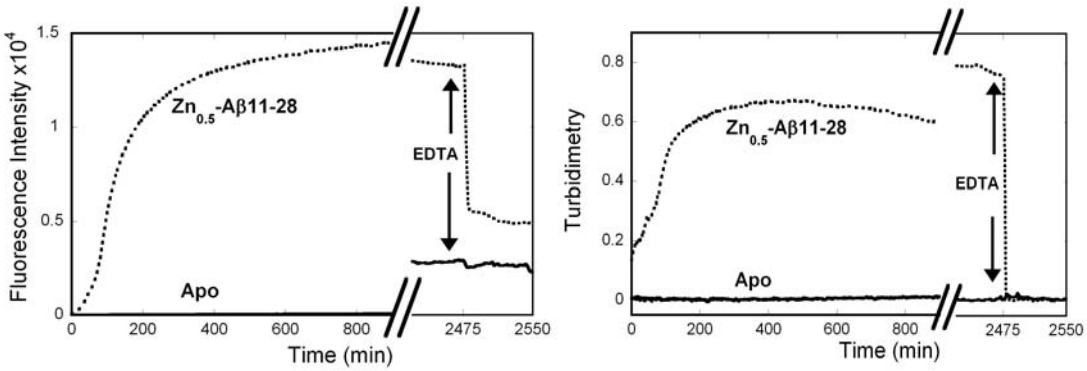

Figure 9 : Fluorescence de la ThT (à gauche) et turbidité (à droite) au cours du temps (// indique la cassure dans l'échelle du temps) de Aβ11-28 en absence (ligne continu) ou en présence de 0.5 équivalent de Zn(II) (lignes en pointillés). L'ajout d'ETDA est indiqué par les flèches. Conditions : [Aβ11-28] = 300µM ; [Zn(II)] = 150µM ; [HEPES] = 100mM ; [ThT] = 10µM ; [EDTA] = 750µM.

Ci-dessus, la figure 9 présente le suivi cinétique par la fluorescence de la ThT et turbidité de Aβ11-28 avec et sans Zn(II) sur une longue période. On constate que même en l'absence de Zn(II), Aβ11-28 peut agréger si l'on est suffisamment patient (voir aussi Fig. 5).

On remarque aussi que l'apoAβ11-28 forme un type d'agrégats différent de celui formé par Aβ11-28 en présence de Zn(II). En effet, dans l'agrégation de apoAβ11-28, on observe une fluorescence de la ThT moins intense (~5-10 fois) qu'avec $Zn_{0.5}$-Aβ11-28 (voir Figure 5 et Figure 9 de gauche). De plus, aucune turbidité des agrégats n'est détectée avec ApoAβ11-28 (contrairement à $Zn_{0.5}$-Aβ11-28, figure 9 de droite). Les fibres apoAβ11-28 sont aussi moins denses que celles de $Zn_{0.5}$-Aβ11-28 (voir Fig. 10, panneau de gauche et de droite). Il y a donc deux types d'agrégats. Ils se distinguent par l'intensité en fluorescence ($Zn_{0.5}$Aβ11-28 > apoAβ11-28) et la présence de turbidité ($Zn_{0.5}$Aβ11-28 >> apoAβ11-28 ~ 0).

Que se passe-t-il lorsqu'on retire le Zn(II) des agrégats $Zn_{0.5}$Aβ11-28 ? L'ajout d'EDTA sur $Zn_{0.5}$-Aβ11-28 provoque un changement du type d'agrégat. D'agrégat de type Zn, on passe à des agrégats de type Apo (voir Figure 9 et Figure 10).

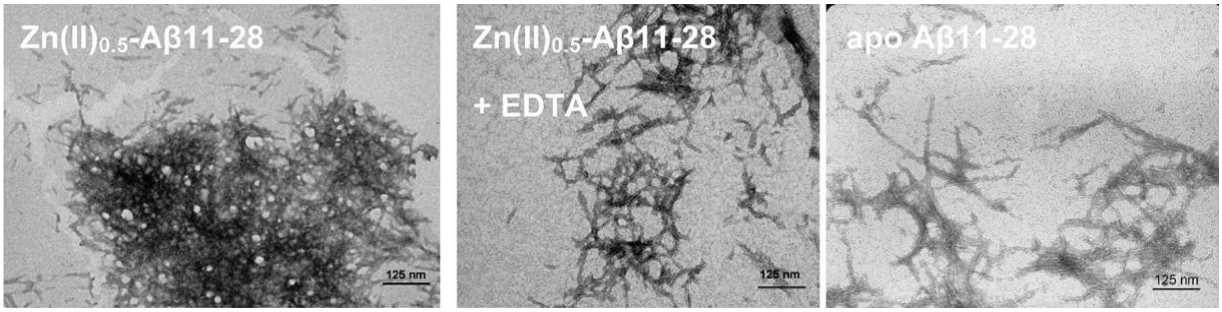

Figure 10 : Image de TEM de $Zn_{0.5}$-Aβ11-28 (gauche), $Zn_{0.5}$-Aβ11-28 + EDTA (milieu) et apoAβ11-28 après un jour d'incubation. Conditions : [Aβ11-28] = 300µM ; [Zn(II)] = 150µM ; [HEPES] = 100mM ; [ThT] = 10µM ; [EDTA] = 750µM.

Plus intéressant encore, le moment de l'ajout de l'EDTA n'a pas d'importance (de t = 2 min jusqu'à plusieurs heures). L'addition d'EDTA sur Aβ11-28 en présence de Zn(II) provoque une formation très rapide d'agrégats de type apo et ce même si l'EDTA est ajouté avant l'augmentation de la fluorescence de la ThT (pendant la phase de nucléation) de $Zn_{0.5}$-Aβ11-28 (données non montrées). La formation d'agrégats de type Apo *via* l'exposition au Zn(II) et puis à l'EDTA est ainsi beaucoup plus rapide que la formation d'agrégat de type Apo avec seulement du Aβ11-28. Cela signifie que lorsque l'Aβ11-28 est en présence de Zn(II) même de manière très temporaire, le Zn(II) pourra induire une modification (comme par exemple la formation d'un dimère) « durable », modification qui accélère l'agrégation même en absence de Zn(II) (voir schéma 3).

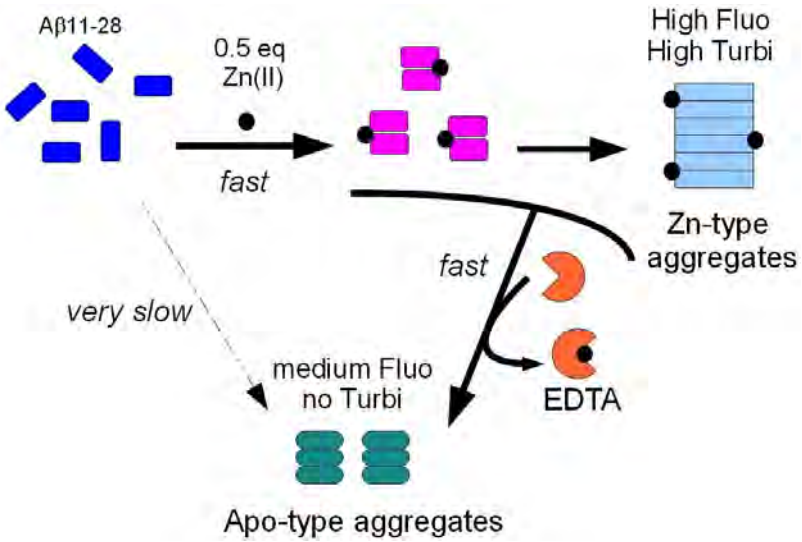

Schéma 3 : Aβ11-28 de la forme monomérique aux agrégats de type « apo » ou « Zn »

Le Zn(II) coordiné sur Aβ11-28, même après agrégation semble donc labile (accessible à la chélation), mais *via* ce chélateur (EDTA), la quantification n'est pas possible.

Aussi, nous avons eu recours au PAR (voir structure en annexe), qui est un chélateur du Zn(II). PAR et le $Zn(PAR)_2$ n'ont pas la même absorption ce qui rend possible le suivi de la chélation du Zn(II). Dans la figure 11 de gauche, le $Zn_{0.5}$Aβ11-28 préalablement agrégé est ajouté à une solution de PAR. On constate que très vite ($t_{1/2}$ < 1min) et totalement, le Zn(II) est chélaté par le PAR. Ainsi, même lorsque que le Zn est co-agrégé au Aβ11-28 et donc sous forme solide, il est accessible en solution. La figure 10 de droite montre la ^{1}H RMN dans la zone des aromatiques de Aβ11-28 en présence de différents équivalents de Zn(II). On notera que les déplacements sur Hε et Hδ de l'His14 (~7.75ppm et ~6.9ppm) augmentent avec les équivalents en Zn(II), et qu'un ajout sub-stœchiométrique provoque le déplacement du signal de tout l'échantillon. Cela caractérise un échange rapide du Zn(II) avec l'ensemble des molécules d'Aβ11-28. Ces deux expériences montrent l'échange rapide du Zn(II) que ce soit entre peptides en solution ou entre peptides agrégés et peptides en solution.

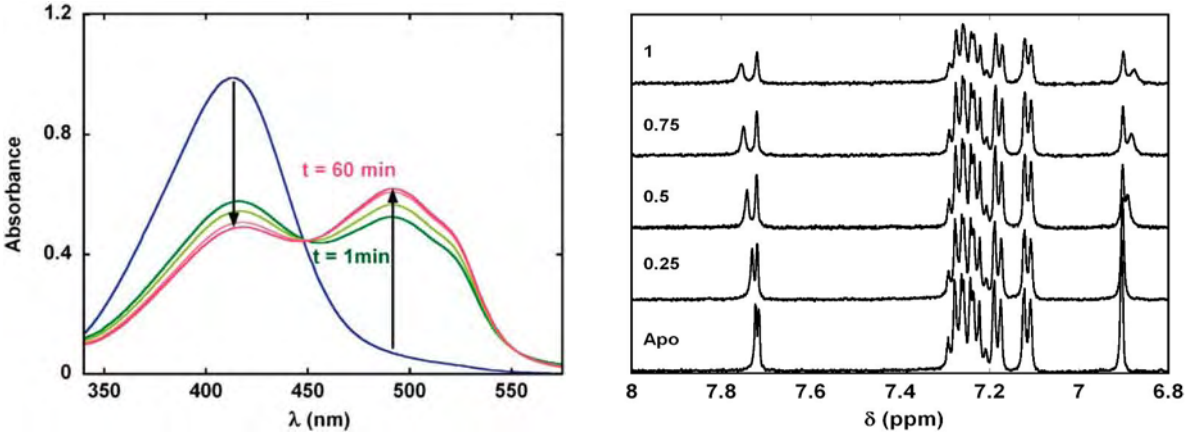

Figure 11 : (A gauche) Suivi UV-vis de l'addition $Zn_{0.5}$-Aβ11-28 pre-agrégé à la solution de PAR. Condition : [PAR] = 300 μM ; pré-agrégé [$Zn_{0.5}$-Aβ11-28] = 160µM ; [HEPES] = 100mM, pH 7,4. (A droite) ^{1}H RMN de Aβ11-28 en absence et présence de différentes stœchiométries de Zn(II). Conditions : [Aβ11-28] = 300µM ; [Zn(II)] = 0-300µM ; [Tris D_{11}]=100mM.

Une autre expérience intéressante est l'effet de « l'ensemencement » (ou seeding en anglais). L'ensemencement consiste à ajouter des agrégats ou des fibres préformés pour déclencher l'agrégation, agrégation qui suit alors normalement la nature de la matrice imposée par la « graine » (comparable à une cristallisation). La figure 12 montre l'ajout de $Zn_{0.5}$-Aβ11-28 pré-agrégé à une solution d'apoAβ11-28. On observe un déclenchement immédiat de l'agrégation. Cette agrégation n'est pas une agrégation de type Zn mais de type Apo. En effet, les caractéristiques spectroscopiques, à savoir, une fluorescence de la ThT faible et pas de

turbidité, sont celles d'une agrégation de type « apo ». Ce comportement peut être expliqué, par l'échange du Zn(II) entre les peptides (voir schéma 4).

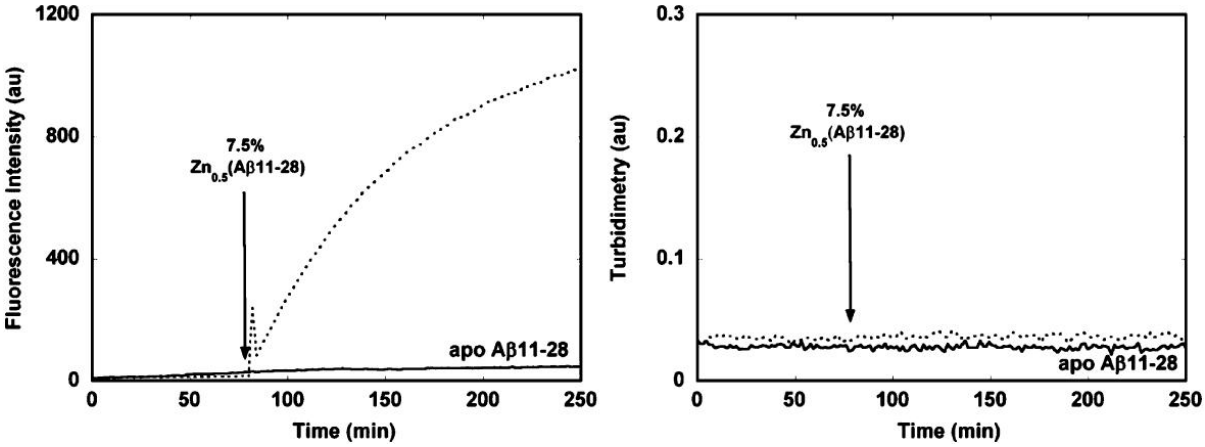

Figure 12 : Fluorescence de la ThT (à gauche) et turbidité (à droite) au cours du temps, suivant l'agrégation de Aβ11-28 en absence (ligne continue) ou en présence d'un ajout Zn0.5-Aβ11-28 pré-agrégé (ligne pointillée) indiqué par les flèches. Conditions : [Aβ11-28] = 300µM ; [$Zn_{0.5}$-Aβ11-28] = 22.5µM ; [HEPES] = 100mM ; [ThT] = 10µM.

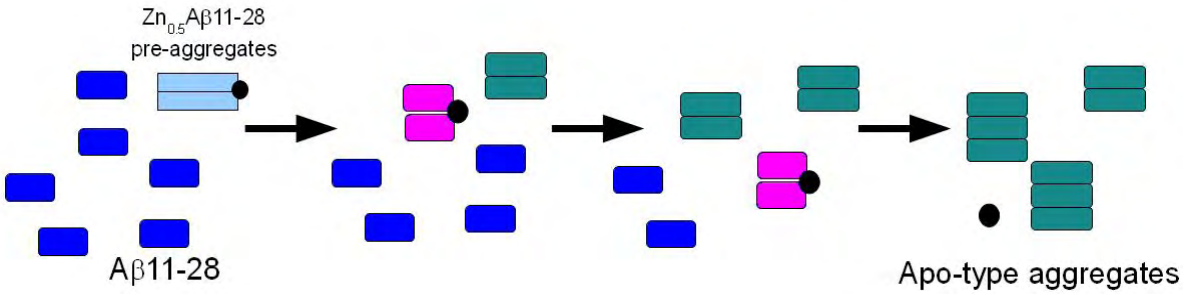

Schéma 4 : L'échange dynamique du Zn(II) induit une agrégation de type « apo » plutôt que de type « Zn ». Ici, le complexe Zn(II)-Aβ11-28 est considéré comme un catalyseur de l'agrégation d'apoAβ11-28

III. 4- Conclusion :

Par ces expériences, nous avons montré que :

- L'agrégation d'un peptide induite par les ions métalliques Cu et Zn dépend du peptide et des ions métalliques.

Ces deux paramètres sont reliés par la coordination de l'ion métallique au peptide.

-Le Zn(II) accélère l'agrégation de l'Aβ11-28 *via* la formation d'un dimère impliquant les Glu11 et His14. L'augmentation du pH change cette coordination (implication du NH_2

terminal) et contribue au ralentissement de la cinétique d'agrégation. La charge globale du dimère $Zn(A\beta 11\text{-}28)_2$ conditionne la précipitation.

- La coordination du Zn(II) au Aβ11-28 est dynamique, même lorsque le Zn est co-précipité, l'échange entre agrégats solides et peptides en solution est très rapide. La coordination du Zn(II) même transitoire ou temporaire, induit des modifications (formation de dimères) non réversibles par le retrait du Zn. Ces modifications accélèrent fortement et durablement l'agrégation même en l'absence de Zn(II).

Références :

1. Liu, K.; Solano, I.; Mann, D.; Lemere, C.; Mercken, M.; Trojanowski, J.; Lee, V., Characterization of Aβ11-40/42 peptide deposition in Alzheimer's disease and young Down's syndrome brains: implication of N-terminally truncated Aβ species in the pathogenesis of Alzheimer's disease. *Acta Neur.* **2006,** *112* (2), 163-174.
2. Breydo, L.; Uversky, V. N., Role of metal ions in aggregation of intrinsically disordered proteins in neurodegenerative diseases. *Metallomics* **2011,** *3* (11), 1163-1180.
3. Brender, J. R.; Hartman, K.; Nanga, R. P. R.; Popovych, N.; de la Salud Bea, R.; Vivekanandan, S.; Marsh, E. N. G.; Ramamoorthy, A., Role of Zinc in Human Islet Amyloid Polypeptide Aggregation. *J. Am. Chem. Soc.* **2010,** *132* (26), 8973-8983.
4. Wetzel, R., Kinetics and Thermodynamics of Amyloid Fibril Assembly. *Acc. Chem. Res.* **2006,** *39* (9), 671-679.
5. Hellstrand, E.; Boland, B.; Walsh, D. M.; Linse, S., Amyloid Î²-Protein Aggregation Produces Highly Reproducible Kinetic Data and Occurs by a Two-Phase Process. *ACS Chem. Neurosci.* **2009,** *1* (1), 13-18.
6. Harford, C.; Sarkar, B., Amino Terminal Cu(II)- and Ni(II)-Binding (ATCUN) Motif of Proteins and Peptides: Metal Binding, DNA Cleavage, and Other Properties *Acc. Chem. Res.* **1997,** *30* (3), 123-130.
7. Pradines, V.; Stroia, A. J.; Faller, P., Amyloid fibrils : modulation of formation and structure by copper(II). *New J. Chem.* **2008,** *32*, 1189-1194.
8. Kozin, S. A.; Mezentsev, Y. V.; Kulikova, A. A.; Indeykina, M. I.; Golovin, A. V.; Ivanov, A. S.; Tsvetkov, P. O.; Makarov, A. A., Zinc-induced dimerization of the amyloid-β metal-binding domain 1-16 is mediated by residues 11-14. *Mol. BioSyst.* **2011,** *7* (4), 1053-1055.

Zinc(II) modulates specifically amyloid formation and structure in model peptides

Bruno Alies, Vincent Pradines, Isabelle Llorens-Alliot,
Stéphanie Sayen, Emmanuel Guillon, Christelle Hureau, Peter Faller

Journal of Biological Inorganic Chemistry
2011, *16 (2)*, 333-340

The following article is described in the previous chapter. The study is about Cu and Zn mediated aggregation on several amyloidergic peptides and theirs different behaviour.

J Biol Inorg Chem (2011) 16:333–340
DOI 10.1007/s00775-010-0729-8

ORIGINAL PAPER

Zinc(II) modulates specifically amyloid formation and structure in model peptides

Bruno Alies · Vincent Pradines · Isabelle Llorens-Alliot · Stéphanie Sayen · Emmanuel Guillon · Christelle Hureau · Peter Faller

Received: 17 August 2010 / Accepted: 20 October 2010 / Published online: 9 November 2010
© SBIC 2010

Abstract Metal ions such as zinc and copper can have dramatic effects on the aggregation kinetics of and the structures formed by several amyloidogenic peptides/proteins. Depending on the identity of the amyloidogenic peptide/protein and the conditions, Zn(II) and Cu(II) can promote or inhibit fibril formation, and in some cases these metal ions have opposite effects. To better understand this modulation of peptide aggregation by metal ions, the impact of Zn(II) binding to three amyloidogenic peptides (Aβ14-23, Aβ11-23, and Aβ11-28) on the formation and structure of amyloid-type fibrils was investigated. Zn(II) was able to accelerate fibril formation for all three peptides as measured by thioflavin T fluorescence and transmission electron microscopy. The effects of Zn(II) on Aβ11-23 and Aβ11-28 aggregation were very different compared with the effects of Cu(II), showing that these promoting effects were metal-specific. X-ray absorption spectroscopy suggested that the Zn(II) binding to Aβ11-23 and Aβ11-28 is very different from Cu(II) binding, but that the binding is similar in the case of Aβ14-23. A model is proposed in which the different coordination chemistry of Zn(II) compared with Cu(II) explains the metal-specific effect on aggregation and the difference between peptides Aβ14-23 and Aβ11-23/Aβ11-28.

Keywords Amyloid · Zinc · Copper · Aggregation · Spectroscopy

Abbreviations

Aβ	Amyloid β
ESRF	European Synchrotron Radiation Facility
EXAFS	Extended X-ray absorption fine structure
Hepes	4-(2-Hydroxyethyl)-1-piperazineethanesulfonic acid
POPSO	Piperazine-1,4-bis-(2-hydroxy-propane-sulfonic acid) dihydrate
ThT	Thioflavin T
XAS	X-ray absorption spectroscopy

Introduction

Amyloid fibrils formed by the assembly of peptides or proteins are widely studied owing to their roles in several disorders, including neurodegenerative diseases [1, 2]. The assembly of these peptides/proteins can be modulated by a

Electronic supplementary material The online version of this article (doi:10.1007/s00775-010-0729-8) contains supplementary material, which is available to authorized users.

B. Alies · V. Pradines · C. Hureau (✉) · P. Faller (✉)
LCC (Laboratoire de Chimie de Coordination),
CNRS, 205 route de Narbonne,
31077 Toulouse, France
e-mail: christelle.hureau@lcc-toulouse.fr

P. Faller
e-mail: peter.faller@lcc-toulouse.fr

B. Alies · V. Pradines · C. Hureau · P. Faller
Université de Toulouse,
UPS, INPT,
31077 Toulouse, France

I. Llorens-Alliot
CEA/DSM/INAC/NRS,
17 rue des Martyres,
38000 Grenoble, France

S. Sayen · E. Guillon
Institut de Chimie Moléculaire de Reims
(ICMR, CNRS UMR 6229),
Groupe Chimie de Coordination,
Université de Reims Champagne-Ardenne,
BP 1039, 51687 Reims Cedex 2, France

variety of cofactors. Metal ions are one cofactor, and in particular, Cu, Zn, and Fe ions are reported to be involved in several neurodegenerative diseases [3–5]. The binding of these metal ions to several peptide/proteins has been proposed. It has been shown that metal ion binding can modulate the kinetics and the structure of several amyloidogenic peptides/proteins [6–13]. Although the importance of metal ions in the formation of peptide/protein aggregates has been recognized, little is known on the underlying molecular mechanisms. Fundamental insight into amyloid fibril formation has been gained with short model peptides (for reviews see [14–16]). This strategy has also been applied for studying fundamental questions of metal-ion-assisted aggregation [17–23].

Here, three model peptides were used deriving from amyloid β (Aβ) peptide (Fig. 1), which plays a central role in Alzheimer's disease. However, the aim was not to model the metal binding to full-length Aβ, as it is known that residues 1–10 play an important role (for recent references see [24–27]); the aim was to gain general insights into the role of metal binding in peptide aggregation. The peptides chosen are able to make amyloid-type fibrils and contain two important features: a hydrophobic core (amino acids 17–21), thought to be involved in initiation of the aggregation process [28], and a metal binding site due to the one or two His residues, which are well known to be anchors for metal binding [21, 22, 29]. The same peptides were used in our previous study, in which we were able to gain interesting insights into the influence of Cu(II) binding on the formation and structure of aggregates [29]. It was found that Cu(II) bound to Aβ11-28 and Aβ11-23 as a mononuclear complex, which inhibited but did not abolish fibril formation (Fig. 2). In contrast Cu(II) bound to Aβ14-23 increased fibril formation by bridging two peptides (Fig. 2).

Aβ11-28: NH_3^+-EVHHQKLVFFAEDVGSNK-COO^-

Aβ11-23: NH_3^+-EVHHQKLVFFAED-COO^-

Aβ14-23: NH_3^+-HQKLVFFAED-COO^-

Fig. 1 Sequences of Aβ11-28, Aβ11-23, and Aβ14-23

The present study focuses on the modulating effect of Zn(II) on the model peptides Aβ11-28, Aβ11-23, and Aβ14-23. Aggregation kinetics and structural methods were employed to better understand the mechanism of Zn(II)-induced aggregation.

Materials and methods

Aβ11-23/Aβ11-28/Aβ14-23 sample preparation

The peptides Aβ11-23 (sequence Glu-Val-His-His-Gln-Lys-Leu-Val-Phe-Phe-Ala-Glu-Asp), Aβ11-28 (sequence Glu-Val-His-His-Gln-Lys-Leu-Val-Phe-Phe-Ala-Glu-Asp-Val-Gly-Ser-Asn-Lys), and Aβ14-23 (sequence His-Gln-Lys-Leu-Val-Phe-Phe-Ala-Glu-Asp) were purchased from either GeneCust (Dudelange, Luxembourg) or GenScript (Piscataway, NJ, USA). The stock solutions of peptides were prepared by first dissolving the peptides in pure water (resistivity 18 MΩ cm^{-1}), which resulted in a final pH 2. Then the solution pH was adjusted to 12 by adding NaOH, to monomerize the peptides. These stock solutions were stored at 253 K. The peptide concentrations were determined by using the molar extinction coefficient $\varepsilon = 390$ M^{-1} cm^{-1} of the two Phe at 258 nm [30]. (As Phe does not absorb at 275 nm, the absorbance at that wavelength was subtracted to remove contributions from the buffer or baseline shifts.). The stock solution of Zn(II) was prepared with $ZnSO_4 \cdot H_2O$ (Strem Chemicals) in water. Aggregation of peptides in the presence of Zn(II) was performed by dissolving peptides from stock solution in a 100 mM 4-(2-hydroxyethyl)-1-piperazineethanesulfonic acid (Hepes) buffer pH 7.4 (the pH was checked at the end of the experiment). We chose to perform "equimolar" experiments with 0.9 equiv of Zn(II) to be sure to avoid any effects of excess Zn(II). All of the experiments measuring either turbidimetry or fluorescence intensity were

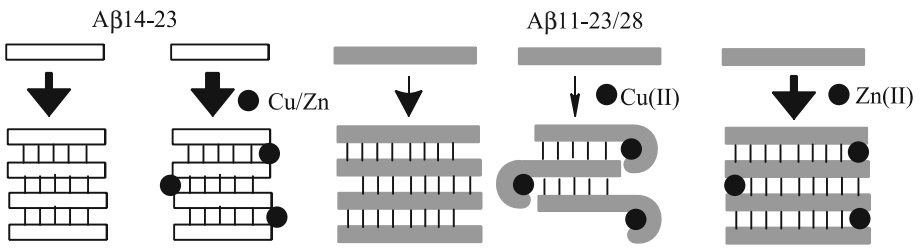

Fig. 2 The modulation of Cu(II) and Zn(II) (*black circles*) on the peptides Aβ14-23 (*white rod*) and Aβ11-23/Aβ11-28 aggregation (*gray rod*). *Black sticks* represent H-bonds in the β-sheets and the *thickness of the arrows* symbolizes the aggregation rate. For Aβ14-23, Cu(II) and Zn(II) accelerate fibril formation by bridging the peptides. Zn(II) has a more important effect than Cu(II), which may be due to the more flexible coordination geometry. For Aβ11-23/Aβ11-28, Zn(II) accelerates fibril formation owing to the bridging of two peptides. In contrast, Cu(II) does not bridge and hence decreases fibril formation owing to the peptides wrapping around Cu(II) in the ATCUN motif and the consequent lower number of H-bonds

realized at room temperature. The kinetic data were obtained at least five times, including from different peptide batches (from different sources, see above) and different preparations. There were variations in the kinetics, but the effects of the metal ions and different peptides were always the same. The data shown are representative measurements. In the X-ray absorption spectroscopy (XAS) measurements, 1 mM peptide and 0.9 mM Zn(II) in 100 mM POPSO at pH 8.6 were used. The first sample ($t = 0$ h) was withdrawn immediately after mixing and transferred to the sample holder and frozen in liquid nitrogen. The second sample was incubated for 24 h at room temperature before being transferred to and frozen in the sample holder.

Turbimetry

Turbidity measurements were done by measuring the absorbance at 350 nm with an Agilent 8453 spectrometer connected to a personal computer (UV–vis ChemStation, revision A.10.01), in a 1 cm path length quartz cuvette or in a 96-well quartz microplate (Hellma) with an flx-Xenius spectrophotometer (SAFAS) connected to a personal computer. Peptide concentrations were 300 μM in 100 mM Hepes pH 7.4 if not otherwise stated.

Fluorescence spectroscopy

Fluorescence spectra were measured using an flx-Xenius spectrophotometer (SAFAS) or a Fluostar Optima (BMG) connected to a personal computer. Thioflavin T (ThT), peptides, and Zn(II) were mixed in 100 mM Hepes buffer pH 7.4 and placed in a 96-well microplate. The time course of ThT fluorescence was then measured (excitation 437 nm, emission 485 nm, bandwidth for emission and excitation 10 nm). The final concentrations of peptides and ThT were 300 and 10 μM, respectively.

If a sigmoidal type of kinetic trace was obtained, the data were fitted with the program KaleidaGraph to the formula $F(t) = F_0 + A/\{1 + \exp[-k(t - t_{1/2})]\}$, where k is the elongation rate, A the amplitude, $t_{1/2}$ the time point when half the maximal intensity is reached, and F_0 the baseline before aggregation [31].

Electronic microscopy

Five microliter of peptide samples incubated for 17–24 h was applied on electron microscopy grids, washed with 5 μL of Milli-Q water, and negatively stained with an aqueous solution (5 μL) of uranyl acetate (1% w/w). Samples were air-dried and examined with a JEOL 1011 transmission electron microscope operating at an accelerating voltage of 100 kV.

X-ray absorption spectroscopy

XAS measurements were carried out at the European Synchrotron Radiation Facility (ESRF; Grenoble, France), which was operating with a ring current of 150–200 mA. Zn K-edge XAS spectra were collected on the BM30B (FAME) beamline using a Si(220) N_2 cryo-cooled double-crystal monochromator [32, 33]. The spectra were measured in fluorescence mode by measuring the Zn K_α fluorescence with a 30-element solid-state Ge detector (Canberra) in liquid cells in a He cryostat. The temperature was kept at 10 K during data collection to prevent sample damage. Three scans of 45 min each were averaged. Data from each detector channel were inspected for glitches or dropouts before inclusion in the final average. Energy calibration was achieved by measuring a Zn foil for the Zn edge and assigning the first inflection point of the Zn foil spectrum to 9,659 eV. Data analysis was performed using the MAX (multiplatform applications for X-ray absorption spectroscopy) package, including Cherokee for the data extraction and Roundmidnight for the shell fitting [34]. X-ray absorption near-edge structure spectra were background-corrected by a linear regression through the pre-edge region and a polynomial through the postedge region and normalized to the edge jump. For the extraction of the extended X-ray absorption fine structure (EXAFS) part, E_0 was defined at the half-height of the absorption edge step. The $\chi(k)$ functions were extracted from the data with a linear pre-edge background, a polynomial atomic-absorption background, and were normalized using the Lengeler–Eisenberg method [35]. The k^2-weighted EXAFS spectra were Fourier-transformed over the k range 2.4–11.9 $Å^{-1}$ using a Kaiser–Bessel window with a smoothness τ parameter of 2.5 (k is the photoelectron wave number). In this work, all Fourier transforms were calculated and presented without phase correction. The peak corresponding to the first coordination shell was then isolated and back-Fourier-transformed into k space to determine the mean coordination number, N, the bond length, R, and the Debye–Waller factor, σ^2, by a fitting procedure realized in the framework of single scattering using the standard EXAFS formula:

$$\chi(k) = S_0^2 \sum_i \left[\frac{N_i}{R_i^2} A_i(k) e^{-2\sigma_i^2 k^2} e^{-2R_i/\lambda(k)} \sin(2kR_i + \Phi_i(k)) \right].$$

The $S_0{}^2$ value was taken as 1 and kept constant. Fits were performed on the Fourier-filtered spectra over the $R + \Delta R$ range 0.8–2.3 Å. Theoretical amplitude and phase shift functions were calculated with the ab initio code FEFF 7.0 [36] using bis(salicylhydrazide)sulfatozinc(II) monohydrate [37] as a structure model from the Cambridge Structural Database (http://www.ccdc.cam.ac.uk/products/csd). The estimated errors for distances and coordination numbers are ±0.02 Å and ±20%, respectively.

Results

During our investigation with the peptides Aβ11-23, Aβ11-28, and Aβ14-23, we realized that the aggregation kinetics followed by ThT (an amyloid-specific fluorescent dye) fluorescence were dependent on the batch (Fig. 3) [38]. This is likely due to a small portion of preaggregated peptide, the quantity or structure of which is batch-dependent. As aggregation can be seeded by a small amount of preaggregated peptide, a very small amount of preaggregated peptide is sufficient for a large kinetic difference. In contrast, in the presence of 0.9 equiv of Zn(II), the aggregation kinetics were more uniform between the batches, indicating that the effect of Zn binding prevails over the seeding effect (not shown). Thus, the peptides were incubated at pH 12, a well-established treatment to monomerize full-length Aβ1-40/Aβ1-42 peptide. After this treatment, the apo form of the model peptides (Aβ11-23, Aβ11-28, Aβ14-23) aggregated more slowly and more uniformly between batches. Thus, for the rest of the study all peptides were incubated at pH 12 to have more homogeneous samples. However, even without the incubation at pH 12, the differences between the different peptides and metal ions were qualitatively the same.

As in our previous study we did not use the pH 12 treatment. The measurements of apo Aβ11-23/Aβ11-28/Aβ14-23 and Cu-Aβ11-23/Cu-Aβ11-28/Cu-Aβ14-23 were reperformed to be able to compare them directly with the measurements for Zn [29]. As shown in Fig. 4, for all three peptides, Aβ11-23, Aβ11-28, and Aβ14-23, Zn had a dramatic effect on the ThT fluorescence traces. In general,

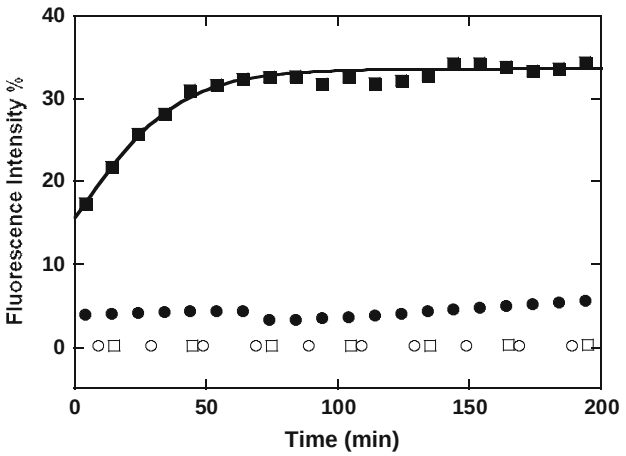

Fig. 3 Representative thioflavin T (ThT) fluorescence of apo-Aβ11-28 (two different batches, *circles* and *squares*) with (*filled symbols*) and without (*open symbols*) preincubation at pH 12. The *solid line* represents a fit (see "Materials and methods" for details). The conditions were as follows: 300 μM Aβ11-28, 100 mM 4-(2-hydroxyethyl)-1-piperazineethanesulfonic acid (Hepes) pH 7.4, 10 μM ThT

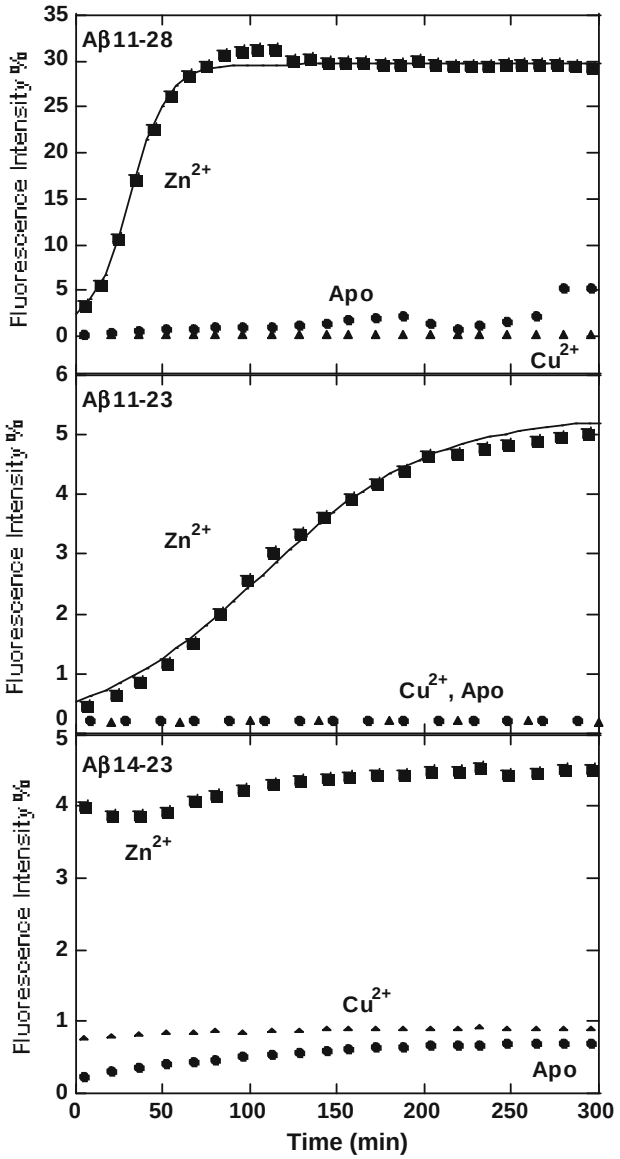

Fig. 4 Metal-specific aggregation: representative kinetic data of ThT fluorescence of Aβ11-28 (*top*), Aβ11-23 (*middle*), and Aβ14-23 (*bottom*) in the presence of Zn(II) (*squares*) and Cu(II) (*triangles*) and without metal ions (*circles*). The conditions were as follows: 300 μM peptides, 270 μM metal ions, 100 mM Hepes pH 7.4, 10 μM ThT. The *solid line* represents a fit (see "Materials and methods" for details)

Zn accelerated and increased ThT fluorescence over time. Comparison with Cu(II) and apo forms showed an important metal-specific effect.

The ThT fluorescence intensity increased instantaneously for Zn-Aβ14-23, more slowly for Zn-Aβ11-28, and even more slowly for Zn-Aβ11-23. The latter two showed a sigmoidal curve, which is typical for amyloid fibril formation. These curves can be fitted with an aggregation model including a nucleation and elongation

process (for a recent review see [39]). In terms of the fluorescence intensity after reaching the plateau, Zn-Aβ11-28 had higher intensity than Zn-Aβ14-23 and Zn-Aβ11-23, showing that the Zn-induced aggregation in amyloid-type structures is peptide-dependent.

In parallel, turbidity was measured. In contrast to ThT fluorescence, turbidity assesses the general state of aggregation (amount and size, but not specific for fibrils). Turbidity increased rapidly for all three peptides after addition of Zn (Fig. 5, top). The turbidity of Zn-Aβ11-28 was the highest, whereas the turbidities of the other two peptides were similar. The turbidity of Zn-Aβ11-28 and that of Zn-Aβ11-23 (but not Zn-Aβ14-23) showed several phases. The changes were small but reproducible, and the same features occurred in Zn-Aβ11-28 and Zn-Aβ11-23, but the turbidity change for the latter was slower. Several phases can be distinguished. This indicates that the aggregation for Zn-Aβ11-28 and Zn-Aβ11-23 occurs in several steps and

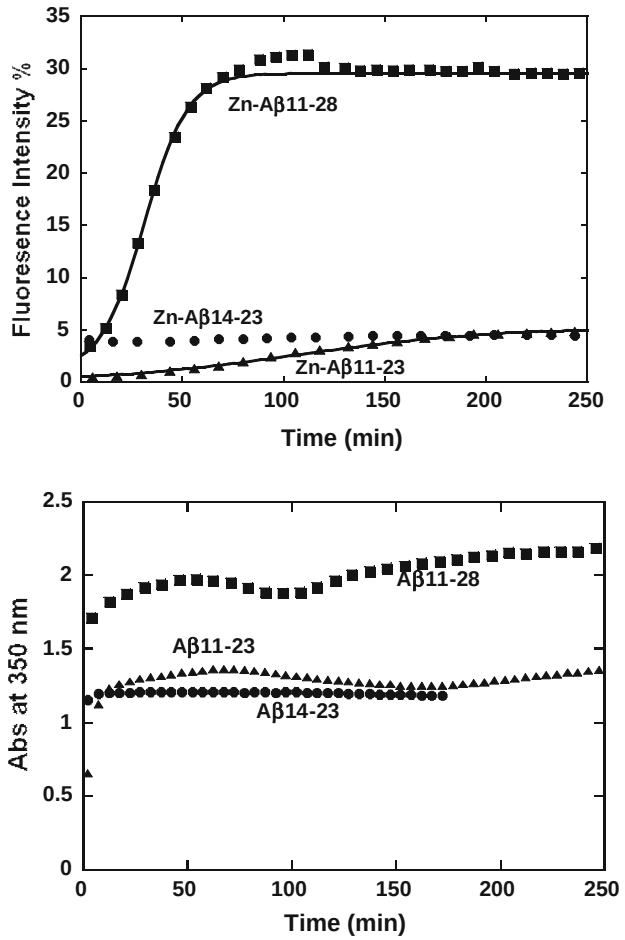

Fig. 5 Representative kinetic data of ThT fluorescence (*top*) and turbidity (*bottom*) of Zn-Aβ11-28, Zn-Aβ11-23, and Zn-Aβ14-23. The conditions were as follows 300 μM peptides, 270 μM Zn(II), 100 mM Hepes pH 7.4. The *solid line* represents a fit (see "Materials and methods" for details)

that the increase in ThT fluorescence is not associated with the first events.

Transmission electron microscopy images were collected at the beginning (just after mixing; 0 h) and after reaching the plateau (24 h) (Fig. 6). Zn-Aβ11-28 and Zn-Aβ11-23 showed aggregates at the beginning, but they were rather amorphous and little fibrils were observed. At the end, clearly fibrillar aggregates can be observed (Fig. 6). This is in line with the turbidity and ThT measurements, as turbidity measures better the degree of aggregation and ThT is more specific for fibrillar aggregates. Zn-Aβ11-28 showed more fibrils than Zn-Aβ11-23, in line with the ThT measurements. In the case of Zn-Aβ14-23, similar fibrillar structures were observed at 0 and 24 h, in line with the very fast increase of turbidity and ThT fluorescence (Fig. 6).

To gain insight into the coordination of Zn to the three different peptides during aggregation, XAS was employed. To have an intense signal, a higher concentration of Zn–peptides was used (approximately 1 mM). The pH was adjusted to 8.6 to slow down the faster aggregation due to higher concentrations. As such we were able to measure XAS spectra at a time point before the ThT fluorescence increased and on the plateau for Zn-Aβ11-28 (see the electronic supplementary material for details of pH and concentration dependence). The X-ray absorption near-edge structures are shown in Fig. 7. All spectra were in agreement with a hexacoordinated Zn(II), which was confirmed by EXAFS (see below), although a pentacoordination cannot be completely ruled out [40]. Moreover, for all three peptides, Zn-Aβ14-23, Zn-Aβ11-23, and Zn-Aβ11-28, no significant difference between the time point at the beginning and after 24 h could be detected, indicating that the type of Zn(II) binding site does not change much during aggregation. The XAS spectra are very similar for Zn-Aβ11-23 and Zn-Aβ11-28, indicating that they have the same binding site and hence amino acids 24–28 do not play an important role in Zn(II) coordination. In contrast, the spectrum of Zn(II)-Aβ14-23 differs, supporting the role of amino acids 11–13 in Zn(II) binding of the Aβ11-23/Aβ11-28 peptides.

These conclusions are supported by the EXAFS data (Table 1; see also the electronic supplementary material). The Zn(II) coordination showed no significant changes between the beginning of the aggregation (time point 0 h) and after 24 h. For all Zn–peptides at different time points, the best fit suggested about four atoms at a distance of 1.96 ± 0.4 Å and about two atoms at a distance of 2.05 ± 0.04 Å. The shorter distance is more in line with carboxylate ligands (from Asp, Glu, or the C terminus) and the longer distance with nitrogen ligands (His or N-terminal amine) [40]. This suggests that in Zn-Aβ14-23 Zn is bound by the N-terminal His via both the amine and the imidazol group. In the case of Zn-Aβ11-23/Zn-Aβ11-28, the two nitrogen ligands are more likely to be the two His.

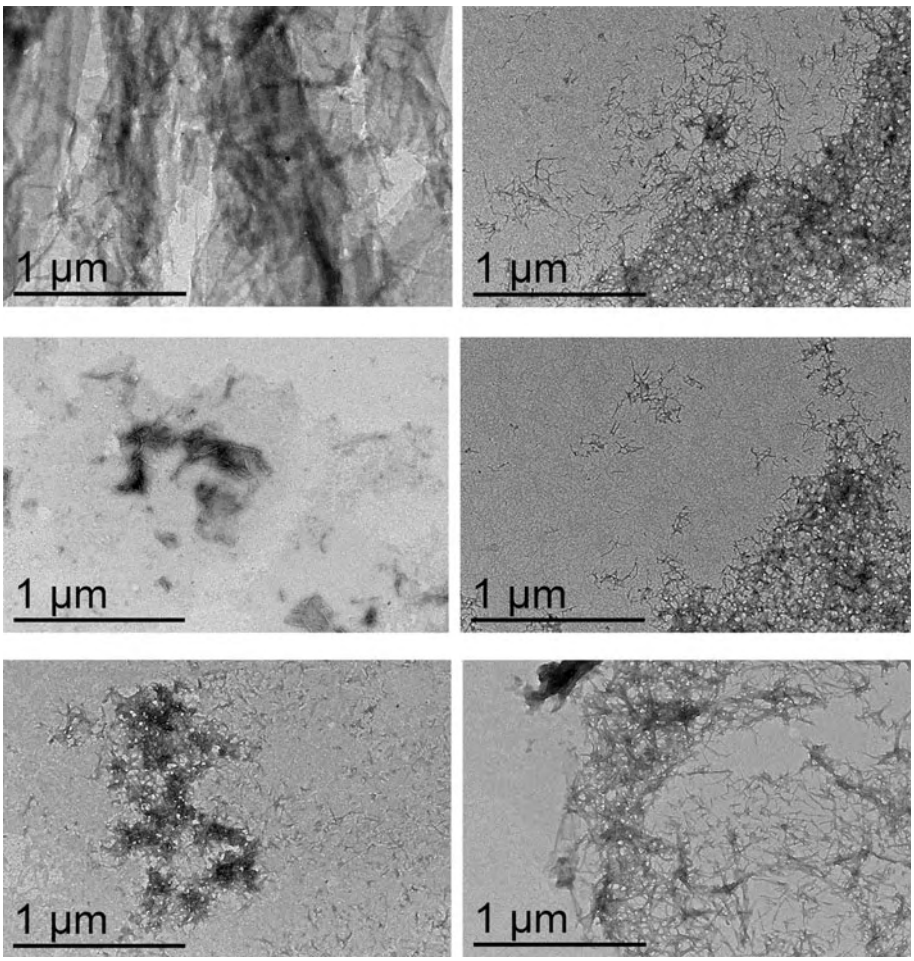

Fig. 6 Representative transmission electron microscopy images of Zn-Aβ11-28 (*top*), Zn-Aβ11-23 (*middle*) and Zn-Aβ14-23 (*bottom*) at 0 h (*left*) and after 24 h (*right*)

Discussion

In general, Zn drastically increased the formation of fibrils and the aggregation intensity for all three peptides, Aβ14-23, Aβ11-23, and Aβ11-28. Moreover, the impact of Zn on the fibrils was metal-specific as Cu(II) behaves very differently. Cu(II) inhibited the formation of fibrils by Aβ11-23 and Aβ11-28. In contrast, Cu(II) slightly increased the formation of fibrils by Aβ14-23, but to a much lower extent when compared with Zn(II).

In the case of Aβ14-23, the fibril-inducing effect of Cu has been assigned to the bridging coordination of Cu(II) at the end of the peptides leading to a stabilization of the aggregates [29] with Cu(II) bound to the N-terminal His and to C-terminal caboxylates. The XAS data are in line with Zn binding to the same ligands as Cu (NH_2 and imidazole of N-terminal His and carboxylates near the C terminus). However, the Zn(II) coordination geometry is more flexible compared with that of Cu(II) as distorted four, five, and six ligand coordinations are well tolerated (Fig. 2). Indeed the XAS data suggest a hexacoordinated Zn(II) in Aβ14-23. In contrast Cu(II)-Aβ14-23 is more square-planar [29]. As such, the aggregation-increasing effect of Zn(II) binding [compared with Cu(II)] can be explained by the more flexible coordination chemistry, which imposes a lower constraint on the aggregation process.

Aβ11-28 and Aβ11-23 have very similar binding modes for either Zn(II) or Cu(II) (see earlier and [29]). Cu(II) binds in the well-defined ATCUN motif, by the His, N-terminal amine, and two amidyl as is typical for peptides with the sequence H_2N-Xxx-Xxx-His-R [41]. The XAS data suggest that Zn(II) is hexacoordinated in Aβ11-23/Aβ11-28, likely including the two His side chains, and hence Zn(II) coordinates differently to the N-terminal portion of Aβ11-23/Aβ11-28. This is also supported by studies reported in the literature of Zn binding to the peptides Asp-Ala-His and Gly-Gly-His showing that Zn did not bind to amidyl, but bound to the His side chain and N-terminal amine and/or carboxylate [42].

This implies that Zn(II) is able to bridge two Aβ11-23/Aβ11-28 peptides and hence promote the formation of amyloid-type structures like in the case of Aβ14-23 (Fig. 2). In contrast, Cu(II) bound to the ATCUN motif has

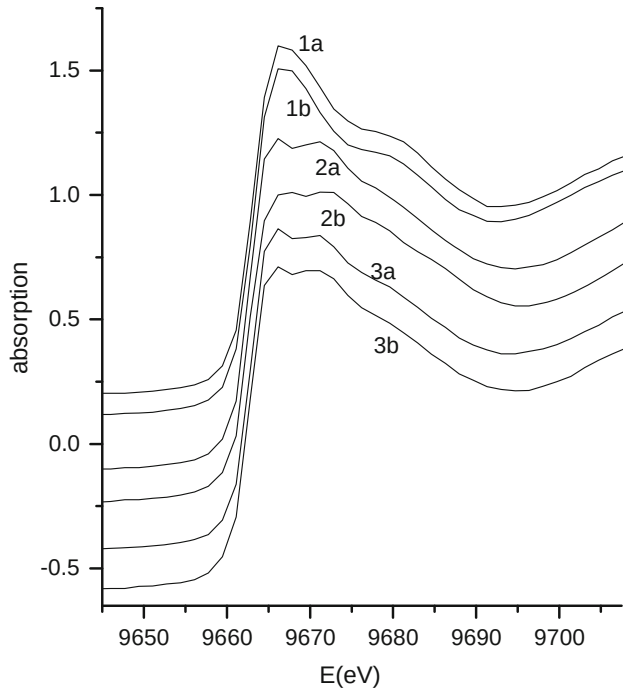

Fig. 7 X-ray absorption near edge structure of Aβ14-23 (*1a*, *1b*), Zn-Aβ11-23 (*2a*, *2b*), and Zn-Aβ11-28 (*3a*, *3b*) just after Zn addition (*1a*, *2a*, *3a*) and after 24 h incubation (*1b*, *2b*, *3b*). The conditions were as follows: 1 mM peptide, 0.9 mM Zn(II), 100 mM POPSO pH 8.6

all ligands on the same Aβ11-23/Aβ11-28 peptide. Therefore, Cu(II) is not able to bridge two Aβ11-23/Aβ11-28 peptides, which could explain the non-promoting effect of Cu(II) on the amyloid formation of Aβ11-23/Aβ11-28.

Another important physico-chemical parameter to consider in aggregation is the charge. Aggregation is faster when the net charge approaches 0 [43, 44]. As Zn(II) and Cu(II) have +2 charges, their binding can change the net charge. Moreover, depending on the binding site, protons can be released and hence for the equally charged Cu(II) and Zn(II), their binding to a peptide at different sites can result in different net charge. Aβ14-23 at physiological pH has a charge of about −1. Zn(II) binding and Cu(II) binding are supposed to displace only the N-terminal proton. This leads to an overall charge of 0 for Zn(II)-Aβ14-23 or Cu(II)-Aβ14-23. This is supposed to contribute to the accelerated fibril formation. However, as the effects of Zn and Cu are different, the effect on charge of metal ion binding does not explain everything and structural effects (see above) are likely to contribute as well. In the case of Aβ11-23/Aβ11-28, Cu(II) and Zn(II) do not bind to the same site. Cu(II) replaces about three protons (ATCUN motif), and therefore the negative charge increases from −2 for apo-Aβ11-23 to −3 for Cu(II)-Aβ11-23 and from −1 for apo-Aβ11-28 to −2 for Cu(II)-Aβ11-28. In contrast, Zn is thought to replace only one proton (no binding to amidyl), and the negative charge decreases from −2 for apo-Aβ11-23 to −1 for Zn(II)-Aβ11-23 and from −1 for apo-Aβ11-28 to 0 for Zn(II)-Aβ11-28. This suggests that changes in overall charge play a role in the effects of metal ion binding to amyloidogenic peptides.

It is interesting to note that at least for Aβ11-23 and Aβ11-28, turbidity evolves much faster than ThT fluorescence, indicating that first non-ThT-positive aggregates are formed, which later transform to ThT-positive amyloid-like aggregates. During the transformation, the turbidity intensity does not change much, suggesting a transformation of aggregates.

In conclusion, Zn(II) is able to accelerate fibril formation for all three peptides. The different coordination chemistry of Zn(II) versus Cu(II) can explain the metal-specific effect on aggregation and the difference between the peptides Aβ14-23 and Aβ11-23/Aβ11-28. These insights could provide mechanistic hypotheses on how Zn can promote and Cu inhibit fibril formation of certain amyloidogenic peptides/proteins [12, 13] (like Aβ11-23 and Aβ11-28) or how in certain cases both metals promote amyloid formation [7, 10].

Table 1 Structural data of the first coordination shell obtained from *R*-space fits of extended X-ray absorption fine structure spectra; *N* number of neighbors, *R* absorber–neighbour distance, σ^2 Debye–Waller factor; uncertainties in coordination numbers are estimated to ± 20%, in *R* to ± 0.02 Å, and in σ^2 to ± 0.001 Å^2

	Scattered/backscattered	*N*	*R* (Å)	σ^2 (Å^2)	*R* factor[a] (%)	ΔE_0 (eV)
ZnAβ14-23 (0 h)	Zn-N/O	4.46	1.93	0.0078	0.38	2.74
		2.43	2.08	0.0025		5.75
ZnAβ14-23 (24 h)	Zn-N/O	4.31	2.00	0.0077	0.51	3.09
		2.47	2.04	0.0044		2.47
ZnAβ11-23 (0 h)	Zn-N/O	4.31	1.95	0.0011	0.35	1.88
		2.47	2.09	0.0075		4.37
ZnAβ11-23 (24 h)	Zn-N/O	4.45	1.93	0.0046	0.53	2.26
		2.41	2.05	0.0080		1.43
ZnAβ11-28 (0 h)	Zn-N/O	4.39	1.95	0.0078	0.87	0.79
		2.38	2.01	0.0056		1.16
ZnAβ11-28 (24 h)	Zn-N/O	4.47	1.92	0.0069	0.36	0.36
		2.39	2.08	0.0058		2.88

[a] *R* factor is the overall goodness of fit

Acknowledgments We acknowledge the ESRF for beamtime provision and the team of beamline FAME 30B, especially Olivier Proux, for their helpful support. We also thank Thomas Lunardi and the EMBL laboratory (Grenoble) for their support in performing UV–vis spectroscopy near the beamline, and Vincent Colliere and Diana Ciuculescu (LCC Toulouse) for part of the transmission electron microscopy experiments. This work was supported by the ESRF (Experiment CH-3015), a grant from the French Ministry (MERT) (B.A.), and a grant from the Agence Nationale de la Recherche (ANR) Programme Blanc NT09-488591, "NEUROMETALS" (P.F. and C.H.).

References

1. Klein WL, Stine WB Jr, Teplow DB (2004) Neurobiol Aging 25:569–580
2. Rousseau F, Schymkowitz J, Serrano L (2006) Curr Opin Struct Biol 16:118–126
3. Drago D, Bolognin S, Zatta P (2008) Curr Alzheimer Res 5:500–507
4. Barnham KJ, Masters CL, Bush AI (2004) Nat Rev Drug Discov 3:205–214
5. Molina-Holgado F, Hider RC, Gaeta A, Williams R, Francis P (2007) Biometals 20:639–654
6. Zou J, Kajita K, Sugimoto N (2001) Angew Chem Int Ed 40:2274–2277
7. Khan A, Ashcroft AE, Higenell V, Korchazhkina OV, Exley C (2005) J Inorg Biochem 99:1920–1927
8. Khan A, Ashcroft AE, Korchazhkina OV, Exley C (2004) J Inorg Biochem 98:2006–2010
9. Binolfi A, Lamberto GR, Duran R, Quintanar L, Bertoncini CW, Souza JM, Cervenansky C, Zweckstetter M, Griesinger C, Fernandez CO (2008) J Am Chem Soc 130:11801–11812
10. Jobling MF, Huang X, Stewart LR, Barnham KJ, Curtain C, Volitakis I, Perugini M, White AR, Cherny RA, Masters CL, Barrow CJ, Collins SJ, Bush AI, Cappai R (2001) Biochemistry 40:8073–8084
11. Suhre MH, Hess S, Golser AV, Scheibel T (2009) J Inorg Biochem 103:1711–1720
12. Ward B, Walker K, Exley C (2008) J Inorg Biochem 102:371–375
13. Wilkinson-White LE, Easterbrook-Smith SB (2007) Biochemistry 46:9123–9132
14. Hamley IW (2007) Angew Chem Int Ed 46:8128–8147
15. Lynn DG, Meredith SC (2000) J Struct Biol 130:153–173
16. Eisenberg D, Nelson R, Sawaya MR, Balbirnie M, Sambashivan S, Ivanova MI, Madsen AO, Riekel C (2006) Acc Chem Res 39:568–575
17. Yang H, Pritzker M, Fung SY, Sheng Y, Wang W, Chen P (2006) Langmuir 22:8553–8562
18. Pagel K, Seri T, von Berlepsch H, Griebel J, Kirmse R, Bottcher C, Koksch B (2008) ChemBioChem 9:531–536
19. Hoernke M, Koksch B, Brezesinski G (2010) Biophys Chem 150:64–72
20. Schlosser G, Stefanescu R, Przybylski M, Murariu M, Hudecz F, Drochioiu G (2007) Eur J Mass Spectrom (Chichester Eng) 13:331–337
21. Dong J, Canfield JM, Mehta AK, Shokes JE, Tian B, Childers WS, Simmons JA, Mao Z, Scott RA, Warncke K, Lynn DG (2007) Proc Natl Acad Sci USA 104:13313–13318
22. Dong J, Shokes JE, Scott RA, Lynn DG (2006) J Am Chem Soc 128:3540–3542
23. Scotter AJ, Guo M, Tomczak MM, Daley ME, Campbell RL, Oko RJ, Bateman DA, Chakrabartty A, Sykes BD, Davies PL (2007) BMC Struct Biol 7:63
24. Dorlet P, Gambarelli S, Faller P, Hureau C (2009) Angew Chem Int Ed 48:9273–9276
25. Hureau C, Coppel Y, Dorlet P, Solari PL, Sayen S, Guillon E, Sabater L, Faller P (2009) Angew Chem Int Ed 48:9522–9525
26. Drew SC, Masters CL, Barnham KJ (2009) J Am Chem Soc 131:8760–8761
27. Drew SC, Noble CJ, Masters CL, Hanson GR, Barnham KJ (2009) J Am Chem Soc 131:1195–1207
28. Esler WP, Stimson ER, Ghilardi JR, Lu YA, Felix AM, Vinters HV, Mantyh PW, Lee JP, Maggio JE (1996) Biochemistry 35:13914–13921
29. Pradines V, Jurca Stoia A, Faller P (2009) New J Chem 32:1189–1194
30. Ciuculescu ED, Mekmouche Y, Faller P (2005) Chem Eur J 11:903–909
31. Hellstrand E, Boland B, Walsh DM, Linse S (2009) ACS Chem Neurosci 1:13–18
32. Proux O, Nassif V, Prat A, Ulrich O, Lahera E, Biquard X, Menthonnex JJ, Hazemann JL (2006) J Synchrotron Radiat 13:59–68
33. Proux O, Biquard X, Lahera E, Menthonnex J-J, Prat A, Ulrich O, Soldo Y, Trevisson P, Kapoujyan G, Perroux G, Taunier P, Grand D, Jeantet P, Deleglise M, Roux J-P, Hazemann JL (2005) Phys Scr T 115:970–973
34. Michalowicz A, Muller-Bouvet D, Provost K (2009) J Phys Conf Ser 012034–012035
35. Lengeler B, Eisenberg P (1980) Phys Rev B Condens Matter Mater Phys 21:4507–4520
36. Zabinsky SI, Rehr JJ, Ankudinov AL, Albers RC, Eller MJ (1995) Phys Rev B Condens Matter 52:2995–3009
37. Luo W, Meng XG, Cheng GZ, Ji ZP (2007) Acta Crystallogr Sect E Struct Rep 63:m2482
38. LeVine H 3rd (1999) Methods Enzymol 309:274–284
39. Morris AM, Watzky MA, Agar JN, Finke RG (2008) Biochemistry 47:2413–2427
40. Giachini L, Veronesi G, Francia F, Venturoli G, Boscherini F (2010) J Synchrotron Radiat 17:41–52
41. Harford C, Sarkar B (1997) Acc Chem Res 30:123–130
42. Lakusta H, Deber CM, Sarkar B (1980) Can J Chem 58:757–766
43. Chiti F, Stefani M, Taddei N, Ramponi G, Dobson CM (2003) Nature 424:805–808
44. Lopez De La Paz M, Goldie K, Zurdo J, Lacroix E, Dobson CM, Hoenger A, Serrano L (2002) Proc Natl Acad Sci USA 99:16052–16057

Insights into the Mechanisms of Amyloid Formation of ZnII-Ab11-28: pH-Dependent Zinc Coordination and Overall Charge as Key Parameters for Kinetics and the Structure of ZnII-Aβ11-28 Aggregates

Bruno Alies, Giovanni LaPenna, Stéphanie Sayen, Emmanuel Guillon, Christelle Hureau, Peter Faller

Inorganic Chemistry
2012, *51* (14), 7897–7902

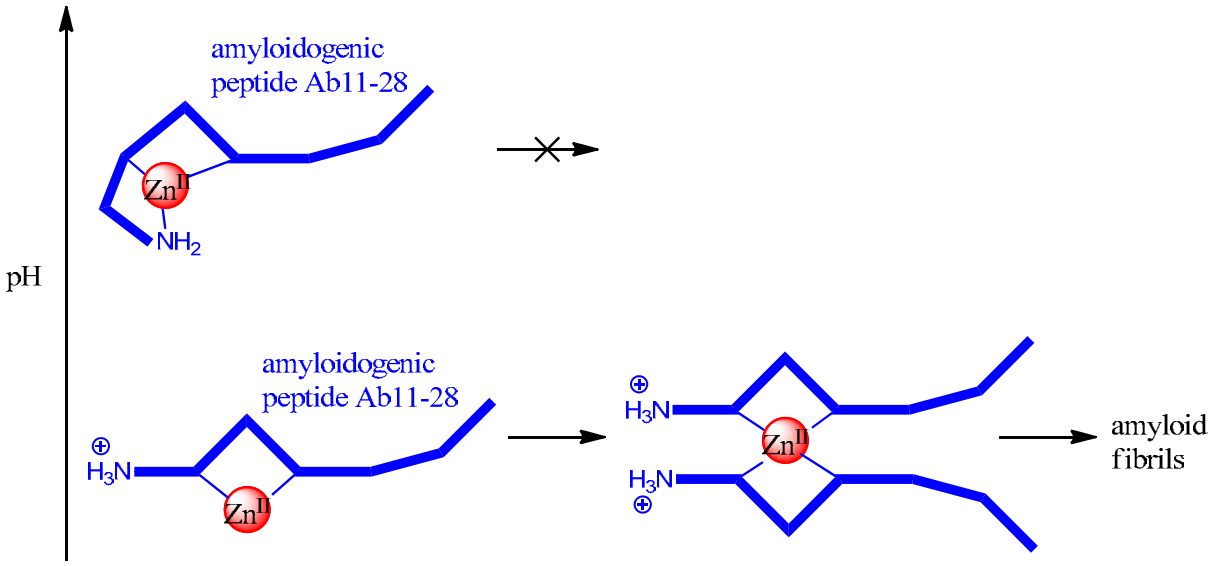

The following article is described in the previous chapter. The study is about the impact of pH on Aβ11-28 Zn-induced aggregation.

Inorganic Chemistry

Article

pubs.acs.org/IC

Insights into the Mechanisms of Amyloid Formation of Zn^{II}-Ab11-28: pH-Dependent Zinc Coordination and Overall Charge as Key Parameters for Kinetics and the Structure of Zn^{II}-Ab11-28 Aggregates

Bruno Alies,[†,‡] Giovanni LaPenna,[§] Stéphanie Sayen,[⊥] Emmanuel Guillon,[⊥] Christelle Hureau,*[,†,‡] and Peter Faller*[,†,‡]

[†]LCC (Laboratoire de Chimie de Coordination), CNRS, 205 route de Narbonne, BP 44099, F-31077 Toulouse Cedex 4, France

[‡]Université de Toulouse, UPS, INPT, F-31077 Toulouse Cedex 4, France

[§]CNR-National Research Council of Italy, ICCOM, via Madonna del Piano 10, 50019 Sesto Fiorentino, Florence, Italy

[⊥]Institut de Chimie Moléculaire de Reims (ICMR, CNRS UMR 7312), Groupe de Chimie de Coordination, Université de Reims Champagne-Ardenne, BP 1039, 51687 Reims Cedex 2, France

Supporting Information

ABSTRACT: Self-assembly of amyloidogenic peptides and their metal complexes are of multiple interest including their association with several neurological diseases. Therefore, a better understanding of the role of metal ions in the aggregation process is of broad interest. We report pH-dependent structural and aggregation studies on Zn^{II} binding to the amyloidogenic peptide Ab11-28. The results suggest that coordination of the N-terminal amine to Zn^{II} is responsible for the inhibition of amyloid formation and the overall charge for amorphous aggregates.

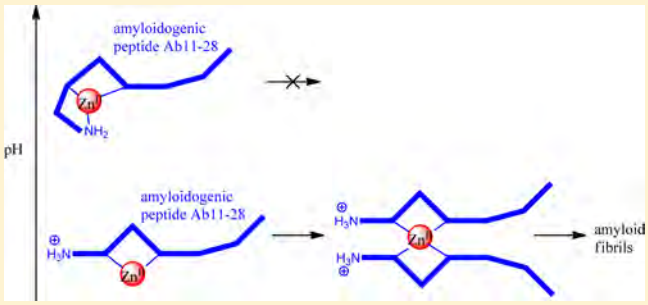

INTRODUCTION

The supramolecular assembly of peptides and proteins into amyloid fibrils is intensively studied owing to their important biological roles including different neurological diseases (Alzheimer's, Parkinson's, etc.)[1−3] and because amyloids are of interest in material science.[4,5] Amyloids are made of peptides or proteins that adopt fibrils based on the cross-β-structure, in which the peptide backbone is orthogonal to the fibril axis.[4,6,7] They are normally formed by a two-step process of slow nucleation, followed by a typically fast, autocatalytic surface growth, leading to a sigmoid curve for amyloid formation.[8]

The binding of metal ions such as zinc, copper, and iron to amyloidogenic peptides modulates the aggregation behavior[9−14] and results in fibrils with embedded metal ions.[15−20] The use of small peptides to model the aggregation of native peptides or to gain general insight into the mechanisms was very helpful in the understanding of amyloid formation[4,21−23] and the role of metal ions.[24−30] Smaller model peptides are often easier to handle and have higher reproducibility in terms of aggregation behavior.

In the past, we investigated the effect of Zn^{II} and Cu^{II} binding on three different amyloidogenic model peptides and found metal- and peptide-specific effects related to the coordination chemistry of the metal ions.[31,32] One of these peptides, Ab11-28, showed suitable properties in terms of mechanistic studies for Zn^{II}-induced aggregation. Ab11-28 is derived from amyloid-β (Aβ) peptide, which plays a crucial role in Alzheimer's disease. Although Ab11-28 is missing the N- and C-terminal parts and, hence, is clearly different from Aβ in terms of aggregation and metal binding,[33] it preserves two important features for metal-induced amyloid formation. These are the two His residues (His13 and His14) known to anchor Zn^{II} and the hydrophobic core (amino acid residues spanning from 17 to 21, sequence LVFFA). Moreover, truncated Aβ peptides starting at position 11 (i.e., Aβ11-x) have been found in human amyloid plaques and are thus physiologically relevant.[34] Therefore, the amyloidogenic Ab11-28 peptide can serve as a model system to gain general insight into metal-induced amyloid formation.

Further studies on Zn^{II} binding to the peptide Ab11-28 at pH 7.4 showed the importance of dynamical Zn^{II} binding for aggregation and suggested that the formation of a transitory complex of two Ab11-28 bound to Zn^{II} (i.e., $Zn^{II}(Ab11\text{-}28)_2$) via His14 and the carboxylate of Glu11 is most prone to fibril formation.[35]

In order to gain insight into the relationships between the structure of Zn^{II} binding and the aggregation behavior, we studied the pH dependence of Zn^{II} binding to Ab11-28 upon aggregation.

Received: May 10, 2012
Published: July 5, 2012

ACS Publications © 2012 American Chemical Society

dx.doi.org/10.1021/ic300972j | Inorg. Chem. 2012, 51, 7897−7902

RESULTS AND DISCUSSION

pH Dependence of $Zn^{II}_{0.5}$-Ab11-28 Aggregation. Our previous studies indicated that $Zn^{II}(Ab11\text{-}28)_2$ is the building block of aggregation into amyloids.[31,35] Changing the pH of metallopeptides like $Zn^{II}(Ab11\text{-}28)_2$ will influence two important parameters concerning aggregation: (i) the overall charge of a peptide is pH-dependent, and aggregation is classically faster when the overall charge approaches zero (Table 1).[36,37] (ii) Metal binding is often pH-dependent, and hence the structure of the metal−peptide complex can change.

Table 1. Expected Charge of Ab11-28 and $Zn^{II}_1(Ab11\text{-}28)_2$

pH	Ab11-28	Zn^{II}_1-$(Ab11\text{-}28)_2$
8.4	−2	−2
7.3	−1	0
6.3	0	+2

The aggregation of Ab11-28 with 0.5 equiv of Zn^{II} was followed by thioflavin T (ThT) fluorescence and turbidimetry at different pH values. ThT is a specific fluorescence dye for amyloid-type aggregates, while turbidity measures more amorphous aggregates because it depends mostly on the amount and size of aggregates.

Figure 1 (top) shows the time courses of the ThT fluorescence and turbidity of Ab11-28 with 0.5 equiv of Zn^{II} at pH 7. For either measurement, the overall curve has a sigmoidal form, and hence a $t_{1/2}$ and a plateau intensity can be estimated as indicated. $t_{1/2}$ of turbidity is shorter than $t_{1/2}$ from ThT, indicating that first amorphous-type aggregates are formed, which are subsequently transformed into amyloid-type aggregates.

The pH dependence of Ab11-28 with 0.5 equiv of Zn^{II} revealed very different ThT fluorescence and turbidity features (Figure 1, middle and bottom), indicating that aggregates and amyloid formation are not directly correlated. The main kinetic phase of ThT fluorescence was faster with lower pH (Figure 1, bottom), but the plateau reached at the end was similar (Figure 1, middle). This indicates that the same amount of amyloid was formed over the present pH range, but the formation was faster at low pH. In contrast, the turbidity increased rapidly in a nonsigmoidal manner and ThT fluorescence preceded (at the pH where it could be well measured, i.e., ≥ pH 7). The kinetics was not very sensitive to the pH (Figure 1, bottom). This suggests that amorphous, unstructured aggregates are formed before amyloids and likely a transformation occurred. The turbidity plateau reached was pH-dependent (Figure 1, middle). It was maximal around pH 7.4, i.e., increased from pH 8.4 to 7.4, and then decreased by a further lowering of the pH to 6.

To gain insight into the structural changes responsible for the pH dependence of turbidity and ThT fluorescence, NMR and X-ray absorption spectroscopies (XAS) were applied.

NMR. The effect of the addition of Zn^{II} to Ab11-28 was studied by ^{1}H NMR at several pH values (Figure 2). Measurements were done immediately after Zn^{II} addition in order to minimize aggregation. Zn^{II}-induced line broadening and shifts for some specific resonances (Figures 2 and S2 in the Supporting Information), indicating the specific binding of Zn^{II} to the affected residues. Figure 2, left panel, shows the aromatic region, including His13, His14, Phe19, and Phe20. Zn^{II} addition at different pH values lead to line broadening and to

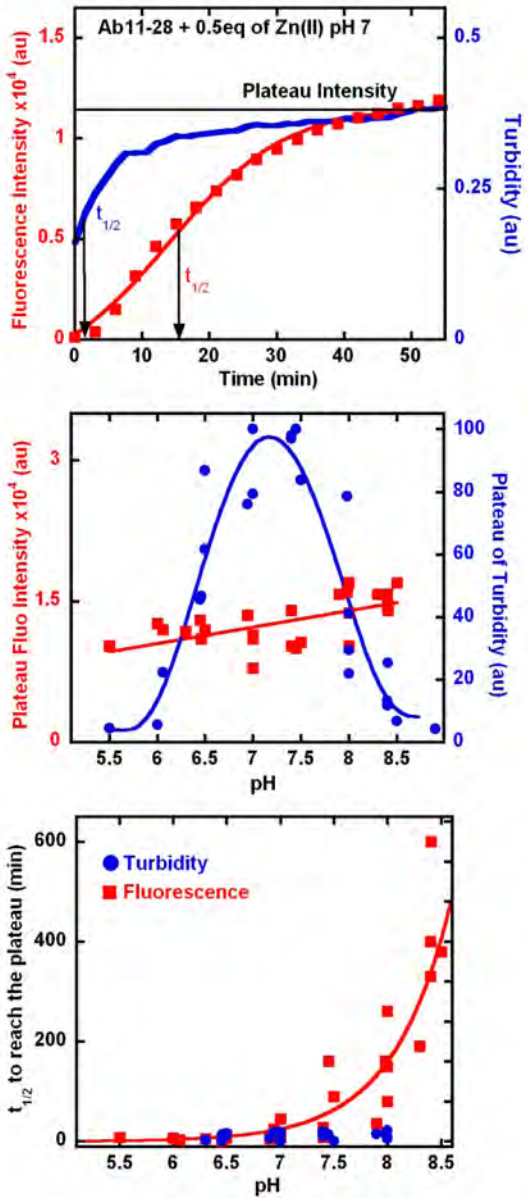

Figure 1. (Top) Time course of turbidity (blue, right scale) and ThT fluorescence (red squares, raw data; red line, fitted data; left scale) of Ab11-28 with 0.5 equiv of Zn^{II} at pH 7.0. The black line indicates the intensity of the plateau. $t_{1/2}$ values are given by the fit. (Middle) pH dependence of the plateau intensity reached in ThT fluorescence (red squares, raw data; red line, linear fit; left scale) and in turbidity (blue circles, raw data; blue line, trendline; right scale) by Ab11-28 with 0.5 equiv of Zn^{II} aggregation. Raw data are from five independent measurements. (Bottom) pH dependence of $t_{1/2}$ to reach the plateau in fluorescence (red square, raw data; red line, trendline) and in turbidity (blue circle) by Ab11-28 with 0.5 equiv of Zn^{II} aggregation. Raw data are from five independent measurements.

shifts of H−Cδ and H−Cε of His14. In contrast, the H−Cδ and H−Cε resonances of His13 were only little affected, showing a slight broadening and a slight chemical shift. The resonances of the two Phe are not affected at all, indicating no binding to or near the Phe. This indicates that over the pH range studied, His14, but not His13, is bound to Zn^{II}.

The resonance of H−Cα of Glu11 in the *apo*-Ab11-28 underwent a large shift over the pH range 7−9, in line with deprotonation of the N-terminal amine (Glu11). A pK_a of 7.8 is

dx.doi.org/10.1021/ic300972j | Inorg. Chem. 2012, 51, 7897−7902

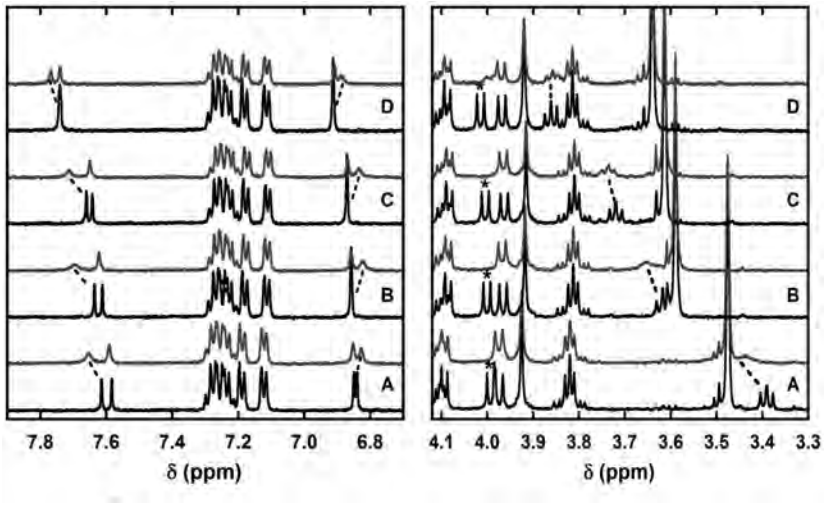

Figure 2. ^{1}H NMR of *apo*-Ab11-28 (lower trace) and Zn^{II}-Ab11-28 (upper trace) at pH 9.1 (A), 8.0 (B), 7.7 (C), and 7.3 (D) in the regions of H−Cδ and H−Cε of His13 and 14 (left) and H−Cα of Glu11 (right). Dotted lines represent the affected H−Cδ and H−Cε of His14 by Ab11-28 (left) and H−Cα of Glu11 (right). H−Cα of Glu11 shifts strongly because of protonation of NH_2. The asterisk indicates the H−Cα attributed to Val 12. Conditions: 300 μM Ab11-28, 270 μM Zn^{2+}, Tris-d_{11} 100 mM.

estimated, a typical value for N-terminal amines in peptides (Figure S3 in the Supporting Information). The addition of Zn^{II} showed a pH-dependent feature; at higher pH, the resonances shifted and were largely broadened; in contrast, at lower pH, no shift was induced and only a little broadening occurred (Figures 2 and S3 in the Supporting Information). This is interpreted in the sense that at higher pH the deprotonated NH_2 of the N-terminal Glu is a ligand to Zn^{II} but not at lower pH, where NH_3^+ is present. The smaller broadening at lower pH is ascribed to the binding of Zn^{II} to the COO^- of Glu11 (in line with ref 38).

These results suggest that Zn^{II} binding occurs to Glu11 and His14. In order to confirm this, we used the shorter, nonaggregating peptide Ab11-14 (Glu-Val-His-His-NH_2), and as expected, the same resonances were affected by the addition of Zn^{II} in a way very similar to that in the longer Ab11-28 (see above). Moreover, the same pH dependence was observed (see Figure S4 in the Supporting Information) and hence supports the binding of Zn^{II} by NH_2 of Glu11 at higher pH.

XAS. X-ray absorption near-edge structure (XANES) spectra give an indication of the dominant zinc species in a given sample. Thus, XANES was used to probe the pH dependence of Zn^{II} coordination to Ab11-28 (Figure 3). The Zn K-edge spectra for the two Ab11-28 with 0.5 equiv of Zn^{II} at pH 6.5 and 7.5 were similar, indicating that no major difference in zinc speciation occurred between these two pH values. On the contrary, the sample at pH 8.5 exhibited a different shape. Indeed, based qualitatively on the shapes of the main white-line peak at ~9665 eV and oscillations on the high energy side of the white-line peak, the solution at pH 8.5 had distinctly a different spectrum compared with those at lower pH. The white-line peak was enlarged with pH, especially between pH 7.5 and 8.5, the peak at 9670 eV was shifted to a higher energy (~9672 eV), and the peak at 9678 eV (dotted line) disappeared. These differences indicate a change in coordination between pH 7.5 and 8.5 in line with the NMR data (see above).

Previous studies suggested that the dimer $Zn^{II}(Ab11\text{-}28)_2$ is the building block, which first forms nonamyloid aggregates (the presence of turbidity but no ThT fluorescence) and then

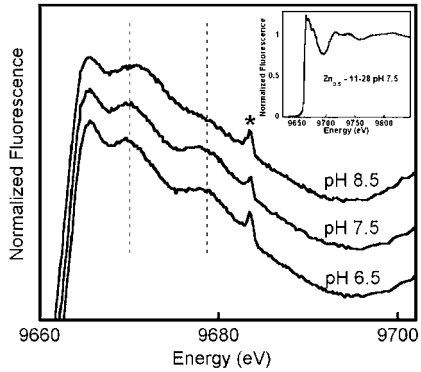

Figure 3. Zoom on XANES of Ab11-28 with 0.5 equiv of Zn^{II} at pH 6.5, 7.5, and 8.5. The asterisk indicates an artifact of the detector (inset: complete XANES of Ab11-28 with 0.5 equiv of Zn^{II} at pH 7.5).

converts to amyloid fibril (increasing ThT fluorescence). Moreover, Zn^{II} was bound by COO^- from two Glu11 and two imidazole of His14 from each peptide[38,39] (see the inset in Figure 4A). As pointed out by a reviewer, the binding of Zn^{II} to Glu11 and His14 is not consistent with a β-sheet structure of this portion of the peptide because the two side chains point in opposite directions. This resembles the structure from solid-state NMR of Aβ1-42, in which the N-terminal part 1−16 is disordered and the β-sheet structure starts around position 17.[40,41] The structural data obtained above suggest that the Zn^{II} binding in $Zn^{II}(Ab11\text{-}28)_2$ is pH-dependent in the region of pH 6−8.5. Two forms exist with an apparent pK_a of about 7.8, the low pH form binds His14 and COO^- of Glu11, and in the high pH form, the N-terminal amine binds additionally to His14. Whether COO^- is still bound cannot be determined.

The pK_a of N-terminal amine binding to Zn^{II} correlates very well with the kinetics of the fibril formation measured by ThT (Figure 1, bottom) and hence suggests that the binding of the N-terminal amine changes the peptide structure to a less aggregation-prone conformation. An explanation would be that additional binding of N-terminal NH_2 to Zn^{II} coordinated by COO^- from Glu11 and His14 of the two peptides might inhibit the alignment of the two portions from amino acids 15−28 in a

dx.doi.org/10.1021/ic300972j | Inorg. Chem. 2012, 51, 7897−7902

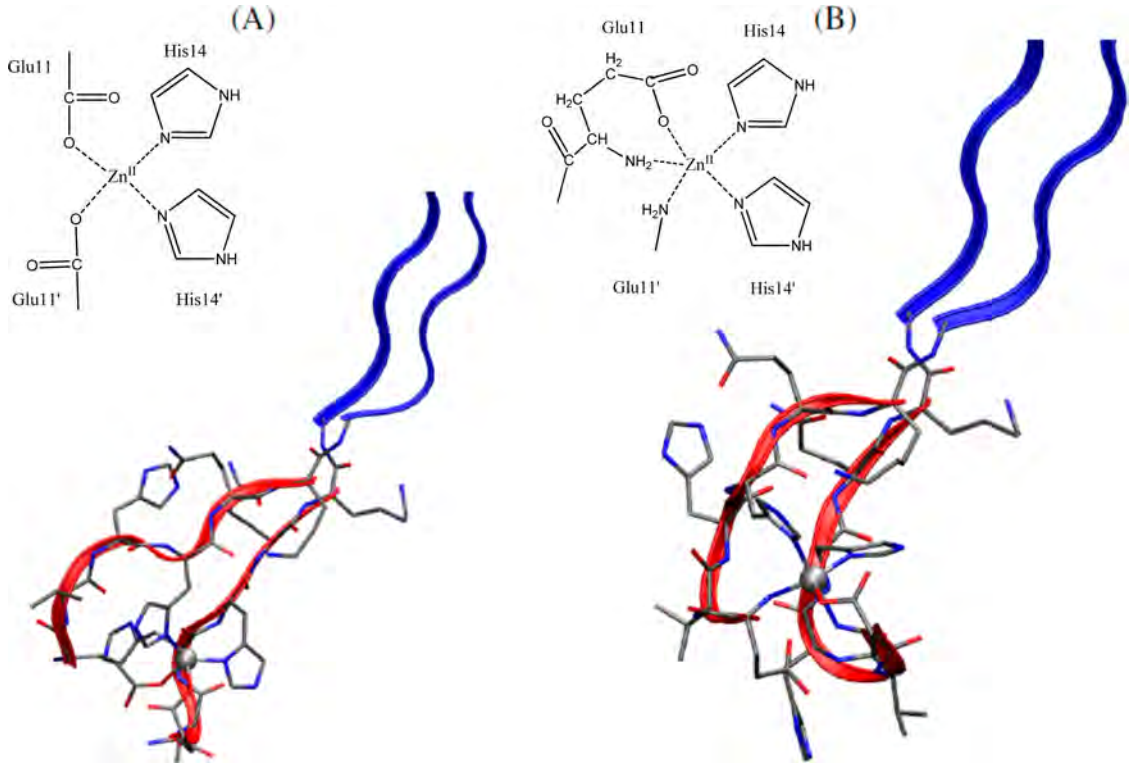

Figure 4. Final configurations (t = 5 ps) for models 1 (low pH, panel A) and 2 (high pH, panel B) for TB-MD at T = 50 K. Residues 17−28 (displayed as ribbons only) are represented with the positions of the empirical models. Residues 11−16 are represented as sticks, and Zn^{II} is represented as a sphere. Bonds involving Zn^{II} are displayed for interatomic distances within 2.2 Å. Atomic radii are arbitrary, and the color scheme is gray for C, red for O, blue for N, and silver for Cu. The *VMD* program was used for this and the following molecular drawings. A schematic view of the first coordination sphere for the two structures is given in the upper left corner.

parallel β-sheet as needed for an amyloid structure. It might also reduce dimerization because the monomeric Zn^{II}_1(Ab11-28)$_1$ is stabilized because of the tripodal binding of NH_2, COO^- from Glu11, and His14.

Modeling. To gain deeper insight into the possible structural changes of the Zn^{II} site at different pH values and of the implications of structural changes on the peptide structure and aggregation, we investigated two semiempirical models of the dimeric Zn^{II}(Ab11−28)$_2$ with NH_3^+-Ab11-28 and NH_2-Ab11-28, respectively, as ligands.

First, Zn^{II}(Ab11-28)$_2$ with two NH_3^+-Ab11-28, in which zinc is bound to both His14 residues via the Nδ atoms, as suggested by ref 38, and to both COO^- groups of Glu11, was constructed and simulated in the vacuum at T = 50 K for 5 ps. This corresponds to Zn^{II}(Ab11-28)$_2$ at pH 6.5, called model 1 hereafter. Then, a second model, Zn^{II}(Ab11-28)$_2$ with two NH_2-Ab11-28, in which the two N atoms of the two Glu11 residues are included in the zinc coordination sphere corresponding to Zn^{II}(Ab11-28)$_2$ at pH 8.5 was simulated in the same conditions (model 2 hereafter).

The result of model 1 is very similar to the structure reported by Kozin and co-workers (Figure 4a in ref 38), although in their peptide, the NH_2 of Glu11 is acetylated. Thus, a significant difference in our model 1 is that the N termini are positively charged and one is in hydrogen-bond distance to COO^- (Figure 4a).

Once the N termini are deprotonated and the approach of N(Glu 11) toward Zn^{II} is forced (model 2), one of the COO^- groups of Glu11 is expelled away from the zinc coordination sphere. This event produces a pentacoordinated Zn^{II} (ligands 2 His, 2 NH_2, and 1 COO^-; Figure 4B), which is stable for the simulated time.

The root-mean-square deviation (rmsd) of backbone heavy atoms in the two models measured for residues 11−16 with respect to the initial extended β-sheet conformation (almost the backbone structure proposed by Luhrs et al.[40]) is smaller for model 1 (low pH) than for model 2 (high pH) (the two 5-ps-range curves in Figure 5). This indicates a distortion of the β-sheet alignment between the two peptides in the high-pH

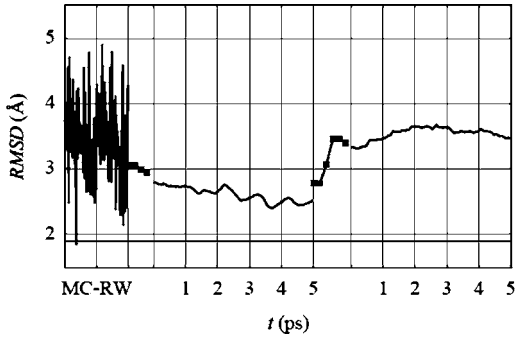

Figure 5. rmsd for heavy backbone atoms along with different trajectories. The first noisy line represents the span of values obtained within the MC-RW of residues 11−13. Square points represent the values along with the manipulations of empirical models (see the text for details). The two lines along with the 5-ps trajectories are the values for the TB-MD at T = 50 K. The first 5-ps part is for model 1, and the second 5-ps part is for model 2.

dx.doi.org/10.1021/ic300972j | *Inorg. Chem.* 2012, 51, 7897−7902

model, induced by the NH_2(Glu 11)−Zn^{II} bond. This observation is in line with a lower propensity to aggregate.

It is interesting to note that the turbidity does not correlate with the changes of Zn^{II} coordination observed because the intensity was highest around pH 7.4 (Figure 1, middle) and the kinetics is much less pH-dependent than it is for ThT (Figure 1, bottom). This can be explained by the overall net charge, which is an important parameter of aggregation because classically proteins precipitate better the closer the pH is to the isoelectric point (pI). The overall expected charges of $Zn^{II}{}_1$(Ab11-28)$_2$ is around 0 at pH 7.4 (Table 1) and thus very well with the profile of turbidity measurements (see Figure 1, middle), where a bell-like curve in aggregation/precipitation dependent on the pH was found with a peak around pH 7.4.

In conclusion, the very different pH dependences of ThT fluorescence (related to amyloids) and turbidity (global aggregation state) can be explained. The precipitation of $Zn^{II}{}_1$(Ab11-28)$_2$ leading to high turbidity is governed by the global charge of $Zn^{II}{}_1$(Ab11−28)$_2$, whereas the amyloid formation is governed by the pH-dependent structure of the zinc(II) peptide complex.

MATERIALS AND METHODS

Ab11-28 Sample Preparation. The peptide Ab11-28 (sequence Glu-Val-His-His-Gln-Lys-Leu-Val-Phe-Phe-Ala-Glu-Asp-Val-Gly-Ser-Asn-Lys) was purchased from GenScript Corp. (Piscataway, NJ). The stock solutions of Ab11-28 (∼1.2 mM) have been prepared by dissolving the peptide in Milli-Q water (resistivity = 18 MΩ cm^{-1}) or in D_2O for an NMR stock solution, which resulted in a final pH of 2. The pH of the solution was then adjusted to pH 12 by the addition of NaOH (or NaOD for NMR) stock solutions, in order to monomerize the peptides. These stock solutions were stored at 253 K. The peptide concentrations were determined by using the molar extinction coefficient ε = 390 M^{-1} cm^{-1} of the two phenylalanines at 258 nm.[30] Because phenylalanine does not absorb at 275 nm, the absorption at that wavelength was subtracted in order to remove contributions from the buffer or baseline drifts. A Zn^{II} stock solution was prepared with $Zn^{II}SO_4$ monohydrate (Strem Chemicals) in water or in D_2O for NMR experiments. Aggregation of peptides in the presence of Zn^{II} has been performed by dissolving peptides from a stock solution into a 100 mM 4-(2-hydroxyethyl)-1-piperazineethanesulfonic acid buffer at pH 7.4, 100 mM piperazine-*N*,*N*′-bis(2-ethanesulfonic acid) for pH 7.0 and 6.5, 2-(*N*-morpholino)-ethanesulfonic acid for pH 6.0, or piperazine-1,4-bis(2-hydroxypropanesulfonic acid) for pH 8.0 and 8.4 and was controlled at the end of the experiment. All of the experiments measuring either turbidity or fluorescence intensity have been performed at 298 K. The experiments were repeated at least five times in different preparations.

UV−Vis Spectroscopy. UV−vis spectra were recorded on an Agilent 8453 UV−visible spectrometer. Measurements were performed at room temperature.

Turbimetry. Turbidity measurements were done by measuring the absorbance at 350 nm with a FLUOstar Optima (BMG Labtech) in a quartz microplate (96-well, Hellma). The final concentrations of Ab11-28 and ThT are 300 and 10 μM, respectively.

Fluorescence Spectroscopy. Fluorescence spectra were measured by using a FLUOstar Optima (BMG Labtech). ThT, Ab11-28, and Zn^{II} were mixed in a 100 mM buffer and placed in a 96-well microplate. The time course of ThT fluorescence was then measured (excitation, 440 nm; emission, 490 nm; bandwidth for emission and excitation, 10 nm). The final concentrations of Ab11-28 and ThT were 300 and 10 μM, respectively.

The sigmoidal ThT curve was fitted with the program *KaleidaGraph* to the formula $F(t) = F_0 + A/\{1 + \exp[-k(t - t^{1/2})]\}$, where k is the elongation rate, A the amplitude, $t_{1/2}$ the time point when half the maximal intensity is reached, and F_0 the baseline before aggregation.[42]

XAS. XANES measurements were carried out at the SOLEIL Synchrotron Facility (St. Aubin, France), which was operating with a ring current of 400 mA. Zn^{II} K-edge XAS spectra were collected on the SAMBA beamline. The measurements were performed using a Si(220) water-cooled double-crystal monochromator and two large silicon mirrors for high-energy harmonics rejection. Energy calibration was achieved by measuring a copper foil and assigning the first inflection point of the absorption spectrum to 8979 eV. The spectra were measured in fluorescence mode by measuring the Zn^{II} Kα fluorescence with a 7-element germanium detector. The liquid samples were injected in special sample holders and cooled down to 20−30 K using a helium-flow cryostat. XANES spectra were background-corrected by a linear regression through the preedge region and a polynomial through the postedge region and normalized to the edge jump.

NMR. NMR experiments were realized on a Avance 500 Bruker NMR spectrometer. Several solutions of the buffer deuterated tris(hydroxymethyl)aminomethane (D_{11}-TRIS) at different pH values were prepared by solubilization of the TRIS powder in D_2O and acidification with D_2SO_4. Ab11-28 samples were freshly prepared from a D_2O stock solution (see the Ab11-28 Sample Preparation section). Ab11-28 (final TRIS concentration of 300 μM) was added to several TRIS solutions at a given pH (final concentration of 100 mM). The solutions were mixed, the pH was measured (to take into account the increase of the pH due to the Ab11-28 solution), and the resulting solution was added to the NMR tube. The residual water signal was suppressed by a presaturation procedure. Zn^{II} was directly added to the NMR tube, and measurements were performed as quickly as possible (less than 1 min 30 s) in order to minimize the aggregation process during spectrum acquisition. The assignment of the resonances at pH 7.4 was published earlier,[35] and titration between pH 7 and 9 in small pH steps allowed the assignment of the resonances over this pH range (see Figure S4 in the Supporting Information).

Calculations. The first two monomers in the structure reported in ref 40 (PDB id2BEG) were used as templates for building the initial Ab11-28 dimer. The φ and ψ dihedral angles of each residue are, in this structure, approaching the pair of values φ = −120°/ψ = 120° typical of a parallel β-sheet. A Zn^{II} ion was docked within the Nd atoms of His14, by using a dummy counterion model,[43] and the two His14 side chains were adapted to bind the Zn^{II} ion in an approximate tetrahedral coordination. A short molecular dynamics (MD) trajectory (20 ps) of this model in the vacuum and at T = 50 K was performed, keeping the N, CA, and C atoms of residues 17−28 fixed in space, in order to adapt the Zn^{II}-bound 11−16 region to the extended β-strand proposed by Luhrs et al.[40]

All of the manipulations of the empirical models were performed with the *NAMD*[44] and *VMD*[45] packages, with external forces implemented via the *PLUMED*[46] plugins. In order to build structures with the two Glu11 side chains in the Zn^{II} coordination sphere already occupied by the two His14 side chains, a Monte Carlo random walk (MC-RW) for the dihedral angles involving heavy atoms in the two 11−13 regions was performed. This random walk[47] samples almost every configuration with nonoverlapping atoms, with residues 14−28 fixed in space. Among the collected configurations, the first configuration with one Zn^{II}Oe(Glu 11) distance (in both Glu11 residues) within 3 Å was extracted. This configuration was then moved into the closest energy minimum and assumed as the starting model for a semiempirical calculation based on the tight-binding (TB) approximation.[48] The system was truncated to the Zn^{II} complex of Ab(11−16)−CO−NH−CH_3. The density functional TB code DFTB +[49] was used with the set of parameters developed for organic Zn^{II} compounds.[50] After 300 steps of energy minimization, a 5-ps-long MD simulation at T = 50 K was performed with the C, O, and N atoms in the two −CO−NH−CH_3 C-terminal groups (mimicking the Lys16−Leu17 linkage) fixed in space. A time step of 1 fs was used with no thermal bath (approximately constant energy or Born−Oppenheimer MD simulation). The result is model 1.

The approach of the two N termini of Glu11 toward Zn^{II} (model 2) was performed by the removal of one proton for each N terminus in the last DFTB configuration. External harmonic forces acting on the

dx.doi.org/10.1021/ic300972j | Inorg. Chem. 2012, 51, 7897−7902

Zn^{II}–N(Glu 11) distances were added to the empirical model. By increasing the equilibrium distance for the harmonic force in steps of 0.5 Å, the N(Glu 11)–Zn(II) distance decreased from 4.5 to 2 Å, ending to a model where both N(Glu 11) atoms are at bonding distance with Zn^{II}. The final configuration obtained with this procedure was used as the starting point for a second DFTB simulation, again at T = 50 K for 5 ps. The result is model 2.

■ ASSOCIATED CONTENT

Ⓢ Supporting Information

ThT fluorescence and turbidity, ^{1}H NMR spectra, and chemical shift of H–Cα of the N-terminal atom. This material is available free of charge via the Internet at http://pubs.acs.org.

■ AUTHOR INFORMATION

Corresponding Author

*E-mail: christelle.hureau@lcc-toulouse.fr (C.H.), peter.faller@lcc-toulouse.fr (P.F.). Tel: +33 5 61 33 31 62.

Notes

The authors declare no competing financial interest.

■ ACKNOWLEDGMENTS

Financial support from the "Region Midi-Pyrénées" (Research Grant APRTCN09004783) is acknowledged. We acknowledge SOLEIL for provision of synchrotron radiation on the SAMBA beamline (Proposal 20100771) and Stéphanie Belin (SOLEIL) and Christian Bijani for XAS and NMR measurements, respectively.

■ REFERENCES

(1) Haass, C.; Selkoe, D. J. *Nat. Rev. Mol. Cell Biol.* **2007**, *8*, 101–112.
(2) Chiti, F.; Dobson, C. M. *Annu. Rev. Biochem.* **2006**, *75*, 333–366.
(3) Fowler, D. M.; Koulov, A. V.; Balch, W. E.; Kelly, J. W. *Trends Biochem. Sci.* **2007**, *32* (5), 217–224.
(4) Hamley, I. W. *Angew. Chem., Int. Ed.* **2007**, *46* (43), 8128–8147.
(5) Gazit, E. *Chem. Soc. Rev.* **2007**, *36* (8), 1263–1269.
(6) Cherny, I.; Gazit, E. *Angew. Chem., Int. Ed.* **2008**, *47* (22), 4062–4069.
(7) Morris, K.; Serpell, L. *Chem. Soc. Rev.* **2010**, *39* (9), 3445–3453.
(8) Morris, A. M.; Watzky, M. A.; Agar, J. N.; Finke, R. G. *Biochemistry* **2008**, *47* (8), 2413–2427.
(9) Exley, C. *J. Alzheimer's Dis* **2006**, *10* (2–3), 173–177.
(10) Barnham, K. J.; Cappai, R.; Beyreuther, K.; Masters, C. L.; Hill, A. F. *Trends Biochem. Sci.* **2006**, *31* (8), 465–472.
(11) Tougu, V.; Tiiman, A.; Palumaa, P. *Metallomics* **2011**, *3* (3), 250–261.
(12) Hong, L.; Simon, J. D. *Metallomics* **2011**, *3* (3), 262–266.
(13) Perez, L. R.; Franz, K. J., *Dalton Trans. 39* (9), 2177–2187.
(14) Calabrese, M. F.; Miranker, A. D. *Prion* **2009**, *3* (1), 1–4.
(15) Brown, D. R. *Dalton Trans.* **2009**, *21*, 4069–4076.
(16) Faller, P.; Hureau, C. *Dalton Trans.* **2009**, 1080–1094.
(17) Drago, D.; Bolognin, S.; Zatta, P. *Curr. Alzheimer Res.* **2008**, *5* (6), 500–507.
(18) Fritz, G.; Botelho, H. M.; Morozova-Roche, L. A.; Gomes, C. M. *FEBS J* **2010**, *277* (22), 4578–4590.
(19) Duce, J. A.; Bush, A. I. *Prog. Neurobiol. 92* (1), 1–18.
(20) Gaggelli, E.; Kozlowski, H.; Valensin, D.; Valensin, G. *Chem. Rev.* **2006**, *106* (6), 1995–2044.
(21) Gazit, E. *Prion* **2007**, *1* (1), 32–35.
(22) Lynn, D. G.; Meredith, S. C. *J. Struct. Biol.* **2000**, *130* (2–3), 153–173.
(23) Eisenberg, D.; Nelson, R.; Sawaya, M. R.; Balbirnie, M.; Sambashivan, S.; Ivanova, M. I.; Madsen, A. O.; Riekel, C. *Acc. Chem. Res.* **2006**, *39* (9), 568–575.
(24) Yang, H.; Pritzker, M.; Fung, S. Y.; Sheng, Y.; Wang, W.; Chen, P. *Langmuir* **2006**, *22* (20), 8553–8562.
(25) Pagel, K.; Seri, T.; von Berlepsch, H.; Griebel, J.; Kirmse, R.; Bottcher, C.; Koksch, B. *ChemBioChem* **2008**, *9* (4), 531–536.
(26) Hoernke, M.; Koksch, B.; Brezesinski, G. *Biophys. Chem.* **2010**, *150* (1–3), 64–72.
(27) Schlosser, G.; Stefanescu, R.; Przybylski, M.; Murariu, M.; Hudecz, F.; Drochioiu, G. *Eur. J. Mass Spectrom. (Chichester, England)* **2007**, *13* (5), 331–337.
(28) Dong, J.; Canfield, J. M.; Mehta, A. K.; Shokes, J. E.; Tian, B.; Childers, W. S.; Simmons, J. A.; Mao, Z.; Scott, R. A.; Warncke, K.; Lynn, D. G. *Proc. Natl. Acad. Sci. U.S.A.* **2007**, *104* (33), 13313–13318.
(29) Dong, J.; Shokes, J. E.; Scott, R. A.; Lynn, D. G. *J. Am. Chem. Soc.* **2006**, *128* (11), 3540–3542.
(30) Scotter, A. J.; Guo, M.; Tomczak, M. M.; Daley, M. E.; Campbell, R. L.; Oko, R. J.; Bateman, D. A.; Chakrabartty, A.; Sykes, B. D.; Davies, P. L. *BMC Struct. Biol.* **2007**, *7*, 63.
(31) Alies, B.; Pradines, V.; Llorens-Alliot, I.; Sayen, S.; Guillon, E.; Hureau, C.; Faller, P. *J. Biol. Inorg. Chem.* **2011**, *16* (2), 333–340.
(32) Pradines, V.; Jurca Stoia, A.; Faller, P. *New J. Chem.* **2009**, *32*, 1189–1194.
(33) Tougu, V.; Palumaa, P. *Coord. Chem. Rev.* **2012**, DOI: 10.1016/j.ccr.2011.12.008.
(34) Tekirian, T. L. *J. Alzheimer's Dis.* **2001**, *3* (2), 241–248.
(35) Alies, B.; Solari, P. L.; Hureau, C.; Faller, P. *Inorg. Chem.* **2012**, *51* (1), 701–708.
(36) Chiti, F.; Stefani, M.; Taddei, N.; Ramponi, G.; Dobson, C. M. *Nature* **2003**, *424* (6950), 805–808.
(37) Lopez De La Paz, M.; Goldie, K.; Zurdo, J.; Lacroix, E.; Dobson, C. M.; Hoenger, A.; Serrano, L. *Proc. Natl. Acad. Sci. U.S.A.* **2002**, *99* (25), 16052–7.
(38) Tsvetkov, P. O.; Kulikova, A. A.; Golovin, A. V.; Tkachev, Y. V.; Archakov, A. I.; Kozin, S. A.; Makarov, A. A. *Biophys. J.* **2010**, *99* (10), L84–L86.
(39) Kozin, S. A.; Mezentsev, Y. V.; Kulikova, A. A.; Indeykina, M. I.; Golovin, A. V.; Ivanov, A. S.; Tsvetkov, P. O.; Makarov, A. A. *Mol. Biosyst.* **2011**, *7* (4), 1053–1055.
(40) Luhrs, T.; Ritter, C.; Adrian, M.; Riek-Loher, D.; Bohrmann, B.; Dobeli, H.; Schubert, D.; Riek, R. *Proc. Natl. Acad. Sci. U.S.A.* **2005**, *102* (48), 17342–17347.
(41) Tycko, R. *Q. Rev. Biophys.* **2006**, *39* (1), 1–55.
(42) Hellstrand, E.; Boland, B.; Walsh, D. M.; Linse, S. *ACS Chem. Neurosci.* **2009**, *1*, 13–18.
(43) Pang, Y. P.; Xu, K.; Yazal, J. E.; Prendergas, F. G. *Protein Sci.* **2000**, *9* (10), 1857–1865.
(44) Phillips, J. C.; Braun, R.; Wang, W.; Gumbart, J.; Tajkhorshid, E.; Villa, E.; Chipot, C.; Skeel, R. D.; Kale, L.; Schulten, K. *J. Comput. Chem.* **2005**, *26* (16), 1781–1802.
(45) Humphrey, W.; Dalke, A.; Schulten, K. *J. Mol. Graph.* **1996**, *14* (1), 33–38, 27–28.
(46) Bonomi, M.; Branduardi, D.; Bussi, G.; Camilloni, C.; Provasi, D.; Raiteri, P.; Donadio, D.; Marinelli, F.; Pietrucci, F.; Broglia, R. A.; Parrinello, M. *Comput. Phys. Commun.* **2009**, *180* (10), 1961–1972.
(47) La Penna, G.; Morante, S.; Perico, A.; Rossi, G. C. *J. Chem. Phys.* **2004**, *121* (21), 10725–10741.
(48) Colombo, L. *Riv. Nuovo Cimento Soc. Ital. Fis.* **2005**, *28* (10), 1–59.
(49) Aradi, B.; Hourahine, B.; Frauenheim, T. *J. Phys. Chem. A* **2007**, *111* (26), 5678–5684.
(50) Moreira, N. H.; Dolgonos, G.; Aradi, B.; da Rosa, A. L.; Frauenheim, T. *J. Chem. Theory Comput.* **2009**, *5* (3), 605–614.

Dynamics of Zn(II) Binding as a Key Feature in the Formation of Amyloid Fibrils by Aβ11-28

Bruno Alies, Pier-Lorenzo Solari, Christelle Hureau, Peter Faller

Inorganic Chemistry
2012, *51* (1), 333-340

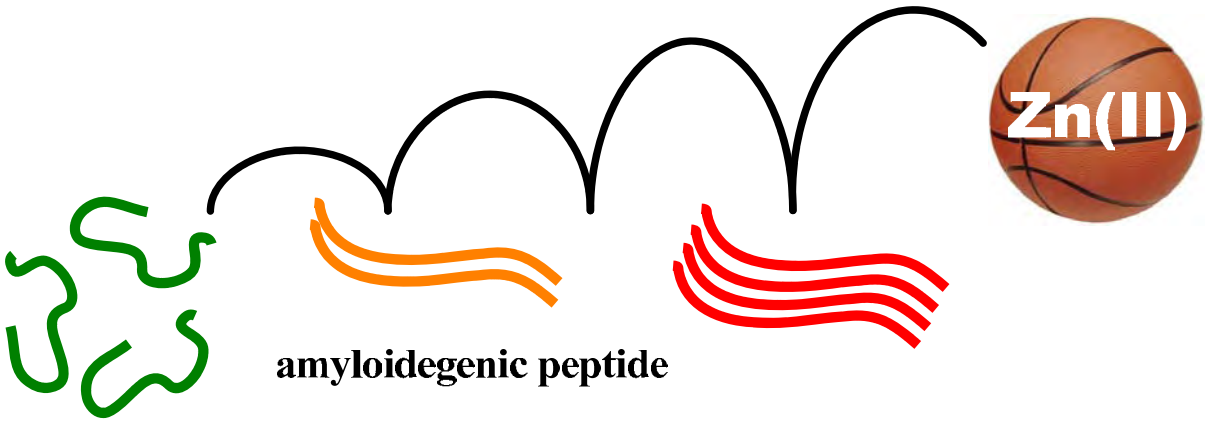

The following article is described in the previous chapter. The study is about Zn coordination to Aβ11-28 and the effect of its dynamic binding on Zn mediated aggregation.

Inorganic Chemistry

Article

pubs.acs.org/IC

Dynamics of Zn^{II} Binding as a Key Feature in the Formation of Amyloid Fibrils by Aβ11-28

Bruno Alies,[†,‡] Pier-Lorenzo Solari,[§] Christelle Hureau,*[,†,‡] and Peter Faller*[,†,‡]

[†]Laboratoire de Chimie de Coordination (LCC), CNRS, 205 route de Narbonne, 31077 Toulouse, France

[‡]LCC, Université de Toulouse, UPS, INPT, 31077 Toulouse, France

[§]Synchrotron SOLEIL, L'Orme des merisiers BP48, Saint-Aubin, F-91192 Gif-Sur-Yvette Cedex, France

Supporting Information

ABSTRACT: Supramolecular assembly of peptides and proteins into amyloid fibrils is of multifold interest, going from materials science to physiopathology. The binding of metal ions to amyloidogenic peptides is associated with several amyloid diseases, and amyloids with incorporated metal ions are of interest in nanotechnology. Understanding the mechanisms of amyloid formation and the role of metal ions can improve strategies toward the prevention of this process and enable potential applications in nanotechnology. Here, studies on Zn^{II} binding to the amyloidogenic peptide Aβ11-28 are reported. Zn^{II} modulates the Aβ11-28 aggregation, in terms of kinetics and fibril structures. Structural studies suggest that Aβ11-28 binds Zn^{II} by amino acid residues Glu11 and His14 and that Zn^{II} is rapidly exchanged between peptides. Structural and aggregation data indicate that Zn^{II} binding induces the formation of the dimeric $Zn^{II}_1(A\beta 11\text{-}28)_2$ species, which is the building block of fibrillar aggregates and explains why Zn^{II} binding accelerates Aβ11-28 aggregation. Moreover, transient Zn^{II} binding, even briefly, was enough to promote fibril formation, but the final structure resembled that of apo-Aβ11-28 amyloids. Also, seeding experiments, i.e., the addition of fibrillar $Zn^{II}_1(A\beta 11\text{-}28)_2$ to the apo-Aβ11-28 peptide, induced aggregation but not propagation of the $Zn^{II}_1(A\beta 11\text{-}28)_2$-type fibrils. This can be explained by the dynamic Zn^{II} binding between soluble and aggregated Aβ11-28. As a consequence, dynamic Zn^{II} binding has a strong impact on the aggregation behavior of the Aβ11-28 peptide and might be a relevant and so far little regarded parameter in other systems of metal ions and amyloidogenic peptides.

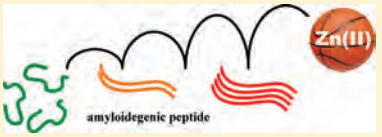

1. INTRODUCTION

The supramolecular assembly of peptides and proteins into amyloid fibrils is intensively studied not only because of their important biological roles in several diseases[1,2] but also because nonpathological roles have been identified.[3] Moreover, amyloids are of interest in nanostructure fabrication and biotechnology.[4,5] Amyloids refer to peptides and proteins that adopt fibrils based on the cross-β structure, in which the peptide backbone is orthogonal to the fibril axis.[4,6,7] They normally form by a two-step process with a slow nucleation phase, followed by a typically fast, autocatalytic surface growth, leading to a sigmoid curve characteristic of amyloid formation, often monitored by thioflavin T (ThT) fluorescence.[8] Binding of metal ions to amyloidogenic peptides is of biological relevance in several cases, including Prion diseases, Alzheimer's disease, Parkinson's disease, amyotrophic lateral scleroses, and type II diabetes, in which specific amyloidogenic peptides or proteins interact with metal ions such as Zn, Cu, Fe, etc.,[9−16] and for which compounds are developed to suppress the effect of the metal ion.[16−21] Also, for biotechnological application or in nanoscience, amyloid fibrils with embedded metal ions are of interest because they can undergo electron-transfer reactions or can serve as catalytic centers.[22−27]

Truncated peptides have been used to model the aggregation of native peptides or to gain general insight into the mechanisms of the aggregating process as well as for nanostructure fabrication.[28] Also, de novo designed peptides were very useful for understanding aggregation and for obtaining nanostructures of the amyloid type.[4,29,30] The interaction of small or truncated amyloidogenic peptides with various metal ions has been studied in the past.[31−37] Recently, we investigated the impacts of stoichiometric Zn^{II} and Cu^{II} binding on three different amyloidogenic model peptides including Aβ11-28 and found metal- and peptide-specific effects related to the coordination chemistry of the metal ions.[38,39] Aβ11-28 is derived from amyloid-β (Aβ) peptide, which plays a central role in Alzheimer's disease. Although Aβ11-28 is missing the N- and C-terminal parts and, hence, is clearly different from Aβ in terms of aggregation and metal binding, it retains two important features for metal-induced amyloid formation. These are the hydrophobic core (amino acid residues spanning from 17 to 21, sequence LVFFA) and the two His residues (His13 and His14) known to anchor the Zn^{II} ion. Thus, this amyloidogenic Aβ11-28 peptide can serve as a model system to gain general insight into metal-induced amyloid formation but does not mimic the special case of native Aβ (although native truncated forms starting from amino acid 11 have been identified in AD[40]).

So far, studies of the effect of metal binding on amyloid formation have focused on the addition of metal ions at the beginning of the aggregation process with the idea that they bind very rapidly[41,42] and stay bound. Only one case is reported

Received: October 17, 2011
Published: December 13, 2011

 © 2011 American Chemical Society dx.doi.org/10.1021/ic202247m | *Inorg. Chem.* 2012, 51, 701−708

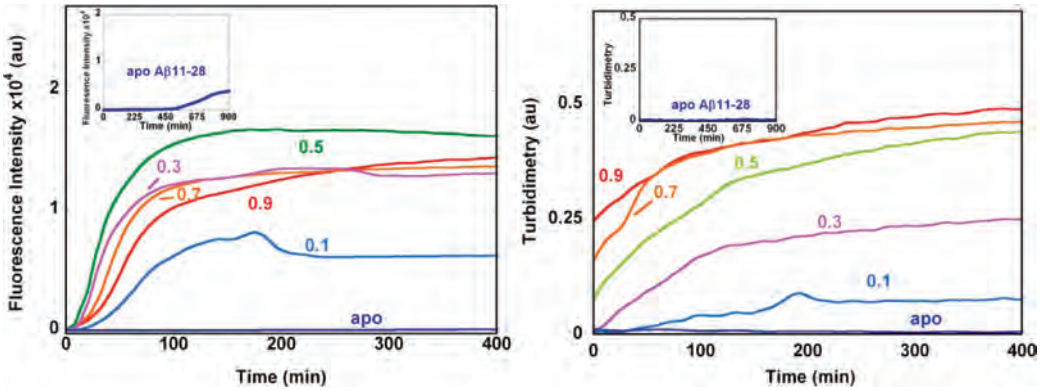

Figure 1. Time-course measurements of ThT fluorescence (left) and turbidity (right) of Aβ11-28 peptide in the presence of Zn^{II}, with Zn^{II} to Aβ11-28 ratios ranging from 0 to 0.9. Conditions: [Aβ11-28] = 300 μM; [Zn^{II}] = 0–270 μM; [HEPES buffer] = 100 mM, pH 7.4; [ThT] = 10 μM. Insets: time-course measurements of ThT fluorescence (left) and turbidity (right) of Aβ11-28 peptide without Zn^{II} (i.e., apo-Aβ11-28) over a longer period.

where transient copper(II) binding to β-2 microglobulin in a 2:1 ratio was sufficient to promote amyloid formation. Copper(II) binding to the natively structured protein β-2 microglobulin induced a conformational change to form an oligomerization-prone structure by exposing a previously buried region. The structural conversion is Cu^{II}-dependent, while the subsequent formation of amyloids is not. The transient copper(II) binding required for conformational change was on the hour time scale.[14,43]

Transient metal ion binding might be of biological relevance because in several biological environments metal-ion concentrations can fluctuate at different time scales; i.e., binding can be dynamic. A well-known example is the Zn^{II} ion in certain glutamatergic neurons, in which Zn^{II} is released in high amounts (up to 300 μM) in the synaptic cleft and taken up in a few seconds.[44,45] Thus, we investigated also dynamical aspects of Zn^{II} binding to the Aβ11-28 model peptide during aggregation, and the results suggest that dynamics can play an important role in the aggregating process and might be of biological relevance.

2. RESULTS

2.1. Aggregation Dependence of the Zn^{II} to Aβ11-28 Ratio. The stoichiometry between metal ions and amyloidogenic peptides can influence the aggregation behavior because of the formation of different types of complexes. Here, the aggregation kinetics were followed by ThT fluorescence and turbidity as a function of the Zn^{II} to Aβ11-28 ratio (Figure 1). ThT is a specific fluorescence dye for amyloid-type aggregates, while turbidity measures all types of aggregates. The Zn^{II} to Aβ11-28 stoichiometry had a pronounced impact on the aggregation behavior, and different changes in the ThT fluorescence and turbidity were observed (Figure 1). The turbidity increased rapidly upon Zn^{II} addition to Aβ11-28. Zn^{II} addition to the buffer only (no peptide) did not show turbidity, hence ruling out that turbidity is due to Zn^{II} precipitation. Increasing the equivalent of Zn^{II} per Aβ11-28 from 0 to 0.9 led to faster kinetics and a higher plateau, a behavior that has often been observed for amyloidogenic peptides (Figure 1, right panel). In contrast, ThT traces did not parallel the one measured by turbidity. The increase in ThT fluorescence was slower and showed the typical sigmoid curve for amyloid-type aggregation due to a nucleation and elongation mechanism.[8] The fastest curve with the most intense plateau was observed for approximately 0.5 equiv of Zn^{II} per Aβ11-28; below and above this stoichiometry, the kinetics and intensity were slower and smaller, respectively (Figure 1, left panel). Turbidity evolved much faster than ThT fluorescence for all Zn^{II} to Aβ11-28 stoichiometries. This indicates that in a first stage ThT-negative amorphous aggregates were formed, which later evolved toward ThT-positive amyloid-like aggregates. During this change, the turbidity intensity stayed more or less constant, suggesting a transformation of the aggregates. This indicates that from 0 to 0.9 equiv of Zn^{II} per Aβ11-28 global aggregation is accelerated and increased, while for fibril formation, 0.5 equiv is the optimum. This can be explained in the most straightforward manner by assuming that a dimeric complex with one Zn^{II} bound to two Aβ11-28 peptides, i.e. $Zn^{II}_1(A\beta 11\text{-}28)_2$, is the building block of the fibrillar-type aggregate. The further addition of Zn^{II} enhanced the formation of aggregates but diminished the fibrillar content, likely by precipitating the $Zn^{II}_1(A\beta 11\text{-}28)_2$ complex via Zn^{II} bridging of two $Zn^{II}_1(A\beta 11\text{-}28)_2$ moieties.

It is important to note that after longer incubation apo-Aβ11-28 aggregated as well (Figure 1, insets) but with different characteristics. Apo-Aβ11-28 reached a plateau of ThT fluorescence approximately 5 times lower than the one observed in the case of $Zn^{II}_{0.5}$-Aβ11-28 and did not show any detectable increase in the turbidity. This strongly indicates that apo-Aβ11-28 forms a different type of amyloid compared to $Zn^{II}_{0.5}$-Aβ11-28. Indeed, transmission electron microscopy (TEM) showed a dense scaffold of fibrillar aggregates for $Zn^{II}_{0.5}$-Aβ11-28, whereas apo-Aβ11-28 formed more isolated fibrillar aggregates (Figure 2).

2.2. Effect of Ethylenediaminetetraacetic Acid (EDTA) on $Zn^{II}_{0.5}$-Aβ11-28. In order to see whether Zn^{II} is involved in the different phases of the aggregation process and if the effect of Zn^{II} binding on Aβ11-28 is reversible, we added the very strong Zn^{II} chelator EDTA (dissociation constant of approximately 10^{-13} M at pH 7.4 compared to approximately 10^{-6} M for Aβ peptide and truncated forms similar to Aβ11-28[46,47]) at different time points. EDTA has been shown to be useful to reverse the effect of Zn^{II} on amyloid formation, like in the case of Aβ1-42, where it abolished completely the inhibitory effect of Zn^{II} on fibril formation.[48] First, as a control, EDTA (5 equiv per Zn^{II} ion) was added just before Zn^{II} and, as expected, the Aβ11-28 aggregation behavior was very similar to that of apo-Aβ11-28, indicating that the Zn^{II}EDTA complex does not interfere with aggregation. Very interestingly, adding EDTA at any time point after the Zn^{II} addition (2 min to 3 h; see Figure S1 in the Supporting Information) did not completely reverse the aggregation profile back to the level of the nonaggregated apo-Aβ11-28 in ThT fluorescence (Figure 3). In other words,

dx.doi.org/10.1021/ic202247m | Inorg. Chem. 2012, 51, 701–708

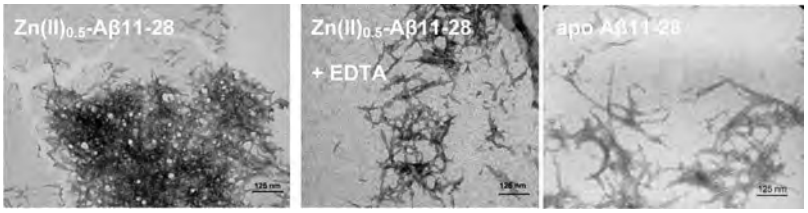

Figure 2. TEM images of $Zn^{II}_{0.5}$-Aβ11-28 (left), $Zn^{II}_{0.5}$-Aβ11-28 + EDTA (middle), and apo-Aβ11-28 (right) after 1 day of incubation. Conditions: [Aβ11-28] = 300 μM; [Zn^{II}] = 0 or 150 μM; [EDTA] = 750 μM; [HEPES buffer] = 100 mM, pH 7.4; [ThT] = 10 μM.

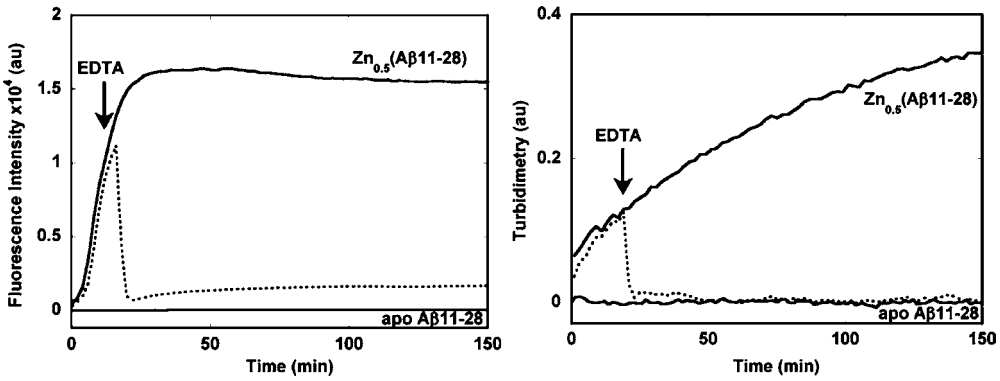

Figure 3. Time course of ThT fluorescence (left) and turbidity (right) of apo-Aβ11-28 and $Zn^{II}_{0.5}$-Aβ11-28 without (solid) and with the addition of EDTA at the time point indicated by the arrow (dashed). Conditions: [Aβ11-28] = 300 μM; [Zn^{II}] = 0 or 150 μM; [EDTA] = 750 μM; [HEPES buffer] = 100 mM, pH 7.4; [ThT] = 10 μM.

the addition of EDTA does not totally reverse the system, and hence even transient Zn^{II} binding is sufficient to induce aggregation. In Figure 3, we are reminded of the fact that apo-Aβ11-28 did not undergo any increase in ThT fluorescence (left panel) or turbidity (right panel) over several hours, while $Zn^{II}_{0.5}$-Aβ11-28 showed the typical sigmoid behavior in ThT fluorescence and a turbidity increase from the beginning. The addition of EDTA to the $Zn^{II}_{0.5}$-Aβ11-28 mixture led to an immediate drop of the turbidity back to the nonaggregated apo-Aβ11-28 level (Figure 3, right). Interestingly, ThT fluorescence did not drop as fast as the turbidity (and sometimes even continued to increase for a while before dropping; data not shown; Figure S1 in the Supporting Information) nor did it drop back to the level of nonaggregated apo-Aβ11-28. At the end, the plateau reached a level similar to that of aggregated apo-Aβ11-28 (compare the left panel in Figure 3 and the inset of the left panel in Figure 1). On the basis of the formation of two types of aggregates, i.e., $Zn^{II}_{0.5}$-Aβ11-28, which exhibits an intense turbidity and high ThT fluorescence, and apo-Aβ11-28, which shows a low ThT fluorescence intensity and no detectible turbidity, the addition of EDTA to $Zn^{II}_{0.5}$-Aβ11-28 resulted in the formation of apo-Aβ11-28-type aggregates, which was much faster compared to that of apo-Aβ11-28 only. This is in line with TEM data (Figure 2), which showed similar types of aggregates for apo-Aβ11-28 and $Zn^{II}_{0.5}$-Aβ11-28 plus EDTA (more isolated fibrillar-type structures), but different from Zn^{II}-Aβ11-28 (more dense).

The addition of EDTA to $Zn^{II}_{0.5}$-Aβ11-28 at different time points did not change the overall feature; i.e., shorter or longer transient Zn^{II} binding modulated the aggregation behavior compared to apo-Aβ11-28 in any case (see Figure S1 in the Supporting Information). There were variations in the kinetics and intensity of the drop of ThT fluorescence, but in all experiments, the decrease of ThT fluorescence was slower than that of turbidity. Moreover, at the end, the fluorescence intensity was similar to that of the aggregated apo-Aβ11-28 peptide (Figure 1, left inset) but was reached much faster (Figure S1 in the Supporting Information). This indicates that Zn^{II} is able to nucleate the amyloid formation of apo-Aβ11-28, even when it binds only transiently.

Aβ11-28, after Zn^{II} and EDTA treatments, aggregates faster than without such treatments. Thus EDTA does not reverse $Zn^{II}_{0.5}$-Aβ11-28 back to nonaggregated apo-Aβ11-28 (Figure 3). This indicates that, after Zn^{II} removal by EDTA, apo-Aβ11-28 is in a different state (likely an oligomeric form) and is more prone to aggregation than monomeric apo-Aβ11-28 (Scheme 1).

To see the effect of Zn^{II} addition to aggregated apo-Aβ11-28 (formed via EDTA-treated $Zn^{II}_{0.5}$-Aβ11-28), Zn^{II} was added again at a concentration equal to that of EDTA, leading to Zn^{II}EDTA and $Zn^{II}_{0.5}$-Aβ11-28 species. ThT fluorescence increased again with a sigmoidal curve similar to that observed in the case of Zn^{II} addition to monomeric apo-Aβ11-28 (Figure 4). This can be most straightforwardly explained assuming that Zn^{II} induces aggregation of a portion of the soluble apo-Aβ11-28 peptide. Because of equilibrium between the aggregated and soluble states in amyloids, aggregated apo-Aβ11-28 is solubilized into monomeric Aβ11-28, leading to further Zn^{II}-induced aggregation. Thus, the aggregated apo-Aβ11-28 is transformed into aggregated $Zn^{II}_{0.5}$-Aβ11-28 (Scheme 1).

2.3. Seeding Experiment and Labile Zn^{II} Binding. Because the previous experiments indicated that two structural different aggregates are formed for apo- and $Zn^{II}_{0.5}$-Aβ11-28, we tested if aggregated $Zn^{II}_{0.5}$-Aβ11-28 can seed apo-Aβ11-28. Indeed, after seeding of soluble apo-Aβ11-28 with 7.5% preaggregated $Zn^{II}_{0.5}$-Aβ11-28, ThT fluorescence immediately started to increase and reached a plateau of intensity similar to that of apo-Aβ11-28 (Figure 5, left). No increase in the turbidity was detected (Figure 5, right). This indicates that indeed $Zn^{II}_{0.5}$-Aβ11-28 can nucleate aggregation of apo-Aβ11-28, but the aggregates formed are of the apo-type, so it is a triggering rather

dx.doi.org/10.1021/ic202247m | Inorg. Chem. 2012, 51, 701−708

Scheme 1. Monomeric Aβ11-28 Peptide (Triangles) Binding Zn^{II} (Red Circles) and Forming $Zn^{II}_1(Aβ11-28)_2$[a]

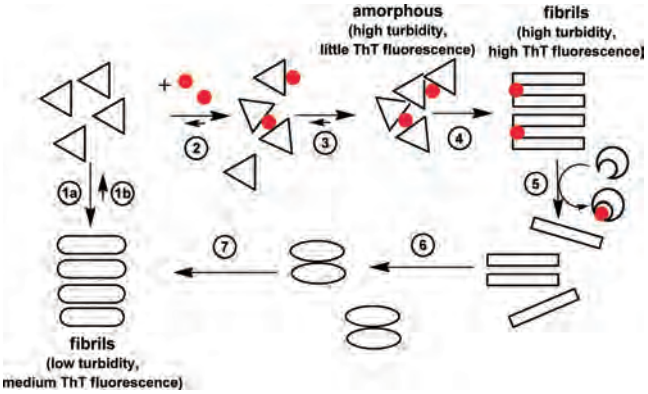

[a] $Zn^{II}_1(Aβ11-28)_2$ rapidly form amorphous-type aggregates (triangles) with high turbidity and very little ThT fluorescence, which then evolve into amyloid-type aggregates (rectangular sticks). The addition of EDTA (open rings) does not reverse the system to monomeric Aβ11-28 (triangles) but induces a form with a different conformation (ellipses) more prone to aggregate into apo-Aβ11-28 amyloid-type fibrils (round sticks).

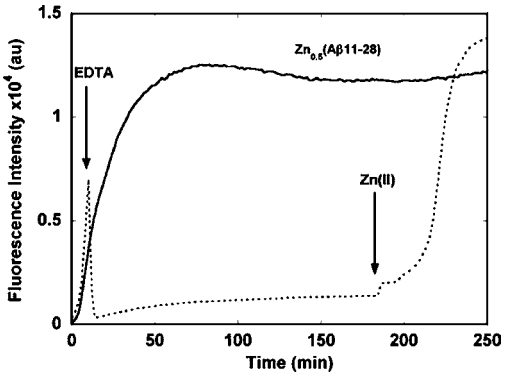

Figure 4. Time course of ThT fluorescence of $Zn^{II}_{0.5}$-Aβ11-28 (solid) and of $Zn^{II}_{0.5}$-Aβ11-28 with the addition of EDTA after ~10 min and of Zn^{II} after ~190 min (dashed). Conditions: [Aβ11-28] = 300 μM; [Zn^{II}] = 150 and 900 μM (after 190 min); [EDTA] = 750 μM; [HEPES buffer] = 100 mM, pH 7.4; [ThT] = 10 μM.

than a seeding effect because the structure of the seed is not propagated (Scheme 2).

Scheme 2. Model for the Triggering of apo-Aβ11-28 (Triangles) with Amyloid-Type Aggregates of $Zn^{II}_{0.5}$-Aβ11-28 (Zn^{II}, Red Circles; Peptides, Rectangular Sticks; See Also Scheme 1)[a]

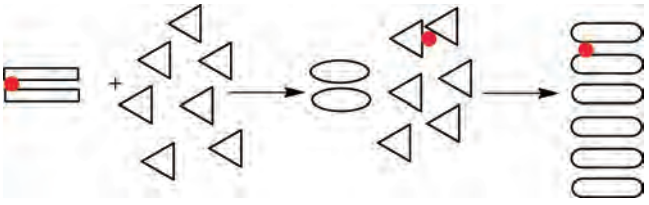

[a] The structure of $Zn^{II}_{0.5}$-Aβ11-28 is not propagated like in a "seeding" process, but Zn^{II} triggers aggregation of monomeric apo-Aβ11-28 to amyloid-type apo-Aβ11-28 (round sticks) because of its fast exchange between the different forms of Aβ11-28 (see also Scheme 1).

The model shown in Scheme 2 is based on a fast exchange of Zn^{II} between peptides. NMR experiments with several amyloid-type peptides indicated that exchange of Zn^{II} between the peptides is faster than that on the NMR time scale (approximately milliseconds).[49−51] This is also the case for the Aβ11-28 peptide because the substoichiometric addition of Zn^{II} affects the resonances of the entire sample (see below and Figure S2 in the Supporting Information). To see if the predicted fast exchange is also possible for the aggregated $Zn^{II}_{0.5}$-Aβ11-28, the Zn^{II}-sensitive chelator 4-(2-pyridylazo)resorcinol (PAR) was used (Figure 6). PAR forms the Zn^{II} complex $[Zn^{II}(PAR)_2]$, which absorbs at λ = 490 nm with $\varepsilon = 73 \times 10^3$ M^{-1} cm^{-1}, while PAR alone absorbs at λ = 413 nm ($\varepsilon = 33 \times 10^3$ M^{-1} cm^{-1}).[52] PAR was able to retrieve Zn^{II} very rapidly and quantitatively (half-time faster than 1 min), indicating indeed that Zn^{II} in aggregated $Zn^{II}_{0.5}$-Aβ11-28 is very labile and suggesting that Zn^{II} exchange between aggregated and soluble Aβ11-28 is also quite rapid. Hence, Zn^{II} in aggregates could have an impact on the aggregation of soluble apo-Aβ11-28 via fast Zn^{II} exchange reactions.

2.4. X-ray Absorption Spectroscopy (XAS). In order to obtain structural information about Zn^{II} binding to Aβ11-28, X-ray absorption near-edge structure (XANES) was used. XANES experiments with 0.5 and 1.0 equiv of Zn^{II} per Aβ11-28 peptide were performed at the beginning and at the end of the aggregation process (Figure 7). All of the spectra are in line with a mononuclear Zn^{II} site and resemble most proteins with tetracoordinated Zn^{II} including two His residues.[53,54]

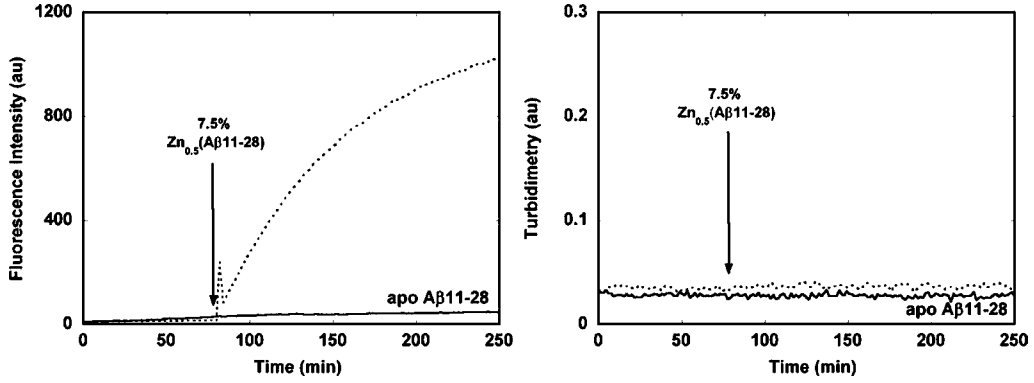

Figure 5. Time course of ThT fluorescence (left) and turbidity (right) of apo-Aβ11-28 without (solid) and with the addition of 7.5% preaggregated $Zn^{II}_{0.5}$-Aβ11-28 (dashed). Conditions: [Aβ11-28] = 300 μM; [$Zn^{II}_{0.5}$-Aβ11-28] = 22.5 μM added after 90 min (indicated by an arrow); [HEPES buffer] = 100 mM, pH 7.4; [ThT] = 10 μM. The addition of preaggregated $Zn^{II}_{0.5}$-Aβ11-28 is indicated by an arrow.

dx.doi.org/10.1021/ic202247m | Inorg. Chem. 2012, 51, 701−708

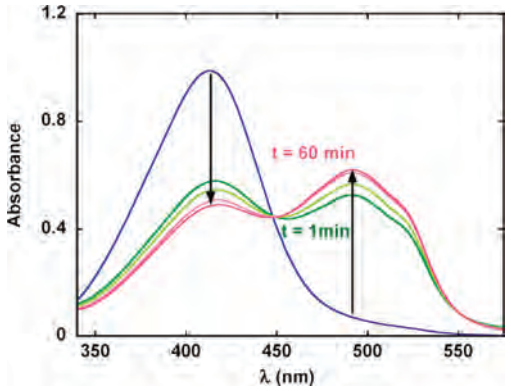

Figure 6. UV−vis monitoring of the addition of preaggregated $Zn^{II}_{0.5}$-Aβ11-28 to PAR. [PAR] = 300 μM; preaggregated [$Zn^{II}_{0.5}$-Aβ11-28] = 160 μM; [Zn^{II}] = 80 μM; [HEPES] = 100 mM, pH 7.4.

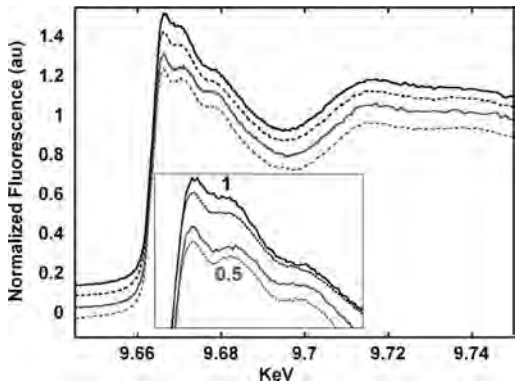

Figure 7. XANES spectra of $Zn^{II}_{0.5}$-Aβ11-28 (gray, **0.5**) and Zn^{II}_{1}-Aβ11-28 (black, **1**) before (dashed) and after (solid) aggregation at pH 7. Inset: magnification of the zone around 9.67 keV. [Aβ11-28] = 2.4 mM; [Zn^{II}] = 1.2 or 2.2 mM; [HEPES] = 50 mM, pH 7.0.

No difference between the beginning and end of the aggregation was observed, indicating that the coordination sphere does not change much during aggregation. The spectra were slightly different compared to previous measurements of Zn^{II}_{1}-Aβ11-28 at pH 8.6, indicating a pH-dependent Zn^{II} coordination.[38]

The measurements at different stoichiometries, i.e., $Zn^{II}_{0.25}$-Aβ11-28, $Zn^{II}_{0.5}$-Aβ11-28, and Zn^{II}_{1}-Aβ11-28, supported the formation of the dimeric Zn^{II}_{1}(Aβ11-28)$_2$ species because Aβ11-28 species with 0.25 and 0.5 equiv of Zn^{II} were identical, but with 1 equiv, features were dampened. This points to a more homogeneous coordination site of the first 0.5 equiv of Zn^{II}, in contrast to a more heterogeneous binding of the second 0.5 equiv of Zn^{II}. This is in line with formation of the dimeric Zn^{II}_{1}(Aβ11-28)$_2$ complex as a building block.

2.5. NMR. As shown by XANES, Zn^{II} coordination does not change significantly during aggregation, suggesting that Zn^{II} binding in the soluble state, as can be probed by NMR, is also relevant for the aggregated state. Hence, the effect of the Zn^{II} addition of the Aβ11-28 peptide was monitored by NMR (Figures 8 and S2−S4 in the Supporting Information). Zn^{II} induced line broadening and chemical shifts of some specific resonances. Figure 8 shows the aromatic region of the ^{1}H NMR spectra of the Aβ11-28 peptide in the absence and presence of 1 equiv of Zn^{II}, including the two His and two Phe residues. Zn^{II} addition leads to line broadening and a shift of only one of the two H_δ and only one of the two H_ε of His13 or His14. The other H_δ and H_ε resonances are only weakly affected, likely

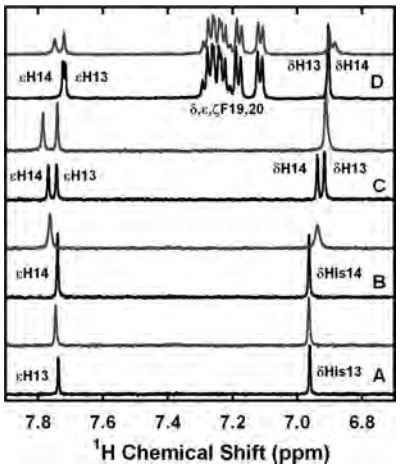

Figure 8. ^{1}H NMR of apo- (lower black trace) and Zn^{II} peptides (upper gray trace) of EVHG (A), EVRH (B), EVHH (C), and Aβ11-28 (D). Conditions: [peptide] = 300 μM; [Zn^{II}] = 270 μM; [Tris-d^{11}] = 100 mM, pH 7.5.

because of perturbation by Zn^{II} binding to the neighboring His. The resonances of the two Phe residues are not affected at all, indicating no binding to or near the Phe residues. The other affected residues were Glu11 and Val12 (see Figures S3 and S4 in the Supporting Information). This is attributed to the involvement of Glu11 in Zn^{II} binding, with Val12 being affected because of its vicinity to Glu11.

Because Aβ11-28 aggregation precluded the attribution of the resonances by longer NMR measurements (2D and ^{13}C experiments), we used model peptides corresponding to the Zn^{II}-binding region Glu-Val-His-His (EVHH-NH_2). Upon Zn^{II} addition to the EVHH peptide, although with slight differences, the Zn^{II} effect observed on the Aβ11-28 spectrum was reproduced, i.e., one of the His is much more affected than the other one (Figure 8C,D). The addition of Zn^{II} to the EVHG peptide lacking the His14 residue did not perturb significantly the NMR spectrum, with the remaining His13 being only weakly affected (Figure 8A). This indicates that the Zn^{II} binding His is His14. This was confirmed by the study of the EVRH peptide lacking His13, in which His14 is affected similarly to the His14 from Aβ11-28 (Figure 8B,D). This allowed assignment of the highly affected His of Aβ11-28 to His14. Moreover, a comparison between the EVHH and Aβ11-28 spectra in the Glu11 H_β and H_γ regions with and without Zn^{II} established the implication of Glu11 in Zn^{II} binding (Figure S4 in the Supporting Information). This agrees with the recent work of Kozin and collaborators, who proposed binding of Zn^{II} to COO^- of Glu11 and to His14 in the peptide Ac-Glu-Val-His-His-NH_2 with an apparent K_d in the lower micromolar range.[47,55] In conclusion, Zn^{II} binds preferentially to Glu11 (COO^-) and His14 in Aβ11-28 (Scheme 3). These structural features are fully in line with the possible formation of a dimeric Zn^{II}_{1}(Aβ11-28)$_2$ species, as indicated by the aggregation experiments (see above).

3. DISCUSSION

The structural studies described above suggest that Zn^{II} binds to Glu11 (COO^-) and His14 and that a dimeric Zn^{II}_{1}(Aβ11-28)$_2$ can be formed in line with recent studies on Ac-EVHH-NH_2.[47,55] These dimers are likely to be formed transiently and dynamically and aggregated further to larger aggregates.

dx.doi.org/10.1021/ic202247m | Inorg. Chem. 2012, 51, 701−708

Scheme 3. Model of the $Zn^{II}_1(A\beta 11\text{-}28)_2$ Complex[a]

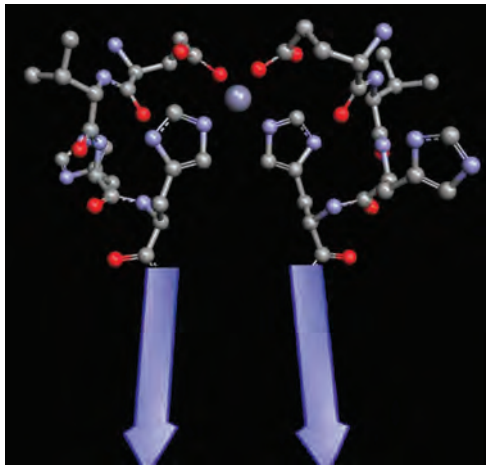

[a]Shown are Glu11, Val12, His13, and His14. Gln15 to Lys28 are represented as arrows. Zn^{II} is bound by Glu11 (COO^-) and His14 of Aβ11-28. Other ligands are possible (e.g., H_2O).

Amyloid-type fibrils are most rapidly and most intensively formed at 0.5 Zn^{II} per Aβ11-28 ratio, suggesting that the dimer $Zn^{II}_1(A\beta 11\text{-}28)_2$ is the building block of fibrils. This is supported by considering the overall charge. Classically, proteins precipitate and often aggregate into amyloids better when the net charge is smaller. At pH 7.4, apo-Aβ11-28 has a charge of 1−. The $Zn^{II}(A\beta 11\text{-}28)$ complex is thus expected to have 1+ charge, while $Zn^{II}_1(A\beta 11\text{-}28)_2$ has an expected charge of 0 and thus fits better with the faster aggregation. Further Zn^{II} addition decreased fibril formation but increased the turbidity, likely because of binding of Zn^{II} between the $Zn^{II}_1(A\beta 11\text{-}28)_2$ units and subsequent distortion of the amyloid-like aggregation of the $Zn^{II}_1(A\beta 11\text{-}28)_2$ units with the formation of more amorphous-like aggregates.

A very important finding is that Zn^{II} binding is very dynamic and Zn^{II} exchange between soluble and aggregated Aβ11-28 is rapid, which has a crucial impact on the aggregation behavior (Schemes 1 and 2). Apo-Aβ11-28 aggregates into amyloid-type fibrils with moderate ThT fluorescence and very little turbidity because the fibrils are not clumped together (Scheme 1, process 1a). Zn^{II} binding to apo-Aβ11-28 is rapid (Scheme 1, process 2) and forms at least transiently a dimeric $Zn^{II}_1(A\beta 11\text{-}28)_2$ complex, which forms amorphous-type aggregates (Scheme 1, process 3) with intense turbidity but no ThT fluorescence. These aggregates evolve toward amyloid-type fibrils (high ThT fluorescence), forming dense meshes (therefore, high turbidity). If Zn^{II} is added to preaggregated apo-Aβ11-28, the same process likely occurs (Scheme 1, processes 2−4) and soluble apo-Aβ11-28 is repopulated by the dissolution of aggregated apo-Aβ11-28 (process 1b). In contrast, when EDTA is added to Zn^{II}-Aβ11-28 aggregates (process 5), apo-Aβ11-28 aggregates are formed but not via the reversed pathway (processes 4 to 2). Instead another pathway is taken (Scheme 1, processes 5−7). This is supported by the findings that the turbidity is dropping faster than ThT fluorescence, indicating an intermediate state and that formation of apo-Aβ11-28 is much faster than expected from a reversible pathway.

As a consequence, transiently adding Zn^{II} to apo-Aβ11-28 results in fibrils like the ones formed by apo-Aβ11-28 only but dramatically accelerates formation. Transient Zn^{II} binding over different time periods shows the effect, but a period of transient Zn^{II} binding of less than 1 min is sufficient to accelerate the formation of apo-Aβ11-28 aggregates. This clearly shows that transient Zn^{II} binding in the second time scale can have a nucleation effect on the aggregation of apo-Aβ11-28. Moreover, transient Zn^{II} binding accelerates the formation of apo-Aβ11-28 at substoichiometric amounts (Figure 1), showing that relatively low concentrations of Zn^{II} can have an important effect on aggregation. The dynamic exchange of Zn^{II} binding to Aβ11-28 did not only involve soluble Aβ11-28 because aggregated Zn^{II}-Aβ11-28 was also able to take part in the exchange. The observation that the addition of a small fraction of preaggregated $Zn^{II}_{0.5}$-Aβ11-28 to soluble apo-Aβ11-28 ("seeding experiment") forms apo-type aggregates and not Zn^{II}-type aggregates is in line with nucleation due to Zn^{II} exchange (see above).

These new findings about the very dynamic Zn^{II} exchange between different forms of Aβ11-28 might also apply to other systems with metal ion and amyloidogenic peptide interactions and have the following important impacts:

i. Transient Labile Metal Pools. Fast transient Zn^{II} binding might be very relevant for certain biological systems, in particular for the Aβ peptide and Zn^{II} in Alzheimer's disease. In certain synapses, Zn^{II} is ejected in the synaptic cleft and taken up on the second time scale[44,45] and plays the role of a neuromodulator. This Zn^{II} has been shown to be involved in the formation of Aβ deposits, and the distribution of histological stainable Zn^{II} resembles the area most prone to amyloid deposit in Alzheimer's disease.[56] Moreover, in vitro Zn^{II} is able to induce Aβ aggregation in milliseconds.[41] A similar transient increase of the metal-ion concentration in certain synaptic clefts has been proposed for copper.[57−59] Another example is the release of Zn^{II} from pancreatic islet β cells into the blood, which includes locally high Zn^{II} concentrations next to the release before dilution out in the blood.[15,16]

ii. Trace Metal Ions. It has been observed, for different metal−amyloidogenic interactions, that trace amounts (large substoichiometric) of metal ions can have a strong impact on aggregation.[60−63] This has classically been assigned to the induction of a stable metal−peptide nucleus with a further elongation phase consisting of apo-peptide addition to the nucleus. The dynamic exchange found here sheds more light on the mechanism: substoichimetric amounts of metal ions will not be bound to a portion of the peptide in a stable 1:1 complex but can be exchanged and thus bound transiently to the entire pool of peptides. Hence, metal ions induce nucleation of a much higher peptide concentration compared to its concentration,and this in a relatively short time.

iii. Binding Constant. For several biological relevant systems of metal−peptide interactions (Aβ, prion, α-synuclein, amylin, etc.), the binding affinity for metal ions is much weaker than that for classical metalloproteins (see, e.g., refs 12, 23, and 64−67), and hence sometimes the biological relevance of metal binding to these peptides has been questioned. However, in light of the present findings, a strong affinity is not required because a substoichiometric amount of transiently bound metal ions is sufficient for having a high impact on the aggregation behavior.

iv. Metal-Ion Source. The dynamic exchange of Zn^{II} binding to Aβ11-28 did not only involve the soluble Aβ11-28 because aggregated Zn^{II}-Aβ11-28 was also able to take part in the exchange. This means that metal−peptide aggregates can provide metal ions for transient binding to soluble apo peptide. This might be particularly relevant for Aβ, where amyloid

dx.doi.org/10.1021/ic202247m | Inorg. Chem. 2012, 51, 701−708

plaques contain a high amount of metal ions available for metal binding by external chelators.[46,68] Moreover, metal ions could also originate from other biomolecules containing labile-bound metal ions, like metallothioneins.[69]

In conclusion, modulators of amyloid formation can interact differently, i.e., covalently, by coordination, or by weak interactions. For the latter two, transient binding is possible. Binding of metal ions has been reported for quite a lot of amyloidogenic proteins/peptides, and in several cases, they seem to be biologically relevant. So far, not that much attention has been paid to dynamic exchange reactions, in particular related to aggregation species. The studies of our model system revealed that dynamic metal exchange reactions between soluble and aggregated peptides are an important mechanism that can strongly impact the aggregation behavior.

4. MATERIALS AND METHODS

Aβ11-28 Sample Preparation. The peptide Aβ11-28 (sequence Glu-Val-His-His-Gln-Lys-Leu-Val-Phe-Phe-Ala-Glu-Asp-Val-Gly-Ser-Asn-Lys) was purchased from GenScript Corp. (Piscataway, NJ). The stock solutions of Aβ11-28 (~1.2 mM) have been prepared by dissolving the peptide in Milli-Q water (resistivity = 18 MΩ cm^{-1}) or in D_2O for an NMR stock solution, which resulted in a final pH of 2. The pH of the solution was then adjusted to pH 12 by adding NaOH (or NaOD for NMR) stock solutions, in order to monomerize the peptides. These stock solutions were stored at 253 K. The peptide concentrations were determined by using the molar extinction coefficient ε = 390 M^{-1} cm^{-1} of the two phenylalanines at 258 nm.[30] Because phenylalanine does not absorb at 275 nm, absorption at that wavelength was subtracted in order to remove contributions from the buffer or baseline drifts. A Zn^{II} stock solution was prepared with $Zn^{II}SO_4$ monohydrate (Strem Chemicals) in water or in D_2O for NMR experiment. Aggregation of peptides in the presence of Zn^{II} has been performed by dissolving peptides from a stock solution in a 100 mM 4-(2-hydroxyethyl)-1-piperazylethanesulfonic acid (HEPES) buffer at pH 7.4 and was controlled at the end of the experiment.

All of the experiments measuring either turbidimetry or fluorescence intensity have been realized at 298 K. The experiments were repeated at least five times in different preparations. There were variations in the kinetics, but the trends shown were always the same. Data shown are representative measurements.

In the XANES measurements, the first sample (t = 0 h) was withdrawn immediately after mixing, transferred to the sample holder, and frozen in liquid nitrogen. The second sample was incubated for 15 h at room temperature before transferring to and freezing in the sample holder.

EDTA. An EDTA solution at 100 mM is prepared from ethylenediaminetetraacetic acid disodium salt (Sigma-Aldrich).

Tetrapeptides. EVHH-NH_2, EVHG-NH_2, and EVRH-NH_2 peptides (N-terminal amine; C-terminal amide) were purchased from GenScript Corp. (Piscataway, NJ). The stock solutions were prepared by dissolving the peptides in D_2O. The peptide concentrations were determined by Cu^{II} titration (see ref 32).

4-(2-Pyridylazo)resorcinol (PAR) Measurement. PAR was purchased from Sigma-Aldrich. UV−vis measurements were done in a 1 mm quartz cuvette in the presence of a HEPES buffer at pH 7.4 (100 mM).[70]

UV−Vis Spectroscopy. UV−vis spectra were recorded on an Agilent 8453 UV−vis spectrometer. Measurements were performed at room temperature.

Turbidimetry. Turbidity measurements were done by measuring the absorbance at 350 nm with a FLUOstar Optima (BMG Labtech) in a quartz microplate (96-well, Hellma).

Fluorescence Spectroscopy. Fluorescence spectra were measured by using a FLUOstar Optima (BMG Labtech). ThT (Acros), Aβ11-28, and Zn^{II} were mixed in a 100 mM HEPES buffer at pH 7.4 and placed in 96-well microplate. The time course of ThT fluorescence was then measured (excitation, 440 nm; emission, 490 nm; bandwidth for emission and excitation, 10 nm). The final concentrations of Aβ11-28 and ThT were 300 and 10 μM, respectively.

TEM. Peptide samples (15 μL) incubated for 17 h were applied on EM grids, washed with 15 μL of Milli-Q water, and negatively stained with an aqueous solution (15 μL) of uranyl acetate (1% w/w). Samples were air-dried and examined with a JEOL 1011 transmission electron microscope operating at an accelerating voltage of 100 kV or on a HU12A transmission electron microscope (75 kV). Conditions: [Aβ11-28] = 300 μM; [Zn^{II2+}] = 0 or 150 μM; [EDTA] = 750 μM; [HEPES buffer] = 100 mM, pH 7.4; [ThT] = 10 μM. EDTA was added after 1 day of incubation and 10 min before grid deposition.

XAS. XANES measurements were carried out at the SOLEIL Synchrotron Facility (St. Aubin, France), which was operating with a ring current of 400 mA. Zn^{II} K-edge XAS spectra were collected on the MARS beamline.[71] The measurements were performed using a Si(220) water-cooled double-crystal monochromator and two large silicon mirrors for high-energy harmonics rejection. Energy calibration was achieved by measuring a copper foil and assigning the first inflection point of the absorption spectrum to 8979 eV. The spectra were measured in fluorescence mode by measuring the Zn^{II} K_α fluorescence with a silicon drift detector (SII Nanotechnology). The liquid samples were injected into special sample holders and cooled to 20−30 K using a helium-flow cryostat. XANES spectra were background-corrected by a linear regression through the preedge region and a polynomial through the postedge region and normalized to the edge jump.

NMR. NMR experiments were realized on a Avance 500 Bruker NMR spectrometer. Aβ11-28 samples were freshly prepared from a D_2O stock solution (see the Aβ11-28 Sample Preparation section). The pH value of Aβ11-28 (300 μM) and a deuterated tris(hydroxymethyl)-aminomethane (Tris) buffer (100 mM) was adjusted to 7.5. The residual water signal was suppressed by a presaturation procedure. Zn^{II} was directly added to the NMR tube, and measurement was performed as quickly as possible (less than 1 min 30 s) in order to minimize the aggregation process during spectrum acquisition. EVHH-NH_2, EVHG-NH_2, and EVRH-NH_2 samples were prepared by diluting stock solutions (see the Tetrapeptide section) to 300 μM in a deuterated Tris buffer (100 mM); the pH value was adjusted to 7.4.

■ ASSOCIATED CONTENT

Ⓢ Supporting Information

Time course of ThT fluorescence and ^1H NMR spectra. This material is available free of charge via the Internet at http://pubs.acs.org.

■ AUTHOR INFORMATION

Corresponding Author

*E-mail: peter.faller@lcc-toulouse.fr (P.F.), christelle.hureau@lcc-toulouse.fr (C.H.). Phone: (+33) 5 61 33 31 62 (P.F.), (+33) 5 61 33 31 62 (C.H.). Fax: (+33) 5 61 55 30 03 (P.F.), (+33) 5 61 55 30 03 (C.H.).

■ ACKNOWLEDGMENTS

Financial support from ANR Neurometals (Agence Nationale de la Recherche Neurometals; Grant NT09-488591) and from "Region Midi-Pyrénées" (Research Grant APRTCN09004783) is acknowledged. We acknowledge SOLEIL for a provision of synchrotron radiation on the MARS beamline (Proposal 20090686).

■ REFERENCES

(1) Haass, C.; Selkoe, D. J. *Nat. Rev. Mol. Cell Biol.* **2007**, *8*, 101−112.
(2) Chiti, F.; Dobson, C. M. *Annu. Rev. Biochem.* **2006**, *75*, 333−366.
(3) Fowler, D. M.; Koulov, A. V.; Balch, W. E.; Kelly, J. W. *Trends Biochem. Sci.* **2007**, *32* (5), 217−224.
(4) Hamley, I. W. *Angew. Chem., Int. Ed.* **2007**, *46* (43), 8128−8147.
(5) Gazit, E. *Chem. Soc. Rev.* **2007**, *36* (8), 1263−1269.

(6) Cherny, I.; Gazit, E. *Angew. Chem., Int. Ed.* **2008**, *47* (22), 4062–4069.
(7) Morris, K.; Serpell, L. *Chem. Soc. Rev.* **2010**, *39* (9), 3445–3453.
(8) Morris, A. M.; Watzky, M. A.; Agar, J. N.; Finke, R. G. *Biochemistry* **2008**, *47* (8), 2413–2427.
(9) Exley, C. *J. Alzheimer's Dis.* **2006**, *10* (2–3), 173–177.
(10) Barnham, K. J.; Cappai, R.; Beyreuther, K.; Masters, C. L.; Hill, A. F. *Trends Biochem. Sci.* **2006**, *31* (8), 465–472.
(11) Tougu, V.; Tiiman, A.; Palumaa, P. *Metallomics* **2011**, *3* (3), 250–261.
(12) Hong, L.; Simon, J. D. *Metallomics* **2011**, *3* (3), 262–266.
(13) Perez, L. R.; Franz, K. J. *Dalton Trans. 39* (9), 2177–2187.
(14) Calabrese, M. F.; Miranker, A. D. *Prion* **2009**, *3* (1), 1–4.
(15) Brender, J. R.; Salamekh, S.; Ramamoorthy, A. *Acc. Chem. Res.* **2011**.
(16) Detoma, A. S.; Salamekh, S.; Ramamoorthy, A.; Lim, M. H. *Chem. Soc. Rev.* **2011**.
(17) Hindo, S. S.; Mancino, A. M.; Braymer, J. J.; Liu, Y.; Vivekanandan, S.; Ramamoorthy, A.; Lim, M. H. *J. Am. Chem. Soc.* **2009**, *131* (46), 16663–16665.
(18) Hureau, C.; Sasaki, I.; Gras, E.; Faller, P. *ChemBioChem* **2010**, *11* (7), 950–953.
(19) Crouch, P. J.; Hung, L. W.; Adlard, P. A.; Cortes, M.; Lal, V.; Filiz, G.; Perez, K. A.; Nurjono, M.; Caragounis, A.; Du, T.; Laughton, K.; Volitakis, I.; Bush, A. I.; Li, Q. X.; Masters, C. L.; Cappai, R.; Cherny, R. A.; Donnelly, P. S.; White, A. R.; Barnham, K. J. *Proc. Natl. Acad. Sci. U.S.A.* **2009**, *106* (2), 381–386.
(20) Bush, A. I.; Tanzi, R. E. *Neurotherapeutics* **2008**, *5* (3), 421–432.
(21) Scott, L. E.; Orvig, C. *Chem. Rev.* **2009**, *109* (10), 4885–4910.
(22) Brown, D. R. *Dalton Trans.* **2009**, *21*, 4069–4076.
(23) Faller, P.; Hureau, C. *Dalton Trans.* **2009**, 1080–1094.
(24) Drago, D.; Bolognin, S.; Zatta, P. *Curr. Alzheimer Res.* **2008**, *5* (6), 500–507.
(25) Fritz, G.; Botelho, H. M.; Morozova-Roche, L. A.; Gomes, C. M. *FEBS J.* **2010**, *277* (22), 4578–4590.
(26) Duce, J. A.; Bush, A. I. *Prog. Neurobiol. 92* (1), 1–18.
(27) Gaggelli, E.; Kozlowski, H.; Valensin, D.; Valensin, G. *Chem. Rev.* **2006**, *106* (6), 1995–2044.
(28) Gazit, E. *Prion* **2007**, *1* (1), 32–35.
(29) Lynn, D. G.; Meredith, S. C. *J. Struct. Biol.* **2000**, *130* (2–3), 153–173.
(30) Eisenberg, D.; Nelson, R.; Sawaya, M. R.; Balbirnie, M.; Sambashivan, S.; Ivanova, M. I.; Madsen, A. O.; Riekel, C. *Acc. Chem. Res.* **2006**, *39* (9), 568–575.
(31) Yang, H.; Pritzker, M.; Fung, S. Y.; Sheng, Y.; Wang, W.; Chen, P. *Langmuir* **2006**, *22* (20), 8553–8562.
(32) Pagel, K.; Seri, T.; von Berlepsch, H.; Griebel, J.; Kirmse, R.; Bottcher, C.; Koksch, B. *ChemBioChem* **2008**, *9* (4), 531–536.
(33) Hoernke, M.; Koksch, B.; Brezesinski, G. *Biophys. Chem.* **2010**, *150* (1–3), 64–72.
(34) Schlosser, G.; Stefanescu, R.; Przybylski, M.; Murariu, M.; Hudecz, F.; Drochioiu, G. *Eur. J. Mass Spectrom. (Chichester, England)* **2007**, *13* (5), 331–337.
(35) Dong, J.; Canfield, J. M.; Mehta, A. K.; Shokes, J. E.; Tian, B.; Childers, W. S.; Simmons, J. A.; Mao, Z.; Scott, R. A.; Warncke, K.; Lynn, D. G. *Proc. Natl. Acad. Sci. U.S.A.* **2007**, *104* (33), 13313–13318.
(36) Dong, J.; Shokes, J. E.; Scott, R. A.; Lynn, D. G. *J. Am. Chem. Soc.* **2006**, *128* (11), 3540–3542.
(37) Scotter, A. J.; Guo, M.; Tomczak, M. M.; Daley, M. E.; Campbell, R. L.; Oko, R. J.; Bateman, D. A.; Chakrabartty, A.; Sykes, B. D.; Davies, P. L. *BMC Struct. Biol.* **2007**, *7*, 63.
(38) Alies, B.; Pradines, V.; Llorens-Alliot, I.; Sayen, S.; Guillon, E.; Hureau, C.; Faller, P. *J. Biol. Inorg. Chem.* **2011**, *16* (2), 333–340.
(39) Pradines, V.; Jurca Stoia, A.; Faller, P. *New J. Chem.* **2009**, *32*, 1189–1194.
(40) Naslund, J.; Schierhorn, A.; Hellman, U.; Lannfelt, L.; Roses, A. D.; Tjernberg, L. O.; Silberring, J.; Gandy, S. E.; Winblad, B.; Greengard, P.; et al. *Proc. Natl. Acad. Sci. U.S.A.* **1994**, *91* (18), 8378–8382.
(41) Noy, D.; Solomonov, I.; Sinkevich, O.; Arad, T.; Kjaer, K.; Sagi, I. *J. Am. Chem. Soc.* **2008**, *130* (4), 1376–1383.
(42) Pedersen, J. T.; Teilum, K.; Heegaard, N. H.; Ostergaard, J.; Adolph, H. W.; Hemmingsen, L. *Angew. Chem., Int. Ed.* **2011**, *50* (11), 2532–2535.
(43) Calabrese, M. F.; Eakin, C. M.; Wang, J. M.; Miranker, A. D. *Nat. Struct. Mol. Biol.* **2008**, *15* (9), 965–971.
(44) Qian, J.; Noebels, J. L. *J. Physiol.* **2005**, *566* (Part3), 747–758.
(45) Frederickson, C. J.; Koh, J. Y.; Bush, A. I. *Nat. Rev. Neurosci.* **2005**, *6* (6), 449–462.
(46) Talmard, C.; Bouzan, A.; Faller, P. *Biochemistry* **2007**, *46*, 13658–13666.
(47) Tsvetkov, P. O.; Kulikova, A. A.; Golovin, A. V.; Tkachev, Y. V.; Archakov, A. I.; Kozin, S. A.; Makarov, A. A. *Biophys. J.* **2011**, *99* (10), L84–L86.
(48) Tougu, V.; Karafin, A.; Zovo, K.; Chung, R. S.; Howells, C.; West, A. K.; Palumaa, P. *J. Neurochem.* **2009**.
(49) Zirah, S.; Kozin, S. A.; Mazur, A. K.; Blond, A.; Cheminant, M.; Ségalas-Milazzo, I.; Debey, P.; Rebuffat, S. *J. Biol. Chem.* **2006**, *281* (4), 2151–2161.
(50) Mekmouche, Y.; Coppel, Y.; Hochgrafe, K.; Guilloreau, L.; Talmard, C.; Mazarguil, H.; Faller, P. *ChemBioChem* **2005**, *6* (9), 1663–1671.
(51) Brender, J. R.; Hartman, K.; Nanga, R. P.; Popovych, N.; de la Salud Bea, R.; Vivekanandan, S.; Marsh, E. N.; Ramamoorthy, A. *J. Am. Chem. Soc.* **2010**, *132* (26), 8973–8983.
(52) Walkup, G. K.; Imperiali, B. *J. Am. Chem. Soc.* **1997**, *119*, 3443–3450.
(53) Giachini, L.; Veronesi, G.; Francia, F.; Venturoli, G.; Boscherini, F. *J. Synchrotron Radiat.* **2010**, *17* (Part 1), 41–52.
(54) Giachini, L.; Francia, F.; Veronesi, G.; Lee, D. W.; Daldal, F.; Huang, L. S.; Berry, E. A.; Cocco, T.; Papa, S.; Boscherini, F.; Venturoli, G. *Biophys. J.* **2007**, *93* (8), 2934–2951.
(55) Kozin, S. A.; Mezentsev, Y. V.; Kulikova, A. A.; Indeykina, M. I.; Golovin, A. V.; Ivanov, A. S.; Tsvetkov, P. O.; Makarov, A. A. *Mol. Biosyst.* **2011**, *7* (4), 1053–1055.
(56) Bush, A. I. *Neurobiol. Aging* **2002**, *23* (6), 1031–1038.
(57) Schlief, M. L.; Craig, A. M.; Gitlin, J. D. *J. Neurosci.* **2005**, *25*, 239–246.
(58) Hartter, D. E.; Barnea, A. *Synapse* **1988**, *2*, 412–415.
(59) Tamano, H.; Takeda, A. *Metallomics* **2011**, *3* (7), 656–661.
(60) Innocenti, M.; Salvietti, E.; Guidotti, M.; Casini, A.; Bellandi, S.; Foresti, M. L.; Gabbiani, C.; Pozzi, A.; Zatta, P.; Messori, L. *J. Alzheimer's Dis.* **2010**, *19* (4), 1323–1329.
(61) Huang, X.; Atwood, C. S.; Moir, R. D.; Hartshorn, M. A.; Tanzi, R. E.; Bush, A. I. *J. Biol. Inorg. Chem.* **2004**, *9* (8), 954–960.
(62) House, E.; Collingwood, J.; Khan, A.; Korchazkina, O.; Berthon, G.; Exley, C. *J. Alzheimer's Dis.* **2004**, *6* (3), 291–301.
(63) Sarell, C. J.; Wilkinson, S. R.; Viles, J. H. *J. Biol. Chem.* **2010**, *285* (53), 41533–41540.
(64) Rozga, M.; Bal, W. *Chem. Res. Toxicol.* **2011**, *23* (2), 298–308.
(65) Meloni, G.; Vasak, M. *Free Radical Biol. Med. 50* (11), 1471–1479.
(66) Kozlowski, H.; Luczkowski, M.; Remelli, M. *Dalton Trans. 39* (28), 6371–6385.
(67) Alies, B.; Badei, B.; Faller, P.; Hureau, C. Reevaluation of Copper(I) Affinity for Amyloid-β Peptides by Competition with Ferrozine–an Unusual Copper(I) Indicator. *Chem. Eur. J.* DOI: 10.1002/chem.201102746.
(68) Cherny, R. A.; Legg, J. T.; McLean, C. A.; Fairlie, D. P.; Huang, X.; Atwood, C. S.; Beyreuther, K.; Tanzi, R. E.; Masters, C. L.; Bush, A. I. *J. Biol. Chem.* **1999**, *274* (33), 23223–23228.
(69) Durand, J.; Meloni, G.; Talmard, C.; Vasak, M.; Faller, P. *Metallomics* **2010**, *2* (11), 741–744.
(70) Ciuculescu, E.-D.; Mekmouche, Y.; Faller, P. *Chem.—Eur. J.* **2005**, *11* (3), 903–909.
(71) Sitaud, B.; Solari, P.-L.; Schlutig, S.; Hermange, H. *Suppl. Proc.: Mater. Process.d Energy Mater.* **2011**, *1*, 61.

Main Findings

The aim of our work was to get a better knowledge about Aβ – metal ions interactions, which are a wide and wild field of research. We decided to mainly focus on two aspects: Cu coordination to altered Aβ sequence and role of metal ions on aggregation by the means of models peptides. Our main findings are stated below in their two respective parts.

Coordination

We have determined:

- the coordination of Cu(II)- and Cu(I)-Aβ species and their pH dependence;
- the importance of the N-terminal amine function in Cu(II) coordination and the dramatic effect of its absence on coordination and affinity;
- the major impacts of non-coordinating residues on the Cu(II) coordination, *i.e.* the importance of second-sphere effects on the first Cu(II) coordination sphere;
- The high dependence of Cu(II) coordination on slight Aβ sequence modifications.

Aggregation

We have demonstrated that:

- aggregation is peptides and metal ions dependent; these two parameters are linked to a specific coordination;
- Zn binding to Aβ11-28 accelerates aggregation via the formation of dimeric species where the Zn ion bridges two peptides;
- a pH increase changes Zn coordination and thus contributes to slowdown the aggregation process and that the total charge of $Zn(A\beta 11\text{-}28)_2$ controls the complex precipitation;
- Zn binding is dynamic and Zn is in exchange within the peptide pool;
- Transiently Zn binding can induce non-reversible modifications even if Zn is later taken off. These modifications dramatically accelerate the peptide aggregation.

V- Perspectives

As explained in the introduction part, AD, metal ions and Aβ seems to be closely interconnected. Our approach was original, in the sense that we perform fundamental research on a highly applied issue (AD). From my point of view, understanding fundamental aspects are prior and required to develop efficient therapeutic tools. In this line, we explored "basic" aspects of metal ions and peptides:

- their coordination to a series of Aβ peptides;
- their role in aggregation of amyloidogenic peptides originating from Aβ .

Having acquired this fundamental knowledge, we can try to find concepts which can be applied to AD and further (as in material science or in catalysis). The following paragraphs are (d/r)eflections from findings to others interesting aspects uncovered in this manuscript.

V.1- Coordination

In the present work, we focused on Cu coordination to Aβ. Using complementary techniques and relevant mutants, we demonstrated the intricacy of simple Cu-peptides complexes. Metals exchange's in the peptide pool is fast and metal coordination on the same peptide might exhibit different types of coordination in equilibrium. This clearly contrasts with proteins, which have mostly one well defined metal-binding site and do not exchange their metal ions. Two parameters control this versatile behaviour: affinity and folding. The higher the affinity is, the slower the exchange rate is. In addition, a better folding induces a lowering of the number of conformations and thus makes less coordination modes available, classically resulting in one strong binding site. So, unstructured peptides like Aβ, with moderate Cu affinity, have the "ideal" profile to be tricky to study! Indeed, even a modification of non-coordinating residue, may lead to a strong shift of the equilibrium (see for instance the D1N mutation) or give rise to different coordination modes (see for instance, the Aβ3-16 truncation). In addition, a modification in the first Cu(II) coordination shell (for instance, acetylation of the N-terminal amine function) can go unnoticed if only one spectroscopic technique is used and/or if the pH range of study is too narrow.

Zn is also of paramount importance in AD. Therefore, studies of Zn coordination to Aβ and its modified forms are worthy. Our preliminary results (not shown) indicate that Zn coordination also differs with the peptide sequence and the pH (around physiological values).

In our Cu(II) coordination studies, we have demonstrated that the majority of sequence alterations in Aβ linked to an early onset of AD or to higher toxic species, also induce strong modifications in Cu(II) coordination. This supports an active role of Cu-Aβ interactions in AD. Nevertheless, in order to know if such modified forms are more toxic *via* a higher ROS production, it would be worthy to quantify and compare Aβ and modified Aβ on Cu induced ROS production.

Contrasting with the plethora of existing methods to quantify ROS (Ascorbate consumption, Coumarin fluorescence, Resorufin production, Nitro blue tetrazolium reduction, DMPO spin trap…), general features of the Cu-peptide ROS production are still poorly understood. Yet, coordination seems to be related to ROS production since ROS are produced by redox cycle of the metal ions and thus depend on its coordination. With regards to parameters such as affinity, metal ions (oxidized and reduced forms) coordination spheres, it seems possible to predict ROS production. However, our preliminary experiments prove that it is not so simple! Anyway, a better understanding of such process will be, in fundamental aspects interesting and challenging, and could also be used to applied research, as for instance the search of drugs. Imagine a ROS hyper-active compound (peptidic complexes or not); it may be a good anti-cancer drug candidate, even better if specific.

V.2- Aggregation

In this part of our studies, we tried to understand “basic” features of peptide aggregation modulated by metal ions. Interactions of metals ions - peptides are diverse and depend of both metal ions and peptide sequence. Metal ions can induce dimerisation and thus promote aggregation (see for instance Cu and Aβ14-23) or in contrast preclude aggregation process by binding in a fashion which destabilizes the β-sheet formation (Cu and Aβ11-28). pH and total charge are also key parameters. On one hand, pH may influence the metal coordination and thus modulate aggregation. On the other hand, the total charge of metal-ions peptide complexe, which is also pH dependent, controls the precipitation.

Another interesting finding was the importance of the metal ions dynamic exchange. Indeed, temporary metal binding may induce change (*i.e.* induce dimerisation) which influences the aggregation even if the metal ion is removed rapidly. Since exchange is fast, a trace of the metal ions is sufficient to interact with the whole pool of peptide and, in our case, to force it to aggregate. Moreover, Zn from solid aggregates is rapidly and fully available to peptide from the bulk solution meaning that amyloid plaques may act as pool of ions metal. In

the synaptic cleft, Zn is released and then taken up; this could be enough to induce modification on surrounding Aβ. We have demonstrated this effect on Aβ11-28, but it would be highly interesting to observe it on the native Aβ1-40 peptide. Affinity is usually use as a proof of biological interaction, but if the affinity is too high, exchange via free Zn becomes slow. The affinity of Aβ for metal ions is rather moderate and lower for Zn compared to Cu. This dynamic exchange allowed by the moderate affinity may be a key point of Aβ aggregation in AD, in line with the fact that Zn is more competent to enhance full-length Aβ aggregation than Cu.

Measurements of aggregation of deleterious modified Aβ peptides will be also worthy to reveal if their toxicity originates from aggregation tendency mediated or not by metal ions rather than by metal ions induced ROS production.

Aggregation is generally follows by Thioflavin T (ThT) fluorescence. Such measurements are adequate to monitor fibrils formation. However, fibrils seem not to be the harmful species. Scientific consensus supports that aggregation intermediate species (called oligomers) are the most toxic species. To the best of our knowledge, those species has been poorly characterised (mainly by TEM). Indeed, with fluorophore such ThT, we are blind to species of interest. Did you ever try to find something you don't know in the dark? Sounds pretty hard, doesn't it? FRET technique could be a major help in oligomer's detection. Indeed, mixtures of fibrils specific and unspecific fluorophores enabled to FRET together may light on "oligomers". This could be great step forward in the AD field that could let us dream of an early diagnostic of AD.

ANNEXE

Structure

Optically active compound :

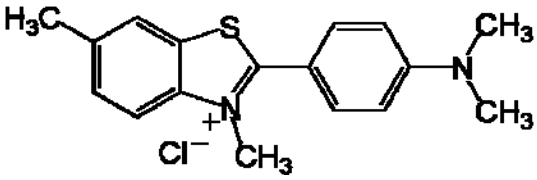

Thioflavin T

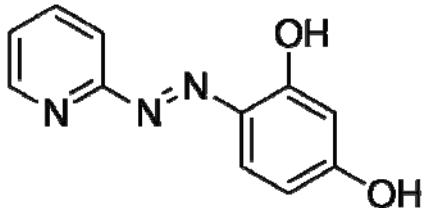

PAR
4-(2-**p**yridyl**a**zo)**r**esorcinol

Buffer :

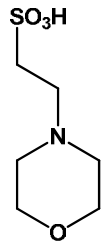

MES
pKa = 6.1

2-(N-Morpholino) ethanesulfonic acid

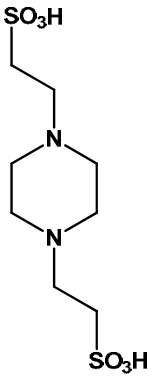

PIPES
pKa = 6.8

1,4-Piperazinediethane sulfonic acid

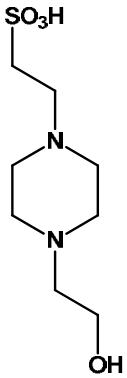

HEPES
pKa = 7.5

4-(2-Hydroxyethyl)piperazine-1-ethanesulfonic acid

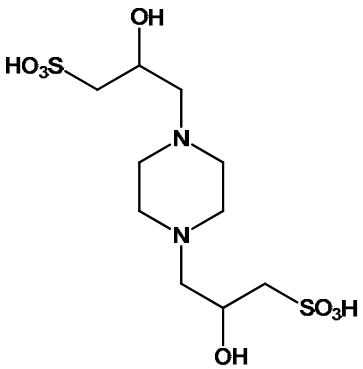

POPSO
pKa = 7.8

Piperazine-1,4-bis(2-hydroxy propanesulfonic acid)

Peptide Aβ1-40

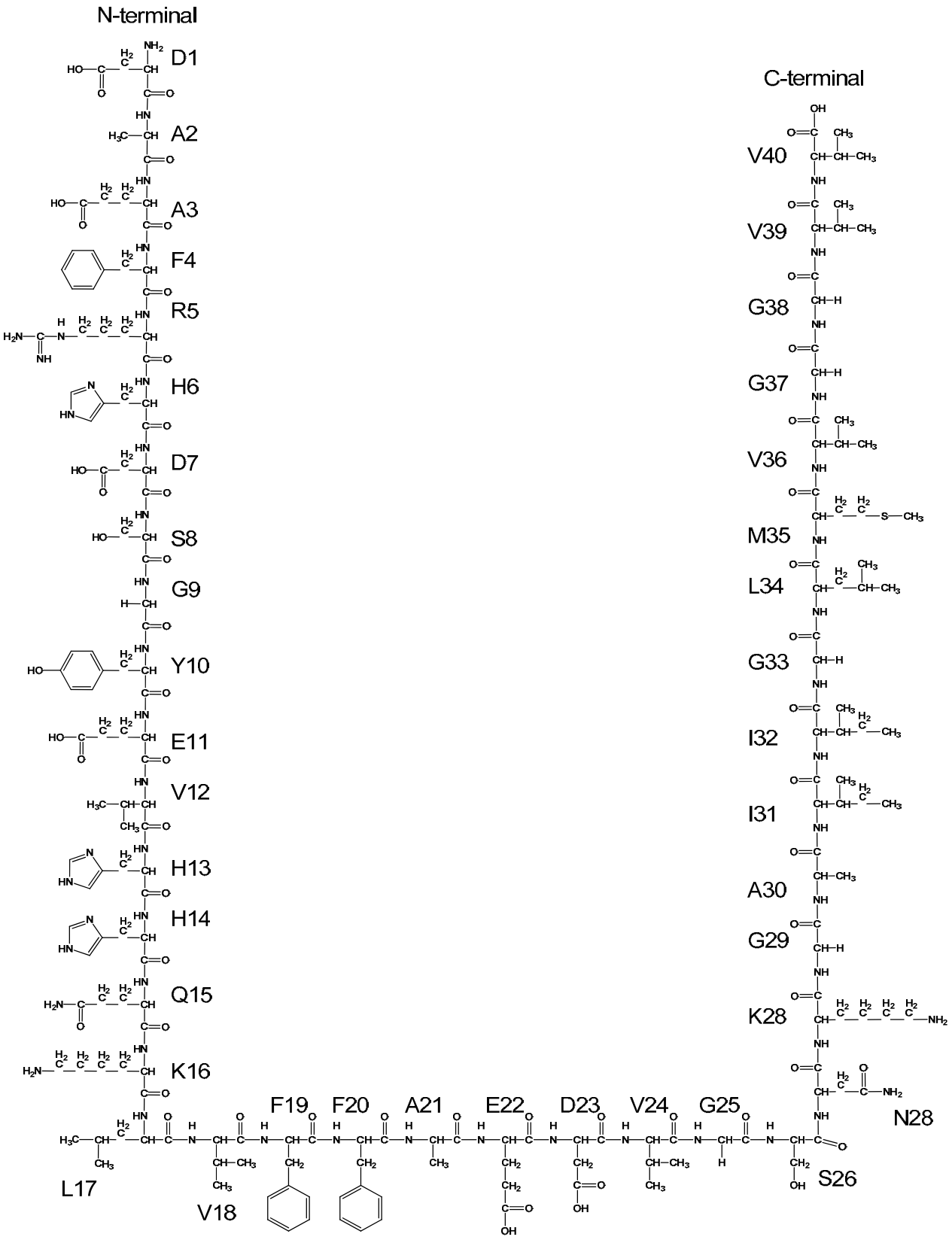

Methods and techniques to study the bioinorganic chemistry of metal–peptide complexes linked to neurodegenerative diseases

Peter Faller, Christelle Hureau, Pierre Dorlet, Petra Hellwig,
Yannick Coppel, Fabrice Collin, Bruno Alies

Coordination Chemistry Reviews
2012, *256*, 2381-2396

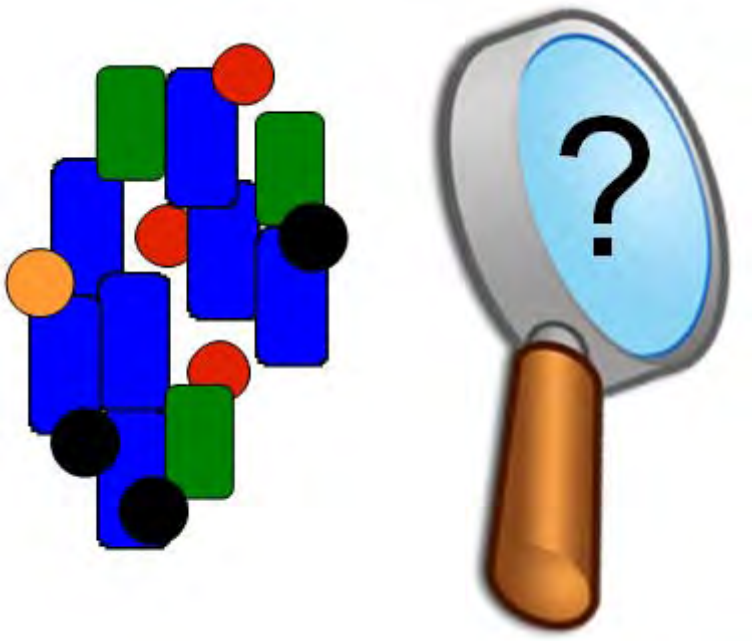

The following article is a review which focuses on peptide sample preparation and common methods used to study peptide – metal ions interactions. I critically reviewed this article and contributed to Figures 1, 3, 8 and Table 2.

Coordination Chemistry Reviews 256 (2012) 2381–2396

Contents lists available at SciVerse ScienceDirect

Coordination Chemistry Reviews

journal homepage: www.elsevier.com/locate/ccr

Review

Methods and techniques to study the bioinorganic chemistry of metal–peptide complexes linked to neurodegenerative diseases

Peter Faller[a,b,*], Christelle Hureau[a,b], Pierre Dorlet[c,d], Petra Hellwig[e], Yannick Coppel[a,b], Fabrice Collin[f], Bruno Alies[a,b]

[a] CNRS, LCC (Laboratoire de Chimie de Coordination), 205 route de Narbonne, 31077 Toulouse, France
[b] Université de Toulouse, UPS, INPT, LCC, 31077 Toulouse, France
[c] CNRS, Laboratoire Stress Oxydant et Détoxication, 91191 Gif-sur-Yvette, France
[d] CEA, iBiTec-S, SB^2 SM, 91191 Gif-sur-Yvette, France
[e] Institut de Chimie, UMR 7177, Laboratoire de spectroscopie vibrationnelle et électrochimie des biomolécules, Université de Strasbourg, 1, rue Blaise Pascal, 67008 Strasbourg, France
[f] PHARMA-DEV, IRD UMR 152, Université Paul Sabatier, 35 chemin des Maraîchers, 31400 Toulouse, France

Contents

ARTICLE INFO

Article history:
Received 22 December 2011
Received in revised form 20 February 2012
Accepted 12 March 2012
Available online 23 March 2012

ABSTRACT

This article provides a review about the most common techniques used to study the interaction of metal ions with amyloidogenic peptides. It is addressed to researchers, who want to know what kind of techniques exists, the information which can be obtained, their advantages, limits and the demands

* Corresponding author at: CNRS, LCC (Laboratoire de Chimie de Coordination), 205 route de Narbonne, 31077 Toulouse, France. Fax: +33 61 55 30 03.
E-mail address: peter.faller@lcc-toulouse.fr (P. Faller).

0010-8545/$ – see front matter © 2012 Elsevier B.V. All rights reserved.
doi:10.1016/j.ccr.2012.03.015

Keywords:
Amyloid
Peptide
Metal ions
Copper
Zinc
Aggregation
Bioinorganic chemistry
Neurodegeneration
Methods
Physico-chemical techniques

concerning sample preparation etc. It is not addressed to specialists of these techniques as the physical principles of the techniques are nor given. First, a general overview is given about sample preparation and treatment, with focus on the metal ions Zn(II), Cu(I/II) and Fe(II/III) and the peptides amyloid-β (but also α-synuclein, prion etc.). Then the methods NMR, EPR, electrochemistry, optical spectroscopy, isothermal titration calorimetry, FTIR, X-ray absorption and mass spectrometry are treated.

© 2012 Elsevier B.V. All rights reserved.

1. Introduction

The aim of this article is to give an overview on the most current different techniques, which are applied for studying the interaction of metal ions (mostly, Cu(I/II), Zn(II) and Fe(II/III) ions) with amyloidogenic peptides, in particular amyloid-β (Aβ), but also prion, α-synuclein etc. The aim is to concentrate on the following questions:

- what kind of information can be obtained by each techniques, and what are the advantages and limits;
- what are the metal and amyloid peptide specific particularities which should be taken into account for proper sample handling and application to the technique.

There is no space to give explanation about the physical principle of the methods. Here we refer to more specialized articles. Moreover, we focus on the most common methods which are particular dedicated to the metal ions. We did not treat other very important techniques, in which the impact of metal ions is less important and can be found in other non metal specific reviews on amyloids (e.g. transmission electron microscopy) or in which we feel not competent enough.

2. Samples preparation

2.1. Metal ions and buffers

Zn(II), Cu(II) and Fe(III): Zn(II), Cu(II) and Fe(III) are the oxidation states stable on air and in aqueous solution. Classical salts used are chlorides, sulfates etc. Best is to take salts which are not hygroscopic and contain a defined amount of water, in order to have a precise quantity by weighting.

The solubility of Zn(II), Cu(II) and Fe(III) around physiological pH is not very high due to the formation of hydroxides and subsequent precipitation (solubility constants Ksp for $Fe(OH)_3 = 6 \times 10^{-38}$; $Zn(OH)_2 = 4.5 \times 10^{-17}$; $Cu(OH)_2 = 1.6 \times 10^{-19}$). Thus the solubility is pH dependent and salts are more soluble at low pH. Concentrated stock solution (mM range) of Zn(II), Cu(II) and Fe(III) should be prepared at low pH (for 1 M stock solutions the volume change due to the dissolution of the salt has to be taken into account, in contrast for 100 mM stock solution this can be neglected). The pH is directly low when salts are dissolved in pure water, due to the Lewis acidity of the metal ions.

Reduced forms Cu(I) and Fe(II): Generally, salts of Cu(I) are less soluble as salts of Cu(II), whereas Fe(II) salts are better soluble than Fe(III). Dissolved Cu(I) and Fe(II) salts are normally not stable on air. Thus stock solutions have to be prepared under inert gas (Ar or N_2) by using degassed aqueous solution (freeze/thaw cycles are appropriate). In the case of Fe(II), $Fe(NH_4)_2(SO_4)_2$ is the only redox stable Fe(II) salt. For Cu(I) the complexes $[Cu(I)(MeCN)_4]^+$ (counterion BF_4^-, ClO_4^- or PF_6^-) can be used.

For Cu(I) an additional problem is that Cu(I) disproportionates in Cu(0) and Cu(II) in aqueous solutions. Thus Cu(I) has to be stabilized, often done by adding a portion of MeCN (classically at least 10%). The presence of MeCN has to be taken into account for further analyses of the sample. Another possibility is to add thiols, like DTT, EtSH or glutathione. Glutathione has the advantage to be the biological reducing agent likely natively involved in Cu(I) coordination/stabilization, and other thiols can be argued to be models for glutathione. In contrast, due to their strong affinity, the thiols have a strong impact on the apparent metal-binding affinity of peptides/proteins. Moreover, Cu(I)-thiolates are not stable under aerobic conditions as Cu(I) oxidizes to Cu(II), which in turn is rereduced to Cu(I) by thiol oxidation to disulfides. This has the advantage that thiols play two roles, impeding disproportionation and oxidation. The drawback is that thiols are consumed and disulfides formed, but under inert atmosphere this is very limited.

Apart from adding thiols which are good ligands and reducing agents, other reducing agents which have lower affinity for metal ions can be added, like dithionite, $NaBH_4$, ascorbate etc. Dithionite works well to keep Fe(II) and Cu(I) reduced and seems not to interfere strongly with metal-binding to Aβ. Dithionite reacts directly with molecular oxygen and hence eats up dissolved oxygen. However, the reaction produces radicals which can attack the sample. Moreover HSO_3^- and HSO_4^- is formed which can acidify the solution. Thus a strong buffer has to be used and the pH checked at the end of the experiment. Ascorbate does not react directly with molecular oxygen and is a weaker reductant.

2.2. Buffers

Important factors about the choice of buffers are [1]:

Interaction of buffer with metal ions: All buffers can have interaction as the base of the buffers has an unpaired electron (often amine) which is able to coordinate metal ions. So there are two possibilities, either take a buffer with little interaction, so that it can be neglected (this is mostly the case for the Good's buffer, Hepes, Pipes, Popso etc.) or take a buffer for which the interaction with the metal ions is well defined, so that it can be corrected (for instance Cu(II) with glycine or Hepes). In the former case, a problem can be that in such buffers metal ions are not stable (at higher concentration) due to the formation of hydroxides. This is less the case for buffers with a stronger interaction (see Table 1).

Precipitation: This is the case for phosphate, $Cu_3(PO_4)_2$, $Zn_3(PO_4)_2$ and $Fe_3(PO_4)_2$ complexes are very insoluble (solubility product constants $Ksp = 1.4 \times 10^{-37}$, 9.0×10^{-33}, and 1.0×10^{-36}, respectively) and hence precipitation could occur, which may invalidate the results. This is pH dependent due to the pH dependent concentration of PO_4^{3-}.

Temperature dependence of pH: The pK_a of the buffers are temperature dependent, i.e. by changing the temperature the pH of the buffer will change. This dependence differs between the different buffers, e.g. it is high for Tris and small for Hepes. This is important

Table 1
Buffers and metal ions.

Buffer	Properties with M^{n+}	Pros	Cons
Phosphate	Forms unsoluble complexes with several metal ions	No ^1H signal in NMR, covers large pH range	$Cu_3(PO_4)_2$ and $Zn_3(PO_4)_2$ complexes are very insoluble
Tris	Binds well metal ions, keep them in solution	Keeps M^{n+} in solution cheap d_{11}-Tris available for NMR	Complexes of M^{n+} not well defined. Strong temperature dependence of pK_a
Hepes	Low interaction	Cu–Hepes (1:1) complex well defined [5]. Zn(II) Hepes interaction can often be neglected. Small temperature dependence of pK_a	Hepes can form radicals (reducing agent)
CAPSO, POPSO, PIPES, MES	Low interaction	Weak M^{n+} binding	Interaction not well defined

for temperature dependent studies and also in techniques using samples in the frozen state (classically in EPR, XAS, etc.).

A specific case is phosphate buffer, because the change in pH upon freezing depends on the presence of sodium (like in PBS). With sodium, phosphate shows an important decrease in pH (up to 3 units) upon freezing. In contrast, the Hepes buffer shows only a moderate change (−0.4 units) and the Tris buffer can increase up to 2 pH units [2].

Side reaction: Buffers can make side reactions. A non negligible one is that Hepes is a weak reducing agent and can form radicals. Hepes was reported to reduce Cu(II), if a Cu(I) stabilizing ligand is present [3]. However, no redox reactions of Cu(II)–Aβ occurred in Hepes over 2 h [4].

Techniques specific issues: In ^1H NMR the choice of buffer is limited as for buffers with ^1H the deuterated form has to be used, at least in the more common case where a large excess of buffer compared to the peptide is used. The only cheap deuterated buffer is Tris, others are very expensive. Alternative is phosphate, which contains no ^1H.

2.3. Peptides

A very detailed review on methods concerning Aβ handling without metal ions has been published recently [6].

Peptide sources: Chemical synthesis or recombinant peptides are commercially available. Chemically synthesized peptides contain counter ions, classically trifluoroacetate (TFA) from HPLC purification. The number of counter ions can be calculated from the charge of the peptide at pH ∼2 and has to be taken into account when the peptide is quantified by weight. For Aβ, the charge at pH 2 is about +7 (N-terminal amine, 3 His, 2 Lys, 1 Arg, but the carboxylates are mostly protonated) and hence ∼7 counterions are present. Moreover, the purification at pH around 2 (e.g. due to presence of 0.1% TFA) and subsequent freeze drying results in peptide, in which the His and carboxylates are mostly protonated. If such a peptide is dissolved in water at higher concentrations (mM), the resulting pH will be quite low. Even when the peptide is dissolved in high concentration of buffer, the pH can drop significantly, so pH should be checked for such preparations.

For longer very amyloidogenic peptides like Aβ1–42, but also Aβ1–40 there are differences between batches in term of their state of aggregation. Differences in batches and between chemically synthesized and recombinant Aβ are often encountered (Fig. 1). Often recombinant Aβ is less preaggregated and hence aggregates slower and often in a more reproducible way.

Monomerization: Several treatments have been described to break preaggregates (or seeds), either using solvents (mostly hexafluoro-isopropanol (HFIP) shown to be better than DMSO [7]), formic acid, chaotropic agents (urea, guanidinium hydrochloride) or incubation at high pH [8] (Fig. 1). However, it seems difficult to obtain completely monomerized Aβ following these methods. To minimize the presence of preaggregates, the sample should be passed over a size-exclusion column and the monomer peak collected [9]. Also ultracentrifugation has been reported to remove preaggregated Aβ [10].

Aggregation: Apart from the presence of preaggregates/seeds, there are a lot of other factors having an effect on aggregation, including pH, temperature, presence of trace amounts of metal ions, agitation and contact with air (e.g. by shaking, bubbles etc.), contact with other surfaces (like wells, tubes, etc.) [9].

Model peptides: Model peptides are used because they are cheaper and/or easier to handle. Normally they are shorter peptides and the idea is that they contain the relevant part of the sequence. As the name says model peptides are models, so they will never be identical to the native peptide. So experiments have to be done showing that the model peptide keeps the property of interest. For instance, it has been well established that Aβ1–16 contains the principle metal binding site, at least for Cu(II), Cu(I), Zn(II) and Fe(II) [11–13]. Similarly, this is the case of α-synuclein, the main metal ion binding sites are in the N-terminal portion (amino acids 1–60) or for prion, it is the octarepeat region (amino acids 60–91), where Cu(II) and Zn(II) are predominantly bound [14]. In several cases, the ligands are present in the model peptide, but they do not form amyloid fibrils, so they are good models for studying the interaction of the metal ions in the monomeric complex, but not for studying the aggregation.

Dosage of apo-peptides by weight: If the peptide is dry and the number and type of counterions known (see above), this can be very accurate, but often this is not the case and it is better to confirm by another method.

Dosage of apo-peptides UV-absorption: Most of the peptides can be dosed by the absorption of the aromatic amino acids via UV spectroscopy. Often the extinction is known or can be calculated upon the amino acid composition. In case of an unstructured peptide this

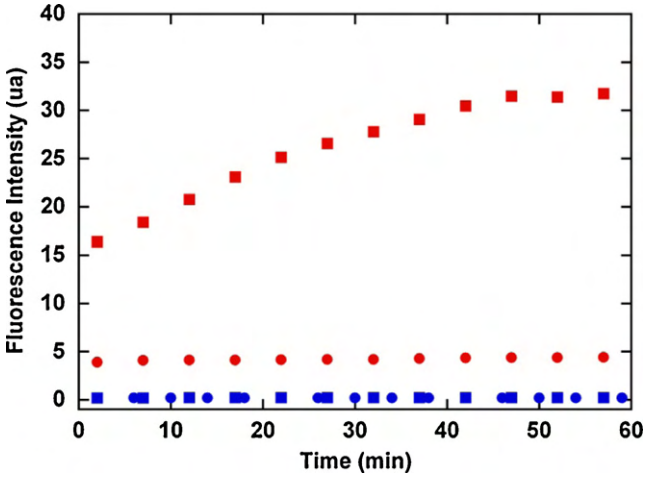

Fig. 1. Aggregation followed by thioflavin T fluorescence of the peptide Aβ11–28 at pH 7.4. Two different batches (square and circles) are shown in red (before incubation at pH 12) and blue (after incubation at pH 12) (*Conditions:* 100 mM Hepes, pH 7.4, 300 μM Aβ11–28).

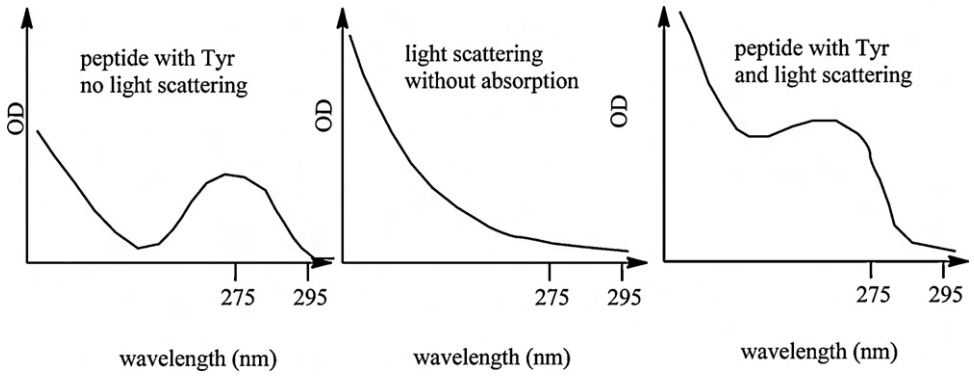

Fig. 2. Schematic absorption spectra of a peptide containing one or more Tyr (but no Trp) like Aβ. The maximum of the Tyr absorption in such a peptide is around 275 nm and no absorption occurs above 295 nm. If there is little light scattering, it can be corrected for by subtracting the value at 295 nm (i.e. use the $\varepsilon_{275}-\varepsilon_{295} = 1410\,M^{-1}\,cm^{-1}$).

is quite accurate, but the absorption of an amino acid can change depending on the structure, in particular in a more hydrophobic environment. However, changes in intensity do rarely exceed 10%, keeping such an approach still relatively correct. A problem which can occur with these often amyloidogenic peptides, is the presence of aggregates and therefore light scattering. Thus the sample is not homogeneous anymore, which has to be taken into account. As such the peptide concentration is overestimated. If light scattering is not too intense, the light scattering can be corrected for by substracting the OD where the peptide does not absorb, but light scattering is similar. For instance Aβ has one Tyr and hence absorbs at 275 nm with an extinction coefficient of $1400\,M^{-1}\,cm^{-1}$ (see Fig. 2).

The interference of light scattering is particularly important for very amyloidogenic peptides like Aβ42. Aβ42 is much more soluble at higher pH (p*I* around 5–6), and hence dosage can be made at high pH. However, the tyrosine becomes deprotonated at around pH 10, and the tyrosinate has a different absorption, the band is moved to the red with a maximum at 293 nm and an extinction coefficient of $2400\,M^{-1}\,cm^{-1}$ (Fig. 3). If one want to dose the peptide at high pH, one has to make sure that tyrosine is completely deprotonated, so a pH clearly above 11, i.e. ~13 should be used and use $\varepsilon_{293}-\varepsilon_{360} = 2400\,M^{-1}$ cm.Classical protein tests like BCA, Bradford Lowry etc. can be also used. They are normally quite accurate if the calibration is made with the same peptide. In contrast if the calibration is made with another protein like BSA the concentration is less accurate. (For instance in our hands BCA test was off by up to a factor of two when using BSA for amyloid-β dosage.) Another

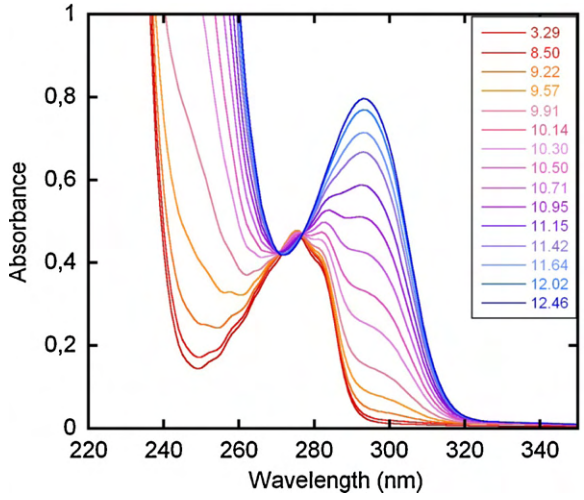

Fig. 3. pH titration of Tyr in Aβ1–16 (300 μM). From tyrosine band (red) to tyrosinate band (blue).

issue is the aggregation state, which is likely to change the reactivity toward the different chemicals used in these tests.There are other methods, like amino acid analysis which is very accurate.

Dosage in the presence of metal ions: UV–Vis is not always valuable as metals bound to the peptide can absorb as well in the region of the aromatic amino acids. This is the case of Cu(II)-bound to Aβ and prion. In contrast Zn(II) binding does not induce absorption and hence dosage based on the absorption of aromatic amino acids is possible given that the metal does not induce aggregation and hence light scattering. A possibility to circumvent this, is to lower the pH to 2, as metal are released and do not contribute to absorption anymore.

3. Isothermal titration calorimetry (ITC)

Isothermal titration calorimetry (ITC) is a method giving access to the thermodynamic parameters of an interaction, like metal ion binding to a protein. It measures directly the enthalpy of a reaction and delivers a model-based binding stoichiometry as well as the dissociation constant. Thus three parameters (stoichiometry, affinity constant and enthalpy) are needed for the fit per metal binding site. Thus, and this is in particular important in the case of more than one binding site, it is important to have independent measurements of stoichiometry and/or affinity constant.

A first prerequisite for such measurements is that the system reaches equilibrium after each titration step, that means that the binding event, e.g. of a metal ion to a peptide is completed before the next titration step is started. Moreover, it is important to note that the heat measured, and as a consequence the thermodynamic parameters (K and ΔH), stem from all the reactions occurring, including dilution, precipitation, oxidation, degradation etc. during the titration of a metal ion to a macromolecule. For instance in the case of Cu(II)-binding to Aβ, the reaction is not limited to Cu(II) and Aβ as the starting reagents and the complex Cu(II)–Aβ is the final product (Fig. 4). At the beginning Aβ and Cu(II) are hydrated and Cu(II) does often bind to the buffer. Upon binding of Cu(II) to Aβ, the water and buffer bound to Cu(II) are (at least partially) released. Moreover, if Cu(II) replaces protons from the Aβ, they will be bound by the buffer. Thus, the measured heat can stem from (1) breaking bonds from Cu(II) to water and/or buffer interactions, (2) bond formation of Cu(II) with peptide, (3) concurrent changes in hydration upon Cu(II)–peptide complex formation, (4) deprotonation of peptide, (5) proton(s) binding to buffer, if proton(s) are displaced upon Cu(II)-binding to Aβ, and (6) structural changes of the peptide due to Cu(II)-binding. Thus, the thermodynamic parameters obtained are apparent. Or in other words, the thermodynamic parameters obtained include all the processes associated. For an excellent recent review going more into details on ITC and metal ions see Wilcox and colleagues [15]. There is the

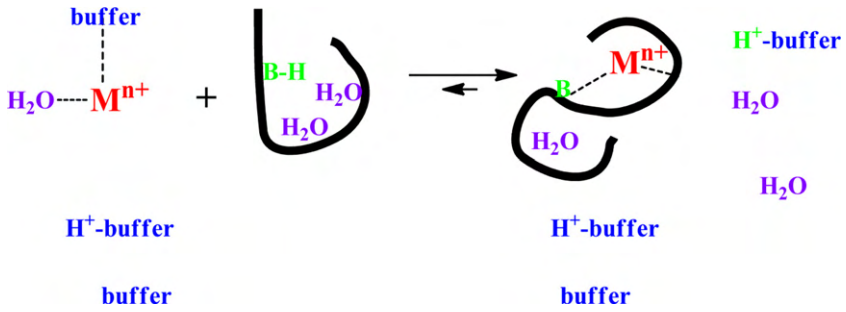

Fig. 4. Possible processes associated to addition of metal ion (M^{n+}) to a peptide (black line) in an aqueous buffered solution. The buffer is present in protonated and deprotonated form. B and B–H depicts a deprotonated and protonated base, respectively, which is able to bind the metal ion.

possibility to have access to the thermodynamic parameters of the pure metal-binding to peptide, if all the associated processes are well known. For instance, if metal-binding to a peptide includes a displacement of protons, the measured ΔH includes the ΔH of the proton-binding to the buffer and the metal-binding. Thus, if the number of displaced protons and the ΔH of buffer protonation are known, the ΔH of the metal-binding to peptide can be corrected. Similarly, one could correct for metal–buffer interaction, however in practice this is often not very easy as the interaction of metal ions with buffers are often ill defined and/or conflicting.

The number of protons displaced upon metal-binding can be determined by using exactly the same condition but different buffers with known ΔH. Then, the difference in ΔH is only due to proton-binding to the buffer (see [16] for a recent example on metal-peptides).

Determination of an apparent dissociation constant is limited in ITC to a range between 1 mM and 10 nM. This is deduced from a parameter $c = n \cdot [M]/Kd$ (with n = binding stoichiometry, [M] = concentration of macromolecule, e.g. peptide; Kd = dissociation constant), which should be ideally between 5 and 500. This means if the Kd is too low, very little concentration should be used to fulfill the requirement for c, but then the concentration are too low to yield measurable enthalpy.

A way around that is the use of a competing ligand, i.e. metal-ion bound to competing ligand is titrated to a peptide. As such the measured Kd drops to the difference between the Kd of peptide and Kd of competing ligand, and hence the parameter c can be moved to the ideal region. In this case, in order to deduce the thermodynamic parameter of the metal ion interaction with the peptide in the absence of the competing ligand, one has to correct them. For that the ΔH, stoichiometry and Kd of the metal ions competing ligand interaction has to be known.

ITC has been mainly applied for Zn(II) and Cu(II)-binding to Aβ [17–19], prion [20–22] and some other amyloid like iAPP [23], mainly by titrating Cu(II) or Zn(II) in a buffer to the peptide. Thus the thermodynamic parameters obtained are apparent, without correction for buffer interaction etc. Simon and colleagues [24,25] used the glycine as a competing ligand to study Cu(II)-binding to Aβ, and were able to obtain a Kd after correcting for the glycine. In this case the buffer does not interfere with the determination of the Kd, and the deduced Kd corresponds to the Kd of Cu(II)-binding to Aβ at the measured pH in the absence of buffer. However, a prerequisite for this analysis is that no ternary complexes are formed. Very recently, Trapaidze et al. [16] extended the methodology of Simon and colleagues to two model peptides. By measuring at different glycine concentrations and with different buffers they were able to correct not only the Kd, but also ΔH (corrected for ΔH of glycine and displaced protons). Thus they obtained formally Kd and ΔH of Cu-binding to peptide in pure water at pH 7.4. Moreover, with this method the formation of a ternary complex peptide–Cu–glycine was evidenced and the Kd of glycine binding to Cu–peptide could be determined.

4. Electron paramagnetic resonance (EPR)

Electron paramagnetic resonance (EPR) is a powerful technique to study species with unpaired electrons. In bioinorganic chemistry, it is widely applied to transition metals and radicals encountered during catalytic reactions. In the case of the interaction of metals with amyloidogenic peptides, the relevant ions and redox states are essentially Cu(I), Cu(II), Zn(II), Fe(II) and Fe(III). Among those, Cu(I) and Zn(II) are diamagnetic and cannot be studied by this technique. Fe(II) can be either diamagnetic (low spin state S = 0) or paramagnetic (high-spin state S = 2). The paramagnetic state can in principle be studied by EPR, however the zero-field splitting (ZFS) effect for such integer spin prevent the use of conventional EPR (signals can in principles be obtained with parallel detection mode EPR or high-field EPR if the Zeeman effect can become competitive with the ZFS). Fe(III) and Cu(II) have half-integer spin-states and are routinely studied by conventional EPR and more advanced techniques. In the case of amyloid peptides, most EPR studies have focused on the coordination of the Cu(II) ion and this will be the case of interest in the remaining of this section.

The electronic configuration of the Cu(II) ion is $3d^9$ and therefore it has an unpaired electron, leading to an electron spin S = 1/2. When there are no strong geometrical constraints, which is the case in peptide systems for Cu(II), the metal center is in a distorted octahedral geometry due to the Jahn–Teller effect (elongated octahedron or usually pentacoordinated square base pyramid) and the unpaired electron is in the orbital $d_{x^2-y^2}$. This orbital extends in the equatorial plane and therefore the equatorial ligands are those most easily studied, the potential axial ligands being only very weakly coupled to the metal ion. In frozen solution, the observed spectrum is anisotropic with axial symmetry. The Zeeman effect gives rise to two resonances at $g_{//}$ and $g_{\perp}$ and ligand field theory indicates that $g_{//}$ and $g_{\perp}$ are both greater than g_e (g-value of the free electron) and $g_{//}$ is greater than $g_{\perp}$. Moreover, the nuclear spin for the two natural isotopes ^{63}Cu(II) and ^{65}Cu(II) (natural proportion 69% and 31%, respectively) is I = 3/2 leading to hyperfine coupling. This interaction is highly anisotropic with the stronger component along $g_{//}$, leading to a splitting in four distinct lines while the perpendicular component of the Cu(II) hyperfine coupling is generally not resolved on the EPR spectra in frozen solution. Furthermore interactions so-called "super-hyperfine" between the electron spin of the Cu(II) ion and the nuclear spins of the atoms of the ligands (mainly nitrogens and protons) are also present. They are usually partially resolved on the EPR spectrum, in particular for the $g_{\perp}$ region. The analysis of the hyperfine coupling is very important for chemists and biologists because it provides information on the distribution of spin density (electronic structure) and structure

(distances obtained through dipolar interactions) of the complex studied.

In the case of Cu(II), the values of $g_{//}$ and $A_{//}$ are very sensitive to the nature of the equatorial ligands. In the 1970s, Peisach and Blumberg have published empirical diagrams that give insights into the coordination sphere of the cupric ion [26]. Practically in our case, a change from O ligands to N ligands induce a decrease of the $g_{//}$ value while the $A_{//}$ increases. The specific values indicate the relative number of O and N ligands. This has been used to propose the binding modes of Cu(II) with proteins and peptides such as prion protein [27–29], Aβ [30–33,18,34], α-synuclein [35–37]. To get insights into the structure of the binding site in greater details, the careful study of the interaction with the atoms from the ligands has to be made, that is the super-hyperfine interactions. The best way to disentangle and analyze the superhyperfine interactions is to use isotopic labeling in conjunction with the EPR experiments. Indeed, different isotopes of the same element often have different nuclear spins (^{1}H I = 1/2 vs. ^{2}H I = 1; ^{14}N I = 1 vs. ^{15}N I = 1/2, ^{12}C I = 0 vs. ^{13}C I = 1/2) resulting in different patterns in the spectra. Specific isotopic labeling can therefore directly attributes the nucleus responsible for the interaction observed. The superhyperfine interaction can be resolved, at least partially, on the EPR spectrum. It is sometimes convenient to record the spectrum at lower frequency (S-band or L-band vs. X-band) to improve the resolution. Studies on prion peptides and Aβ-peptides are example of this [27,38,39]. When the (super)hyperfine couplings are not directly measurable on the EPR spectrum or their analysis is too complex, other EPR methods such as ENDOR (electron nuclear double resonance), ESEEM (electron spin echo envelope modulation) or HYSCORE (hyperfine sublevels correlation) are used to obtain direct measurements of hyperfine couplings. These two techniques are complementary, the ENDOR being particularly suitable for strong couplings (typically the nitrogen atoms directly coordinated to Cu(II)) and high frequency resonances while the ESEEM is most successful for weak couplings and low frequency ranges (coupled deuterons, non-coordinated nitrogen from His, amides, etc.). In addition to measure the hyperfine couplings unresolved in EPR spectra, these techniques also allow the determination of the nature of the coupled nuclei (H, N, etc.) because they are sensitive to the Larmor frequency, characteristic of a given nucleus. This information is not available in the EPR spectra. An important and recurring case in the Cu(II) complexes is the ligation of a His residue by the imidazole ring of the side chain which is a very good ligand for Cu(II). The coupling of the nitrogen atom linked directly to the Cu(II) is too strong to be detected by ESEEM, but can be measured by ENDOR. In contrast, the remote nitrogen atom of the imidazole ring has a very weak coupling, which gives a characteristic signal in ESEEM and HYSCORE. At X-band for which the exact cancellation condition ($|a_{iso}| = 2\nu_n$) is achieved for this nucleus, the spectrum obtained for 3-pulse ESEEM consists of three narrow peaks in the range 0–2 MHz corresponding to the quadrupole transitions and a broad peak around 4 MHz (Fig. 5). When multiple equivalent nitrogen nuclei are coupled to Cu(II) (coordination of several His residues in equatorial position) so-called combination peaks are observed at frequencies sum of the three basic frequencies, therefore it is possible to distinguish between single or simultaneous His binding in equatorial position. Although theoretically possible, it is more difficult to determine without ambiguities the exact number of residues coordinated simultaneously when several of them are involved. Detection of coordinating His is quite systematic in Cu(II)–amyloid peptide studies [27,38,40–43]. Another nitrogen atom routinely detected in ESEEM and HYSCORE in Cu-peptide complexes is the one from a peptide bond when the carbonyl is a ligand to the Cu(II) ion. This coupling has been described for example in the case of the octarepeat domain of the prion protein [27] and observed also in the case of the Aβ peptide. Labeling

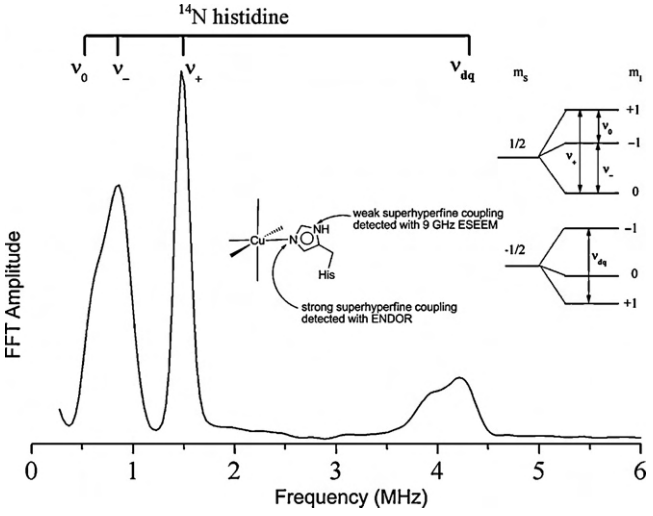

Fig. 5. Frequency domain of a 3-pulse ESEEM experiment for an equatorial His bound Cu(II) complex. The nitrogen nucleus sublevels are presented on the right within the exact cancellation condition. In the center, the scheme of the Cu–His complex indicates which N nucleus is detected by which technique at X-band.

with ^{13}C can also be used to detect couplings with carbon atoms. This has been applied for example to study the involvement of the Asp1 residue of the Aβ peptide in the coordination of Cu(II) [38,42,44].

All these measurements are best applied when there is no mixture of species in the sample. However, in the case of amyloid peptides it is usual that there is a strong pH dependence in the complexes that can be formed with Cu(II). This leads to a mixture of species at physiological pH which plagues the analysis of the data since working on difference spectra can prove not to be obvious in particular with pulse techniques. One way to work around this is to study the predominance diagram for the complexes as a function of pH and poise the sample at those pHs for which the complex of interest are predominant, when possible. With respect to sample preparation, a typical volume to work with at X-band is 100–150 μL of sample, the concentration of which can range from tens of μM up to 1 mM. For the usual case of aqueous samples, 10% of glycerol should be added to the samples to enhance the glass property of the solvent and improve the detection/resolution of the EPR spectrum. Isotopic labeled samples should be prepared in parallel to unlabeled samples under the same conditions to allow direct comparisons.

With the development of new pulse-sequences, the availability of different frequencies, the technical improvements on spectrometers and the rather straightforward isotopic labeling possible on peptides synthesized chemically, EPR remains a method of choice and a powerful technique to study the coordination of paramagnetic transition metals to amyloid peptides.

5. Nuclear magnetic resonance (NMR)

NMR spectroscopy provides detailed information at the atomic level about the structure and dynamics of metal–peptide interactions in solution.

The peptide concentration is usually in the range from 0.05 to 2 mM for ^{1}H NMR spectroscopy. The higher concentration limit is imposed by peptide aggregation that will broaden the NMR signals.

Higher aggregates cannot not be measured by solution NMR, due too slow tumbling and poor solubility. However, during the last years solid state NMR provided important insights into the structure of aggregated amyloidogenic peptides, on their interaction with metal ions [45] and on the interaction of metal–peptide

with lipids [46]. In contrast to solution NMR, solid state NMR needs site specific labeling and is more demanding in sample preparation and measurements. We do not considered solid state NMR as a routine technique and we refer to a recent review for more details [47]. Peptide–peptide aggregation phenomena or oligomer formation, possibly mediated by metal binding, can be studied by translational diffusion coefficient measurement (DOSY NMR). The lower concentration depends on the NMR spectrometer used. The signal to noise ratio and the spectral dispersion both increase with the magnetic field strength. Today NMR spectrometers can operate at ^{1}H NMR frequency up to 1 GHz but 500 MHz may be sufficient in many cases. Spectrometer equipped with cryogenic probe can allow for reduction of the protein concentration by approximately a factor of four compare to conventional probes. NMR experiments on ^{13}C and/or ^{15}N nuclei notably with the usual 2-D or even 3-D correlation experiments (HSQC, HNCO, HNCA, etc.) can also be interesting or necessary. For low concentrated samples, the peptides need to be enriched with the magnetically active isotopes. For highly soluble peptides (short model peptides for example), ^{13}C NMR can be perform at natural abundance. The solvent is usually 90% H_2O/10% D_2O or 100% D_2O. In the later case, labile protons (NH, OH, etc.) are deuterated and are no more observable. Sometimes DMSO-d_6 has been chosen but its use is subject of extensive debate about its biological relevance. Buffer choice for NMR is limited to deuterated buffers or buffers that contain no ^{1}H (see above). The pH should be adjusted with deuterated salts for 100% D_2O (DCl and NaOD).

Peptide–metal ion complexes are dynamic systems and therefore the time scale at which the components of the protein–metal ion complex exchange between free and bound forms is an important factor that needs to be addressed [48]. The time scale of the experimental method (chemical shift, relaxation time or diffusion coefficient monitoring for example) has to be comparable to the time scale of the dynamic process studied (usually on the micro to milli-second time scale). For a system in slow exchange on the chemical shift time scale (in general terms this would be a peptide–metal ion system with high binding affinity and low dissociation constant, Kd = μM or lower), resolved signals might be expected for the free and bound states. For a system in fast exchange, the observed NMR responses are the mole fraction weighted average of the NMR parameters of the free and bound states. At the intermediate chemical exchange rate regime with respect to the chemical shift time scale, resonance broadenings are observed. Investigation of the dynamic processes can be done by recording NMR experiment at different temperatures. Temperature changes will influence the dynamics, i.e. increase exchange rates (k_{on} and k_{off}), but will also have an influence on the equilibrium populations (Kd) [49].

5.1. Diamagnetic Zn(II) and Cu(I)

The binding of diamagnetic metal ions is usually investigated through the chemical shift variations upon metal binding (chemical shift mapping). The titration experiments where the concentration of the metal ion is increased gradually can be used to estimate the binding constant and the rate constant of the complex formation [50]. (Caution has to be taken about a stable pH, as metal ion solutions are often acid (see above) and hence addition of concentrated metal ion solution may drop the pH and could lead to chemical shift variations).

The chemical shift variations are mostly due to conformational changes caused by the metal binding and from the electric field induced by the charge of the metal ion. Amino acid residues whose resonances are perturbed upon metal ion addition are involved in the metal coordination and/or are close to the metal binding site (Fig. 6). This is particularly true for flexible unstructured peptides.

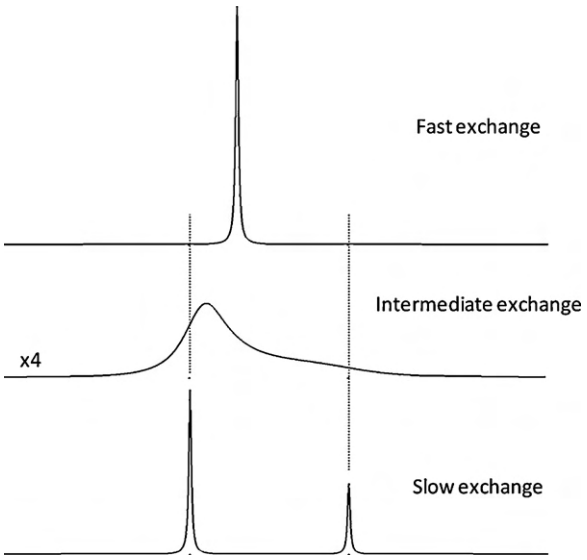

Fig. 6. Simulation of a ^{1}H NMR spectrum of one proton in a ligand close to a Zn-binding site, where 30% of the ligand is bound to diamagnetic Zn(II) and 70% is not bound to Zn. Under slow exchange (bottom) the resonance of Zn-bound and Zn-free ligand is detected with the ratio of 0.3–0.7. Under fast exchange (top) only one resonance is observed, in between the shifts of free and Zn-bound ligand (bottom) and with a shift reflecting the % of Zn(II) load. Intermediate exchange broadens the resonances.

For peptide with ordered organization, small chemical shift variations far from the metal binding site can result from an overall change of the peptide structure following metal binding. In this case of well defined peptide framework, the three dimensional structure can be studied by ^{1}H nuclear Overhauser enhancements (NOEs) that give information about inter-proton distances.

However, most of the times exchange between the metal-free and metal-bound peptide is fast compared to the chemical shift differences between the two form ($k_{ex} \gg \Delta\nu$) so that only single exchange-averaged signals are observed making precise geometric structure less straightforward (Fig. 6). In these cases the coordination environment of the metal can be monitored by following changes to the NMR spectrum upon metal ion concentration. Furthermore, a peptide may have a number of different coexisting binding sites in fast exchange among themselves, making it difficult to localize and identify the different binding sites.

Sometimes non-selective broadening of basically all the observed signals, including those of the non-coordinating amino acid residues, occurred even at a small proportion of metal ion. This phenomenon refers to the presence of several complexes, which are in relatively intermediate mutual exchange (with respect to the chemical shift time scale) with each other and with the free ion. Global line broadening can also indicate the formation of peptide–peptide aggregates mediated by metal binding. If these aggregates are insoluble, an overall signal intensity decrease will be observed. For oxygen sensitive Cu(I), line broadenings can also result from the presence of contaminating paramagnetic Cu(II). Local resonance broadening can also be due to protonation–deprotonation equilibrium influenced by the metal binding.

^{63}Cu(II) (or ^{65}Cu(II)) and ^{67}Zn(II) nuclei are too insensitive to be studied by NMR at the peptide concentration. Substitutions with more sensitive nuclei like ^{113}Cd (or ^{111}Cd) and ^{109}Ag can be done in order to obtain information at the metal level about the type and number of the bound ligands.

The metal ion binding can also change locally the flexibility of the peptide. NMR spectroscopy can provide information about the backbone dynamics on the pico to milli-second time scale.

Dynamics information on the peptide backbone are retrieved from ^{15}N R_1 and R_2 relaxation rates and ^{1}H–^{15}N NOEs and side chain dynamics can be studied using relaxation rates of ^{13}C, ^{1}H or ^{2}H (^{15}N, ^{13}C and ^{2}H sample labeling necessary) [51].

5.2. Paramagnetic Cu(II) and Fe(II)

The binding of paramagnetic metal ions to peptide has a pronounced effect on the NMR spectra of the peptide. The reason for this pronounced effect is the presence of unpaired electrons that strongly interact with surrounding peptide nuclei. The unpaired electrons can affect the chemical shift and/or the relaxation rates of the nearby nuclei. The paramagnetic contribution to the nucleus chemical shift are the Fermi contact shift (through bond effect: the paramagnetic equivalent of scalar couplings) and pseudocontact shift (through space effect due to dipolar interactions with unpaired electrons). Contact shifts are restricted to nuclei in the immediate vicinity of the paramagnetic center. Pseudocontact shifts (PCS) depend on the anisotropy of the magnetic susceptibility tensor. PCSs depend also on the distance (with an inverse-three power) and on the spherical position of the nuclei with respect to the metal ion. PCS are usually very small for Cu(II) (less than ±10 ppm), contact shift can be more important (up to ±50 ppm). For Fe(II), the situation is more complex as the electron spin quantum number can take different values depending of the complex nature (from S = 0 (diamagnetic, see above) to S = 2). For Fe(II) with S = 2, paramagnetic contribution to the chemical shift are usually more important than for Cu(II). Fast exchange between bound and free paramagnetic metal ion lead to much reduced weighted average paramagnetic contribution to the chemical shift that depend on the metal bound fraction [52]. Intermediate exchange cases are more complicated to study [52].

Paramagnetic relaxation enhancements (PRE) depend on the electron spin quantum number, the electron spin relaxation time, the gyromagnetic ratio of the nuclear spin and the distance (with an inverse-sixth power) from the paramagnetic center. PRE decays much more rapidly with increasing distance from the paramagnetic metal than the PCS. However paramagnetic metal ions are generally at the center of a "blind" sphere in which the NMR signals are too broad to be detected, due to the paramagnetic enhancement of the transverse relaxation rates R_2. However, the R_2 rates are difficult to interpret quantitatively [53]. Measuring spin-lattice relaxation R_1 is usually preferable for obtaining structural information on the metal ion peptide complex [54]. The line broadening effects are less severe for low gyromagnetic nuclei as ^{13}C or ^{15}N (compared to ^{1}H) making NMR detection of these nuclei advantageous for the identification of residue in the proximity of the paramagnetic center [55]. Again exchange rate between bound and free paramagnetic metal ion is an important factor to evaluate (Fig. 7). Slow exchange rate level off the paramagnetic contribution to the nuclear relaxation rates necessitating adding higher amount of the metal ion [49]. For fast exchange rate, paramagnetic nuclear relaxation rates depend on the metal-bound fraction and on the distances between the paramagnetic center and the corresponding peptide residues (Fig. 7). Selective line broadening effects can be use to locate the metal binding sites even in the presence on several lowly populated states in fast exchange [53]. Localization of metal ion binding sites can also be done by using the paramagnetic longitudinal relaxation rates R_{1p} that are exclusively dependent on: (i) metal bound complex molar fraction; (ii) the kinetic off rate (k_{off}) and (iii) metal bound proton relaxation rates T_{1b} [49]. T_{1b} strongly depends on the Cu(II) proton distances and it is shortening with the metal–nucleus distance. Cu(II) has a long electron spin relaxation time but a small electron spin quantum number (S = 1/2) [56]. Cu(II) can induce important line broadening effects that supply direct qualitative evidence for residues involved in binding. Cu(II) is also known to affect

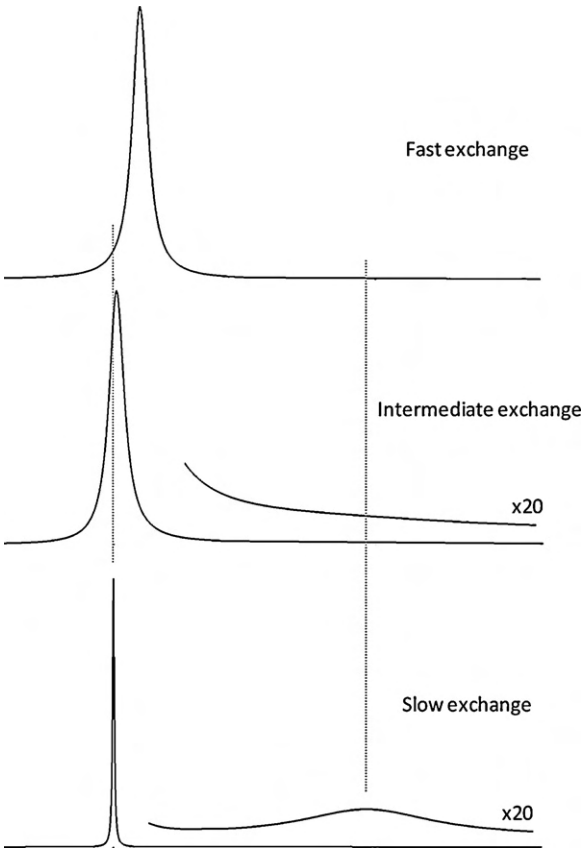

Fig. 7. Simulation of a ^{1}H NMR spectrum of one proton in a ligand close to the Cu(II)). 10% of the ligand is bound to paramagnetic Cu(II) and 90% is not bound to Cu(II). Under slow exchange (bottom) the resonance of Cu(II)-bound state is broadened beyond detection due to PRE; the Cu(II)-free ligand is detected. Under fast exchange (top) only one resonance is observed, in between the shifts of free and Zn-bound ligand (bottom) and with a shift reflecting the % of Cu(II) load (i.e. with 10% Cu(II) load the shift is small). The average resonance also broadens due to the proportional averaging of the R_2 relaxation rates of the free and bound states. Intermediate exchange broadens also the signal with a very small shift.

the paramagnetic longitudinal relaxation rates R_{1p} through dipolar interaction and so R_{1p} can provide metal-nucleus distance information [52]. Fe(II) has much shorter spin electron spin relaxation times than Cu(II) resulting in nearly no effect on R_1 relaxation rates [56]. However Fe(II) can induce more important broadening effects than Cu(II) due to more important Curie relaxation contributions [56].

6. Electrochemistry, cyclic voltammetry

Among the various electrochemical techniques available, cyclic voltammetry is commonly used and will be detailed below. It is based on the detection of the variation of current intensity (i) as a function of an applied potential (E) that depends linearly with time (t).

6.1. Experimental setup

Cyclic voltammetry (CV) measurements are performed in three-electrodes electrochemical cells combining the working electrode (WE), the reference electrode (ref) and the counter electrode (CE). The controlled electrical variable is the potential of the working electrode. It is measured between the WE and the reference electrode and the current circulates between the WE and the CE. In aqueous medium, well-suited reference electrodes are SCE (Saturated Calomel Electrode) or Ag/AgCl electrodes. The CE has to

conduct the current and has not to interfere with the bulk solution. In general, it is a Pt wire. The electron transfer of interest takes place at the WE, the nature of which is crucial for an ideal detection of the electrochemical process. Carbon-based electrodes (glassy carbon GC, graphite), Pt and Au electrodes are the most common working electrodes. In the particular case of small peptides complexes, good experimental CV traces have been reported with GC electrodes (for recent examples, see Refs. [28,57–59]). Careful polishing of the WE before each CV record is strictly required in case of peptidic complexes and an insufficiently well-polished electrode may preclude the correct measurement of the CV traces. Electrodes are fixed in the electrochemical cell and the solution is not stirred to ensure diffusion controlled current transport required for the CV analysis. The measured current is the sum of two contributions: the faradic current (i_f) corresponding to the electron transfer of interest and the capacitive current depending on the electrochemical setup. Thus ideally, the current recorded in absence of the studied species (capacitive current (i_c)) should be subtracted from the total current to obtain only the faradic contribution.

Supporting electrolyte is required in order to ensure a correct conductivity. In case of aqueous solution, the supporting electrolyte can be either the buffer itself or NaCl. Considering its electroactive domain, i.e. the potential range inside which the measurement can be performed, phosphate buffer may be the best choice. Indeed, other commonly used buffer such as Hepes or Tris contain amine functions that can be easily oxidized and thus restricts the electroactive domain. However, due to precipitation issues with phosphate (see above) it should be used with cautious and the metal ions should not be added to the buffer without prior addition of the peptidic ligand.

In case of peptidic species, residues like Cys, Met, Tyr and Trp may also contribute to restrict the electroactive domain due to their oxidation at "low" potential (i.e. at pH 7.4 approx. 0.9 vs. NHE for Cys [60], 1.4 vs. NHE for Met [60], 1.0 V vs. NHE for Tyr, pH 7.4 [61] and 1.1 V vs. NHE for Trp pH 7.4 [62]). In most cases, the electrochemical cell containing the solution of interest should be flushed with argon to prevent from any O_2 contribution.

6.2. Useful insights obtained from CV

6.2.1. Electrochemical reaction

Case of fast electron transfer: This case is encountered when the electron transfer is sufficiently fast compared to the electrochemical diffusion rate, given by $\sqrt{FvD/RT}$, where v is the scan rate and D the diffusion coefficient of the studied species, F being the Faraday constant, R the perfect gas constant and T the temperature). A direct consequence is that, depending on the scan rate, a system can be considered slow or fast. Experimentally a system will considered fast if (in the scan rate range used, classically between 50 mV s^{-1} and 500 mV s^{-1}) the faradic current i_f varies linearly with $\sqrt{v}$, the maximum intensity in the anodic scan i_p^a equals the maximum intensity in the reverse (cathodic) scan i_p^c, and the difference between the potential at the two maximum of intensity $\Delta E_p = |E_p^c - E_p^a| = 2.22RT/F = 57$ mV at 25 °C for a mono-electronic transfer.

In that present case, thermodynamic equilibrium is reached at any potential point in the scan and concentrations of oxidant and reductant at the electrode are given by the Nernst Law. Two parameters can then be deduced from the CV trace: (1) the $E_{1/2} = (1/2)(E_p^c + E_p^a)$, which is the apparent standard potential in the recording conditions (pH, T, ionic strength etc.) used for the measurement and (2) the diffusion coefficient D obtained according to $i_p = 0.446FSC^0\sqrt{D}\sqrt{Fv/RT}$, where C^0 is the concentration of the studied species in the bulk. From this last equation it clearly appears that the intensity of the recorded current will decrease with the decrease in the diffusion coefficient of the molecule and thus with the increase in its size. This is the reason why proteins cannot be studied by classical voltammetry. Instead Protein Film Voltammetry investigations where the protein is attached to the electrode surface are performed (see Ref. [63] for an example and Ref. [64] for a review).

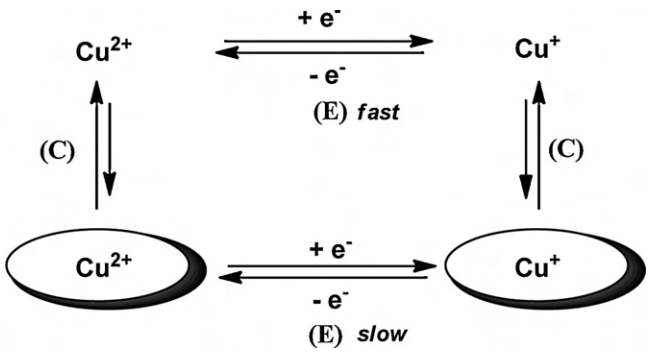

Scheme 1. Square scheme mechanism showing an ECEC mechanism between unbound Cu(II)/Cu(I) and peptide-bound Cu(II)/Cu(I) redox couples (oval). If the chemical reaction(s) is (are) equilibrated and if the electron transfer is slow when the Cu(I/II) is bound to the peptide then electron transfer via unbound Cu(I/II) may occur predominantly.

Case of slow electron transfer: In such conditions, the kinetics of the electron transfer are rate determining and the electrochemical equilibrium is not reached. As a direct consequence the oxidant and reductant concentrations are not given by the Nernst Law but by the Butler–Volmer law allowing access to the kinetics of the electron transfer described by two parameters (see Refs. [65,66] for more details).

6.2.2. Chemically coupled electrochemical reactions

More complicated CV traces can be observed when chemical reaction (C) interferes with the electrochemical reaction (E). If the rate of the chemical reaction is fast compared with the scan rate, insights into the chemical reaction can be obtained. In case of Cu(I)/Cu(II) redox couples, structural rearrangement is often observed between Cu(I) and Cu(II) redox states. This will give rise to an ECEC square-scheme mechanism that can be probed by varying the scan rate [67,68]. Another process (ECE) has also been recently proposed for Cu–Aβ species [57]. These mechanisms are very intricate and detailed analysis can be found in Refs. [57,67,68].

Two important cases of coupled chemical–electrochemical reactions is given below in case of Cu(I/II) peptidic species.

1. *Square scheme between unbound Cu(I/II) and coordinated Cu(I/II):* In case of low Cu(I/II) affinity for the peptide and in case of slow electron transfer inside the Cu(I/II)–peptide species, the electron transfer can occur via unbound Cu(I/II) for which the electron transfer is fast (Scheme 1). As a consequence, data should be recorded in excess of peptide to minimize contribution of unbound Cu(I/II) in the electron transfer process.
2. *O_2 reduction catalysis:* An interesting EC mechanism in case of Cu(I/II)–peptide species is O_2 (or H_2O_2) catalytic reduction [69,70] (Scheme 2) due to their proposed involvement in reactive oxygen species production [71]. If Cu(I/II)–peptide species catalyze O_2 reduction, then the catalytic reduction will be centered on the reduction peak of the Cu(II)-peptidic species and a more intense cathodic current should be observed, the intensity of which increases with increase in O_2 concentration and the shape of which depends on O_2 diffusion rate to the electrode.

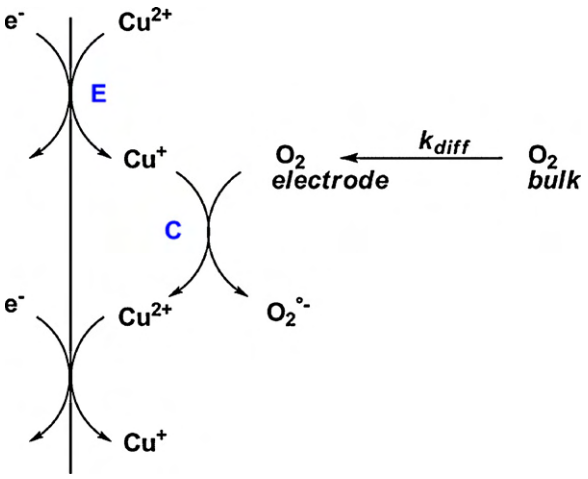

Scheme 2. Catalytic reduction of dioxygen (C) by Cu(I) species electrochemically generated at the electrode (E). Intensity and shape of the reduction wave depends on O_2 concentration at the electrode and of O_2 diffusion rate to the electrode.

7. Optical methods: (UV–Vis, circular dichroism and fluorescence)

7.1. Fluorescence

Intrinsic fluorescence: Intrinsic fluorescence can be well measured on tryptophan and tyrosin (phenylalanine is more difficult due to the lower intensity). For instance Aβ contains one tyrosine and no tryptophan, which makes the system relatively simple, as fluorescence originates from the single Tyr only. This fluorescence has been used to measure coordination of Cu(II), as Cu(II) like other paramagnetic ions (e.g. Fe(III)) quenches the fluorescence quite strongly. Based on this approach binding affinities have been measured [32,18,72]. Similar approach was performed on prion protein with tryptophan and tyrosine for α-synuclein [62,73]. Fluorescence changes on addition of diamagnetic metal ions (Cu(I), Zn(II), Al(III)) are not easy to detect due to the absence of the paramagnetic effect. Hence a conformational change is needed to affect fluorescence, which is often less pronounced. Thus Zn-binding to Aβ was reported to increase or decrease fluorescence. We never observed a robust fluorescence change of Zn(II) on Aβ1–16, under non aggregating conditions. As tyrosine fluorescence changes with aggregation [74] and Zn(II) induces aggregation, observed fluorescence changes might be due to aggregation and hence only indirectly to Zn-binding [4] (Table 2).

Covalent linked fluorophores: There are several fluorophore tagged peptides commercially available or kits to produce them, mostly with a classical fluorophore, like rhodamine, often covalently bound to the N-terminal amine or to a cysteine [75]. As the N-terminus is often involved in metal-binding (like in Aβ, α synuclein), a C-terminal tagged peptide might be more suitable. In any case, controls have to be performed in order to show that the linked fluorophore does not interfere (too much) with the properties of the peptide. This is in particular difficult in aggregation studies as small changes can have a considerable impact on the aggregation behavior [75].

Table 2
Fluorophores.

Name/wavelength	λ_{ex}	λ_{emi}
Intrinsic		
Tyrosine	270–280	300–320
Tryptophan	280–290	310–360
Extrinsic		
Thioflavin T	440–450	480–490
ANS	350–380	495–515
Bis-ANS	385–400	485–500
Nile Red	540–580	620–660
Covalent linked		
TRITC – tetramethyl-rhodamine-isothiocyanate	535–545	565–575
FITC – fluorescein isothiocynate	490–500	515–525

Fluorophore labeled amyloidogenic peptides allows the monitoring of the peptide at very low concentrations and to follow the aggregation by different fluorescence based methods, e.g. a change in intensity or shift of the emission upon aggregation, fluorescence anisotropy [76] or fluorescence correlation spectroscopy [77]. Another very valuable technique is FRET, which detects the proximity of two fluorophores and hence can be used to evidence interaction of two molecules, like a metallo-peptide with a potential binding partner.

Extrinsic fluorescence: Several extrinsic fluorophores are available to monitor the formation of amyloids, including thioflavin T (ThT), ANS, bis-ANS, Nile-Red, etc. [78,79] The most widely used is ThT [80]. In principle there is a risk that paramagnetic ions, like Cu(II), Fe(III), etc. quench the ThT fluorescence, and hence change in ThT fluorescence cannot be correlated directly with the aggregation state. This was for instance the case for the model peptide Aβ14–23 [81]. In the case of Cu(II)-binding to Aβ aggregates, no such quenching was observed at least if Cu(II) was not added in a large excess. Thus ThT is a valuable tool to monitor amyloid in the presence Cu(II). ThT is also suitable for the in real-time observation of fibrillation in solution in solution [82]. Care has to be taken when organic molecules (in particular potential aggregation inhibitors) are present, as they might interfere with ThT-binding assay rather than inhibiting the aggregation [83].

7.2. UV–Vis spectroscopy

UV–Vis is mainly used to measure concentrations of peptides (see above). Moreover, metal-binding can be studied via the charge transfer (CT) and the d–d bands. Cu(II) has d–d bands in the visible, which give information about the type of coordination sphere [84]. Zn(II) and Cu(I) do not have d–d bands and even the charge transfer bands of O and N (His, amine etc.) are often too high in energy to be observed. In contrast thiolates bound to Zn(II) and Cu(I) give rise to ligand to metal CT band in the UV (around 225 nm and 250, respectively).

However, very often the CT and d–d band are better resolved in circular dichroism and hence this technique is preferred (see next Section 7.3 and Fig. 8).

7.3. Circular dichroism

Secondary structure: Classically circular dichroism is used to obtain information about the secondary structure of proteins. The spectrum of the peptide bands (around 190–230 nm) depends on the content of α-helix, β-sheet, turns and random coil. CD is particularly sensitive to α-helix and is often used to detect structural changes to the mostly β sheet structure found in amyloids. It seems to be tempting to use CD to monitor secondary structural changes induced by metal binding. However, attention has to be paid on the fact that metal-binding to proteins can have charge transfer bands in the same region, and this band are also CD active. In other words, in the case a charge transfer band is in the same region (like if Cu(II) binds to His, or Zn(II) to Cys), then changes upon Cu(II)-binding are the sum of secondary structure change and charge transfer bands and hence no clear statement about secondary structure can be made. This is the case of Cu(II)–Aβ and Cu(II)–prion, both of them employ His residues to bind Cu(II). However, in the absence of CT bands in this region, like for Zn-binding to Aβ or prion, changes in secondary structure can be unambiguously made.

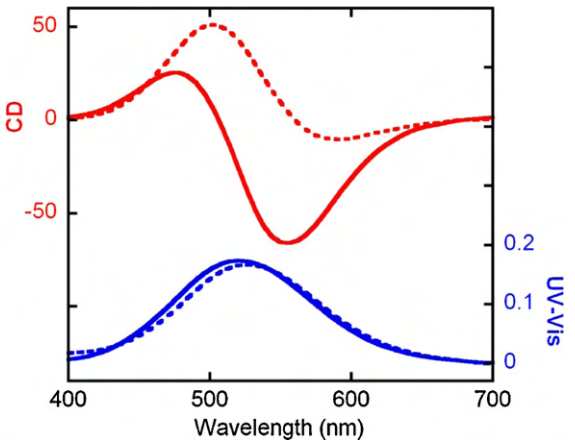

Fig. 8. Circular dichroism (red) and absorption spectrum (blue) of the visible region of Cu(II)-Glu-Val-His-Gly (solid) and Cu(II)-Gly-Gly-His-Gly (dashed) (*Conditions:* 1.8 mM Cu(II), 2 mM peptide, Hepes 100 mM, pH 7.4). Although the absorption spectrum of the d–d bands of the two Cu(II) peptides are very similar, the circular dichroism spectra differ a lot. This is an example of the possible higher sensitivity toward subtle and/or second coordination sphere changes of circular dichroism compared to absorption.

Charge transfer and d–d bands: The other interesting use of CD is to measure the charge transfer and d–d bands. Cu(II) shows d–d bands in the visible and often CT bands in the UV. In contrast Cu(I) and Zn(II) have no d–d and only CT bands connected to Cys (in proteins) are low enough in energy to be detected. These bands are also detected in UV–Vis absorption, but the advantage of CD is often the better resolution (as band can be positive and negative) and that they are often sensitive to the structural environment (Fig. 8). Several charge transfer bands for certain ligand–Cu(II) interaction have been assigned, like the amide to Cu(II) charge transfer band around 315 nm [31]. This helped for instance to deduce the ligands in Cu(II)-binding to Aβ or prion [31,85].

Also the d–d bands of Cu(II) are quite sensitive to structural changes even in the second coordination sphere. Although this is not well understood [86], it allows the use of CD signals as signatures for certain type of Cu(II) environment. As such, CD spectrum of the d–d bands were used to evidence differences in the second sphere of Cu(II) in certain mutants in Aβ [34].

8. Infrared (IR) spectroscopy

Infrared (IR) spectroscopy is a well-established technique for the investigation of the structural properties of molecules and was extensively used for the study of amyloid structures. Although the theory of infrared spectroscopy is thoroughly worked out, its scientific basis is undergoing a current boost, with the application of this analytical technique in biology and biomedicine and the development of new time and space resolved techniques. The analysis of the IR data is based on the presence of specific vibrational marker modes of reactant, intermediate or product states. The outcome or kinetics of a studied reaction can then be interpreted by inspection of the transitions of these marker modes. When, in comparing the experimentally observed vibrational mode pattern with predictions from quantum chemical calculations a full correspondence is possible, the three-dimensional structure is derivable. Current quantum chemical calculation routines, such as density functional theory (DFT), allow for the estimation of the electronic ground state structure of medium-sized molecules.

Different experimental setups can be used in order to obtain absorption data. Experiments in transition mode can be realized by stabilizing two windows with a spacer. The strong absorbance of water at the same position as the amide I band, however, makes it necessary to work with very thin cells of 10 μm path only and to subtract the solvents contribution. Alternatively experiments with difference spectroscopic approaches are possible. Here the difference between two states is measured in one cell and the solvent absorption is omitted. Most studies, however, are performed in reflection mode and more specifically by attenuated total reflection (ATR). The samples are deposited as a film or as a solid on the crystal and the samples are monitored by the infrared beam. ATR cells have been optimized in a way that only a few microliters of sample are necessary.

Most infrared studies in the field use the spectral range between 1700 and 1600 cm^{-1} that includes the coordinates of the ν(C=O) vibration (amide I) [87,88]. The exact position of the amide I band is dependent on the hydrogen bonding strength and is thus specific for the secondary structure of the peptide. In order to obtain the exact position of each structural element the amide I signal is fitted on the basis of a second derivative method or a Fourier self deconvolution [89]. The technique has an error of up to 10% and is highly complementary to CD spectroscopy and X-ray [90]. The amide signal analysis contributed to the understanding of the structures of the amyloid fibrils and more specifically on the 'β-sheet core structure'. Vibrational spectroscopy was extensively used for the study of the aggregation process in the absence of metal ions [91–96].

Linear IR dichroism and polarization studies gives information on the orientation of a functional group, here for example the C=O vibration of the peptide backbone [97,98]. Oriented fibrils have been studied by this technique and two kinds of β-sheets were detected [99]. Isotopic substitution reveals the involvement of certain nuclei in the vibrational motions and the labeling of the C=O group gave further insight in the structure of the amyloid fibril and a six-residue parallel β-sheet over the F22-V27 region of the peptide were deduced [100]. The antiparallel β-sheet structure was reported for the toxic peptide [101].

The combination of microscopic techniques and infrared spectroscopy added the possibility to study surfaces and tissues at molecular resolution and has led to the development of infrared imaging [102]. Chemical, biochemical and biomedical information can be combined with spatial information. Imaging has become one of the main applications of synchrotron light based infrared spectroscopies [103]. In vivo and in vitro studies with this technique confirmed the correlation of the antiparallel β-sheet structure with toxicity [104].

Site-specific information can be obtained for vibrational marker modes that involve nuclear motions of specific molecular side group and the analysis completed by isotope labeling. Labeling may also be performed by H/D exchange of the solvent, supporting among others the attribution of NH or COOH vibrational modes. The side chain contributions of individual amino acids have been examined by a number of infrared spectroscopists [105,106] and are well established in the mid infrared spectral range. Few studies are available on individual amino acids since most of the signal is buried in the strong amid absorptions. The role of individual amino acids in the aggregation process is followed on the basis of the perturbation of the amide I signal [107]. The analysis of the contribution of specific amino acids in the interaction of Cu(II) with the amyloid β-16 was recently presented in function of pH. At pH 7.4 two forms exist, called components I and II. Components I and II are predominant at pH 6.5 and 9, respectively. Combined with isotopic labeling of the amino acids involved in the coordination sphere, the data pointed toward the coordination of Cu(II) via the carboxylate of Asp1 for components I and II in a pseudo-bridging monovalent fashion. At low pH (i.e. component I), His6 bound Cu(II) via Nτ while His13 and His14 are bound via Nπ. At high pH (i.e. component II), direct evidence was given on the coordination of Cu(II) via the Nτ atom of His6 [108].

Exciting developments have been performed in the field of two-dimensional infrared (2D-IR) spectroscopy in recent years. This spectroscopic tool combines structural and ultrafast time resolution. The idea is based on the transferability of the concepts of multidimensional nuclear magnetic resonance (NMR) spectroscopy to IR spectroscopy which was postulated already in the earliest publications on 2D-NMR [109]. The first 2D-IR spectrum was measured about 12 years ago [110]. Despite the fact, that multidimensional optical techniques are analogs of their NMR counterparts, the time resolution is significantly improved: from ms in NMR to fs in IR. This technique provides a unique view into the structure, dynamics, and fluctuating environments of molecules, such as signatures of conformational and hydrogen-bonding fluctuations, protein folding, and chemical-exchange processes.

Since vibrational spectra of large molecules are complex and congested, the use of a vibrational marker for 2D-IR is essential. Stretching modes with a large transition dipole such as C=O, Amide-I, Amide-II, O—H, and N—H, are often used in 2D-IR measurements. In addition, isotope labeling can be used to support the analysis [111–113]. The interpretation is made on the basis of theoretical tools and simulation protocols, based on different approaches, including for example vibrational-exciton Hamiltonians [114] or united residue models [112,115].

The application of 2D spectroscopy to amyloid research is thus sensible toward the structural evolution of the aggregates and the dynamics of hydrogen bonding [112,116–119]. The technique revealed that some amino acids form nearly linear chains within the fibrils. The rigidity of the fibrils has been analyzed and a fast dynamics and the role of water molecules incorporated during the fibrillization process demonstrated. The inhomogeneously broadened β-sheet peak and strong coupling to random coil conformations in 2D IR spectra reveal that the β-sheet fibers have a large structural distribution.

9. X-ray absorption spectroscopy (XAS)

9.1. Information obtained from XAS

In general, X-ray absorption spectroscopy gives information about the binding site of the metal, i.e. the first coordination shell and if good signal to noise also second or further shell. Thus it gives information about the number and type of ligand, the geometry and metal–ligand distance. The spectrum obtained is an average over all centers, i.e. in the case of heterogeneous sites or several distinct sites; the spectrum obtained is the average over the sites. One of the advantages of X-ray absorption (XAS) is that it can be applied to all the metals in their different redox states. This is in particular interesting for elements where less other methods are available, i.e. Zn(II) and Cu(I). XAS gives information about the oxidation state, so Cu(II) and Cu(I) could be distinguished, see e.g. [120], as well as Fe(II) and Fe(III). XAS can be divided into two zones, X-ray absorption near edge structure (XANES) and extended X-ray absorption fine structure (EXAFS), which can give complementary information.

XANES: fingerprint of the metal ion coordination sphere, that means XANES can qualitatively used to compare coordination's spheres as differences in the XANES suggest a different sphere. In the case of Cu(I) the XANES allows relatively well the distinction between bi, tri and tetra-coordinated Cu(I). For Cu(I)–Aβ the XANES was diagnostic for a diagonal coordination [85,121].

For Zn, the shape of the XANES was linked to the tetra-, penta- and hexa-coordination [122], but the distinctions are not that straight forward as probably the type of ligand and the exact geometry influences the shape. For instance the use of several truncated peptide of Aβ, showed that the Zn-binding is in Aβ1–16, as the XANES of Zn–Aβ16 resembled more Zn–Aβ than Zn(II)–Aβ17–40 [94]. Another example is that the XANES of the model peptide Aβ11–28 bound to Zn(II) did not change with its aggregation state, indicating that the binding sphere is similar in the monomeric and aggregates state [123].

EXAFS: EXAFS gives very accurate information about the bond-length (average) between the metal ion and sulfur ligands or nitrogen/oxygen (the distinction between N and O is very difficult). Conclusions about the number of ligands can also be made based on the fact that the bond length increases with an increasing number of ligands. Compared to XANES, the EXAFS features are smaller and hence a better signal to noise is required. This means often a higher concentrated sample or longer acquisition time.

9.2. Samples preparation and damages induced by the beam

XAS of Cu(I/II) Aβ has been recorded in the frozen solution (classically) but also at room temperature. In the frozen state damage by the beam is expected to be lower. Adding of cryoprotectant like 10% glycerol or ethyleneglycol leads to more homogeneous freezing and often to a better signal to noise. Possible pH changes due to freezing of the sample should be considered (see above). Damaging the sample at room temperature is expected to be higher, however, in the liquid phase flow can occur (in particular due to heating by the beam) which can lead to a renewal of the sample in the beam. In any case it is important to assess damage of the sample by the beam. This can be reached by performing several scans and to see if the spectrum evolves with time. If the spectrum evolve the sample is not stable and hence best is to move the beam after each scan to a different place when several accumulation are performed.

A classical form of beam induced damage is photo reduction or photo oxidation. In the case of Zn(II) this is not a problem as Zn(II) is redox inert under the conditions, and indeed XAS on Zn(II)–Aβ did not suffer from this problem. In contrast, photo reduction is very common for Cu(II) samples (see Fig. 9) [71,124]. This can be a problem as the a mixture of Cu(I) and Cu(II) is present, which can complicate the interpretation [85,125]. Photo oxidation of Cu(I) is less observed and has not been reported for Cu(I)–Aβ [71,124].

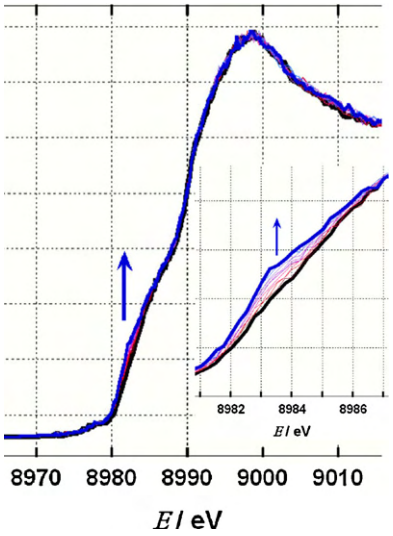

Fig. 9. Photoreduction of Cu(II)–Aβ16: evolution of the edge of X-ray absorption of Cu(II)–Aβ16 at pH 8.7 for consecutive X-ray scans at the same position of the sample. First scan (black) and last scan (blue). The growing of a shoulder around 8983 eV is observed, typical for the edge of Cu(I). Inset: magnification of the spectrum around 8984 eV.

10. Mass spectrometry

In the past decade, mass spectrometry (MS) has become a powerful analytical tool for studying bioorganic and bioinorganic molecule. This evolution can be mainly attributed to electrospray ionization (ESI) and matrix-assisted laser desorption ionization (MALDI), because of their gentle nature that allowed analysis of biomolecule – usually fragmented if ionized by electron impact (EI). MALDI is less applicable for studies of non-covalent interaction, generally lost during ionization, but indirect strategies for determining metal/peptide coordination mode can be applied and provide valuable information. Thus mostly ESI Mass spectrometry was applied for studying metal–peptide complexes linked to neurodegenerative diseases as it preserves best noncovalent interactions. In addition, tandem mass spectrometry (MS/MS) could provide accurate determination of the binding sites involved in metal coordination.

In the case of Alzheimer's disease, the general use of mass spectrometry to study Aβ peptide has recently been reviewed [126]. ESI/MS is commonly employed to identify the formation of Aβ complex with Cu(II) [127,128], Zn(II) [129], Pt(II) [130], Ni(II), Ag(I), or Fe(III) [131], by mass measurement of whole metal–peptide complexes. The coordination mode of metal ions with Aβ peptide was thus revealed as being pH-dependent and influencing Aβ conformation [131,34,132]. Model peptides, mimicking Aβ, have also been investigated by mass spectrometry to understand Cu(II)-induced conformational changes [133]. The binding affinity of palladium complexes – $Pd(phen)Cl_2$, $Pd(bipy)Cl_2$ and $Pd(en)Cl_2$ – to synthetic peptide PrP106–126 of prion protein, involved in transmissible spongiform encephalopathies, was easily investigated by ESI/MS [134]. After identification by high resolution mass spectrometry (HRMS), $Pd(bipy)Cl_2$ was found the most efficient in inhibiting the toxicity of PrP106–126 toward human SH-SY5Y cells. While not essential when working in vitro with model peptides, HRMS provides accurate mass measurement (precision of few ppm) facilitating the identification. α-Synuclein, a 140-amino acid residue presynaptic brain protein involved in Parkinson's disease, has also been identified by ESI/MS mass measurement in complex with Cu(II) [135,136], Fe(II) [137] or Tb(III) [138]. In this case, and generally for high mass proteins complexed with metal ion, the use of MALDI/TOF (time-of-flight mass spectrometry) could be a smart analytical tool as it provides the mass of the monoprotonated ion [139]. Multiprotonated ions generated during ESI ionization can overlap the ones with each other, making sometimes the mass spectra confused and difficult to analyze. Moreover, the use of solvent free mini-ball mill (MBM) MALDI/TOF facilitates the detection of hydrophobic peptides, such as Aβ1–42, more difficult to observe by ESI/MS [140].

For some complexes, and despite the gentle nature of ESI, the metal–protein interaction is lost during desolvation and ionization because coordination bond is weaker than covalent one. If Zn(II)–Aβ interaction can be partially preserved during ionization and fragmentation [141], recent work has demonstrated that ESI–MS of Zn(II) peptide systems are subject to Zn(II) deposition in the ESI emitter. This deposition affects the mass spectral intensities and is thus a significant obstacle for quantification of Zn(II)-bound species [142]. No similar process has been described for other metal ion. Platinum, in complex with peptide, usually exhibits coordination bonds strong enough for mass determination by ESI, while coordination bonds with Cu(II) may have various energies, being or not preserved during ionization. Whatever the metal–peptide complex, probing protein conformation remains possible even when metal–peptide interaction is lost during ionization. This has been recently developed and named as Selective Noncovalent Adduct Protein Probing Mass Spectrometry (SNAPP-MS) [143]. By utilizing specific interactions of 18-crown-6-ether (18C6) with lysine residues, 18C6/α-synuclein distribution was studied and found dependent on the presence of Al(III), confirming that aluminum binding induced significant changes in structural reorganization of α-synuclein.

Most often, the determination of the binding site location of metal coordination is based on nuclear magnetic resonance (NMR) or circular dichroism (CD) measurements. The use of tandem mass spectrometry (MS/MS) is one complementary strategy that could provide valuable information. Briefly, the selected metal–peptide complex ion (most likely a multicharged ion) is fragmented and give rise to a set of *b* and *y* ions that are dependent on the peptide sequence ('*b*' and '*y*' refers to the common Biemann nomenclature [144], where '*b*' are N-terminal and '*y*' are C-terminal fragment ions). The coordination of the metal with one residue will affect the mass of the corresponding ion and will be thus identified.

Tandem mass spectrometry can be applied if the metal–peptide interaction is preserved in the gas phase during fragmentation, which is usually dependent on the metal complex. For weak metal peptide interaction, identifying oxidized residue after metal-catalyzed oxidation (MCO) is a possible strategy for giving information about the residues involved in the coordination with the metal ion [145,146]. When metal–peptide interaction is strong enough, as for Zn(II)–Aβ1–16 complex, ESI–MS/MS could provide accurate information on the coordination mode. Zn(II) binding sites of Aβ1–16 were thus identified as Arg^5, His^6, His^{13} and His^{14} [141], even if MS/MS spectra exhibited partial set of *b* and *y* ions. Both histidyl residues His^6 and His^{14} from Aβ1–16 were also involved in Pt(II) coordination, as deduced from ESI–MS/MS spectra [147]. Four major and five minor products were actually identified – after separation by high performance liquid chromatography (HPLC) – each one corresponding to one coordination mode involving one or two platinum complexes. The binding sites were deduced from ESI–MS/MS spectra of both 3+ and 4+ charged Pt(phen)/Aβ1–16 ions, as presented in Fig. 10 for one of the major products detected. By comparison between Pt-free and platinated *b*/*y* ions, histidyl residues His^6 and His^{14} were identified as being involved in the coordination of Pt(phen). The same approach successfully leads to the determination of the coordination mode of Cu(II), Pd(II), Co(III) and Pt(II) to a model peptide mimicking the octarepeat region in the N-terminal domain of the human prion protein [148].

If necessary, tryptic digestion may be performed prior to collision-induced peptide fragmentation analysis. This is needed for high mass metal–protein complexes for which direct fragmentation is difficult to reach and often needs specific mass spectrometer (such as FT-ICR, i.e. Fourier Transform-Ion Cyclotron Resonance). Such approach coupled to MALDI/MS–MS revealed for example that Met^1 was involved as the primary anchoring residue for Cu(II) in α-synuclein [139]. In all cases, tandem mass spectrometry had allowed an unambiguous determination of the residues involved in the metal coordination.

The development of imaging mass spectrometry (for a general review of the technique, see [149]) is becoming of significant importance as it provides the distribution analysis of metals in biological tissues, which is of key interest in neurodegenerative diseases. Laser ablation inductively coupled mass spectrometry (LA-ICP-MS) has been successfully applied for the determination of metal distribution in thin tissue sections of human or rodent brain and has provided quantitative images of detailed regionally specific element (for a review, see [150]). Time of Flight Secondary Ion Mass Spectrometry (TOF-SIMS) is also becoming of interest for studying amyloid peptides [151]. However, these techniques are not suited for studying metal/peptides interaction as they do not preserve non covalent bond during ionization.

Mass spectrometry plays an important role in several aspects of metal–peptide investigation, linked to neurodegenerative diseases. Detailed information on peptide/protein interaction with

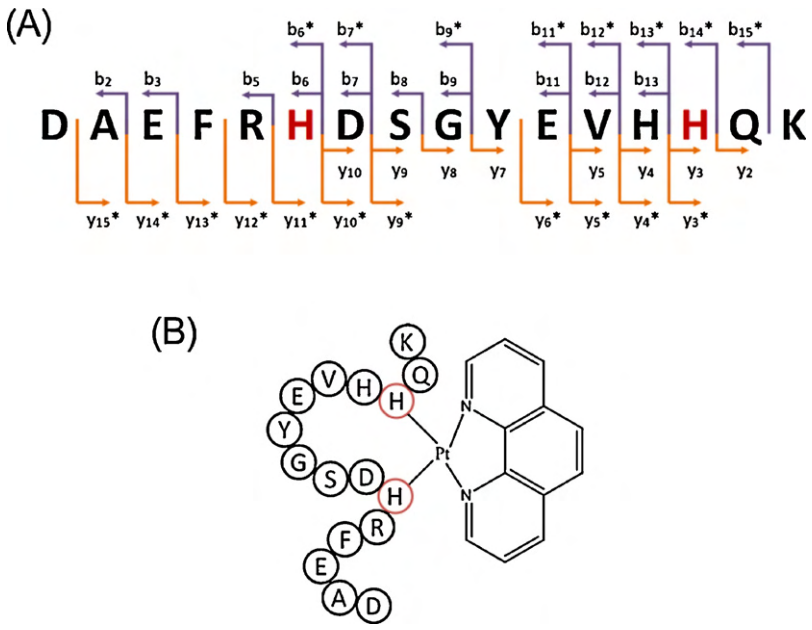

Fig. 10. (A) Fragmentation scheme of one Pt(phen)/Aβ1–16 complex deduced from ESI–MS/MS spectra of both 3+ and 4+ charged ions, including b_n/y_n ions of Pt-free fragments and b_n^*/y_n^* ions of platinated fragments. The lowest platinated and Pt-free ions detected are, respectively, b_6^*/y_3^* and b_5/y_2, showing that histidyl residues His^6 and His^{14} are involved in Pt coordination. (B) The binding model proposed for His^6/His^{14} chelation.
Adapted from Ref. [147].

various metal ions, metal-induced conformational changes and unambiguous MS assignment of coordination modes and binding sites are easily achievable, and have allowed the elucidation of fundamental issues regarding the amyloid fibril assembly pathway. For these reasons, the use of mass spectrometry should stay on the increase in the future and new MS approaches, combining existing MS analytical tools with other experimental techniques, should be developed.

Acknowledgments

We would like to thank Dr. Kevin Barnham (Melbourne) who suggested to us to write a chapter on the methods in this special issue, Dr. Youssef El Khoury (Strasbourg) for helpful discussion and all the collaborators (students, beam line scientist, collaborating groups etc.), without their contribution in applying these methods it would have not been possible to write this review. Research on the interaction of metal ions with amyloidogenic peptides, that allowed us to write on their methods and techniques, was funded by Agence Nationale de la Recherche, Programme Blanc NT09-488591, "NEUROMETALS" and 05-JCJC-0010-01, "NEUROARPE" and the "Region Midi-Pyrénées" (Research Grant APRTCN09004783).

References

[1] A.G. Aslamkhan, A. Aslamkhan, G.A. Ahearn, J. Exp. Biol. 292 (2002) 507.
[2] D.L. Williams-Smith, R.C. Bray, M.J. Barber, A.D. Tsopanakis, S.P. Vincent, Biochem. J. 167 (1977) 593.
[3] K. Hegetschweiler, P. Saltman, Inorg. Chem. 25 (1986) 107.
[4] V. Tõugu, A. Karafin, P. Palumaa, J. Neurochem. 104 (2008) 1249.
[5] M. Sokołowska, W. Bal, J. Inorg. Biochem. 99 (2005) 1653.
[6] A. Jan, D.M. Hartley, H.A. Lashuel, Nat. Protoc. 5 (2010) 1186.
[7] W.B. Stine Jr., K.N. Dahlgren, G.A. Krafft, M.J. LaDu, J. Biol. Chem. 278 (2003) 11612.
[8] Y. Fezoui, D.M. Hartley, J.D. Harper, R. Khurana, D.M. Walsh, M.M. Condron, D.J. Selkoe, P.T. Lansbury Jr., A.L. Fink, D.B. Teplow, Amyloid 7 (2000) 166.
[9] E. Hellstrand, B. Boland, D.M. Walsh, S. Linse, ACS Chem. Neurosci. 1 (2010) 13.
[10] T. Luhrs, C. Ritter, M. Adrian, D. Riek-Loher, B. Bohrmann, H. Dobeli, D. Schubert, R. Riek, Proc. Natl. Acad. Sci. U.S.A. 102 (2005) 17342.
[11] S. Zirah, S. Rebuffat, A. Kozin, P. Debey, F. Fournier, D. Lesage, J.-C. Tabet, Int. J. Mass Spectrom. 228 (2003) 999.
[12] F. Bousejra-Elgarah, C. Bijani, Y. Coppel, P. Faller, C. Hureau, Inorg. Chem. 50 (2011) 9024.
[13] S. Zirah, S.A. Kozin, A.K. Mazur, A. Blond, M. Cheminant, I. Ségalas-Milazzo, P. Debey, S. Rebuffat, J. Biol. Chem. 281 (2006) 2151.
[14] C. Migliorini, E. Porciatti, M. Luczkowski, D. Valensin, Coord. Chem. Rev. 256 (2012) 352.
[15] N.E. Grossoehme, A.M. Spuches, D.E. Wilcox, J. Biol. Inorg. Chem. 15 (2010) 1183.
[16] A. Trapaidze, C. Hureau, W. Bal, M. Winterhalter, P. Faller, J. Biol. Inorg. Chem. 17 (2012) 37.
[17] C. Talmard, A. Bouzan, P. Faller, Biochemistry 46 (2007) 13658.
[18] L. Guilloreau, L. Damian, Y. Coppel, H. Mazarguil, M. Winterhalter, P. Faller, J. Biol. Inorg. Chem. 11 (2006) 1024.
[19] P.O. Tsvetkov, A.A. Kulikova, A.V. Golovin, Y.V. Tkachev, A.I. Archakov, S.A. Kozin, A.A. Makarov, Biophys. J. 99 (2010) L84.
[20] P. Davies, F. Marken, S. Salter, D.R. Brown, Biochemistry 48 (2009) 2610.
[21] M.W. Brazier, P. Davies, E. Player, F. Marken, J.H. Viles, D.R. Brown, J. Biol. Chem. 283 (2008) 12831.
[22] A.R. Thompsett, S.R. Abdelraheim, M. Daniels, D.R. Brown, J. Biol. Chem. 280 (2005) 42750.
[23] S. Salamekh, J.R. Brender, S.J. Hyung, R.P. Nanga, S. Vivekanandan, B.T. Ruotolo, A. Ramamoorthy, J. Mol. Biol. 410 (2011) 294.
[24] L.Q. Hatcher, L. Hong, W.D. Bush, T. Carducci, J.D. Simon, J. Phys. Chem. B 112 (2008) 8160.
[25] L. Hong, T.M. Carducci, W.D. Bush, C.G. Dudzik, G.L. Millhauser, J.D. Simon, J. Phys. Chem. B 114 (2010) 11261.
[26] J. Peisach, W.E. Blumberg, Arch. Biochem. Biophys. 165 (1974) 691.
[27] C.S. Burns, E. Aronoff-Spencer, C.M. Dunham, P. Lario, N.I. Avdievich, W.E. Antholine, M.M. Olmstead, A. Vrielink, G.J. Gerfen, J. Peisach, W.G. Scott, G.L. Millhauser, Biochemistry 41 (2002) 3991.
[28] C. Hureau, L. Charlet, P. Dorlet, F. Gonnet, L. Spadini, E. Anxolabéhère-Mallart, J.-J. Girerd, J. Biol. Inorg. Chem. 11 (2006) 735.
[29] F. Berti, E. Gaggelli, R. Guerrini, A. Janicka, H. Kozlowski, A. Legowska, H. Miecznikowska, C. Migliorini, R. Pogni, M. Remelli, K. Rolka, D. Valensin, G. Valensin, Chem. Eur. J. 13 (2007) 1991.
[30] J.W. Karr, L.J. Kaupp, V.A. Szalai, J. Am. Chem. Soc. 126 (2004) 13534.
[31] T. Kowalik-Jankowska, M. Ruta, K. Wisniewska, L. Lankiewicz, J. Inorg. Biochem. 95 (2003) 270.
[32] C.D. Syme, R.C. Nadal, S.E. Rigby, J.H. Viles, J. Biol. Chem. 279 (2004) 18169.
[33] C.C. Curtain, F. Ali, I. Volitakis, R.A. Cherny, R.S. Norton, K. Beyreuther, C.J. Barrow, C.L. Masters, A.I. Bush, K.J. Barnham, J. Biol. Chem. 276 (2001) 20466.
[34] B. Alies, H. Eury, C. Bijani, L. Rechignat, P. Faller, C. Hureau, Inorg. Chem. 50 (2011) 11192.

[35] T. Kowalik-Jankowska, A. Rajewska, E. Jankowska, Z. Grzonka, Dalton Trans. (2006) 5068.
[36] T. Kowalik-Jankowska, A. Rajewska, K. Wisniewska, Z. Grzonka, J. Jezierska, J. Inorg. Biochem. 99 (2005) 2282.
[37] R.M. Rasia, C.W. Bertoncini, D. Marsh, W. Hoyer, D. Cherny, M. Zweckstetter, C. Griesinger, T.M. Jovin, C.O. Fernandez, Proc. Natl. Acad. Sci. U.S.A. 102 (2005) 4294.
[38] S.C. Drew, C.J. Noble, C.L. Masters, G.R. Hanson, K.J. Barnham, J. Am. Chem. Soc. 131 (2009) 1195.
[39] J.M. Kowalski, B. Bennett, J. Am. Chem. Soc. 119 (2011) 1814.
[40] C.S. Burns, E. Aronoff-Spencer, G. Legname, S.B. Prusiner, W.E. Antholine, G.J. Gerfen, J. Peisach, G.L. Millhauser, Biochemistry 42 (2003) 6794.
[41] B.K. Shin, S. Saxena, Biochemistry 47 (2008) 9117.
[42] P. Dorlet, S. Gambarelli, P. Faller, C. Hureau, Angew. Chem. Int. Ed. 48 (2009) 9273.
[43] M. Bortolus, M. Bisaglia, A. Zoleo, M. Fittipaldi, M. Benfatto, L. Bubacco, A.L. Maniero, J. Am. Chem. Soc. 132 (2010) 18057.
[44] S.C. Drew, C.L. Masters, K.J. Barnham, J. Am. Chem. Soc. 131 (2009) 8760.
[45] S. Parthasarathy, F. Long, Y. Miller, Y. Xiao, D. McElheny, K. Thurber, B. Ma, R. Nussinov, Y. Ishii, J. Am. Chem. Soc. 133 (2011) 3390.
[46] T.L. Lau, E.E. Ambroggio, D.J. Tew, R. Cappai, C.L. Masters, G.D. Fidelio, K.J. Barnham, F. Separovic, J. Mol. Biol. 356 (2006) 759.
[47] R. Tycko, Annu. Rev. Phys. Chem. 62 (2011) 279.
[48] M.R. Jensen, M.A. Hass, D.F. Hansen, J.J. Led, Cell. Mol. Life Sci. 64 (2007) 1085.
[49] E. Gaggelli, N. D'Amelio, D. Valensin, G. Valensin, Magn. Reson. Chem. 41 (2003) 877.
[50] L. Fielding, Prog. Nucl. Magn. Reson. Spectrosc. 51 (2007) 219.
[51] D.D. Boehr, H.J. Dyson, P.E. Wright, Chem. Rev. 106 (2006) 3055.
[52] I. Bertini, C. Luchinat, S. Aime, Coord. Chem. Rev. 150 (1996) R7.
[53] G.M. Clore, J. Iwahara, Chem. Rev. 109 (2009) 4108.
[54] I. Bertini, C. Luchinat, M. Piccioli, Methods Enzymol. 339 (2001) 314.
[55] S. Balayssac, I. Bertini, C. Luchinat, G. Parigi, M. Piccioli, J. Am. Chem. Soc. 128 (2006) 15042.
[56] J. Koehler, J. Meiler, Prog. Nucl. Magn. Reson. Spectrosc. 59 (2011) 360.
[57] V. Balland, C. Hureau, J.-M. Savéant, Proc. Natl. Acad. Sci. U.S.A. 107 (2010) 3367.
[58] R.P. Bonomo, G. Impellizzeri, G. Pappalardo, E. Rizzarelli, G. Tabbì, Chem. Eur. J. 6 (2000) 4195.
[59] C. Hureau, H. Eury, R. Guillot, C. Bijani, S. Sayen, P.L. Solari, E. Guillon, P. Faller, P. Dorlet, Chem.: Eur. J. 17 (2011) 10151.
[60] T.A. Enache, A.M. Oliveira-Brett, Bioelectrochemistry 81 (2011) 46.
[61] M.d. Vestergaard, K. Kerman, M. Saito, N. Nagatani, Y. Takamura, E. Tamiya, J. Am. Chem. Soc. 127 (2005) 11892.
[62] C. Hureau, C. Mathé, P. Faller, T.A. Mattioli, P. Dorlet, J. Biol. Inorg. Chem. 13 (2008) 1055.
[63] J. Shearer, P. Soh, Inorg. Chem. 46 (2006) 710.
[64] C. Léger, P. Bertrand, Chem. Rev. 108 (2008) 2379.
[65] J.-M. Savéant, Elements of Molecular and Biomolecular Electrochemistry, John Wiley and Sons, Hoboken, NJ, 2006.
[66] A.J. Bard, L.R. Faulkner, Electrochemical Methods. Fundamentals and Applications, John Wiley and Sons, Hoboken, NJ, 2001.
[67] D.B. Rorabacher, Chem. Rev. 104 (2004) 651.
[68] N. Le Poul, M. Campion, B. Douziech, Y. Rondelez, L. Le Clainche, O. Reinaud, Y. Le Mest, J. Am. Chem. Soc. 129 (2007) 8801.
[69] D. Jiang, L. Man, J. Wang, Y. Zhang, S. Chickenyen, Y. Wang, F. Zhou, Biochemistry 46 (2007) 9270.
[70] L. Liu, D. Jiang, A. McDonald, Y. Hao, G.L. Millhauser, F. Zhou, J. Am. Chem. Soc. 133 (2011) 12229.
[71] C. Hureau, V. Balland, Y. Coppel, P.L. Solari, E. Fonda, P. Faller, J. Biol. Inorg. Chem. 14 (2009) 995.
[72] M. Rozga, A.M. Protas, A. Jablonowska, M. Dadlez, W. Bal, Chem. Commun. (Camb.) (2009) 1374.
[73] J.C. Lee, H.B. Gray, J.R. Winkler, J. Am. Chem. Soc. 130 (2008) 6898.
[74] S.K. Maji, J.J. Amsden, K.J. Rothschild, M.M. Condron, D.B. Teplow, Biochemistry 44 (2005) 13365.
[75] L.M. Jungbauer, C. Yu, K.J. Laxton, M.J. LaDu, J. Mol. Recognit. 22 (2009) 403.
[76] D. Allsop, L. Swanson, S. Moore, Y. Davies, A. York, O.M. El-Agnaf, I. Soutar, Biochem. Biophys. Res. Commun. 285 (2001) 58.
[77] K. Garai, R. Sureka, S. Maiti, Biophys. J. 92 (2007) L55.
[78] A.A. Reinke, J.E. Gestwicki, Chem. Biol. Drug Des. 77 (2011) 399.
[79] A. Hawe, M. Sutter, W. Jiskoot, Pharm. Res. 25 (2008) 1487.
[80] M. Biancalana, S. Koide, Biochim. Biophys. Acta 1804 (2010) 1405.
[81] V. Pradines, A. Jurca Stoia, P. Faller, New J. Chem. 32 (2009) 1189.
[82] M. Lindgren, K. Sorgjerd, P. Hammarstrom, Biophys. J. 88 (2005) 4200.
[83] S.A. Hudson, H. Ecroyd, T.W. Kee, J.A. Carver, FEBS J. 276 (2009) 5960.
[84] H. Sigel, R.B. Martin, Chem. Rev. 82 (1982) 385.
[85] C. Hureau, Y. Coppel, P. Dorlet, P.L. Solari, S. Sayen, E. Guillon, L. Sabater, P. Faller, Angew. Chem. Int. Ed. 48 (2009) 9522.
[86] M. Klewpatinond, J.H. Viles, FEBS Lett. 581 (2007) 1430.
[87] S. Venyaminov, N.N. Kalnin, Biopolymers 30 (1990) 1259.
[88] E. Goormaghtigh, R. Gasper, A. Benard, A. Goldsztein, V. Raussens, Biochim. Biophys. Acta 1794 (2009) 1332.
[89] E. Goormaghtigh, J.M. Ruysschaert, V. Raussens, Biophys. J. 90 (2006) 2946.
[90] A. Barth, Biochim. Biophys. Acta 1767 (2007) 1073.
[91] E. Cerf, R. Sarroukh, S. Tamamizu-Kato, L. Breydo, S. Derclaye, Y.F. Dufrene, V. Narayanaswami, E. Goormaghtigh, J.M. Ruysschaert, V. Raussens, Biochem. J. 421 (2009) 415.
[92] N. Benseny-Cases, M. Cocera, J. Cladera, Biochem. Biophys. Res. Commun. 361 (2007) 916.
[93] P. Juszczyk, A.S. Kolodziejczyk, Z. Grzonka, J. Pept. Sci. 15 (2009) 23.
[94] V. Minicozzi, F. Stellato, M. Comai, M. Dalla Serra, C. Potrich, W. Meyer-Klaucke, S. Morante, J. Biol. Chem. 283 (2008) 10784.
[95] R. Sarroukh, E. Cerf, S. Derclaye, Y.F. Dufrene, E. Goormaghtigh, J.M. Ruysschaert, V. Raussens, Cell. Mol. Life Sci. 68 (2011) 1429.
[96] E.L. Karjalainen, H.K. Ravi, A. Barth, J. Phys. Chem. B 115 (2011) 749.
[97] J.T. Jarrett, P.T. Lansbury Jr., Biochemistry 31 (1992) 12345.
[98] K. Belbachir, S. Lecomte, H.P. Ta, C. Petibois, B. Desbat, Anal. Bioanal. Chem. 401 (2011) 3263.
[99] H. Hiramatsu, Y. Goto, H. Naiki, T. Kitagawa, J. Am. Chem. Soc. 126 (2004) 3008.
[100] H. Hiramatsu, T. Kitagawa, Biochim. Biophys. Acta 1753 (2005) 100.
[101] O.N. Antzutkin, J.J. Balbach, R.D. Leapman, N.W. Rizzo, J. Reed, R. Tycko, Proc. Natl. Acad. Sci. U.S.A. 97 (2000) 13045.
[102] P. Lasch, D. Naumann, Biochim. Biophys. Acta 1758 (2006) 814.
[103] L.M. Miller, P. Dumas, Biochim. Biophys. Acta 1758 (2006) 846.
[104] K. Berthelot, H.P. Ta, J. Gean, S. Lecomte, C. Cullin, J. Mol. Biol. 412 (2011) 137.
[105] S. Venyaminov, N.N. Kalnin, Biopolymers 30 (1990) 1243.
[106] M. Wolpert, P. Hellwig, Spectrochim. Acta A: Mol. Biomol. Spectrosc. 64 (2006) 987.
[107] A. Peralvarez-Marin, L. Mateos, C. Zhang, S. Singh, A. Cedazo-Minguez, N. Visa, L. Morozova-Roche, A. Graslund, A. Barth, Biophys. J. 97 (2009) 277.
[108] Y. El Khoury, P. Dorlet, P. Faller, P. Hellwig, J. Phys. Chem. B 115 (2011) 14812.
[109] R.R. Ernst, G. Bodenhausen, A. Wokaun, Principles of Nuclear Magnetic Resonance in One and Two Dimensions, Clarendon, Oxford, 1987.
[110] P. Hamm, M.H. Lim, R.M. Hochstrasser, J. Phys. Chem. B 102 (1998) 6123.
[111] Y.S. Kim, L. Liu, P.H. Axelsen, R.M. Hochstrasser, Proc. Natl. Acad. Sci. U.S.A. 105 (2008) 7720.
[112] W. Zhuang, T. Hayashi, S. Mukamel, Angew. Chem. Int. Ed. Engl. 48 (2009) 3750.
[113] C.T. Middleton, A.M. Woys, S.S. Mukherjee, M.T. Zanni, Methods 52 (2010) 12.
[114] P. Hamm, J. Helbing, J. Bredenbeck, Annu. Rev. Phys. Chem. 59 (2008) 291.
[115] M. Khalili, A. Liwo, A. Jagielska, H.A. Scheraga, J. Phys. Chem. B 109 (2005) 13798.
[116] L. Wang, C.T. Middleton, S. Singh, A.S. Reddy, A.M. Woys, D.B. Strasfeld, P. Marek, D.P. Raleigh, J.J. de Pablo, M.T. Zanni, J.L. Skinner, J. Am. Chem. Soc. 133 (2011) 16062.
[117] Y.S. Kim, L. Liu, P.H. Axelsen, R.M. Hochstrasser, Proc. Natl. Acad. Sci. U.S.A. 106 (2009) 17751.
[118] S.H. Shim, D.B. Strasfeld, Y.L. Ling, M.T. Zanni, Proc. Natl. Acad. Sci. U.S.A. 104 (2007) 14197.
[119] G. Stirnemann, P.J. Rossky, J.T. Hynes, D. Laage, Faraday Discuss. 146 (2010) 263.
[120] V.A. Streltsov, J.N. Varghese, Chem. Commun. (Camb.) (2008) 3169.
[121] J. Shearer, V.A. Szalai, J. Am. Chem. Soc. 130 (2008) 17826.
[122] L. Giachini, G. Veronesi, F. Francia, G. Venturoli, F. Boscherini, J. Synchrotron Radiat. 17 (2010) 41.
[123] B. Alies, V. Pradines, I. Llorens-Alliot, S. Sayen, E. Guillon, C. Hureau, P. Faller, J. Biol. Inorg. Chem. 16 (2011) 333.
[124] V.A. Streltsov, S.J. Titmuss, V.C. Epa, K.J. Barnham, C.L. Masters, J.N. Varghese, Biophys. J. 95 (2008) 3447.
[125] J. Shearer, P.E. Callan, T. Tran, V.A. Szalai, Chem. Commun. (Camb.) 46 (2010) 9137.
[126] G. Grasso, Mass Spectrom. Rev. 30 (2011) 347.
[127] M.L. Giuffrida, G. Grasso, M. Ruvo, C. Pedone, A. Saporito, D. Marasco, B. Pignataro, C. Cascio, A. Copani, E. Rizzarelli, J. Neurosci. Res. 85 (2007) 623.
[128] C.A. Damante, K. Osz, Z. Nagy, G. Pappalardo, G. Grasso, G. Impellizzeri, E. Rizzarelli, I. Sovago, Inorg. Chem. 47 (2008) 9669.
[129] C.A. Damante, K. Osz, Z. Nagy, G. Pappalardo, G. Grasso, G. Impellizzeri, E. Rizzarelli, I. Sovago, Inorg. Chem. 48 (2009) 10405.
[130] K.J. Barnham, V.B. Kenche, G.D. Ciccotosto, D.P. Smith, D.J. Tew, X. Liu, K. Perez, G.A. Cranston, T.J. Johanssen, I. Volitakis, A.I. Bush, C.L. Masters, A.R. White, J.P. Smith, R.A. Cherny, R. Cappai, Proc. Natl. Acad. Sci. U.S.A. 105 (2008) 6813.
[131] G. Drochioiu, M. Manea, M. Dragusanu, M. Murariu, E.S. Dragan, B.A. Petre, G. Mezo, M. Przybylski, Biophys. Chem. 144 (2009) 9.
[132] H. Eury, C. Bijani, P. Faller, C. Hureau, Angew. Chem. Int. Ed. Engl. 50 (2011) 901.
[133] M. Murariu, E.S. Dragan, G. Drochioiu, Biomacromolecules 8 (2007) 3836.
[134] Y. Wang, L. Feng, B. Zhang, X. Wang, C. Huang, Y. Li, W. Du, Inorg. Chem. 50 (2011) 4340.
[135] L. Hong, J.D. Simon, J. Phys. Chem. B 113 (2009) 9551.
[136] C. Wang, L. Liu, L. Zhang, Y. Peng, F. Zhou, Biochemistry 49 (2010) 8134.
[137] Y. Peng, C. Wang, H.H. Xu, Y.N. Liu, F. Zhou, J. Inorg. Biochem. 104 (2010) 365.
[138] L.L. Liu, K.J. Franz, J. Biol. Inorg. Chem. 12 (2007) 234.
[139] A. Binolfi, G.R. Lamberto, R. Duran, L. Quintanar, C.W. Bertoncini, J.M. Souza, C. Cervenansky, M. Zweckstetter, C. Griesinger, C.O. Fernandez, J. Am. Chem. Soc. 130 (2008) 11801.
[140] S. Trimpin, M.L. Deinzer, J. Am. Soc. Mass Spectrom. 18 (2007) 1533.
[141] S. Zirah, S. Rebuffat, S.A. Kozin, P. Debey, F. Fournier, D. Lesage, J.C. Tabet, Int. J. Mass Spectrom. 228 (2003) 999.

[142] H. Mattapalli, W.B. Monteith, C.S. Burns, A.S. Danell, J. Am. Soc. Mass Spectrom. 20 (2009) 2199.
[143] T. Ly, R.R. Julian, J. Am. Soc. Mass Spectrom. 19 (2008) 1663.
[144] K. Biemann, Annu. Rev. Biochem. 61 (1992) 977.
[145] C. Schoneich, T.D. Williams, Chem. Res. Toxicol. 15 (2002) 717.
[146] K. Inoue, A. Nakagawa, T. Hino, H. Oka, Anal. Chem. 81 (2009) 1819.
[147] G. Ma, F. Huang, X. Pu, L. Jia, T. Jiang, L. Li, Y. Liu, Chemistry 17 (2011) 11657.
[148] M.J. Pushie, A.R. Ross, H.J. Vogel, Anal. Chem. 79 (2007) 5659.
[149] L.A. McDonnell, R.M. Heeren, Mass Spectrom. Rev. 26 (2007) 606.
[150] J.S. Becker, M. Zoriy, A. Matusch, B. Wu, D. Salber, C. Palm, Mass Spectrom. Rev. 29 (2010) 156.
[151] S. Sole-Domenech, B. Johansson, M. Schalling, J. Malm, P. Sjovall, Anal. Chem. 82 (2010) 1964.

Reevaluation of Copper(I) Affinity for Amyloid-β Peptides by Competition with Ferrozine—An Unusual Copper(I) Indicator

Bruno Alies, Bertrand Badei, Peter Faller, and Christelle Hureau

Chemistry - A European Journal
2012, *18 (4), 1161-1167*

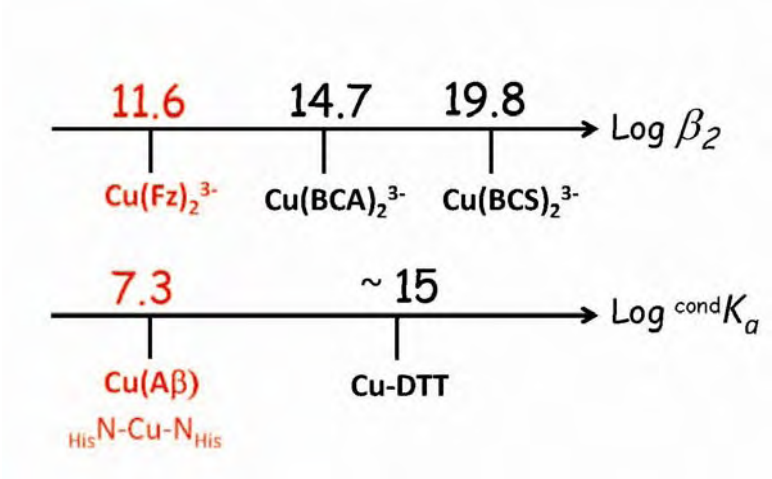

The following article demonstrates the use of Ferrozine as an unusual Cu(I) chelator (generally used as Fe(II) chromophore) with moderate affinity. This property was used to re-evaluated the affinity of Aβ-Cu(I) and other mutants. I strongly participated to Bertrand Badei's supervision and to data acquisition and analysis.

DOI: 10.1002/chem.201102746

Reevaluation of Copper(I) Affinity for Amyloid-β Peptides by Competition with Ferrozine—An Unusual Copper(I) Indicator

Bruno Alies,[a, b] Bertrand Badei,[a, b] Peter Faller,[a, b] and Christelle Hureau*[a, b]

Abstract: The association constant of ferrozine (5,6-diphenyl-3-(2-pyridyl)-1,2,4-triazine-4,4″-disulfonic acid) with Cu^{I} to form the chromophoric $[Cu^{I}(Fz)_2]^{3-}$ complex was determined by UV/Vis titration experiments in Hepes buffer (0.1 M, pH 7.4). An association constant close to $10^{12}\,M^{-2}$, which is significantly weaker than those of the well-known, water-soluble, Cu^{I} chelators bicinchoninic acid and 2,9-dimethyl-4,7-diphenyl-1,10-phenantroline disulfonic acid, was found. The $[Cu^{I}(Fz)_2]^{3-}$ chromophore was used in UV/Vis competition experiments to determine Cu^{I} binding affinity for the amyloid-β peptide involved in Alzheimer's disease and for a series of pertinent mutants. An association constant of approximately $10^{7}\,M^{-1}$ was found; this is much weaker than that reported for dithiothreitol and confirms that imidazoles are harder ligands than thiolates. Each His mutation (H6A, H13A, and H14A) impacts the peptide affinity for Cu^{I}. The native human amyloid-β peptide was found to be a fourfold-stronger Cu^{I} ligand than the murine peptide, which differs by three point mutations (R5G, Y10F, and H13R) from the human one.

Keywords: amyloid-beta peptides · binding affinity · chromophores · copper · ferrozine

Introduction

Copper is an essential trace element involved in several essential biological functions and is used as cofactor in many redox proteins. However, Cu dyshomeostasis is responsible for several diseases. For instance, Cu^{I} overload in the cytosol is the fingerprint of the genetic disorder Wilson's disease (WD). A disturbed Cu^{I} supply is also encountered in the Menkes syndrome.[1,2] In addition, Cu has been involved in neurodegenerative diseases, such as Alzheimer disease (AD),[3–5] in which both Cu^{I} and Cu^{II} oxidation states have been proposed to intervene in deleterious processes linked to the development of the pathology, possibly through the production of reactive oxygen species (ROS).[6,7]

Some therapeutic approaches rely on the use of Cu chelators. For instance for WD, the chelators should have a high affinity to sequester Cu^{I} and should ideally target the liver where Cu^{I} accumulates.[8] However, to determine directly Cu^{I} binding affinity is often difficult. As a consequence, affinities of most of chelators have been obtained by competition with Cu^{I}-specific dyes with known formation constants, such as the BCS (2,9-dimethyl-4,7-diphenyl-1,10-phenanthroline disulfonic acid, $\log \beta_2 = 19.8$)[9] and BCA (bicinchoninic acid, $\log \beta_2 = 14.7$[10] or 17.2)[11] reagents (Scheme 1 and Table 1) that form 1:2 Cu/ligand complexes. No dye with lower Cu^{I} affinities has been studied so far. Herein, we reported on the determination of the apparent formation constant ($\beta_2 = 10^{11.6}$ in Hepes 0.1 M, pH 7.4) of the $[Cu^{I}(Fz)_2]^{3-}$ species (Fz = ferrozine = 5,6-diphenyl-3-(2-pyridyl)-1,2,4-triazine-4,4″-disulfonic acid). This complex shows a visible signature at 470 nm ($\varepsilon = 4320\,M^{-1}cm^{-1}$, Scheme 1 and Table 1).[12]

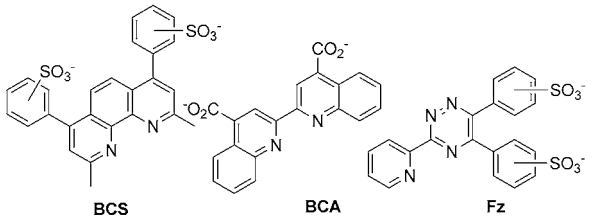

Scheme 1. Structures of the BCS, BCA, and Fz ligands.

Secondly, competition with the chromophoric $[Cu^{I}(Fz)_2]^{3-}$ complex was applied to determine Cu^{I} binding affinity to amyloid-β (Aβ) peptides involved in AD, including the full-length Aβ42 peptide (sequence: DAEFRHDSGYEVHHQKLVFFAEDVGSNK GAIIGLMVGGVVIA). Recently, it was shown that Cu^{I} binds to the soluble form of Aβ through two of the three His residues in positions 6, 13, and 14 with a preference for the His diad His13-His14.[18–22] In the 1:1 Cu/Aβ complex obtained, the metal center is

[a] B. Alies, B. Badei, Prof. Dr. P. Faller, Dr. C. Hureau
CNRS, LCC (Laboratoire de Chimie de Coordination)
205, route de Narbonne, 31077 Toulouse, (France)

[b] B. Alies, B. Badei, Prof. Dr. P. Faller, Dr. C. Hureau
Université de Toulouse
UPS, INPT, LCC, 31077 Toulouse (France)
Fax: (+33) 5-61-55-30-03
E-mail: christelle.hureau@lcc-toulouse.fr

Supporting information for this article is available on the WWW under http://dx.doi.org/10.1002/chem.201102746, including UV/Vis detection (at 470 nm) of reverse titration experiment (Fz into a Cu^{I} solution) and UV/Vis monitoring of competition between Aβ and BCA.

 © 2012 Wiley-VCH Verlag GmbH & Co. KGaA, Weinheim

Table 1. Formation constants and spectroscopic data of $[Cu^{I}(L)_2]^{3-}$ complexes.

Ligand	Log β_2	Comment	Ref	λ_{max} [nm]	ε_{max} [$M^{-1}cm^{-1}$]	Ref
BCS	19.8	from $[Cu(BCS)_2]^{2-}$ association constant and redox potential of $[Cu(BCS)_2]^{2-/3-}$ complexes	[9]	483	1300	[9]
	22.1	competition with cyanide (pH 6.0)	[13]	485		[13]
BCA	14.7	by calorimetry in Hepes (50 mM, NaCl 200 mM, pH 7.5, 25 °C)	[10]	562	7700	[10]
	17.2	by indirect competition with BCS	[11]	562	7900	[14]
	11.4	by spectrophotometric titration pH 6.0	[13]	560		[13]
Fz	11.6	by spectrophotometric titration in Hepes (100 mM, pH 7.4)	[b]	290	49500	[b]
				470	4320	[b]
				(562)[a]	2600	[b]
				470	4320	[12]
				(562)[a]	3300	[12]
MeCN	4.35					NIST[c]
	≈4.0	kinetics of $[Co^{III}(NH_3)_5X]^{2+}$ reduction by Cu^{I} (0.11 M $NaClO_4$, 0.033 M $HClO_4$, 21 °C)				[15]

[a] Data for comparison with $[Fe^{II}(Fz)_3]^{4-}$, which exhibits a λ_{max} at 562 nm. ε of $[Fe^{II}(Fz)_3]^{4-}$ at 562 and 470 nm (the maximum of $[Cu^{I}(Fz)_2]^{3-}$ absorption) were determined herein to be 25 000 $M^{-1}cm^{-1}$ and 8600 $M^{-1}cm^{-1}$, respectively. These values are slightly lower than those previously reported.[12,16,17] [b] This work. [c] NIST = National Institute of Standards and Technology database.

linearly bound by two imidazole rings from His residues.[18,20] Another key parameter to determine is the strength of the Cu^{I}–Aβ interaction. From our measurements, an apparent affinity of $(1.9\pm0.8)\times10^{7}\,M^{-1}$ for the Aβ42 peptide (in 0.1 M Hepes, pH 7.4) was deduced. This result is discussed with respect to contradictory data obtained very recently by Feaga et al., who reported a dissociation constant in the femtomolar range.[23] We also investigated the C-terminally truncated peptide that contains the 16 first amino acid residues of Aβ42 (including the three His ligands), noted Aβ16. The Cu^{I} affinity for the corresponding Aβ16-H6A, Aβ16-H13A, and Aβ16-H14A mutants and the N-terminally protected peptide Ac-Aβ16 were studied to confront affinity data with the actual $[Cu^{I}(Aβ)]$ structural model proposed on the basis of spectroscopic data. Furthermore, as mice and rats, whose peptide differs from the human Aβ peptide by three point mutations (R5G, Y10F, and H13R), do not develop AD, we have also studied Cu^{I} binding to the murine Aβ (mAβ) peptide and the impact of each point mutation on Cu^{I} affinity.

Results and Discussion

Association constant of $[Cu^{I}(Fz)_2]^{3-}$: Fz is a well-known water-soluble spectrophotometric indicator for Fe^{II} and is widely used to titrate Fe^{II} in biological medium or in potable water.[16,17,24] The use of Fz as a Cu^{I} spectrophotometric indicator has been proposed,[12] but has remained unexploited due to possible interference with Fe^{II} concomitants present in natural media.[25] Herein, such interferences with Fe^{II} was avoided or at least corrected and we could thus investigate Cu^{I} binding to Fz. In a first attempt, competition experiments between Fz and BCA for Cu^{I} binding were performed and revealed that Fz was a significantly weaker Cu^{I} ligand than BCA. However, formation of the ternary $[Cu^{I}(Fz)(BCA)]^{3-}$ species (for which the spectroscopic data are not known) during the competition experiment precluded any straightforward quantitative analysis. Moreover, at physiological pH, two different association constants are reported for the $[Cu^{I}(BCA)_2]^{3-}$ complex,[10,11] and thus the $[Cu^{I}(Fz)_2]^{3-}$ association constant deduced from competition experiments would have been a relative value. That is the reason why the $[Cu^{I}(Fz)_2]^{3-}$ association constant was determined by UV/Vis titration, a technique that led to particularly accurate and independently confirmed results in case of the parent $[Fe^{II}(Fz)_3]^{4-}$ species.[17,26] Indeed in such a way, only a small error is detected on the order of magnitude of the constant, because it mainly depends on the concentration at which the reaction between the metal ion and the chromophore is equilibrated. In the present case, the ideal concentrations to observe the equilibrium between Cu^{I} and Fz was below 50 μM, a concentration at which the absorbance of $[Cu^{I}(Fz)_2]^{3-}$ is still high enough to be correctly evaluated (under the usual working conditions, i.e., a pathlength of 1 cm). It is worth noting that such a direct titration is not straightforward for evaluation of the stronger $[Cu^{I}(BCA)_2]^{3-}$ and $[Cu^{I}(BCS)_2]^{3-}$ association constants. Two kinds of titration experiments were performed: either Cu^{I} was added into a Fz solution (direct titration) or Fz was added into a Cu^{I} solution (reverse titration) and all the titrations were repeated at least three times with [Fz] = 30 or 50 μM (direct titration) or $[Cu^{I}]$ = 15 or 25 μM (reverse titration). In the former case (Figure 1a), it was possible to monitor both the absorption band at 470 nm, the increase of which corresponds to the formation of the $[Cu^{I}(Fz)_2]^{3-}$ complex, and the absorption band near 290 nm, which was slightly modified by the addition of Cu^{I}. Addition of Cu^{I} led to the increase of the 470 nm absorption band that followed the titration curve shown in Figure 1b. In the UV region, addition of Cu^{I} (up to half of the Fz concentration) led to the formation of a new absorption band at a higher wavelength. Concomitantly three isosbestic points were detected; this indicates that two chromophores, identified as [Fz] and $[Cu^{I}(Fz)_2]^{3-}$, are in equilibrium in solution. At higher Cu^{I} amounts, the UV band slightly increased and was still weakly shifted toward a higher wavelength. This is due to the formation of a third chromophore, which may be the $[Cu^{I}(Fz)]^{-}$ species. The association constants (β_2) deduced from direct measurement is $(3.7\pm1.5)\times10^{11}$ and from the reverse measurement (2.5±

 © 2012 Wiley-VCH Verlag GmbH & Co. KGaA, Weinheim

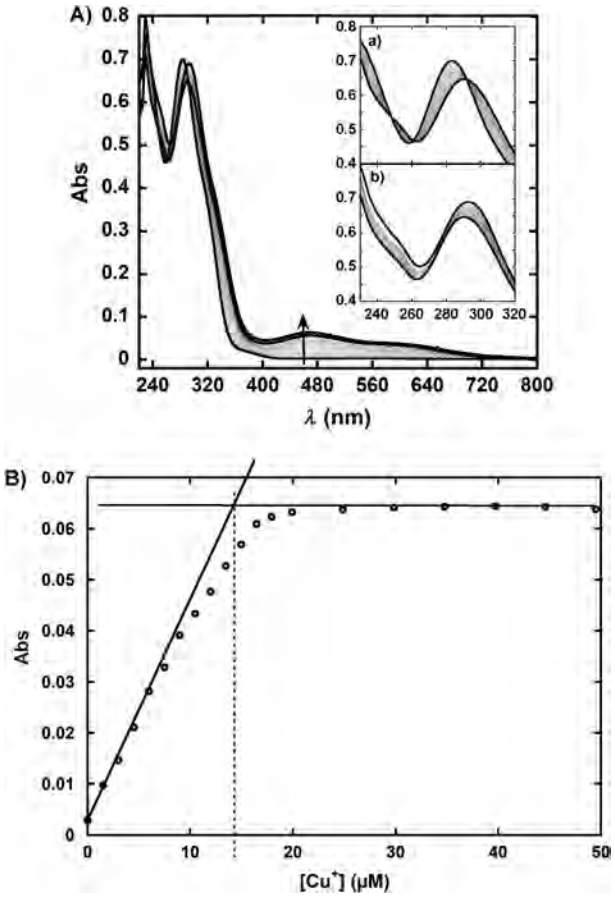

Figure 1. A) UV/Vis spectra of successive additions of Cu^{I} into a Fz solution: [Fz] = 30 μM (Hepes 0.1 M pH 7.4), bold traces correspond to [Cu^{I}] = 0 μM, 15 μM, and 75 μM. Insets: a) [Cu^{I}] from 0 to 15 μM and b) [Cu^{I}] from 15 to 75 μM in the UV region. B) Titration curve of successive additions of Cu^{I} into a Fz solution with the absorbance measured at 470 nm: solid lines correspond to asymptotes for which [Cu^{I}]→0 and [Cu^{I}]→∞. The theoretical absorbance value obtained for total complexation between Cu^{I} and Fz is given by the [Cu^{I}]→∞ asymptote. The *x* value of the intersection between the two asymptotes gives access to the Cu/Fz ratio in the complex formed (dashed line) and the real absorbance value detected due to an equilibrated reaction corresponds to the intersection of the dashed line with the titration curve.

$0.5) \times 10^{11}$ (see example of titration curve in Figure S1 in the Supporting Information and the Experimental Section for detailed calculations). The weak difference observed between the two kinds of titrations may originate from contributions of the $[Cu^{I}(Fz)]^{-}$, which is more important in the reverse titration. A β_2 value of $(3.7 \pm 1.7) \times 10^{11}$, which covers the whole error range, was used in the results described below. Note that 1) in these experiments, we used $[Cu(MeCN)_4]^{+}$ as a starting Cu^{I} source. The MeCN concentration at the break point of the titration curve is approximately 2.5 mM. Because MeCN is a weak Cu^{I} chelator (Table 1), we ensured in a preliminary study that the MeCN concentration up to 20 mM did not interfere with the determination of the β_2 value. 2) The experiments were performed in Hepes buffer (0.1 M) and as a consequence the β_2 value is an apparent constant. However Hepes, due to its chemical structure, is anticipated to have only weak Cu^{I} binding ability. Potentiometric determination of absolute constants, as performed for quinoline Zn^{II} sensors by Fahrni and O'Halloran,[27] was not tried due to the redox sensitivity of Cu^{I}.

Affinity constants of [Cu^{I}(Aβ)] species: To determine the Cu^{I} binding affinity for Aβ peptides, a first attempt was performed by using the known BCA ligand. However, even after addition of 40 equivalents of Aβ16 peptide per Cu^{I}, the UV/Vis signature of the $[Cu^{I}(BCA)_2]^{3-}$ species did not evolve enough to determine precisely the binding affinity of [Cu^{I}(Aβ)] (Figure S2 in the Supporting Information). That was the reason why association of Cu^{I} with Fz was determined (see above). In Figure 2, the effect of successive addition of the Aβ16 peptide to a solution of $[Cu^{I}(Fz)_2]^{3-}$ is shown. Addition of the Aβ16 peptide led to a significant decrease in the 470 nm absorption band characteristic of the $[Cu^{I}(Fz)_2]^{3-}$ complex. Concomitantly a weak increase of the absorbance is observed at 562 nm; this indicates the formation of the $[Fe^{II}(Fz)_3]^{4-}$ complex and is attributed to the presence of small amount of Fe in the peptide batch. Analysis of UV/Vis data, according to Equation (4) in the Experimental Section, gave the affinity values of Cu^{I} for the various Aβ peptides that are reported in Table 2. Note that UV/Vis data have been corrected for contribution of the small amounts of $[Fe^{II}(Fz)_3]^{4-}$ formed during the titration.

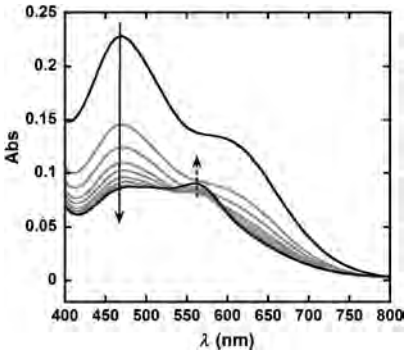

Figure 2. UV/Vis spectra of successive additions of Aβ16 (ca. 100 μM per addition) into a solution of $[Cu^{I}(Fz)_2]^{3-}$ (55 μM) in Hepes (0.1 M, pH 7.4): Bold traces correspond to [Aβ] = 0 and 720 μM. The solid arrow indicates the decrease of the 470 nm absorption band characteristic of the $[Cu^{I}(Fz)_2]^{3-}$ complex. The dashed arrow indicates the increase of the 562 nm absorption band characteristic of the $[Fe^{II}(Fz)_3]^{4-}$ complex, the formation of which is due to the presence of very small amount of Fe in the peptide batch.

An independent method to illustrate the competition between [Cu^{I}(Aβ)] and $[Cu^{I}(Fz)_2]^{3-}$ species is NMR spectroscopy. Indeed, it was previously evidenced that Cu^{I} binding to the Aβ peptide lead to shifts in the position of the His resonances (Figure 3 spectra a and b).[19] Addition of two equivalents of Fz per Cu^{I} ion shifts the His resonances towards those of the apo peptide (Figure 3, spectrum c). The proportion of Cu^{I} bound to the Aβ peptide can thus be deduced from the differences in the peak positions of the His

 © 2012 Wiley-VCH Verlag GmbH & Co. KGaA, Weinheim

Table 2. Affinity constants of [Cu^{I}(L)] species (Hepes 0.1 M, pH 7.4) and corresponding standard-deviation constants calculated by competition with Fz and a β_2 value of 3.7×10^{11}.

Ligand	K_a [10^6 M^{-1}]	Ligand	K_a [10^6 M^{-1}]
Aβ42	19 ± 8.2[a]	–	–
Aβ16	7.5 ± 1.0	mAβ16	1.9 ± 0.15
Aβ16-H6A	2.7 ± 0.30	Aβ16-R5G	12 ± 1.2
Aβ16-H13A	1.1 ± 0.17	Aβ16-Y10F	9.2 ± 0.88
Aβ16-H14A	2.1 ± 0.13	Aβ16-H13R	0.8 ± 0.15
Ac-Aβ16	12 ± 1.3	Aβ16-R5G-H13R	1.7 ± 0.20

[a] The high value of the standard deviation is attributed to a possible heterogeneity of the Aβ42 peptide stock solution due to aggregation.

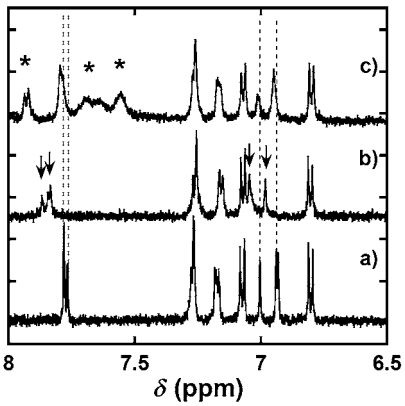

Figure 3. The aromatic region of the NMR spectra of a) Aβ16 peptide ([Aβ] = 200 μM), b) Aβ16 peptide ([Aβ] = 200 μM in presence of 0.9 equivalents of Cu^{I}), and c) Aβ16 peptide ([Aβ] = 200 μM in presence of one equivalent of Cu^{I} and two equivalents of Fz, phosphate buffer 40 mM, pH 7.4). Peaks from [$Cu^{I}(Fz)_2$]$^{3-}$ are represented by *. Dashed lines indicate the position of the His peaks in the apo peptide and arrows indicate the position of the His peaks in the [Cu^{I}(Aβ)] complex.

resonance of the apo-peptide spectrum (Figure 3, spectrum a) and of the mixture of [Cu^{I}(Aβ)] and [$Cu^{I}(Fz)_2$]$^{3-}$ (Figure 3, spectrum c) compared with the differences in the peak positions of the His resonances of the apo-peptide spectrum and of the [Cu^{I}(Aβ)] species (Figure 3, spectrum b). From the NMR data a binding constant of $(8\pm4)\times10^6$ M^{-1} was deduced by using Equation (4) in the Experimental Section. This value agrees well with that determined by UV/Vis titration.

The affinity value obtained herein for the [Cu^{I}(Aβ16)] complex (7.5×10^6 M^{-1}) is very different from the one of approximately 6×10^{14} M^{-1} obtained recently by Feaga et al.[23] To better understand the possible origin of such discrepancy, we tried to reproduce the data obtained by Feaga et al. However, instead of pure water or *N*-ethylmorpholine buffer (20 mM, pH 7.0), we worked in Hepes (0.1 M, pH 7.4) and used a Cu^{I} source, instead of reducing Cu^{II} by ascorbate. Under such conditions, we were unable to see any competition between Aβ16 and BCS for Cu^{I} binding, contrary to what was reported by Feaga et al., and we detected only a weak competition with the weaker chelator BCA (see Figure S2 in the Supporting Information) for Cu^{I}. Our conditions are probably more appropriate because in unbuffered conditions the pH can shift significantly down to pH < 4, pH values at which Cu^{I} decoordination from BCS is anticipated. The pH shift may originate from 1) successive addition of Aβ16 (the stock solution is usually around pH 2 due to peptide purification in trifluoroacetic acid) and 2) the addition of ascorbate to reduce the Cu^{II}. This is the reason why we also performed the experiments in unbuffered solutions and indeed found that addition of Aβ and a concomitant pH shift induce the removal of Cu^{I} from BCS. Even though this explanation may account for the discrepancy between the values found by Feaga et al. and those determined herein, this may not be the sole reason. It is worth noting that the Cu^{I} association constant with dithiothreitol (DTT) has been reported to be weaker than 10^{15} (β_1).[28,29] On the basis of the HSAB (hard–soft acid–base) theory, the affinity of [Cu^{I}(Aβ)], for which Cu^{I} is linked by two imidazole rings instead of thiolate functions when bound to DTT, is expected to be weaker than that of [Cu^{I}(DTT)].

The impact of mutations on Cu^{I} affinity for Aβ was also investigated to better disentangle Cu^{I} binding to Aβ peptides (Table 2). The full-length Aβ42 peptide is a threefold-stronger Cu^{I} ligand than the truncated Aβ16 peptide. This result may be due to participation of Met35 in Cu^{I} coordination. However, this contradicts XAS data that show no spectroscopic differences between Cu^{I} bound to monomeric full-length Aβ and truncated Aβ16 peptides.[20] Moreover Met35 did not bind to other metal ions associated with AD, including the intermediate Lewis acid Fe^{II}.[30] Increased Cu^{I} affinity for the full-length peptide compared with the truncated one may originate from contributions of oligomeric species in the Aβ42-peptide sample compared with the monomeric form in the Aβ16-peptide sample. Indeed different Cu^{I} coordination spheres in monomeric and oligomeric species have been recently proposed based on XAS data. Met35 was, however, not involved in this coordination.[22]

Among the various mutations studied herein, the His replacement by an Ala leads to the most important impact observed on Cu^{I} binding affinity. The three mutants—Aβ16-H6A, Aβ16-H13A, and Aβ16-H14A—are all weaker Cu^{I} ligands than the corresponding Aβ16 truncated peptide; this suggests that all three His residues intervene in Cu^{I} coordination. However, the decrease in the affinity is not drastic, in line with results that show that the Cu^{I} binding site consists of two of the three His residues,[20] with the three possible couples of His being in equilibrium.[19] More precisely, the affinity follows the trend Aβ16 > Aβ16-H6A > Aβ16-H14A > Aβ16-H13A. This result agrees with the fact that the diad that is most frequently involved in Cu^{I} coordination is His13-His14.[19,21] However, the H13A mutation has a more important impact on the affinity than the H14A one; this suggests that the His6-His13 couple is more involved in Cu^{I} coordination than the His6-His14 couple. We also measured Cu^{I} affinity for the N-terminally protected Ac-Aβ16 peptide, and a slightly higher affinity than that of the Aβ16 peptide was found. These results suggest that the N terminus of Aβ is not involved in Cu^{I} coordination; this agrees with the spectroscopic data available at present.[19,20] It can be an-

 © 2012 Wiley-VCH Verlag GmbH & Co. KGaA, Weinheim

ticipated that the higher Cu^{I} affinity found for Ac-Aβ16 is due to second-sphere effects, in which, for instance, the unfavorable formation of salt bridges or H bonds between the $-NH_3^+$-terminal function and a negatively charged residues will be precluded by the N-terminal protection.

Lastly, the affinity for Cu^{I} of the mAβ16 and of the Aβ16-R5G, Aβ16-Y10F, Aβ16-H13R, Aβ16-R5G-H13R mutants was measured. Contrary to what was observed for Cu^{II} binding, for which a threefold-higher affinity was detected for the mAβ16 peptide compared with the human one,[31,32] the human Aβ16 peptide is a fourfold-stronger Cu^{I}-binding ligand than the mAβ16 peptide. Studies of mutants reveals that the decrease in the Cu^{I} affinity for mAβ16 compared with human Aβ16 is mainly due to the H13R mutation. However, it is worth noting that the R5G mutation has an opposite effect that leads to a slightly higher Cu^{I} affinity either for Aβ16 compared with Aβ16-R5G or for Aβ16-H13R compared with Aβ16-R5G-H13R. This may be attributed to a better accessibility of the His6 residue when the bulky and charged Arg amino acid is replaced by the Gly.

Conclusion

The main information deduced from the present study is that Cu^{I} binding to Aβ is weaker than Cu^{II} binding to Aβ; the $[Cu^{II}(A\beta)]$ association constant is in the subnanomolar range,[3] whereas that of $[Cu^{I}(A\beta)]$ is in the submicromolar range. This may be linked to the different binding sites occupied by the two ions: a square planar site composed of -NH_2, two His, and a CO function from the peptide backbone for the main Cu^{II} species present at physiological pH,[33–35] and two His in a linear mode for Cu^{I}.[19,20] This implies that in the extracellular medium, Cu bound to Aβ is likely in the +II valence state, although this can be modulated by the presence of other Cu^{I} and Cu^{II} chelators. Nevertheless, Cu^{I} bound to Aβ can be transiently found during ROS-production processes; this requires a redox switch between the +I and +II valence states of the $[Cu^{II}(A\beta)]$ species.[6]

It was previously conjectured that the higher Cu^{II} affinity for mAβ compared with human Aβ alters the distribution of Cu^{II} bound to human Aβ in transgenic murine AD models, which produce both human and mAβ peptides in contrast to AD cases that produce only human Aβ.[31] For Cu^{I}, such alteration is not anticipated because Cu^{I} affinity for the mAβ peptide is about a fourth of that of human Aβ.

Last but not the least, the affinity range of chromophoric Cu^{I} complexes has been enlarged by the determination of a significantly weaker association constant for the $[Cu^{I}(Fz)_2]^{3-}$ species compared with those already reported in the literature for $[Cu^{I}(BCA)_2]^{3-}$ and $[Cu^{I}(BCS)_2]^{3-}$ (Table 1). A wider affinity range allows determination of Cu^{I} affinity of biologically relevant molecules, such as α-synuclein or prion proteins, and of synthetic chelators by straightforward UV/Vis competition experiments.

Experimental Section

Chemicals: The monosodium salt hydrate of Fz was bought from Alfa-Aesar. A stock solution (0.1 M) was prepared in water. BCS and the disodium salt of BCA were bought from Sigma-Aldrich. A stock solution (0.1 M) was prepared in water. Hepes buffer (sodium salt of 2-(4-(2-hydroxyethyl)piperazin-1-yl)ethanesulfonic acid) were bought from Fluka (bioluminescence grade). $[Cu(MeCN)_4](BF_4)$ was bought from Sigma–Aldrich and kept under inert atmosphere until used. A Cu^{I} stock solution (0.2 M) was prepared in MeCN. For titration experiments, Cu^{I} stock solutions (10 or 5 mM) were prepared in Ar-degassed Hepes (0.1 M, pH 7.4, containing 10 or 5% v/v MeCN) and degassed with water-saturated Ar just before use. UV/Vis monitoring of the stock solution under Ar was performed to ensure that under these conditions no dismutation occurred. Less than 2% of Cu^{II} was detected, a content that can be neglected in the analysis of the titration curve. The Aβ16 peptide (sequence DAEFRHDSGYEVHHQK) was bought from GeneCust (Dudelange, Luxembourg). The other peptides, that is, the mAβ16 peptide (sequence DAEF*G*HDSG*F*EV*R*HQK), the Aβ16-R5G, Aβ16-Y10F, Aβ16-H13R, and Aβ16-H13R-R5G human mutants (sequences DAEF*G*HDSGYEVHHQK, DAEFRHDSG*F*EVHHQK, DAEFRHDSGYEV*R*HQK and DAEF*G*HDSGYEV*R*HQK) as well as the full-length Aβ42 (sequence DAEFRHDSGYEVHHQKLVFFAEDVGSNKGAIIGLMVGGVVIA) peptide were bought from GenScript (Piscataway, USA).

Truncated peptides: A stock solution of peptide (ca. 10 mM) was prepared by dissolving the powder in milliQ water (resulting pH≅2). The peptide concentration was then determined by UV/Vis absorption of Tyr10, which was considered as free tyrosine ($(\varepsilon_{276}-\varepsilon_{296})=1410\,M^{-1}cm^{-1}$) for a tyrosine-containing peptide, and of two Phe ($(\varepsilon_{258}-\varepsilon_{280})=390\,M^{-1}cm^{-1}$) for the mAβ and Y10F peptides. The human Aβ42 peptide was prepared by dissolving the powder in milliQ water and the peptide concentration was then determined by UV/Vis absorption of Tyr10, which was considered as free tyrosine ($(\varepsilon_{293}-\varepsilon_{360})=2410\,M^{-1}cm^{-1}$) in NaOH (0.1 M).

Techniques: *UV/Vis spectroscopy*: UV/Vis spectra were recorded on a Hewlett Packard Agilent 8453 UV/Vis spectrometer at 25 °C.

NMR spectroscopy: 1D ^1H NMR experiments were recorded on a Bruker Avance 500 spectrometer equipped with a 5 mm triple resonance inverse Z-gradient probe (TBI ^1H, ^{31}P, BB). Spectra were collected at 298 K in D_2O. All UV/Vis and NMR experiments were performed on Ar-degassed solutions and in an Ar atmosphere.

Association constants: Regarding $[Cu^{I}(Fz)_2]^{3-}$-association-constant determination, freshly prepared dithionite or ascorbate (10 mM) was added at the end of the titration experiment to reduce possible $[Cu^{II}(Fz)_2]^{2-}$ formed during the experiment. Absorbance values showed only a slight increase corresponding to the presence of less than 5% $[Cu^{II}(Fz)_2]^{2-}$. This value is sufficiently weak to neglect trace amounts of Cu^{II} in the calculation of the $[Cu^{I}(Fz)_2]^{3-}$ association constant.

Regarding $[Cu^{I}(A\beta)]$-association-constant determination, ascorbate (10 mM) was added to the stock solution of peptides (ca. 1 equiv of ascorbate per peptide) just before use to avoid any possible oxidation of Cu^{I} to Cu^{II} during the peptide additions in the competition experiments. Under these conditions, the pH of the solution does not change. Moreover, it is worth noting that in competition experiments, interference with ascorbate (or with any other weak chelators) has no impact on the determination of the association constant. A typical competition experiment consisted in addition of aliquots of the stock peptide solution into a $[Cu^{I}(Fz)_2]^{3-}$ solution. The equilibration time after each peptide addition was approximately 2 min, that is, the time requested for homogenization of the sample and stabilization of the UV/Vis spectrum.

Calculations: The $[Cu(Fz)_2]^{3-}$ formation constant was determined according to Equation (2).

$$\beta_2 = \frac{[Cu(Fz)_2]}{[Cu][Fz]^2} \quad (1)$$

See Table 3 for the reaction considered. Two kinds of titrations were performed: Cu^{I} into a solution of Fz of a known concentration (direct titra-

 © 2012 Wiley-VCH Verlag GmbH & Co. KGaA, Weinheim

Table 3.

	Cu^+	+	2Fz	⇄	$[Cu(Fz)_2)]^{3-}$	
	C_0		C_1		0	initial
$C_1<2C_0$	C_0-x; $0<x<0.5C_1<C_0$		C_1-2x		x	equilibrium: $0<x<0.5C_1<C_0$
	$C_1(C_0/C_1-a)$		$C_1(1-2a)$		C_1a	$0<a<0.5$; $a=x/C_1$
$C_1>2C_0$	C_0-x; $0<x<C_0<0.5C_1$		C_1-2x		x	equilibrium: $0<x<C_0<0.5C_1$
	$C_0(1-a)$		$C_0(C_1/C_0-2a)$		C_0a	$0<a<1$; $a=x/C_0$

tion) or Fz into a Cu^I solution of a known concentration (reverse titration). $C_0=[Cu^+]_0$, $C_1=[Fz]_0$, $a=x/C_1$ (direct titration) or x/C_0 (reverse titration), and x is the $[Cu(Fz)_2)]^{3-}$ concentration determined by UV/Vis absorption. When $C_0\rightarrow\infty$ (in case of direct titration) or $C_1\rightarrow\infty$ (in case of reverse titration), $a\rightarrow1$ and then it is possible to deduce $\varepsilon([Cu(Fz)_2]^{3-})$. When $C_1=2C_0$, the conditions of Equation (2) are fulfilled:

$$\beta_2=\frac{a}{4(C_0)^2(1-a)^3}, a=\frac{x}{C_0} \quad (2)$$

Determination of the [Cu(Aβ)] formation constant: Competition experiments between $[Cu(Fz)_2]^+$ and Aβ are described by Table 4 and Equation (3) and (4):

Table 4.

Cu^+	+	2Fz	⇄	$[Cu(Fz)_2]^{3-}$	
C_0		C_1		0	initial
$C_0-x_{Fz}-x_{A\beta}$		C_1-2x_{Fz}		x_{Fz}	$\boldsymbol{C_1>2C_0}$ $(0<x_{Fz}<C_0)$
$C_0(1-a_{Fz}-a_{A\beta})$		$C_0(C_1/C_0-2a_{Fz})$		C_0a_{Fz}	equilibrium is described by $0<a<1$; $a_{Fz}=x_{Fz}/C_0$
Cu^+	+	Aβ	⇄	[Cu(Aβ)]	
C_0		C_2		0	initial
$C_0-x_{Fz}-x_{A\beta}$		$C_2-x_{A\beta}$		$x_{A\beta}$	$\boldsymbol{C_2>C_0}$ $(0<x_{A\beta}<C_0)$
$C_0(1-a_{Fz}-a_{A\beta})$		$C_0(C_2/C_0-a_{A\beta})$		$C_0a_{A\beta}$	equilibrium is described by $0<a<1$; $a_{A\beta}=x_{A\beta}/C_0$

$$\frac{\beta_2}{K_a^{A\beta}}=\frac{\frac{[Cu(Fz)_2]}{[Cu][Fz]^2}}{\frac{[Cu(A\beta)]}{[Cu][A\beta]}}=\frac{\frac{C_0a_{Fz}}{(C_0)\left(\frac{C_1}{C_0}-2a_{Fz}\right)^2}}{\frac{C_0a_{A\beta}}{(C_0)\left(\frac{C_2}{C_0}-a_{A\beta}\right)}}=\frac{\frac{a_{Fz}}{(C_0)\left(\frac{C_1}{C_0}-2a_{Fz}\right)^2}}{\frac{(1-a_{Fz})}{\left(\frac{C_2}{C_0}-1+a_{Fz}\right)}}=\frac{a_{Fz}}{(1-a_{Fz})}\frac{\left(\frac{C_2}{C_0}-1+a_{Fz}\right)}{(C_0)\left(\frac{C_1}{C_0}-2a_{Fz}\right)^2} \quad (3)$$

$$K_a^{A\beta}=\beta_2C_0\frac{(1-a_{Fz})}{a_{Fz}}\frac{\left(\frac{C_1}{C_0}-2a_{Fz}\right)^2}{\left(\frac{C_2}{C_0}-1+a_{Fz}\right)} \quad (4)$$

for which a_{Fz} is determined by UV/Vis (470 nm) or NMR spectroscopy. $C_0=50$ μM, $C_1=105$ μM, and C_2 was varied from 100 μM to 1 mM (ca. five to ten C_2 values were used). The affinity constant of Cu^I towards Aβ was determined by solving Equation (4) for each C_2 concentration used in one experiment (with the Kaleidagraph software). Data given in Table 2 correspond to the mean value and the standard deviation obtained for the different C_2 values.

Contribution to the absorbance at 470 nM from $[Fe(Fz)_3)]^{4-}$ was calculated by solving Equations (5) and (6) with the ε values reported in Table 1.

$$A^{470nm}=\varepsilon_{Fe}^{470nm}[Fe(Fz)_3]+\varepsilon_{Cu}^{470nm}[Cu(Fz)_2] \quad (5)$$

$$A^{562nm}=\varepsilon_{Fe}^{562nm}[Fe(Fz)_3]+\varepsilon_{Cu}^{562nm}[Cu(Fz)_2] \quad (6)$$

Acknowledgements

The authors thank the ANR (Agence Nationale de la Recherche) for financial support (ANR Grant Neurometals NT09–488591). Dr. C. Bijani (Laboratoire de Chimie de Coordination) is acknowledged for recording the NMR data.

[1] V. Lalioti, G. Muruais, Y. Tsuchiya, D. Pulido, I. V. Sandoval, *Front. Biosci.* **2009**, *14*, 4878.
[2] B. Sarkar, *Chem. Rev.* **1999**, *99*, 2535.
[3] P. Faller, C. Hureau, *Dalton Trans.* **2009**, 1080 and references therein.
[4] E. Gaggelli, H. Kozlowski, D. Valensin, G. Valensin, *Chem. Rev.* **2006**, *106*, 1995.
[5] K. J. Barnham, A. I. Bush, *Curr. Opin. Chem. Biol.* **2008**, *12*, 222.
[6] C. Hureau, P. Faller, *Biochimie* **2009**, *91*, 1212.
[7] D. G. Smith, R. Cappai, K. J. Barnham, *Biochim. Biophys. Acta Biomembr.* **2007**, *1768*, 1976.
[8] A. M. Pujol, M. Cuillel, O. Renaudet, C. Lebrun, P. Charbonnier, D. Cassio, C. Gateau, D. Pascal, E. Mintz, P. Delangle, *J. Am. Chem. Soc.* **2011**, *133*, 286–296.
[9] Z. Xiao, F. Loughlin, G. N. George, G. J. Howlett, A. G. Wedd, *J. Am. Chem. Soc.* **2004**, *126*, 3081 and refrences therein.
[10] L. A. Yatsunyk, A. C. Rosenzweig, *J. Biol. Chem.* **2007**, *282*, 8622.
[11] Z. Xiao, P. S. Donnelly, M. Zimmermann, A. G. Wedd, *Inorg. Chem.* **2008**, *47*, 4338.
[12] S. K. Kundra, M. Katyal, R. P. Singh, *Anal. Chem.* **1974**, *46*, 1605.
[13] R. Miras, I. Morin, O. Jacquin, M. Cuillel, F. Guillain, E. Mintz, *J. Biol. Inorg. Chem.* **2008**, *13*, 195.
[14] K. Y. Djoko, Z. Xiao, D. L. Huffman, A. G. Wedd, *Inorg. Chem.* **2007**, *46*, 4560.
[15] P. Kamau, R. B. Jordan, *Inorg. Chem.* **2001**, *40*, 3879.
[16] L. Stookey, *Anal. Chem.* **1970**, *42*, 779.
[17] C. R. Gibbs, *Anal. Chem.* **1976**, *48*, 1197.
[18] R. A. Himes, G. Y. Park, G. S. Siluvai, N. J. Blackburn, K. D. Karlin, *Angew. Chem.* **2008**, *120*, 9224; *Angew. Chem. Int. Ed.* **2008**, *47*, 9084.
[19] C. Hureau, V. Balland, Y. Coppel, P. L. Solari, E. Fonda, P. Faller, *J. Biol. Inorg. Chem.* **2009**, *14*, 995.
[20] J. Shearer, V. A. Szalai, *J. Am. Chem. Soc.* **2008**, *130*, 17826.
[21] S. Furlan, C. Hureau, P. Faller, G. La Penna, *J. Phys. Chem. B* **2010**, *114*, 15119.
[22] J. Shearer, P. E. Callan, T. Tran, V. A. Szalai, *Chem. Commun.* **2010**, *46*, 9137.
[23] H. A. Feaga, R. C. Maduka, M. N. Foster, V. A. Szalai, *Inorg. Chem.* **2011**, *50*, 1614.
[24] V. V. S. Eswara Dutt, A. Eskander-Hanna, H. A. Mottola, *Anal. Chem.* **1976**, *48*, 1207.
[25] A. C. I. Anusiem, G. B. Ojo, *Anal. Chem.* **1978**, *50*, 531.
[26] J. C. Thompsen, H. A. Mottola, *Anal. Chem.* **1984**, *56*, 755.
[27] C. J. Fahrni, T. V. O'Halloran, *J. Am. Chem. Soc.* **1999**, *121*, 11448.
[28] Z. Xiao, J. Brose, S. Schimo, S. M. Ackland, S. La Fontaine, A. G. Wedd, *J. Biol. Chem.* **2011**, *286*, 11047.
[29] A. Krezel, W. Leśniak, M. Jeżowska-Bojczuk, P. Młynarz, J. Brasuñ, H. Kozłowski, W. Bal, *J. Inorg. Biochem.* **2001**, *84*, 77.

 © 2012 Wiley-VCH Verlag GmbH & Co. KGaA, Weinheim

[30] F. Bousejra-ElGarah, C. Bijani, Y. Coppel, P. Faller, C. Hureau, *Inorg. Chem.* **2011**, *50*, 9024.
[31] H. Eury, C. Bijani, P. Faller, C. Hureau, *Angew. Chem.* **2011**, *123*, 931; *Angew. Chem. Int. Ed.* **2011**, *50*, 901.
[32] L. Hong, T. M. Carducci, W. D. Bush, C. G. Dudzik, G. L. Millhauser, J. D. Simon, *J. Phys. Chem. B* **2010**, *114*, 11261.
[33] P. Dorlet, S. Gambarelli, P. Faller, C. Hureau, *Angew. Chem.* **2009**, *121*, 9437; *Angew. Chem. Int. Ed.* **2009**, *48*, 9273.
[34] C. Hureau, Y. Coppel, P. Dorlet, P. L. Solari, S. Sayen, E. Guillon, L. Sabater, P. Faller, *Angew. Chem.* **2009**, *121*, 9686; *Angew. Chem. Int. Ed.* **2009**, *48*, 9522.
[35] S. C. Drew, C. J. Noble, C. L. Masters, G. R. Hanson, K. J. Barnham, *J. Am. Chem. Soc.* **2009**, *131*, 1195.

Received: September 2, 2011
Published online: December 21, 2011

 © 2012 Wiley-VCH Verlag GmbH & Co. KGaA, Weinheim

Cu(II) affinity for the Alzheimer's peptide: Tyrosine fluorescence studies revisited

Bruno Alies, Emelyne Renaglia, Malgorzata Rozga, Wojciech Bal, Peter Faller, Christelle Hureau

Analytical Chemistry
Submitted

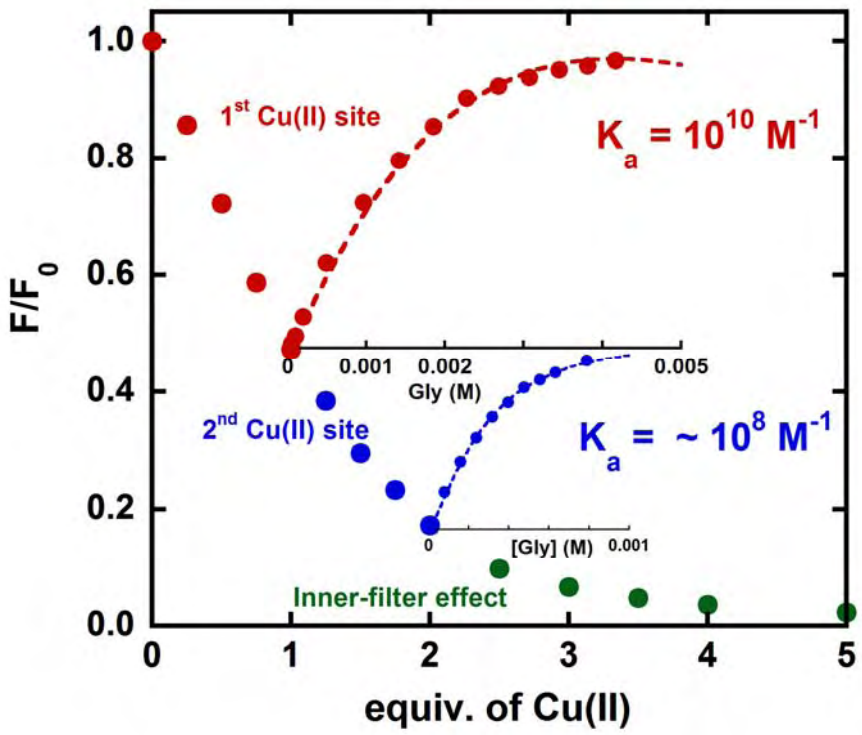

The following article is a comprehensive fluorescence study that aims to determine accurately the Cu(II)-Aβ affinity and to get a standardized value from inconsistent values published in literature. I initiated this work, co-supervised Emelyne Renaglia and contributed significantly to data analysis.

Cu(II) affinity for the Alzheimer's peptide: Tyrosine fluorescence studies revisited.

Bruno Alies,[a,b⊥] *Emelyne Renaglia,*[a,b⊥] *Malgorzata Rózga,*[c] *Wojciech Bal,*[c] *Peter Faller*[a,b,*] *and Christelle Hureau*[a,b,*]

[a,b] CNRS; LCC (Laboratoire de Chimie de Coordination) ; 205, route de Narbonne, F-31077 Toulouse, France. Université de Toulouse; UPS, INPT ; LCC ; F-31077 Toulouse, France

[c] Institute of Biochemistry and Biophysics, Polish Academy of Sciences, Pawińskiego 5A, 02-106 Warsaw, Poland

⊥ These authors contribute equally to this work.

Corresponding authors: peter.faller@lcc-toulouse.fr and christelle.hureau@lcc-toulouse.fr.

Abstract.

Cu(II) binding to the amyloid-β peptide has been proposed to be a key event in the cascade leading to Alzheimer disease. As a direct consequence, the strength of the Cu(II) to Aβ interaction, i.e. the Cu(II) affinity of Aβ, is a very important parameter to determine. Because Aβ peptide contain one Tyr fluorophore in its sequence and because Cu(II) does quench Tyr fluorescence, fluorescence measurements appear to be a straightforward way to obtain this parameter. However, this proved to be wrong, mainly due to data misinterpretation in some previous studies that leads to a conflicting situation. In the present paper, we have investigated in details a large new set of fluorescence data that were analyzed with a new method taking into account the presence of two Cu(II) sites and the inner-filter effect. This leads to re-interpretation of the published data and to the determination of a unified affinity value in the 10^{10} M^{-1} range.

Introduction.

Alzheimer's disease (AD) is the most prevalent cause of dementia in the elderly population, affecting about 40 million people world-wide.[1] This clearly underlines the need to find more efficient medical treatments for AD. In order to find such drugs, the better understanding of the mechanisms, from the origin of the disease to the death of neurons is of central interest.

The underlying mechanism of AD is not clear, but there is evidence and a relatively wide agreement that the so-called amyloid cascade is a key and early event in the development of AD.[1-4] This hypothesis suggests that the mismetabolism of the amyloid-β (Aβ) peptide is the initiating event in AD pathogenesis. The amyloid cascade contains several aggregation stages: oligomers, protofibrils and fibrils that are found in the senile plaques, a traditional hallmark of AD. Aβ is a 39–43 residue polypeptide encompassing a hydrophilic N-terminal domain (1–28)

and a C-terminal hydrophobic domain (29–39/43). *In vivo*, the most prevalent forms consist of 40 (Aβ40) and 42 amino acids (Aβ42). The longer form Aβ42 is more prone to aggregation and more toxic to neurons than Aβ40, in agreement with the amyloid cascade hypothesis.[1]

A large body of evidence also indicates that transition metal ions are involved in the neurodegenerative process.[5, 6] *In vivo, in cellulo* and *in vitro* experiments strongly suggest that metal ions and in particular Cu ions can indeed intervene in the amyloid cascade process.[5, 7-13] Aggregation intermediates (often called oligomers) are now considered to be more toxic than the senile plaques or higher molecular weight aggregates,[14-16] via various events including the production of Reactive Oxygen Species (ROS). As a consequence, metal ions and the amyloid cascade is a central target of anti-AD molecules.[17-19] In such a context, a very important parameter to know is the affinity of Cu(II) for the Aβ peptide. Indeed, it determines: (i) the possibility to have the Cu-Aβ interaction *in vivo* and (ii) it drives the design of Cu(II) chelator, one of the possible therapeutic strategy recently developed.[18]

However, as recently pointed out by some of us in a detailed review,[20] the value of Cu(II) affinity for the amyloid-β peptide (Aβ) is still a matter of debate. While conditional affinity values obtained by potentiometry and isothermal calorimetry (ITC) are in the 10^9 to 10^{10} M^{-1} range, those obtained by Tyr10 fluorescence lie mainly in the 10^7 to 10^8 M^{-1} range (Table 1). Conditional affinity constants describe the effective affinity at a given (pH, T) couple in absence of any competitor. Here, unless specified, these data are given for pH 7.4 and 25 °C. Two possibilities to explain such important discrepancies are: (i) there is a systematic error in the Tyr10 fluorescence or in the potentiometry and ITC experiments (ii) the value found depends on the Aβ concentration since Tyr10 fluorescence studies are performed at much lower concentrations than the other two types of experiments. In parallel with the concentration issue, the nature of the peptide used is different in the two kinds of experiments: short truncated Aβ16

peptide in the latter ones, because relatively high concentration are required for ITC and potentiometry measurements and full-length Aβ peptide for fluorescence experiments that required lower concentration.

Taken into account those considerations, here, we report a new set of Tyr10 fluorescence experiments to evaluate the Cu(II) affinity to Aβ. Concentration of Aβ was varied by two orders of magnitude to search for possible concentration dependence. We get consistent results over a wide range of concentrations, with Aβ16 and Aβ40 peptides of different sources. Also affinity for the second Cu(II) site was evaluated.

Table 1. Summary of conditional affinity constants obtained by fluorescence, ITC and potentiometry. Entries 1 - 11, data obtained by fluorescence, entries 12 - 18, data obtained by calorimetry and entries 19 - 20, data obtained by potentiometry.

Aβ peptide	${}^{app}K_d$ (μM)	Buffer/pH	competitor	${}^{cond}K_a$ (10^7 M^{-1})[a]	${}^{cond}K_a$ (10^{10} M^{-1})[b]	Addition[c]	ref	entry
40/42	1.6/2.0	10 mM tris, 0.1 M NaCl/7.4	10 mM tris	1.4/1.1	0.20/0.16	Cu	21	1
28		H_2O / 7.8	Gly / His	0.2 - 70	N.A.	competitor	22	2
16/28/40	47/28/11	100 mM tris, 0. 15 M NaCl/7.4	100 mM tris	1.9 / 3.1 / 8.3	250/100/60	Cu	23	3
40	8	50 mM PBS, 0.1 M NaCl/7.4	50 mM Phosphate	N.A.	N.A.	Cu	24	4
16		H_2O / 7.8	Gly / His	~ 1	N.A.	competitor	25	5
28	2.5 0.4	10 mM hepes/7.2 10mM phosphate/7.2			N.A. N.A.	Cu	26	6
40	0.5/1.2/3.8/30 0.6/0.9/2.5	10/20/50/100 mM tris, 0.1 M NaCl/7.3 20/50/100 mM hepes,0.1M NaCl/7.4	10/20/50/100 mM tris	2.7/2.9/4.2/1.9 2.8/4.2/2.9	0.63/3.3/36/69 N.A.	Cu	27	7a 7b
42	0.8	20 mM hepes,0.1M NaCl/7.4	20 mM hepes		N.A.	Cu	27	8
40			20-100mM hepes	1.8	N.A.	Cu	28	9
42		H_2O/7.4	Gly/His/NTA	1.7 - 17 x 10^3		competitor	29	10
16/40		100 mM hepes/7.4	Gly	1.1/ 2.7 x 10^3	N.A.	Cu and Competitor	This work	11
16/40	Not given	20mM hepes/7.2 I = 0.16 M, 37°C	Gly: 4 Equiv per	1.5 / 1.1 x 10^3			30	12

			Cu(II)					
16/40	Not given	20mM Pipes/7.2 I = 0.16 M, 37°C	Gly: 4 Equiv per Cu(II)	2.9 / 2.4 x 10^3			[30]	13
16/40	Not given	20 mM hepes/7.4,I = 0.16 M, 37°C	Gly: 4 Equiv per Cu(II)	3 / 9 x 10^3			[31]	14
16/28	0.1	50 mM hepes/7.4		N.A.	N.A.		[32]	15
16	8	50 mM tris	50 mM tris	2	1.7 x 10^{11}		[32]	16
16		20/50/100 mM ACES, 0.1 M NaCl/7.4	20/50/100 mM ACES	1.1/1.04/1.06 x 10^2			[33]	17
28		20 mM ACES, 0.1 M NaCl/7.4	20 mM ACES	0.58 x 10^2			[33]	18
16/28		100mM KNO3		0.48 / 4.1 x 10^3			[34]	19
16				0.83 x 10^2			[35]	20

[a] Correction for tris competition according to ref. [27] and for hepes competition according to [36].

[b] Correction for tris competition according to ref. [30].

[c] Cu means: addition of Cu into a solution of Aβ peptide and competitor means: addition of a competitor to a solution of Cu(Aβ) species.

N.A. Not Applicable; PBS: Phosphate Buffer Saline, ACES : N-(2-acetamido)-2-aminoethanesulfonic acid.

Results.

New analysis of Cu(II)-induced quenching of Tyr10 fluorescence: The full-length Aβ sequence contains only one Tyr residue at position 10 and three Phe residues at position 4, 19 and 20. Hence, upon excitation at 275 nm (and emission at 305 nm), the intrinsic fluorescence of the peptide is predominantly due to the sole Tyr. Figure 1 and S1 show the effect of Cu(II) addition on the Tyr10 fluorescence of Aβ16, considered as a valuable model of Cu(II) binding site in the monomeric full-length Aβ (reviewed in ref. [37]). Full-length Aβ40 has also been studied (Figure S2) but because its aggregation can significantly interfere with fluorescence measurements (see Experimental section), Aβ16 has been preferred, especially when high concentrations are used. Due to its paramagnetic character, Cu(II) quenches the Tyr10 fluorescence. Intensity of the quenching increases with the number of Cu(II) equivalents added and three parts can be identified in the Tyr10 fluorescence quenching curve (Figure 1, left): (i) a linear portion between 0 and 1 Cu(II) equivalent; (ii) a second linear portion with a weaker slope between 1 and 2 Cu(II) equivalents and (iii) an exponential decrease above 2 Cu(II) equivalents. While two break points at 1 and 2 Cu(II) equivalents can be well-observed on this data set, it appears that in most of similar data previously published,[27, 28] they are ill-defined. It is mainly due to a low number of points in the first part of the curve or to irregularly placed points. In such cases, curves reminiscent of the equilibrated formation of the Cu:Aβ 1:1 are observed, leading to the conclusion that Cu(II) affinity lies in the range of the Aβ concentration used for the measurement. Also the Aβ concentration (classically below 10 µM) and the buffer concentration influence the observation of those two break-points.

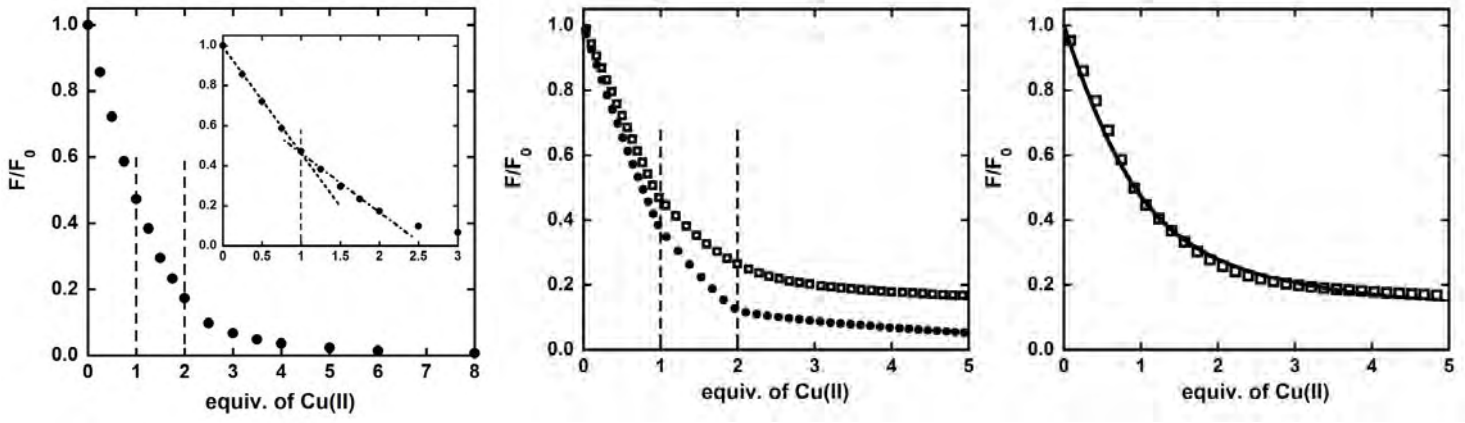

Figure 1. Left panel: Tyr10 fluorescence titration curve showing the three portions of the curve. Inset shows the two first portions of the titration curve, with slope change observed at 1 Cu(II) equivalent per peptide. F_0 corresponds to the fluorescence measured in absence of Cu(II). Central panel: Illustration of impact of Aβ and hepes concentrations on the Cu(II)-induced quenching of Tyr10 fluorescence. *Calculated* points using equations 1 to 4, ${}^{abs}K_a$ of 1.12 10^{10} M^{-1} (see below) and the following conditions: [Aβ16] = 10 µM, [hepes] = 100 mM, pH 7.4 (open squares) or [Aβ16] = 80 µM, [hepes] = 20 mM, pH 7.4 (solid circles). Right panel: fit (solid line) of the former calculated data points (from left panel, open squares) using classical equation for the formation of a 1:1 Cu(II):Aβ complex, where one equivalent of Cu(II) is assumed to quench integrally the Tyr fuorescence (${}^{app}K_d$ = 3.5 10^{-6} M^{-1}). F_0 corresponds to the fluorescence in absence of Cu(II).

To better illustrate this issue, calculated curves using the affinity value determined in this paper and obtained for two extreme conditions are compared in Figure 1, center. For Aβ = 10 µM and [hepes] = 100 mM, the two break points are ill-defined and in such a case, the curve can be well-reproduced with classical model for the equilibrated formation of a Cu:Aβ complex,

yielding an ^{app}Kd of 3.5 10^{-6} M which leads to a conditional affinity of 2 x 10^{7} M^{-1} after correction for competition with hepes buffer according to constants determined in Ref.[36] (Figure 1, right). This value is close to those reported in Table 1, when the fluorescence experiments have been carried out in hepes buffer, a very weak Cu(II) competitor (see Supporting Information).

Analysis of the presently obtained data leads to drastically different conclusions: (i) linearity of the first portion of the titration curve (Figure 1, left, 0 to 1 Cu(II) equivalent) is due to the total (not equilibrated) formation of the Cu(Aβ) complex. Formation of the Cu(Aβ) complex leads to a partial quenching of the Tyr10 fluorescence, with approximately 50% of residual fluorescence observed in presence of one equivalent of Cu(II). (ii) the linearity of the second portion of the curve (1 to 2 Cu(II) equivalents) is due to the total formation of the Cu_2(Aβ) complex leading to approximately 20% of residual fluorescence. (iii) The trend of the third portion of the curve (above 2 Cu(II) equivalents) is due to an inner-filter effect that becomes predominant and leads to a complete Tyr10 fluorescence quenching.

The inner-filter effect is often omitted in Tyr10 fluorescence experiments, inducing misinterpretation of the data. It originates from absorbance of the sample at the excitation (x) and emission (y) points ($I_i(x,y)$), where x and y are the dimensions of the cuvette parallel and perpendicular to the excitation beam. It differs from the maximum intensity (I_o), according to the Beer-Lamber law, $I_i(x,y) = I_0 10^{-(abs(x)+abs(y))}$, where abs(x) and abs(y) are the absorbance at the (x,y) position and the fluorescence of a molecule M defined as $F^M = \varphi^M.[M].I_i$. In the present case,

$$abs(x) = \varepsilon^{A\beta}_{278nm}.[A\beta].x + \varepsilon^{Cu(A\beta)}_{278nm}.[Cu(A\beta)].x + \varepsilon^{Cu_2(A\beta)}_{278nm}.[Cu_2(A\beta)].x + \varepsilon^{Cu(buffer)}_{278nm}.[Cu(buffer)].x$$

and

$$abs(y) = \varepsilon^{A\beta}_{305nm}.[A\beta].y + \varepsilon^{Cu(A\beta)}_{305nm}.[Cu(A\beta)].y + \varepsilon^{Cu_2(A\beta)}_{305nm}.[Cu_2(A\beta)].y + \varepsilon^{Cu(buffer)}_{305nm}.[Cu(buffer)].y$$

and the experimental setup is such as x = 0.5 cm and y = 0.05 cm. Taken into account that the absorbing species absorb at 275 nm but almost not at 305 nm, the second term abs(y) was neglected. Validity of such approximation was checked by addition of the Cu(DAHK) chromophore to a solution of a water-soluble non-coordinating fluorophore (i.e. a phenol sulfonate) (Figure S3). In the following, fluorescence of Aβ containing species will be considered according to Equations 1 and 2 detailed in the Experimental Section.

Glycine as a weak Cu(II) competitor to determine Cu(II) affinity of Aβ. From the Cu(II) addition to Aβ peptide experiment, it appears that it is not possible to determine directly the conditional Cu(II) affinity for Aβ due to a too strong value and thus a non-equilibrated reaction between Cu(II) and Aβ (first part of the titration curve in Figure 1, left). Else, the experiment would require using extremely low Aβ concentrations (nM to pM range). This is the reason why further experiments were performed in presence of the weak competitor, glycine (Gly). Gly was chosen because it proved to be a very-well defined Cu(II) ligand, the formation constants of which has been accurately determined.[38] More particularly, we have used such competitor in the past to evaluate the Cu(II) affinity of GHK and DAHK peptides and obtained results in a close agreement with those obtained by other techniques without Gly competitor.[39] In this case, the affinity value obtained is the apparent affinity, *i.e.* the affinity in presence of a competitor, which thus depends on the competitor concentration according to equation 3 (see Experimental Section).

Two kinds of complementary experiments were performed: (i) Gly addition to Cu(Aβ) species leading to the recovery of the Tyr10 fluorescence (Figure 2, left) or (ii) Cu(II) addition to Aβ in presence of various amounts of Gly (Figure 2, right).

In Figure 2, left, recovery of Tyr10 fluorescence for [Cu(Aβ)] ranging from 20 µM to 200 µM is reported together with simulation of the curves according to the procedure described in the Experimental Section. Also the decrease of the circular dichroism (CD) absorption band at 315 nm (corresponding to the N^- to Cu(II) ligand to metal charge transfer transition in the Cu(Aβ) complex) induced by the formation of the achiral Cu-Gly complexes has been reproduced (Figure S4). A unique value of 1.12×10^{10} M^{-1} M has been used to reproduce the five curves, obtained for [Cu(Aβ)] ranging from 20 µM to 1 mM. This strongly supports that the affinity value of Cu(II)-Aβ binding depends neither on Aβ concentration nor on the technique used for the competition experiments. This also indicates that formation of a ternary Gly-Cu-Aβ complex is unlikely or that the formation constant is very weak.

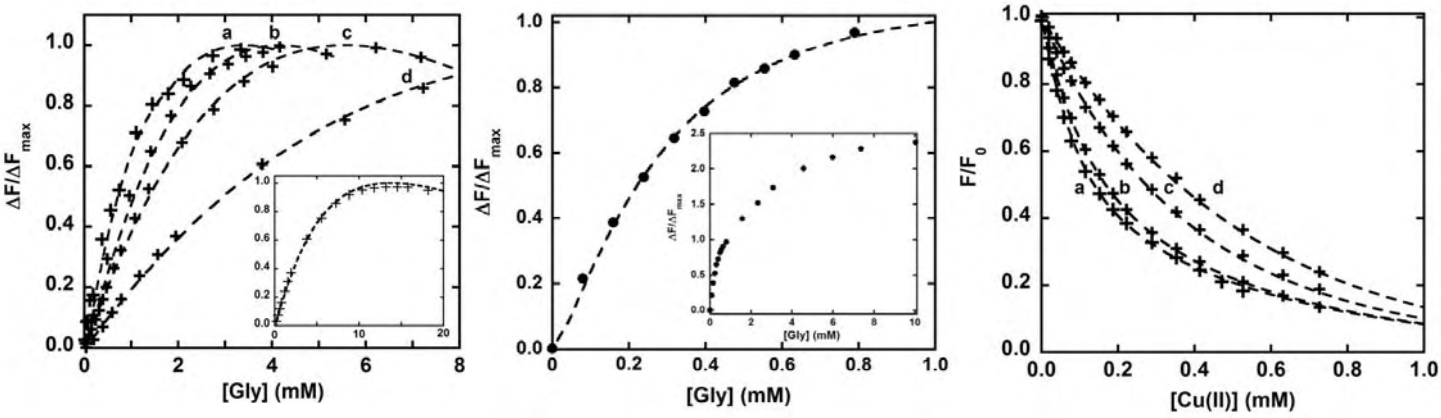

Figure 2. Left panel: Gly induced recovery of [Cu(Aβ16)]-Tyr10 fluorescence, [Cu(Aβ16)] = 20 (a), 50 (b), 80 (c) and 200 μM (d), [hepes] = 100 mM, pH 7.4. Inset shows the data obtained for [Cu(Aβ16)] = 200 μM on a larger scale of Gly concentration. Dashed lines represent the fitting of the Tyr10 fluorescence recovery according to equations 1 to 4 (see Experimental Section), with ${}^{cond}K$= 1.12 10^{10} M^{-1}. Note that Tyr10 fluorescence decrease at high Gly concentration is due to dilution effects (that are taken into account in the fitting procedure). ΔF = F_0-F with F_0 the fluorescence value in absence of Gly. Central panel: Gly induced recovery of [Cu_2(Aβ16)]-Tyr10 fluorescence, [Cu_2(Aβ16)] = 50 μM, [hepes] = 100 mM, pH 7.4 and the corresponding calculated curve (dashed line). Inset: Gly induced recovery of [Cu_2(Aβ16)]-Tyr10 fluorescence on a larger scale of Gly concentrations, including Cu removal from the first site. ΔF = F_0-F, F_0 the fluorescence value in absence of Gly and F_{max} is the fluorescence value for [Gly] = 1 mM. Right panel: Cu(II) induced quenching of Aβ16-Tyr10 fluorescence, [Aβ16] = 80 μM, [hepes] = 100 mM, pH 7.4, in presence of various concentration of glycine, [Gly] = 2 (a), 4 (b), 8 (c) and 16 mM (d). Dashed lines represent the fitting or the Tyr10 fluorescence quenching with ${}^{cond}K$= 1.12 10^{10} M^{-1}. F_0 is the fluorescence value in absence of Cu(II).

Affinity of the second Cu(II) binding site. A second Cu(II) binding site has been identified by Tyr10 fluorescence quenching (Figure 1, left, second portion of the titration curve). To better characterize this second Cu(II) site, CD and EPR measurements were performed (Figure S5). It appears that, in line with previous reports,[22, 29, 32, 35, 40] it is possible to insert a second Cu(II) site into the Aβ16 sequence and that the second Cu(II) binding is sequential.

By addition of Gly to the Cu_2(Aβ) species, Tyr10 fluorescence is recovered in a two-step process (Inset in Figure 2, center). The first steep step (up to 1 mM Gly) corresponds to the removal of the second Cu(II) ion and the second flatter step to the removal of the first Cu(II) ion. Reproduction of the first part of the curve, taking into account that the two Cu(II) ions bind to the Aβ sequentially, leads to an affinity constant of approximately 5×10^7- 1×10^8 M^{-1} for the second Cu(II) ion, in agreement with that evaluated by ITC measurements, with Aβ peptide used as the titrant of a Cu(II) solution.[32] This value is also reminiscent of the Cu(II) affinity for Ac-Aβ peptide measured by ITC.[41]

Cu(II)-induced quenching of Tyr10 fluorescence in presence of Gly. Because the two affinity constants determined for the first and the second Cu(II) ion differs by more than a factor of 100, it is also possible to determine the affinity for the binding of the first Cu(II) to Aβ by monitoring the Tyr10 quenching induced by Cu(II) addition to Aβ in presence of Gly. The second Cu(II) site can be neglected in presence of the Gly concentration required for having an equilibrated reaction between the first Aβ site and the Cu(II). In Figure 2, right, such Cu(II) titration to Aβ has been obtained for [Gly] ranging from 2 mM to 16 mM. A unique affinity value was used to reproduce the four curves: $1.12\ 10^{10}$ M^{-1}, equal to the value determined by Tyr10 recovery in presence of Gly (Figure 2, left).

Cu(II) affinity for full-length human and murine Aβ peptides. Similar affinity value is anticipated for Cu(II) binding to the full-length Aβ (Aβ40) compared to the truncated Aβ16 (compared Figure 1 and S1). Because the Cu(II) titration of Tyr10 fluorescence performed on the Aβ40 was very similar to that obtained for Aβ16, and because Aβ40 is much more complicated to handle and the results less reproducible, Cu(II) affinity for Aβ40 was deduced from competition experiment with the Aβ16 lacking the Tyr10 (Y10F-Aβ16 or murine peptide, i.e. the triple R5G-Y10F-H13R-Aβ16 mutant noted mAβ16). Indeed, such measurements require recording less data compared to the titration curve. In the first step, Cu(II) affinity for Y10F-Aβ16 was deduced from a competition experiment with Aβ16 (Figure 3, bottom data, plain squares). Addition of Cu(II) to Aβ16 leads to a linear decrease of fluorescence (left part of the curve) as observed previously (Figure 1, left). Upon addition of the mAβ16 mutant, fluorescence is recovered (right part of the curve). Taking into account this effect, the affinity ratio between Aβ16 and mAβ16 peptides can be calculated. The same holds for competition between Aβ40 and mAβ16, and Aβ40 and mAβ40. Affinity values thus calculated are reported in Table 2. Aβ16 and Y10F mutant have very similar affinities while the murine Aβ16 binds Cu(II) three times stronger than the human counterpart, in line with previous measurement by competition in circular dichroism (CD).[42] Aβ40 is also stronger than Aβ16, in line with previous publications reporting measurements on both Aβ16 and Aβ40.[23, 31]

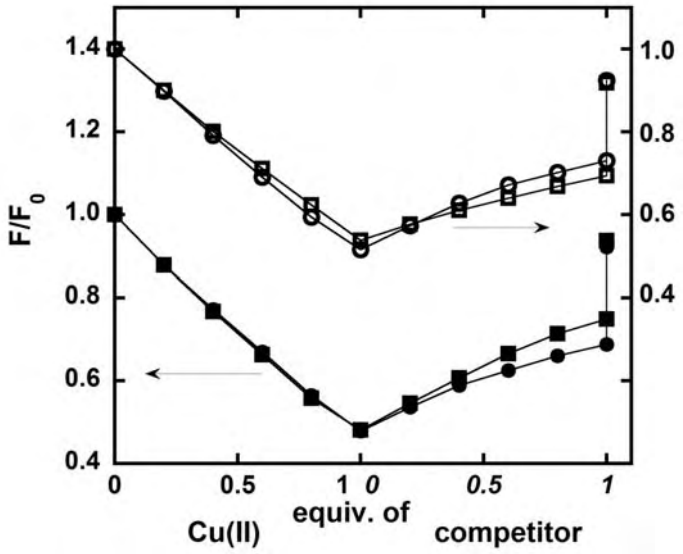

Figure 3. Competition experiments using Tyr10 fluorescence. In the first part of the curves, the fluorescence of Aβ16 (bottom data in solid symbols) or Aβ40 (top data in open symbols) is quenched by addition of Cu(II) while in the second part, fluorescence is recovered by addition of a competing peptide lacking the Tyr10, *i.e.* Y10F-Aβ16 (bottom data, plain circles), mAβ16 (bottom data, plain squares or top data, open circles) or mAβ40 (top data, open squares). Last points on the four curves correspond to the Tyr10 fluorescence recovery after addition of two equiv. of a strong competitor (DAHK). Initial fluorescence is not recovered due to an increased inner filter effect at the end of the experiment compared to the beginning. . [peptide] = 50 µM, [hepes] = 100 mM, pH 7.4. F_0 is the fluorescence value in absence of Cu(II).

Table 2. Conditional affinity relative to conditional affinity of Aβ16. Errors are indicative and come from variation in three independent measurements. Note that a very weak change in fluorescence value impacts significantly the $^{cond}K_a$ ratio.

peptide	Aβ16	Y10F-Aβ16	Aβ40	mAβ16	mAβ40
$^{cond}K_a/^{cond}K_a$(Aβ16)	1	~1±0.2	~2.5±1	~3±1.5	~1±0.5

Discussion.

In the present report, we detail a new method to analyze Cu(II) induced quenching of Tyr10 fluorescence data, that can apply to other quencher - fluorophore couples. In a very weak coordinating buffer such as hepes, the titration curve is made of the three independent parts (Figure 1, left), due to coordination of the first Cu(II) ion, of the second Cu(II) ion and to inner-filter effect induced by increased absorbance of the sample due to Cu(II) addition and binding to the buffer, respectively. These three events are usually ill-defined in the titration curves that can then appears as a classical titration curve of an equilibrated reaction (Cu + Aβ ↔ Cu(Aβ)).[27, 28] Contribution of the inner-filter effect has always been underestimated in all previous reports using fluorescence. The inner-filter effect becomes predominant after the second Cu(II) ion binding to Aβ but also contributes to fluorescence decrease in the first two parts of the titration curve, explaining why Cu(II) induces different ratio in Tyr10 fluorescence quenching depending on the conditions (compare F/F_0 value at one Cu(II) equivalent in Figure 1, center). For instance, in our experiments in presence of one Cu(II) equivalent residual Tyr10 fluorescence was 53 % for Aβ16 = 20 µM, 50 % for Aβ16 = 50 µM, 45 % for Aβ16 = 80 µM (data not shown).

This new analysis leads to Cu(II) affinity of Aβ of about 10^{10} M^{-1} similar to those obtained by other techniques (compare entry 11 with entries 12-20 in Table 1). If a more coordinating buffer such as tris (Figure S6) is used, the Cu(II) induced quenching of Tyr10 fluorescence gives a titration curve characteristic of an equilibrated reaction. This is due to the non-negligible Cu(II) affinity of tris that acts as a weak Cu(II) competitor. Fitting of the titration curve and calculation of the conditional affinity from the apparent one should thus gives a correct evaluation of Cu(II) affinity of Aβ. However, because complexes formation between Cu(II) and tris is still unclear, it is difficult to account for tris competition correctly. Using formation constants from ref. [27], the conditional Cu(II) affinity of Aβ is underestimated (Table 1, entries 1, 3, 7 and 16). Using those from ref. [30] gives results in better agreement with Cu(II) affinity of Aβ obtained by other techniques, but there is a strong dependence on tris concentration (Table 1, entry 7). As pointed out in a recent review,[10] it may originate from tris-Cu formation constants that are not fully correct or from the formation of tris-Cu-Aβ ternary species.

This is the reason why we performed our experiments with Gly as a weak Cu(II) competitor, formation constants of Cu-Gly species being very-well defined.[38] Regarding the use of Gly as weak competitor, some of us raised a possibility that Gly may form ternary complexes with Cu(II) and Aβ, which could explain the discrepancies presented in Table 1 (compare entries 7b and 9 with entries 10 and 12 to 14).[20] The experimental results presented here do not support this concept. The fitting of the affinity constant, which was based upon the absence of such complex, was successful under a broad range of experimental conditions. Even stronger and more direct evidence comes from the CD titration (Figure S5), in which the Gly additions affected only the intensity of the spectrum, but not its shape. CD is very sensitive to perturbations of the d-d chromophore.[43] Thus, we can state that Gly did not bind to the Cu(Aβ) ion in the course of titration.

The competitive titrations using other Aβ analogs are based on a similar assumption, but in this case it is less solid, because we have no evidence that the ternary (Aβ)Cu(Aβ'), where Aβ and Aβ' are the two peptides in competition, isn't present in solution. The existence of such ternary $Cu(A\beta)_2$ species was described as transient species in ref. [44] and later on, reported in ref. [45] on the basis of NMR relaxation rates as a minor species. Hence we have conjectured that the formation of $Cu(A\beta)_2$ was not very significant.

We also evaluate the Cu(II) affinity for the second site (5×10^7 M^{-1} - 10^8 M^{-1}), which is about 100 fold weaker than the first site. Such value involves that hepes in classical concentration range (i.e. 0.1 M) can interfere with Cu(II) binding to the second site. This explains why the slope of the second part of the titration curve is less pronounced in presence of high hepes concentration and weak Aβ concentration (Figure 1, center). This also contributes to the ill-defined break-point at 2 Cu(II) equivalent in most of the titration curves reported, using classical concentration ranges ([Aβ] = 10μM, [hepes] = 100 mM)). Recently, Viles and coworkers[29] proposed that the second Cu(II) site is only observed in the shorter truncated Aβ16 and Aβ28 peptide or in Aβ42 in presence of alcoholic solvent. This proposition was based on EPR signal quantification. Here, by fluorescence, no significant difference in the titration curve measured for the full-length Aβ40 and the shorter Aβ16 peptides has been detected, suggesting that the second Cu(II) binding site is also present in the Aβ40 peptide. Cu((II) affinity for Aβ lies in the 10^{10} M^{-1} range, close to affinity of other neurodegenerative proteins (reviewed in ref. [20]), such as the α-synuclein involved in Parkinson disease (10^9 - 10^{10} M^{-1})[46] and the Prion Protein (10^6 M^{-1} for the octarepeat domain occupied with 4 Cu(II) ions and 10^{10} M^{-1} for the octarepeat domain occupied with 1 Cu(II) ion).[20] Affinity is lower than those of Cu proteins (10^{17} M^{-1} for the SOD),[47] and to a lesser extent to those of other biologically relevant peptides, the N-terminal Cu(II) site of Human

Serum Albumin (10^{12} M^{-1} [48]- 10^{14} M^{-1} [39]) and the cell growth factor GHK (10^{13} M^{-1}).[39] Hence, affinity of Cu(II) chelators designed in the context of AD should thus lie in a relatively narrow range to not disturb the native Cu(II) distribution.

Experimental Section.

Chemicals.

Sodium 4-hydroxybenzenesulfonate dihydrate (phenol sulfonate) was bought from sigma aldrich. Hepes buffer (sodium salt of 2-[4-(2-hydroxyethyl)piperazin-1-yl]ethanesulfonic acid), tris (tris (hydroxymethyl) aminomethane), popso (piperazine-1, 4-bis-(2-hydroxy-propane-sulfonic acid) dihydrate) and pipes (piperazine-N, N'-bis (2-ethanesulfonic acid) buffer were bought from Fluka (bioluminescence grade).

Human and murine Aβ40 peptide (sequences DAEFRHDSGYEVHHQKLVFFAEDVGSNKGAIIGLMVGGVV and DAEF*G*HDSG*F*EV*R*HQKLVFFAEDVGSNKGAIIGLMVGGVV) and the corresponding C-terminally truncated form at position 16 were bought from GeneCust (Dudelange, Luxembourg) with a minimum purity grade of 95%. The Aβ16-Y10F peptide was bought from Genscript (Piscataway, USA).

For truncated peptides: approx. 10 mM stock solution of peptide was prepared by dissolving the powder in milliQ water (resulting pH ~ 2). Peptide concentration was then determined by UV-visible absorption of Tyr10 considered as free tyrosine ($(\varepsilon_{276}-\varepsilon_{296})$ = 1410 $M^{-1}cm^{-1}$) for tyrosine-containing peptide and by UV-visible of two Phe ($(\varepsilon_{258}-\varepsilon_{280})$ = 390 $M^{-1}cm^{-1}$) for the mAβ and Y10F peptides.

Human Aβ40 peptide was prepared by dissolving the powder in milliQ water and peptide concentration was then determined by UV-visible absorption of Tyr10 considered as free tyrosine ($(\varepsilon_{293}-\varepsilon_{360})$ = 2400 $M^{-1}cm^{-1}$) in NaOH 1 M.

For some titration experiments the Aβ40 peptide was obtained by expression in E. coli and purified using HPLC as described before.[28] The identity of this peptide was verified by a ESI Q-ToF Premier mass spectrometer (Waters). Its purity was assessed by HPLC to exceed 98%.

Techniques.

UV-Vis spectra were recorded on a Hewlet Packard Agilent 8453 UV-Vis spectrometer at 25°C. The circular dichroism (CD) spectra were recorded at 25 °C on a J-815 spectropolarimeter (JASCO). Fluorescence measurements were recorded on a on a FluoroMax-4 spectrofluorometer in triplicate and representative data are given in the text. In all measurements, after each addition of Cu(II) or Gly, the solution was gently mixed up and fluorescence recorded until a stabilization of the value. In case of the full-length Aβ peptide, mixing of the solution was challenging even for very low concentration (below 10 µM) due to foam formation and maybe aggregation of the peptide Thus, it was difficult to obtain correct measurements reproducibly. It was also checked that the quenching of Tyr fluorescence was only due to specific Cu interaction with the Aβ peptides since no intensity decrease was observed for Cu addition to a non-coordination phenol water soluble molecule, except decrease due to inner-filter effect.

Equations.

For a molecule M, the fluorescence is given by $\Phi^M = \frac{F^M}{I_a^M}$

where F^M is the fluorescence intensity and $I_a{}^M$ the absorbed intensity given by:

$$I_a^M = I_i - I_t = I_i\left(1 - 10^{-\varepsilon^M_{\lambda exc}[M]l}\right)$$

where I_i is the incident intensity and I_t the transmitted intensity.

Because l is very small, it comes that $I_a^M = I_i . \ln 10 . \varepsilon^M_{\lambda exc} . l . [M]$

then, $F^M = I_i . \Phi^M . \ln 10 . \varepsilon^M_{\lambda exc} . l . [M]$

and $F^M = \varphi^M . [M] . I_t$,

with $I_t(x,y) = I_0 10^{-(abs(x)+abs(y))}$, where

$abs(x) = \varepsilon^M_{\lambda_{exc}} \cdot [M] \cdot x$ and $abs(y) = \varepsilon^M_{\lambda_{emt}} \cdot [M] \cdot y$

Finally, for a molecule M $F^M = \Phi_M . [M] . 10^{-(abs(x)+abs(y))}$

In the present case,

$$F = ([A\beta]\Phi_{A\beta} + [Cu(A\beta)]\Phi_{Cu(A\beta)} + [Cu_2(A\beta)]\Phi_{Cu_2(A\beta)}) . 10^{-abs(x)}$$ (**Eq. 1**), with

$$abs(x) = \varepsilon^{A\beta}_{278nm} \cdot [A\beta] \cdot x + \varepsilon^{Cu(A\beta)}_{278nm} \cdot [Cu(A\beta)] \cdot x + \varepsilon^{Cu_2(A\beta)}_{278nm} \cdot [Cu_2(A\beta)] \cdot x + \varepsilon^{Cu(buffer)}_{278nm} \cdot [Cu(buffer)] \cdot x$$
(**Eq. 2**)

Fitting procedures.

The apparent dissociation constant is defined as:

$$^{app}Kd = \frac{(M)(L)}{(ML)}$$

where $(M) = (M)_0 - (ML)$

$(L) = (L)_0 - (ML)$

Hence, it comes that (ML) is given by:

$$(ML) = \frac{1}{2}\left((M)_0 + (L)_0 + {}^{app}Kd - \sqrt{([M]_0 + [L]_0 + {}^{app}Kd)^2 - 4[M]_0[L]_0}\right)$$ (**Eq. 4**)

For each titration curve, an initial value of the conditional affinity is supposed and the apparent dissociation constant is calculated according to Eq. 3:

$$({}^{cond}K^{A\beta} = {}^{app}K^{A\beta}$$

$$\times\left(1 + \frac{[Gly]_0}{K^{Gly}_{d_1}} \times \frac{1}{\left(1 + 10^{-pH+pK^{Gly}_a}\right)} + \frac{[Gly]_0^2}{K^{Gly}_{d_1}K^{Gly}_{d_2}} \times \frac{1}{\left(1 + 10^{-pH+pK^{Gly}_a}\right)^2} + \frac{[Hepes]_0}{K^{Hepes}_d\left(1 + 10^{-pH+pK^{Hepes}_a}\right)}\right)$$

(**Eq. 3**)

where competition with hepes buffer has also been included but is negligible compared to competition with Gly, except for very low Gly concentration. $pK_a^{Hepes} = 7.41$, $K_d^{Hepes} = 10^{-3.28}$;[36] $pK_a^{Gly} = 9.53, K_{d_1}^{Gly} = 10^{-8.6}, K_{d_2}^{Gly} = 10^{-6.9}$ (hepes data from ref. [38], Gly data from the NIST database and ref. [38]).

Then, concentration of Cu, Aβ and Cu(Aβ) species are calculated according to Eq. 4 and the resulting fluorescence according to Eq. 1 to 3. Next, the initial conditional affinity value is adjusted to improve similarity between the experimental data and the calculated curve.

The intrinsic fluorescence coefficients Φ have been evaluated by dependence of the Tyr10 fluorescence on the fluorophore (Aβ, Cu(Aβ) and Cu_2(Aβ)) concentration (Figure S7).

Buffers.

Another important parameter to control is the nature of the buffer to use for the fluorescence experiments. The buffer should not interfere with Cu(II) binding to Aβ and have the maximum buffering effect near pH 7.4. The effect of various buffers on fluorescence of the Cu(Aβ16) complex was tested (Figure S6). Hepes has been chosen for the following reasons:

(i) hepes is a weak Cu(II) competitor,

(ii) Its buffering power lies in the best pH range (pKa = 7.4)

(iii) Its constant formation with Cu(II) has been evaluated and thus its contribution can be corrected.[36]

In specific cases, pipes has been used. They are: in the calibration curve of the Cu_2(Aβ) species, because hepes can compete with the second Cu site, the Tyr10 fluorescence recovery upon buffer addition for the initial point and EPR and CD experiments on the second Cu(II) binding.

Acknowledgments. Authors thank the ANR (Agence Nationale de la Recherche) for financial support (ANR Grant Neurometals NT09-488591). The support of grant 2741/B/H03/2010/38 by National Centre for Science, Poland is also acknowledged.

Supporting Information is available free of charge via the internet at http://pubs.acs.org.

References.

1. Holtzman, D. M.; Morris, J. C.; Goate, A. M., *Sci. Transl. Med.* **2011,** *3*, 77sr1.
2. Cappai, R.; Barnham, K. J., *Neurochem. Res.* **2008,** *33*, 526-532.
3. Hardy, J.; Selkoe, D. J., *Science* **2002,** *297*, 353-356.
4. Maccioni, R. B.; Muñoz, J. P.; Barbeito, L., *Arch. Med. Res.* **2001,** *32*, 367-381.
5. Bush, A. I., *Trends Neurosci.* **2003,** *26*, 207-214.
6. Multhaup, G.; Masters, C. L., *Met. Ions Biol. Syst.* **1999,** *36*, 365-387.
7. Roychaudhuri, R.; Yang, M.; Hoshi, M. M.; Teplow, D. B., *J. Biol. Chem.* **2009,** *284*, 4749-4753.
8. Kozlowski, H.; Janicka-Klos, A.; Brasun, J.; Gaggelli, E.; Valensin, D.; Valensin, G., *Coord. Chem. Rev.* **2009,** *253*, 2665-2685.
9. Hureau, C., *Coord. Chem. Rev.* **2012,** *256*, 2164-2174.
10. Faller, P.; Hureau, C., *Dalton Trans.* **2009**, 1080-1094.
11. Donnelly, P. S.; Xiao, Z.; Wedd, A. G., *Curr. Opin. Chem. Biol.* **2007,** *11*, 128-133.
12. Cuajungco, M. P.; Faget, K. Y., *Brain Res. Rev.* **2003,** *41*, 44-56.
13. Adlard, P. A.; Bush, A. I., *J Alzheimers Dis.* **2006,** *10*, 145-163.
14. Ono, K.; Yamada, M., *J. Neurochem.* **2011,** *117*, 19-28.
15. Haass, C.; Selkoe, D. J., *Nat. Rev. Cell. Mol. Biol.* **2007,** *8*, 101-112.
16. Gadad, B. S.; Britton, G. B.; Rao, K. S., *J. Alzheimers Dis.* **2011,** *24*, 223-232.
17. Hureau, C.; Sasaki, I.; Gras, E.; Faller, P., *ChemBioChem* **2010,** *11*, 950-953.
18. Rodriguez-Rodriguez, C.; Telpoukhovskaia, M.; Orvig, C., *Coord. Chem. Rev.* **2012,** *256*, 2308-2332.
19. Scott, L. E.; Orvig, C., *Chem. Rev.* **2009,** *109*, 4885-4910.
20. Zawisza, I.; Rozga, M.; Bal, W., *Coord. Chem. Rev.* **2012,** *256*, 2297-2307.
21. Garzon-Rodriguez, W.; Yatsimirsky, A. K.; Glabe, C. G., *Bioorg. Med. Chem. Lett.* **1999,** *9*, 2243-2248.
22. Syme, C. D.; Nadal, R. C.; Rigby, S. E.; Viles, J. H., *J. Biol. Chem.* **2004,** *279*, 18169-18177.
23. Karr, J. W.; Akintoye, H.; Kaupp, L. J.; Szalai, V. A., *Biochemistry* **2005,** *44*, 5478-5487.

24. Raman, B.; Ban, T.; Yamaguchi, K.; Sakai, M.; Kawai, T.; Naiki, H.; Goto, Y., *J. Biol. Chem.* **2005,** *280*, 16157-16162.

25. Ma, Q.-F.; Hu, J.; Wu, W.-H.; Liu, H.-D.; Du, J.-T.; Fu, Y.; Wu, Y.-W.; Lei, P.; Zhao, Y.-F.; Li, Y.-M., *Biopolymers* **2006,** *83*, 20-31.

26. Danielsson, J.; Pierattelli, R.; Banci, L.; Graslund, A., *FEBS J.* **2007,** *274*, 46-59.

27. Tõugu, V.; Karafin, A.; Palumaa, P., *J. Neurochem.* **2008,** *104*, 1249-1259.

28. Rozga, M.; Kłoniecki, M.; Dadlez, M.; Bal, W., *Chem. Res. Toxicol.* **2010,** *23*, 336-340.

29. Sarell, C. J.; Syme, C. D.; Rigby, S. E.; Viles, J. H., *Biochemistry* **2009,** *48*, 4388-4402.

30. Hatcher, L. Q.; Hong, L.; Bush, W. D.; Carducci, T.; Simon, J. D., *J. Phys. Chem. B.* **2008,** *112*, 8160-8164.

31. Hong, L.; Bush, W. D.; Hatcher, L. Q.; Simon, J. D., *J. Phys. Chem. B.* **2008,** *112*, 604-611.

32. Guilloreau, L.; Combalbert, S.; Sournia-Saquet, A.; Marzaguil, H.; Faller, P., *ChemBioChem* **2007,** *8*, 1317-1325.

33. Sacco, C.; Skowronsky, R. A.; Gade, S.; Kenney, J. M.; Spuches, A. M., *J. Biol. Inorg. Chem.* **2012,** *17*, 531-541.

34. Kowalik-Jankowska, T.; Ruta, M.; Wisniewska, K.; Lankiewicz, L., *J. Inorg. Biochem.* **2003,** *95*, 270-282.

35. Damante, C. A.; Osz, K.; Nagy, Z.; Pappalardo, G.; Grasso, G.; Impellizzeri, G.; Rizzarelli, E.; Sóvágó, I., *Inorg. Chem.* **2008,** *47*, 9669-9683.

36. Sokołowska, M.; Bal, W., *J. Inorg. Biochem.* **2005,** *99*, 1653-1660.

37. Hureau, C.; Dorlet, P., *Coord. Chem. Rev.* **2012,** *256*, 2175-2187.

38. Kiss, T.; Sovago, I.; Gergely, A., *Pure Appl. Chem.* **1991,** *63*, 597-638.

39. Trapaidze, A.; Hureau, C.; Bal, W.; Winterhalter, M.; Faller, P., *J. Biol. Inorg. Chem.* **2012,** *17*, 37-47.

40. Karr, J. W.; Szalai, V. A., *Biochemistry* **2008,** *47*, 5006-5016.

41. Hong, L.; Carducci, T. M.; Bush, W. D.; Dudzik, C. G.; Millhauser, G. L.; Simon, J. D., *J. Phys. Chem. B.* **2010,** *114*, 11261-11271.

42. Eury, H.; Bijani, C.; Faller, P.; Hureau, C., *Angew. Chem., Int. Ed. Engl.* **2011,** *50*, 901-905.

43. Faller, P.; Hureau, C.; Dorlet, P.; Hellwig, P.; Coppel, Y.; Collin, F.; Alies, B., *Coord. Chem. Rev.* **2012,** *256*, 2381-2396.

44. Hureau, C.; Coppel, Y.; Dorlet, P.; Solari, P. L.; Sayen, S.; Guillon, E.; Sabater, L.; Faller, P., *Angew. Chem., Int. Ed. Engl.* **2009,** *48*, 9522-9525.

45. Pedersen, J. T.; Teilum, K.; Heegaard, N. H. H.; Østergaard, J.; Adolph, H.-W.; Hemmingsen, L., *Angew. Chem., Int. Ed. Engl.* **2011,** *50*, 2532-2535.

46. Binolfi, A.; Quintanar, L.; Bertoncini, C. W.; Griesinger, C.; Fernández, C. O., *Coord. Chem. Rev.* **2012,** *256*, 2188-2201.

47. Crow, J. P.; Sampson, J. B.; Zhuang, Y.; Thompson, J. A.; Beckman, J. S., *J. Neurochem.* **1997,** *69*, 1936-1944.

48. Rozga, M.; Sokolowska, M.; Protas, A. M.; Bal, W., *J. Biol. Inorg. Chem.* **2007,** *12*, 913-918.

Table of content.

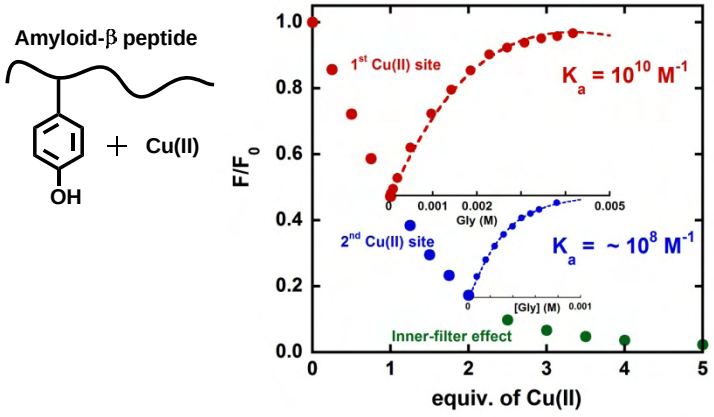

Zn impact on Cu coordination to the Alzheimer's peptide and its associated cell toxicity

Bruno Alies, Isabelle Sasaki, Stéphanie Sayen, Emmanuel Guillon, Peter Faller, Christelle Hureau

Chemical Communications
In preparation

The following article is about simultaneous coordination of Cu and Zn, the impact of their respective coordination and associated cell toxicity.

Journal Name

Dynamic Article Links ►

Cite this: DOI: 10.1039/c0xx00000x

www.rsc.org/xxxxxx

ARTICLE TYPE

Zn impact on Cu coordination to the Alzheimer's peptide and its associated cell toxicity.

Bruno Alies,[a] Isabelle Sasaki,[a] Stéphanie Sayen,[b] Emmanuel Guillon,[b] Peter Faller[a] and Christelle Hureau[a]

Received (in XXX, XXX) Xth XXXXXXXXX 20XX, Accepted Xth XXXXXXXXX 20XX

DOI: 10.1039/b000000x

Combined coordination of Zn^{II} and Cu^{I} or Cu^{II} to the amyloid-β peptide has been investigated by XANES, EPR and NMR spectroscopies. While Zn^{II} does alter CuII binding to Aβ, this has no effect on (Aβ)Cu induced ROS production and cell toxicity.

Extracellular amyloid deposits are one of the main morphological hallmark of Alzheimer's Disease (AD).[1] They are made of aggregated forms of a 40 to 42 residues peptide called amyloid-β (Aβ). In addition, they contain high levels of metal ions, mainly Cu and Zn, which are coordinated to the Aβ peptide. Aβ aggregation that can be modulated by metal ions is the central event of the amyloid cascade, a process proposed to initiate the AD pathology.[2, 3and refs therein] Reactive Oxygen Species (ROS) production linked to aberrant binding of the redox-active Cu ion has also been involved as a deleterious mechanism.[4] The Aβ peptide possesses multiple binding sites with the N-term amine, three His at positions 6, 13 and 14 and four carboxylic acids at positions 1, 3, 7 and 11. Zn level in the synaptic cleft can reach up to 300µM while Cu level is less well determined with reported concentrations in the µM to 100µM range (reviewed in ref. [3]). Hence, for those two reasons studies on simultaneous binding of Cu and Zn to Aβ are biologically relevant. In addition, although Zn is redox-silent, it has recently been proposed[5, 6] that it may change Cu binding to Aβ and, as a consequence, the associated ROS production. In contrast to Prion protein,[7-9] the simultaneous coordination of Cu and Zn to Aβ has only been scarcely investigated. In a pioneering report, Sovago and coworkers studied the impact of Zn addition on (Aβ)Cu^{II} species by speciation and EPR on an highly hydrosoluble PEG derivative of the Aβ peptide (PEG-Aβ16).[5] In contrast, independent Cu and Zn binding to Aβ have been extensively studied in the past ten years. Cu^{II} coordination is pH-dependent and two species noted components I and II coexist at physiological pH. In I (*resp.* II), Cu^{II} is linked to the N-term amine, the adjacent CO group, and two His imidazole rings, (*resp.* N-term amine, the adjacent deprotonated amide group, a CO group and one His imidazole ring).[10 and refs therein] Cu^{I} lies in a linear geometry between two His imidazole rings.[11, 12] Regarding Zn, the coordination picture is less clear, but involvement of at least two His residues, a carboxylate group and the N-term amine has been proposed.[13, 14 and refs therein] In the present report, we use a set of complementary spectroscopies to investigate the concomitant Cu and Zn binding to Aβ as well as interference of Zn in Cu mediated ROS production and cell toxicity.[1]

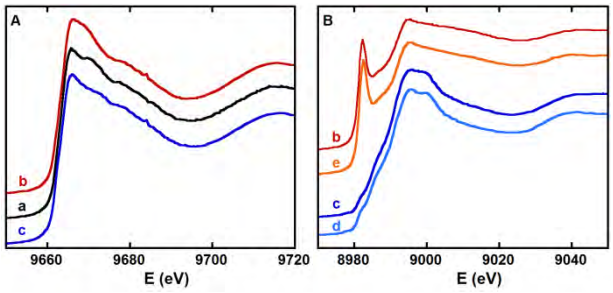

Figure 1. The X-ray absorption near edge structure (XANES) of the normalized absorption amplitude versus energy at the Zn (panel A) and Cu (panel B) K-edges of (a) (Aβ16)Zn, (b) (Aβ16)$ZnCu^{I}$, (c) (Aβ16)$ZnCu^{II}$, (d) (Aβ16)CuII and (e) (Aβ16)Cu^{I} complexes. [complexes] = 2 mM, [hepes] = 0.1 M, pH 7.4, T = 20 K.

To evaluate the effect of simultaneous Cu and Zn binding to Aβ, X-ray absorption spectroscopy is the most powerful technique since it permits to record both Zn and Cu^{I} or Cu^{II} signatures on the same sample depending on the chosen K-edge.[2] The Zn K-edge is reproduced in Figure 1, panel A. Presence of Cu^{I} or Cu^{II} modifies significantly the Zn XANES signature indicating changes in the Zn coordination site upon binding of either Cu^{I} or Cu^{II}. In contrast, the Cu^{I} XANES signature is not perturbed by the presence of Zn (Figure 1, panel B, (e) and (b)). This is particularly clear for the pre-edge associated with the 1s → 4p transition characteristic of a Cu^{I} coordinence of 2. For Cu^{II}, the situation is less obvious with a slight modification of the XANES signature observed at 9.00 keV. These changes due to Zn binding are reminiscent of what has been observed for component II of the (Aβ)Cu^{II} complex.[15] These first characterizations indicate that: (i) Zn can adopt several geometries, with Cu governing Zn coordination in the mixed Cu,Zn complexes. This is line with Cu^{II} and Cu^{I} having affinities higher than Zn affinity for Aβ.[16] (ii) in the (Aβ)$ZnCu^{I}$ complex, change in Zn coordination site is due to the requirement of two His residues for Cu^{I} binding, leaving only one His available for Zn binding which was proposed to require at least two His residues.[13] The unchanged Cu^{I} environment is also deduced from NMR

experiments (Figure 2, panel B) in which the shift of the aromatic His resonances is not modified by the presence of Zn, whatever the addition order of metal ions to the Aβ peptide (compare (d) and (e)). (iii) in the (Aβ)ZnCu^{II} complex, the situation is similar excepted that Cu^{II} requires more potential Zn ligands, such as for instance the -NH$_2$ terminal amine. This would explained why the (Aβ)ZnCu^{I} and the (Aβ)ZnCu^{II} signatures are different. In addition, Zn also induces a reshuffling of the Cu^{II} coordination sphere, with a Cu^{II} XANES spectrum that evolves towards that of component II. This effect is quite weak and can hardly be observed by XANES.

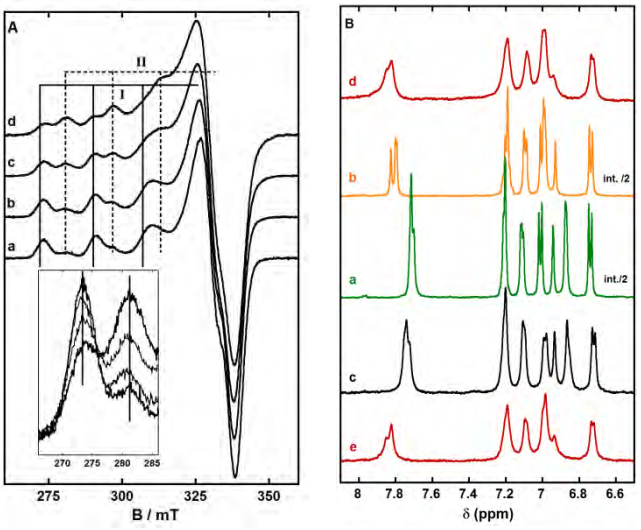

Figure 2. Panel A: EPR spectra of (Aβ16)Cu^{II} complex in presence of increasing equiv. of Zn^{II}: (a) without Zn, (b) 0.5 equiv., (c) 1 equiv. and (d) 2 equiv. Inset: amplification of the first hyperfines lines of spectra (a) to (d). [(Aβ16)Cu^{II}]= 1mM, [hepes] = 0.1 M, pH 7.4, *T* = 110 K, mod. ampl. 1 mT, microwave power: 20 mW, ν = 9.51 GHz. Panel B: NMR spectra of (a) Aβ16 peptide and complexes (b) (Aβ16)Cu^{I}, (c) (Aβ16)Zn, (d) (Aβ16)ZnCu^{I} where Cu^{I} was added to (Aβ16)Zn and (e) (Aβ16)Cu^{I}Zn where Zn was added to (Aβ16)Cu^{I}. [complexes]= 1mM, [d^{11}-Tris] = 50 mM pH = 7.4, *T* = 300 K, ν = 500 MHz.

In contrast, modifications of the (Aβ)Cu^{II} EPR traces upon addition of increasing equivalent of Zn are unambiguous (Figure 2, panel A). Indeed the ratio between the EPR signatures of components I and II evolves from 80/20[3] for the (Aβ)Cu^{II} to 55/45 for the (Aβ)ZnCu^{II} and to 40/60 in presence of one additional Zn equiv.. Similar trends were previously observed for mixed Zn and Cu coordination to the PEG-Aβ16.[5, 4] Such reorganization of the Cu^{II} sphere is in line with the reported involvement of at least two His residues in Zn binding.[13] In addition as Cu^{II} can change its coordination, Zn succeeds in pushing it toward a component II environment, as previously deduced for the PEG-Aβ16 by EPR and speciation study.[5] Such reorganization of the Cu^{II} site might induce a change in the redox properties of the Cu centre and thus of its ability to produce ROS and to induce cell damages.

In Figure 3, the (Aβ)Cu mediated ROS production is monitored by consumption of Ascorbate used here as the Cu^{II} reductant (panel A) and has been confirmed by classical Amplex Red and CCA assays (data not shown). Addition of Zn in the course of the experiment does not change the Asc consumption. Same results are obtained when Zn is initially present and incubated with the (Aβ)Cu species. In addition, (Aβ)Cu induced cell toxicity is not influenced by the presence of Zn in the media (Figure 3, panel B).

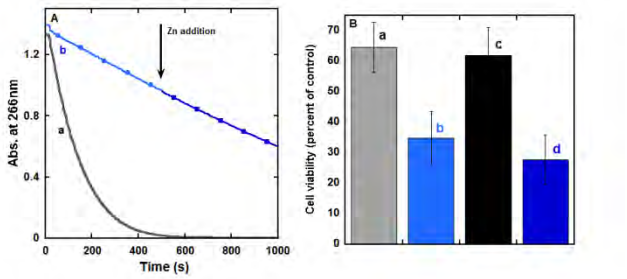

Figure 3. Panel A: Consumption of ascorbate by (a) unbound Cu^{II} and (b) (Aβ40)Cu^{II} without Zn (plain circles) and with Zn (plain squares). [Aβ40] = 7 µM, [Cu^{II}] = 5 µM, [Zn^{II}] = 5 µM, [Asc] = 100 µM, [PO$_4$] = 50 mM pH 7.4. Panel C: Cell viability measurements by MTT assay of (a) Aβ40, (b) (Aβ40)Cu^{II}, (c) (Aβ40)Zn and (d) (Aβ40)ZnCu^{II}, [Aβ40] = 10 µM, [Cu] or [Zn] = 9 µM, [Asc] = 500 µM.

Conclusions

Altogether these data indicate that modification of the Cu^{II} coordination site induced by the Zn ion is not sufficiently important to significantly interfere with (Aβ)Cu ROS production, in contrast to what was proposed in previous reports.[5, 6] More importantly, Zn does not influence the (Aβ)Cu induced cell Hence, the proposed protective role of Zn (for a recent article, see ref. [17]) may be related to modulation of Aβ aggregation ability or to other mechanisms linked to the AD aetiology and not only to variation of the (Aβ)Cu cell toxicity associated to ROS production.

Acknowledgements. We acknowledge the ESRF for provision of synchrotron radiation on the FAME beamline (Proposals CH 3245 and CH 3469). C. Bijani (LCC) is acknowledged for NMR measurements.

Notes and references

[a] *CNRS ; LCC (Laboratoire de Chimie de Coordination) ; 205, route de Narbonne, F-31077 Toulouse, France. Université de Toulouse; UPS, INPT ; LCC ; F-31077 Toulouse, France, +33 5 61 33 31 62, christelle.hureau@lcc-toulouse.fr*

[b] *Institut de Chimie Moléculaire de Reims (ICMR, CNRS UMR 7312), Groupe de Chimie de Coordination, Université de Reims Champagne-Ardenne, BP 1039, 51687 Reims Cedex 2, France*

†Electronic Supplementary Information (ESI) available: [Material and Methods section, EPR and NMR data at [peptide] = 200 µM, ROS productions assays for the Aβ16 peptide]. See DOI: 10.1039/b000000x/

1. D. M. Holtzman, J. C. Morris and A. M. Goate, *Sci. Transl. Med.*, 2011, **3**, 77sr71.
2. D. J. Selkoe, *Science*, 2002, **298**, 789-791.
3. C. Hureau, *Coord. Chem. Rev.*, 2012, **256**, 2164-2174.

This journal is © The Royal Society of Chemistry [year]

4. S. Chassaing, F. Collin, P. Dorlet, J. Gout, C. Hureau and P. Faller, *Current Topics in Medicinal Chemistry*, 2012, **in press**.
5. C. A. Damante, K. Ösz, Z. Nagy, G. Grasso, G. Pappalardo, E. Rizzarelli and I. Sóvágó, *Inorg. Chem.*, 2011, **50**, 5342-5350.
6. L. Liu and X. Ning, *Biochem. Biophys. Res. Commun.*, 2012, **417**, 153-155.
7. F. Stellato, A. Spevacek, O. Proux, V. Minicozzi, G. Millhauser and S. Morante, *Biophys. J.*, 2011, **40**, 1259-1270.
8. E. D. Walter, D. J. Stevens, M. P. Visconte and G. L. Millhauser, *J. Am. Chem. Soc.*, 2007, **129**, 15440-15441.
9. V. Jószai, I. Turi, C. Kállay, G. Pappalardo, G. Di Natale, E. Rizzarelli and I. Sóvágó, *J. Inorg. Biochem.*, 2012, **112**, 17-24.
10. C. Hureau and P. Dorlet, *Coord. Chem. Rev.*, 2012, **256**, 2175-2187.
11. C. Hureau, V. Balland, Y. Coppel, P. L. Solari, E. Fonda and P. Faller, *J. Biol. Inorg. Chem.*, 2009, 995-1000.
12. J. Shearer and V. A. Szalai, *J. Am. Chem. Soc.*, 2008, **130**, 17826-17835.
13. C. Migliorini, E. Porciatti, M. Luczkowski and D. Valensin, *Coord. Chem. Rev.*, 2012, **256**, 352-368.
14. V. Tôugu and P. Palumaa, *Coord. Chem. Rev.*, 2012, **256**, 2219-2224.
15. C. Hureau, Y. Coppel, P. Dorlet, P. L. Solari, S. Sayen, E. Guillon, L. Sabater and P. Faller, *Angew. Chem., Int. Ed. Engl.*, 2009, **48**, 9522-9525.
16. I. Zawisza, M. Rozga and W. Bal, *Coord. Chem. Rev.*, 2012, **256**, 2297-2307.
17. C. Corona, F. Masciopinto, E. Silvestri, A. D. Viscovo, R. Lattanzio, R. L. Sorda, D. Ciavardelli, F. Goglia, M. Piantelli, L. M. Canzoniero and S. L. Sensi, *Cell Death Dis.*, 2010, **1**.

1 Note that for the spectroscopic studies the short truncated Aβ16 peptide was used. It is a valuable model of metal ions binding to the full-length Aβ40/42 peptides (reviewed in ref. 3). For the ROS production studies Aβ40 or Aβ16 were used and give the same results (Aβ16 data are in the Supporting Information). For cell studies Aβ40 was used. For simplicity purpose, Aβ is used in the text while the nature of the peptide used is given in the Figure captions.

2 The order of Zn or Cu addition does not change the XANES signatures detected.

3 For quantification of each component, the EPR spectra of the pure components I and II were recorded in absence of Zn at pH 6.5 and 8.7, respectively and the proportion of I and II were deduced from linear combination for [Zn]-dependent spectra.

4 Note that as was previously pointed out in ref. 5, Zn addition to (Aβ)Cu complex at [Aβ] = 1mM induces a partial precipitation of the corresponding species. With [Aβ] = 0.2mM, no precipitation occurs. As a consequence, we have checked that the partial precipitation observed at [Aβ] = 1mM did not lead to a change in the spectroscopic signatures of the mixed Cu,Zn complexes (See Supporting Information).

A new water-soluble Cu(II) chelator that retrieves Cu from Cu(amyloid-β) species, stops associated ROS production and prevents Cu(II) induced Aβ aggregation

Sabrina Noël, Fabien Perez, Jeppe T. Pedersen, Bruno Alies, Sonia Ladeira, Stéphanie Sayen, Emmanuel Guillon, Emmanuel Gras, Christelle Hureau

Journal of Inorganic Biochemistry
2012

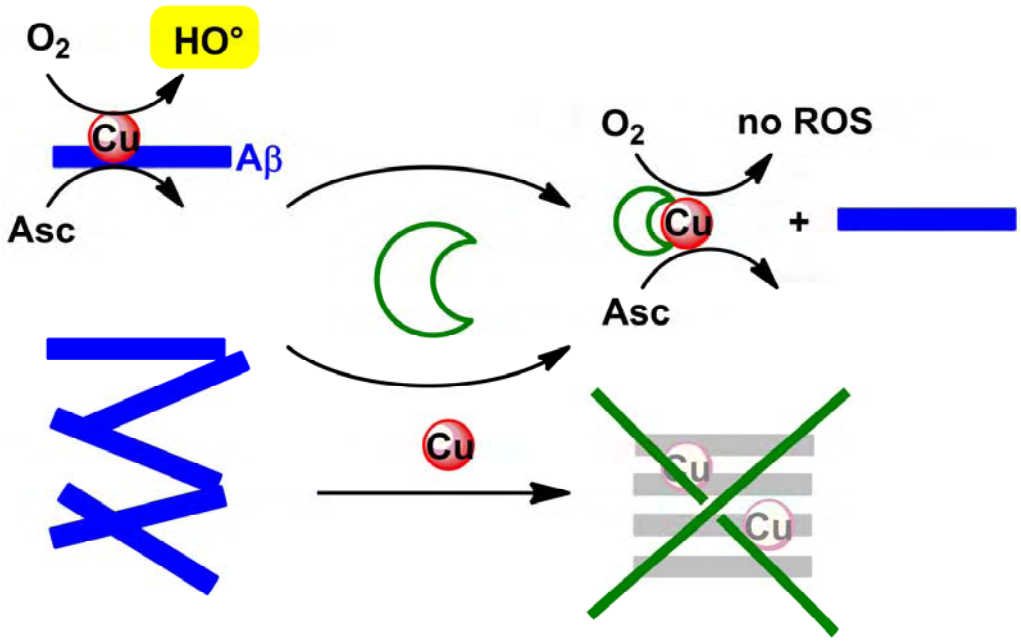

The following article is about synthesis and physicochemical studies of new water soluble Cu(II) chelator. This chelator is enabled to stop Aβ-Cu induced ROS production and aggregation. Due to my experience in peptide aggregation, I contributed to the Aβ1-40 aggregation studies.

Journal of Inorganic Biochemistry xxx (2012) xxx–xxx

Contents lists available at SciVerse ScienceDirect

Journal of Inorganic Biochemistry

journal homepage: www.elsevier.com/locate/jinorgbio

A new water-soluble Cu(II) chelator that retrieves Cu from Cu(amyloid-β) species, stops associated ROS production and prevents Cu(II)-induced Aβ aggregation ☆

Sabrina Noël [a,b], Fabien Perez [a,b], Jeppe T. Pedersen [c], Bruno Alies [a,b], Sonia Ladeira [a,b], Stéphanie Sayen [d], Emmanuel Guillon [d], Emmanuel Gras [a,b], Christelle Hureau [a,b,*]

[a] CNRS, LCC (Laboratoire de Chimie de Coordination), 205 route de Narbonne, BP 44099, F-31077 Toulouse Cedex 4, France
[b] Université de Toulouse, UPS, INPT, F-31077 Toulouse Cedex 4, France
[c] Department of Chemistry, Faculty of Science, University of Copenhagen, Universitetsparken 5, DK-2100 Copenhagen, Denmark
[d] Institut de Chimie Moléculaire de Reims (ICMR, CNRS UMR 7312), Groupe de Chimie de Coordination, Université de Reims Champagne-Ardenne, BP 1039, 51687 Reims Cedex 2, France

ARTICLE INFO

Article history:
Received 1 March 2012
Received in revised form 30 May 2012
Accepted 30 May 2012
Available online xxxx

Keywords:
Copper
Chelator
Peptide
Alzheimer
ROS
Aggregation

ABSTRACT

The synthesis of the H_2L^{2-} ligand (*N*,*N*′-Bis[(5-sulfonato-2-hydroxy)benzyl]-*N*,*N*′-dimethyl-ethane-1,2-diamine) and characterizations of the corresponding Cu(II) complex $[Cu(L)(H_2O)]^{2-}$ (**1**) by X-ray diffraction, EPR, UV–Visible and potentiometry are described. At pH 7.4, the affinity of Cu(II) for this ligand is approximately 4×10^{14} M^{-1}. Coordination of redox active metal ions such as copper or iron to the amyloid-β (Aβ) peptide has been linked to deleterious processes encountered in the etiology of Alzheimer disease (AD), such as Aβ aggregation and reactive oxygen species (ROS) production. In this context, the ability of the H_2L^{2-} to extract Cu(II) from Cu(Aβ) species where Aβ is the peptide involved in AD, is reported as well as its capacity to redox silence the Cu(Aβ) induced ROS formation and to prevent Cu(II)-induced Aβ aggregation. Such water soluble sulfonato-derivatives of Cu(II) chelators are very interesting counterparts for *in vitro* study of chelators' properties required to attend further biological applications as therapeutic tools against AD.

© 2012 Elsevier Inc. All rights reserved.

1. Introduction

Alzheimer disease (AD) is a neurodegenerative disorder characterized by extracellular deposits of amyloid-β (Aβ) peptides, known as senile plaques. High concentration of metal ions, mainly Cu, Zn and Fe have been found co-localized with the senile plaques and deleterious interactions of these ions with soluble and aggregated forms of Aβ peptide have been associated to the development of AD [1–5]. Metal ions can modulate the Aβ peptide aggregation leading to amyloid deposits [6]. Furthermore, redox active Cu and Fe ions impact the production of reactive oxygen species (ROS) [7,8]. A conceptual view of ROS formation is shown in Scheme 1. A valuable approach to fight against AD relies on the design and development of Cu chelators that should be strong enough to remove Cu(II) from Aβ but not from essential metalloproteins. Recently several groups have conceived such new molecules (see Refs. [9–16] and for recent reviews, Refs. [17–19]). More particularly, in a pioneering work, Orvig has developed gluco-conjugated schiff based ligands, namely H_2GL^1 (*N*,*N*′-Bis[(5-β-D-glucopyranosyloxy-2-hydroxy)benzyl]-*N*,*N*′-dimethyl-ethane-1,2-diamine) and H_2GL^2 (*N*,*N*′-Bis[(5-β-D-glucopyranosyloxy-3-*tert*-butyl-2-hydroxy)benzyl]-*N*,*N*′-dimethyl-ethane-1,2-diamine) that have shown promising *in vitro* properties as therapeutic tools against AD [15]. Herein, we report the study of a related ligand, H_2L^{2-}(*N*,*N*′-Bis[(5-sulfonato-2-hydroxy)benzyl]-*N*,*N*′-dimethyl-ethane-1,2-diamine) in which the phenolato groups are sulfonated, leading to a water-soluble counterpart of the well-known $(Me)_2$salan (*N*,*N*′-Bis[(2-hydroxy)benzyl]-*N*,*N*′-dimethyl-ethane-1,2-diamine). Such water-soluble ligands are perfectly designed for *in vitro* biophysical investigations (determination of Cu(II) affinity, spectroscopic characterizations of the Cu(II)

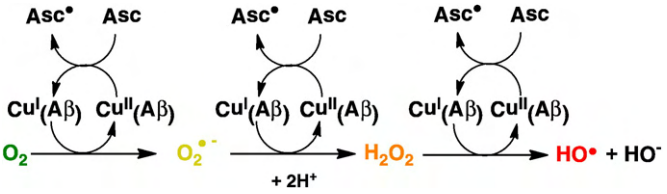

Scheme 1. Cu(Aβ) mediated ROS production.

☆ We thank H. Eury and P.-L. Puyjalon for preliminary results, M. van de Weert and S. L. Svenningsen for use of plate reader systems, and C. Valentin for potentiometric titrations. P. Faller is acknowledged for valuable discussion. This work was supported by the Région Midi-Pyrénées (funding of S. N.) and Villum Kann Rasmussen (funding of J. T. P.).

* Corresponding author at: CNRS, LCC (Laboratoire de Chimie de Coordination), 205 route de Narbonne, BP 44099, F-31077 Toulouse Cedex 4, France.
E-mail address: christelle.hureau@lcc-toulouse.fr (C. Hureau).

0162-0134/$ – see front matter © 2012 Elsevier Inc. All rights reserved.
doi:10.1016/j.jinorgbio.2012.05.016

ARTICLE IN PRESS

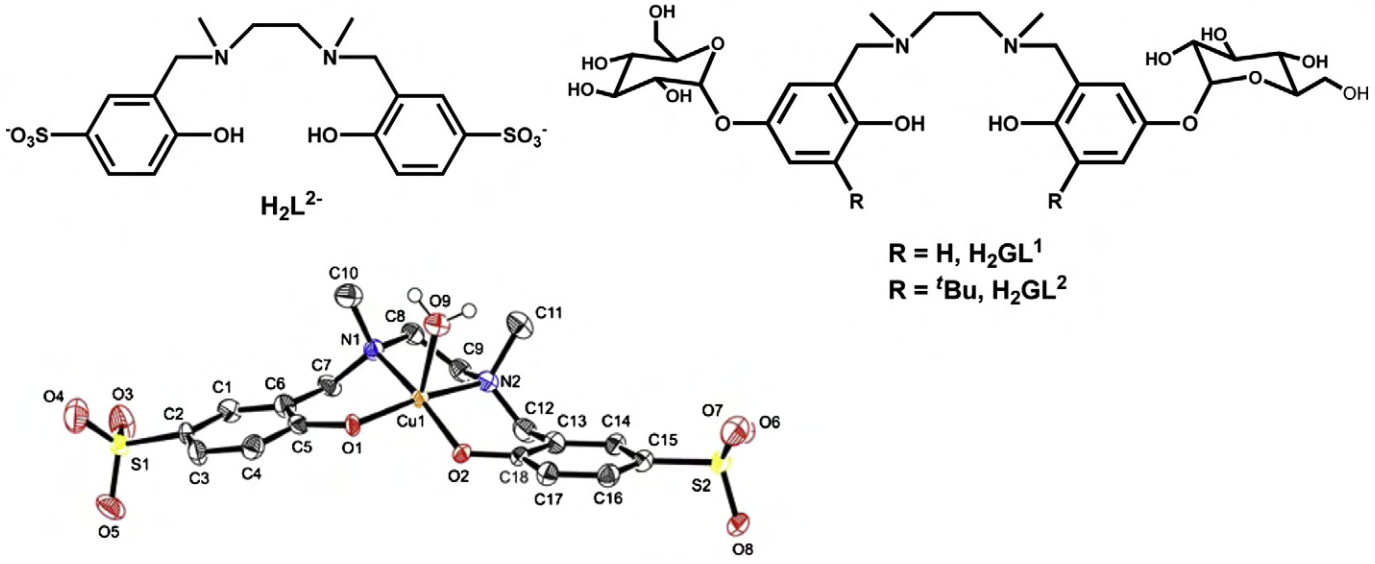

Fig. 1. Top: Ligand H_2L^{2-}, H_2GL^1 and H_2GL^2 for comparison. Bottom: Ellipsoid plot (50% level, H and disorders atoms are omitted for clarity, excepted for the apical water molecule) of $[Cu(L)(H_2O)]^{2-}$ (**1**).

complexes…). Furthermore, the properties of the chelating scaffold are anticipated to vary minimally between the water-soluble and its parent ligand that should be preferred for further biological applications. Although sulfonation is the most straightforward way to obtain water-soluble counterparts, such strategy has still been poorly investigated in the context of AD.

Ligand H_2L^{2-} has been obtained by a Mannich reaction according to Ref. [15]. Reaction with $CuCl_2$ in a methanol/water mixture gave access to crystals of $[Cu(L)(H_2O)]^{2-}$ (**1**) suitable for X-ray crystallography study (Fig. 1,[1] Table 1 and see details in the Supporting information).

1.1. Physico-chemical properties of **1**

Complex **1** has been characterized by EPR ($g_{//} = 2.23(5)$ and $A_{//}(^{63}Cu) = 190\times10^{-4}\,cm^{-1}$) and UV–Vis ($\varepsilon_{390} = 1200$ and $\varepsilon_{620} = 240\,M^{-1}.cm^{-1}$) (Fig. 2c). The parameters are comparable to those of the H_2GL^1 ligand although the later ones have been determined in MeOH. [15] The H_2L^{2-} ligand and its corresponding Cu complexes have been studied by potentiometry. The overall acidity constants of the ligand (β_{01h}) and of the Cu(II) complexes (β_{11h}) are given in Table 2.[2] At pH 7.4, the ligand is mainly obtained as H_3L^- and the Cu(II) species as $[Cu(L)(H_2O)]^{2-}$ (**1**) that predominates in a 5-pH unit range around pH 7.4. From the parameters determined by potentiometry, a conditional affinity value of $4.4\times10^{14}\,M^{-1}$ is found at pH 7.4 (Eq. (S3)), 50 times stronger than that reported for the H_2GL^1 ligand [15]. We have also performed competition experiments with the DAHK (Asp-Ala-His-Lys) peptide to confirm[3] our value. Indeed, the Cu(II) conditional affinity for DAHK has been evaluated by several groups which concur to a value of $4.7\times10^{13}\,M^{-1}$ at pH 7.4 [20]. Competition between H_2L^{2-} and DAHK for Cu(II) was monitored by EPR and UV–Vis spectroscopies (compare a), b) and c) in Fig. 2) and showed that H_2L^{2-} is about a 7 ± 3 times stronger Cu(II) ligand than DAHK, leading to a conditional affinity value of $3\pm1.5\times10^{14}\,M^{-1}$ in full agreement with potentiometric titration. The ability of ligand H_2L^{2-} to remove Cu(II) from Cu(Aβ) species at physiological pH is expected from the value of the conditional affinity reported for Aβ (10^{-10} M) [1]. Competition experiments by EPR and UV–Vis (compare c) d) and e)) in Fig. 2) confirm that in the presence of H_2L^{2-}, Cu(II) is completely removed from Cu(Aβ) species.

1.2. Prevention of Cu(II)-induced Aβ aggregation

As anticipated based on previously reported data for the parent H_2GL^1 ligand [15], ligand H_2L^{2-} prevents Cu(II)-induced aggregation of the native Aβ40 peptide (Fig. 3) as probed by the well-known Thioflavine T (ThT) fluorescence experiments, in which an enhanced ThT fluorescence indicates the formation of fibrillar Aβ aggregates (see Supporting information for details). Because Aβ aggregation is highly intricate and versatile by itself, [5] we have performed two series of measurements with different conditions (pH, peptide source, etc.). Although Cu(II) provokes different Aβ aggregation profiles in the two experiments, the H_2L^{2-} ligand prevents Cu(II)-induced Aβ aggregation whatever the conditions. In the first case (Fig. 3A), it delays the Cu(II)-induced aggregation of Aβ40 and decreases the quantity of fibrillar aggregates formed. In the second case (Fig. 3B), addition of the H_2L^{2-} ligand to Cu(II) Aβ40 mixture leads to an aggregation process reminiscent of what is observed in absence of Cu(II).

Table 1
Selected bond lengths and angles for **1**.

Bond length (Å)		Angle (°)	
Cu–O1	1.924 (4)	O1–Cu–O2	84.20 (16)
Cu–O2	1.936 (4)	O1–Cu–N1	93.29 (18)
Cu–N1	2.017 (5)	N1–Cu–N2	87.4 (3)
Cu–N2	2.018 (7)	O2–Cu–N2	94.3 (2)
Cu–O9	2.495 (5)		

[1] The Cu(II) ion lies in a distorted square-based pyramid, where the equatorial plan is made of two nitrogen atoms from the tertiary amines and two oxygen atoms from the phenolato groups. A water molecule occupies the apical position. This structure differs from that of $Cu(GL^2)$ reported by Orvig and coworkers [15] in line with different crystal packing effects observed in the two crystals. Indeed, in the present case, complex **1** is obtained as a sodium-bridged dinuclear species (Fig. S1).

[2] Attribution of pKa values show that in contrast to what was observed for the H_2GL^1 ligand, [15] the two phenolic functions are deprotonated before the second tertiary amine.

[3] The difference in the conditional affinity observed at pH 7.4 between the H_2L^{2-} and H_2GL^1 ligands might be unexpected based only on the electron-withdrawing/electron-donating properties of both ligands but may have several other origins. Indeed, this value is a multiple function of β_{11h} and of the ligand basicity. It may reflect difference in charge distribution and steric effects and may also originate from differences in the experimental conditions. In particular, in the Orvig's study, [15] the ionic strength was 0.16 M in NaCl. Although chloride is a weak Cu(II) ligand, in such a 1000-fold excess, it can interfere in the determination of the β_{mlh}.

Please cite this article as: S. Noël, et al., A new water-soluble Cu(II) chelator that retrieves Cu from Cu(amyloid-β) species, stops associated ROS product..., J. Inorg. Biochem. (2012), doi:10.1016/j.jinorgbio.2012.05.016

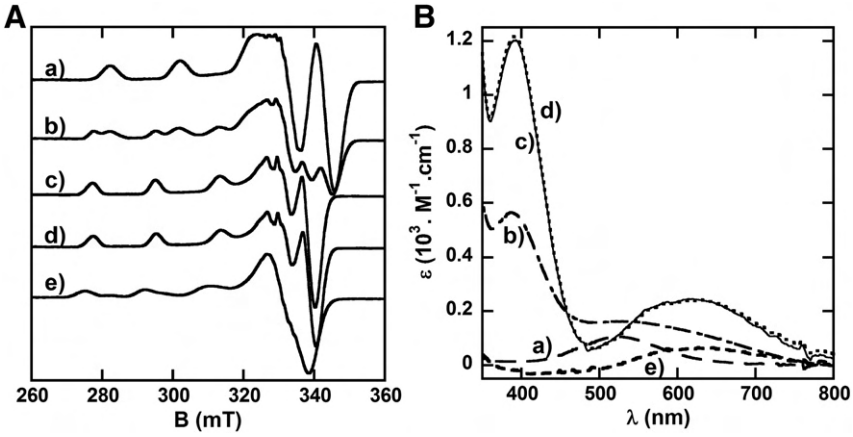

Fig. 2. ^{63}Cu EPR (panel A) and UV–Vis spectra (panel B) of a) [Cu(DAHK)], b) **1** in presence of 5 equiv. of DAHK, c) **1**, d) Cu(Aβ) in presence of 1 equiv. of H_2L^{2-}, e) Cu(Aβ). [Cu(II)] = 0.9 mM, [ligand] = 1 mM. [hepes] = 50 mM, pH 7.4. UV–Vis recording conditions: ℓ = 1 cm, T = 25 °C; EPR recording conditions: ν = 9.53 GHz; T = 100 K, microwave power = 20 mW, modulation amplitude 0.5 mT.

1.3. Inhibition of Cu(Aβ) ROS production

In contrast to prevention of Cu(II)-induced Aβ aggregation that was previously shown by Orvig, [15] no direct measurement of impact of the $(Me)_2$salan scaffold on ROS production by Cu(Aβ) has been reported in the literature. Ligand H_2L^{2-} was therefore probed for its ability to stop Cu(Aβ) ROS production using recently developed *in vitro* tests [9,10]. As ROS production by Cu species requires the reduction of the air-stable Cu(II) by ascorbate (Asc) (Scheme 1), the rate of Asc consumption is indicative of the Cu species' ability to produce ROS. Alternatively, $HO^{\bullet}$ formation is monitored by formation of the fluorescent 7-OH-CCA dye from 3-CCA (coumarin-3-carboxylic acid). As illustrated in Fig. 4, "free" Cu(II), *i.e.* Cu weakly bound to buffer is the most efficient species in consuming Asc and producing $HO^{\bullet}$. Cu(II) coordination to Aβ significantly slows down both processes, in line with a sluggish redox cycling of the Cu(Aβ) complex compared to "free" Cu [21]. Cu(II) coordination to H_2L^{2-} lowers Asc consumption and $HO^{\bullet}$ formation to the background level, in line with no cathodic process observed down to −0.6 V *vs.* NHE (normal hydrogen electrode) by voltammetry (Fig. S7). Also, when H_2L^{2-} is added to Cu(Aβ) species after incubation, Asc consumption and $HO^{\bullet}$ formation are reduced to the background level.

The data reported here strongly support that the salan scaffold is well-appropriate to eliminate deleterious effects related to Cu binding to Aβ. *In cello* study on ligands H_2L^{2-} and $(Me)_2$salan is under investigation in our group to determine whether the *in vitro* encouraging results are confirmed in biological conditions.

Table 2
Logarithmic values of the overall acidity constants of the ligand (β_{01h}) and of the overall stability constants of Cu(II) complexes (β_{m1h}), standard deviation is indicated in parenthesis for the last digit. I = 0.1 M KNO_3, T = 25 °C (see speciation diagrams in Figs. S3 and S4). Attribution of pKa values has been performed by UV–Vis and ^{1}H NMR titrations (Figs. S5 and S6).

log β_{mlh} [a]	L	pK_a	Attribution
log β_{0l4}	34.24 (7)	5.05 (3)	Tertiary amine
log β_{0l3}	29.19 (6)	7.79 (3)	Phenol
log β_{0l2}	21.40 (4)	9.72 (2)	Phenol
log β_{0l1}	11.68 (4)	11.68 (4)	Tertiary amine
log β_{112}	29.1 (2)	–	
log β_{111}	25.75 (4)	–	
log β_{110}	21.79 (3)	10.7	
log $\beta_{11\text{-}1}$	11.09 (4)	–	

[a] $\beta_{mlh} = \frac{[M_mL_lH_h]}{[M]^m[L]^l[H]^h}$ where $mM + lL + hH \rightleftharpoons M_mL_lH_h$.

Appendix A. Supplementary data

Supplementary data to this article can be found online at http://dx.doi.org/10.1016/j.jinorgbio.2012.05.016.

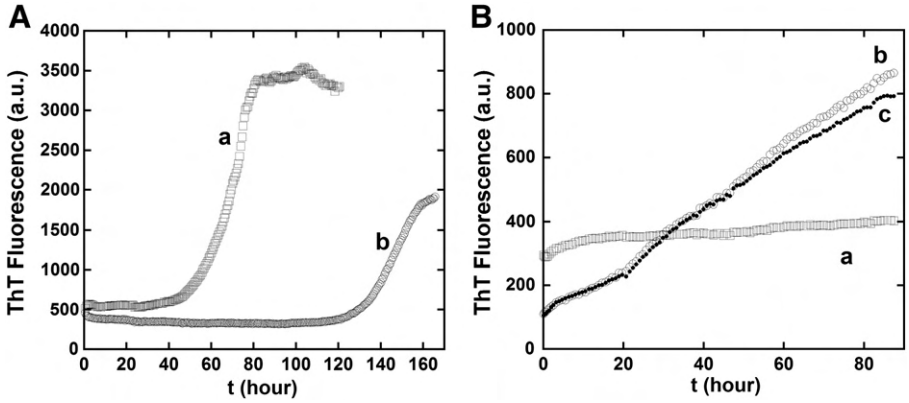

Fig. 3. Prevention of Cu(II)-induced Aβ40 aggregation, Panel A: a) [peptide A] = 40 μM, [Cu(II)] = 20 μM, b) [peptide A] = 40 μM, [Cu(II)] = 20 μM, [H_2L^{2-}] = 40 μM; [ThT] = 20 μM, T = 37 °C, [Hepes] = 20 mM, pH 7.4, NaCl 0.1 M. Panel B: a) [peptide B] = 40 μM, [Cu(II)] = 20 μM, b) [peptide A] = 40 μM, [Cu(II)] = 20 μM, [H_2L^{2-}] = 40 μM, c) [peptide B] = 40 μM; [ThT] = 10 μM, T = 25 °C, [Pipes] = 100 mM, pH 6.5. (For source and preparation of peptides A and B, see Supporting information).

ARTICLE IN PRESS

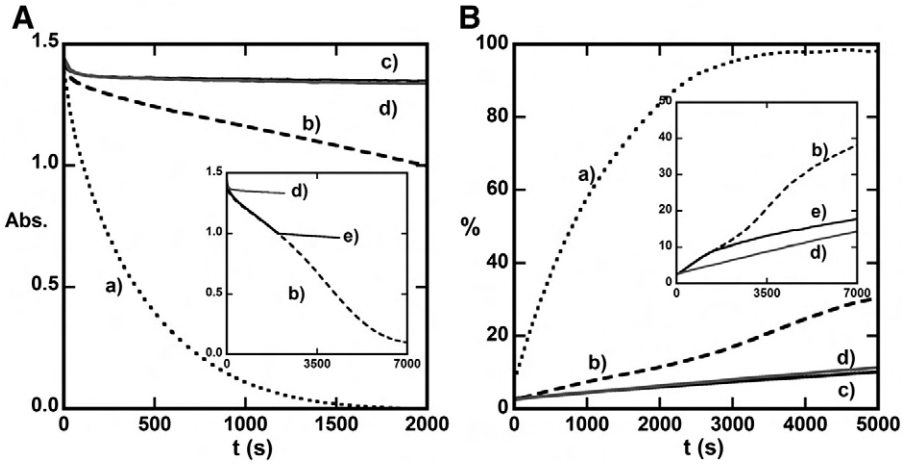

Fig. 4. Panel A: Cu(II) induced ascorbate consumption, a)[Cu(II)] = 1 μM, b) in presence of 1.2 equiv. of Aβ peptide, c) in presence of 1.2 equiv. of H_2L^{2-}, d) control experiment without Cu(II). Inset: e) in presence of 1.2 equiv. of Aβ peptide and after addition of 1.2 equiv. of H_2L^{2-} at t = 1400 s. λ = 265 nm, [Asc] = 100 μM, [hepes] = 50 mM, pH 7.4, ℓ = 1 cm, T = 25 °C, vigorous stirring. Panel B: Cu(II) induced 7-OH-CCA formation, a)[Cu(II)] = 10 μM, b) in presence of 1.2 equiv. of Aβ peptide, c) in presence of 1.2 equiv. of H_2L^{2-}, d) control experiment without Cu(II). Inset: e) in presence of 1.2 equiv. of Aβ peptide and after addition of 1.2 equiv. of H_2L^{2-} at t = 1000 s. λ_{em} = 452 nm, [Asc] = 1 mM, [PO_4] = 50 mM, pH 7.4, [CCA] = 0.5 mM, T = 25 °C.

References

[1] P. Faller, C. Hureau, Dalton Trans. (2009) 1080–1094.
[2] Y.H. Hung, A.I. Bush, R.A. Cherny, J. Biol. Inorg. Chem. 15 (2010) 61–76.
[3] R.R. Crichton, D.T. Dexter, R.J. Ward, Coord. Chem. Rev. 252 (2008) 1189–1199.
[4] P.S. Donnelly, Z. Xiao, A.G. Wedd, Curr. Opin. Chem. Biol. 11 (2007) 128–133.
[5] C. Hureau, Coord. Chem. Rev. (in press) http://dx.doi.org/10.1016/j.ccr.2012.03.037.
[6] R. Roychaudhuri, M. Yang, M.M. Hoshi, D.B. Teplow, J. Biol. Chem. 284 (2009) 4749–4753.
[7] C. Hureau, P. Faller, Biochimie 91 (2009) 1212–1217.
[8] K.J. Barnham, C.L. Masters, A.I. Bush, Nat. Rev. Drug Discov. 3 (2004) 205–214.
[9] M. Jensen, A. Canning, S. Chiha, P. Bouquerel, J.T. Pedersen, J. Østergaard, O. Cuvillier, I. Sasaki, C. Hureau, P. Faller, Chem. Eur. J. 18 (2012) 1161–1167.
[10] L. Perrone, E. Mothes, M. Vignes, A. Mockel, C. Figueroa, M.C. Miquel, M.L. Maddelein, P. Faller, ChemBioChem 11 (2010) 110–118.
[11] D.S. Folk, K.J. Franz, J. Am. Chem. Soc. 132 (2010) 4994–4995.
[12] A. Lakatos, E. Zsigó, D. Hollender, N.V. Nagy, L. Fülöp, D. Simon, Z. Bozsó, T. Kiss, Dalton Trans. 39 (2010) 1302–1315.
[13] D.E. Green, M.L. Bowen, L.E. Scott, T. Storr, M. Merkel, K. Böhmerle, K.H. Thompson, B.O. Patrick, H.J. Schugar, C. Orvig, Dalton Trans. 39 (2010) 1604–1615.
[14] C. Deraeve, C. Boldron, A. Maraval, H. Mazarguil, H. Gornitzka, L. Vendier, M. Pitié, B. Meunier, Chem. Eur. J. 14 (2008) 682–696.
[15] T. Storr, M. Merkel, G.X. Song-Zhao, L.E. Scott, D.E. Green, M.L. Bowen, K.H. Thompson, B.O. Patrick, H.J. Schugar, C. Orvig, J. Am. Chem. Soc. 129 (2007) 7453–7463.
[16] W.H. Wu, P. Lei, Q. Liu, J. Hu, A.P. Gunn, M.S. Chen, Y.F. Rui, X.Y. Su, Z.P. Xie, Y.F. Zhao, A.I. Bush, Y.M. Li, J. Biol. Chem. 283 (2008) 31657–31664.
[17] C. Hureau, I. Sasaki, E. Gras, P. Faller, ChemBioChem 11 (2010) 950–953.
[18] L. Perez, K.J. Franz, Dalton Trans. 39 (2010) 2177–2187.
[19] L.E. Scott, C. Orvig, Chem. Rev. 109 (2009) 4885–4910.
[20] A. Trapaidze, C. Hureau, W. Bal, M. Winterhalter, P. Faller, J. Biol. Inorg. Chem. 17 (2012) 37–47.
[21] V. Balland, C. Hureau, J.-M. Savéant, Proc. Natl. Acad. Sci. U. S. A. 107 (2010) 17113–17118.

Please cite this article as: S. Noël, et al., A new water-soluble Cu(II) chelator that retrieves Cu from Cu(amyloid-β) species, stops associated ROS product..., J. Inorg. Biochem. (2012), doi:10.1016/j.jinorgbio.2012.05.016

Résumé

La maladie d'Alzheimer est caractérisée par la présence de plaques amyloïdes qui sont constituées d'agrégats de peptides amyloïdes-β (Aβ) et d'ions métalliques. Dans ce contexte, nous nous sommes intéressés à l'interaction des ions Cu et Zn avec des formes tronquées de peptides Aβ en se concentrant sur deux aspects : la coordination des ions métalliques et son impact sur les propriétés d'agrégation du peptide.

Dans la première partie, nous avons étudié la coordination du Cu sur des peptides Aβ dont la séquence diffère de celle du peptide original. Ces peptides modifiés sont considérés comme plus délétères. En combinant l'utilisation de plusieurs techniques spectroscopiques (RPE, DC, RMN...), nous avons ainsi: (i) déterminé les différents modes de coordination des Cu(II) et Cu(I) sur ces peptides en fonction du pH; (ii) montré l'importance de la fonction N-terminale dans la coordination du Cu(II); (iii) mis en évidence le rôle majeur de la seconde sphère sur la coordination des différentes espèces Cu(II)-peptides observées en fonction du pH; (iv) démontrer des différences de coordination du Cu(II) entre l'Aβ et ses formes modifiées, à mettre en parallèle avec une toxicité différente.

Dans la seconde partie, notre but a été de mieux de comprendre les mécanismes d'agrégation des peptides modulée par les ions métalliques. L'agrégation de peptides est un domaine vaste allant des maladies neurodégénératives à la nanotechnologie. Grâce à différents peptides (sous-séquences du Aβ) et à plusieurs techniques complémentaires (Fluorescence, Turbidité, MET...), nous avons montré que (i) la modulation de l'agrégation par un ion métallique dépend de sa sphère de coordination; (ii) l'accélération de l'agrégation du peptide Aβ11-28 induit par le Zn est due à la formation d'un complexe dimérique; (iii) la coordination du Zn change en fonction du pH, ce qui modifie la vitesse de l'agrégation; (iv) la charge du dimère est déterminante dans la précipitation du complexe peptidique; (v) la coordination du Zn au Aβ11-28 est dynamique : la coordination du Zn, même transitoire, induit des modifications non réversibles. Ces modifications accélèrent fortement et durablement l'agrégation de peptide même en forte sous-stœchiométrie de Zn.

Summary

Amyloid plaques are a hallmark of Alzheimer's disease. These plaques are formed by amyloid-β (Aβ) aggregates and metal ions. In this context, we studied the interaction of Cu and Zn ions with truncated forms of Aβ peptides. We focused on two aspects: Metals coordination and its impact on the aggregation of Aβ peptides.

In a first part, we studied coordination of Cu on modified Aβ peptides compared to the original one. These native modified peptides are considered more deleterious. Using many complementary spectroscopies (EPR, CD, NMR...), we have shown that (i) Cu(II) coordination is pH dependent; (ii) the importance of N-terminal amine in Cu(II) binding; (iii) the major role played by the second sphere in Cu(II) coordination; (iv) Cu Coordination differences between Aβ and its modified forms, that might be linked to their different toxicity.

In a second part, our aim was to gain insights into peptides aggregation mechanisms modulated by metal ions. Aggregation of peptides is a wide field of interest from neurological diseases to nanotechnology. Using different peptides (derived from Aβ sequence) and several complementary techniques (Fluorescence, Turbitity, TEM...), we have shown that (i) the aggregation depends on the metal ion coordination; (ii) the acceleration of Aβ11-28 aggregation induced by Zn is due to a dimer formation; (iii) pH induced changes in Zn coordination contribute to modify the aggregation rate; (iv) total charge of the dimer determine the precipitation; (v) Zn coordination to Aβ11-28 is highly dynamic: Zn coordination, even transiently, induced non-reversible modifications. These modifications dramatically and durably accelerate peptide aggregation even in large sub-stoichiometric amount of Zn.